FAKULTÄT FÜR
INFORMATIK

Institut für Simulation und Graphik

Visual Exploration and Analysis of Perfusion Data

Dissertation
zur Erlangung des akademischen Grades
Doktoringenieur (Dr.-Ing.)

angenommen durch die Fakultät für Informatik
der Otto-von-Guericke-Universität Magdeburg

von: Dipl.-Ing. Steffen Oeltze
geb. am 22.09.1977 in Magdeburg

Gutachter: Prof. Dr. Bernhard Preim
Prof. Dr. Helwig Hauser
Prof. Dr. Frits H. Post

Magdeburg, den 25. August 2010

Oeltze, Steffen (Dipl.-Ing.):
Visual Exploration and Analysis of Perfusion Data
Dissertation, Otto-von-Guericke-Universität Magdeburg,
25. August 2010.

Für Marlene und Edith

Kurzfassung

Perfusionsdaten sind dynamische medizinische Bilddaten, welche den regionalen Blutfluss in Gewebe charakterisieren. Sie besitzen ein großes Potential in der medizinischen Diagnose, da sie, verglichen mit statischen Daten, eine bessere Differenzierung und eine frühere Erkennung von Krankheiten ermöglichen. Diese Dissertation konzentriert sich auf Perfusionsdaten, welche mit Hilfe der Magnet-Resonanz-Tomographie (MRT) akquiriert wurden und auf deren Analyse in der Diagnostik des ischämischen Schlaganfalls und der Früherkennung und Diagnostik der Koronaren Herzkrankheit (KHK). An passender Stelle werden Beispiele aus der Brustkrebsdiagnostik hinzugezogen, um die Flexibilität der zur visuellen Exploration und Analyse entwickelten Techniken zu illustrieren. Die Übertragbarkeit auf weitere Anwendungsgebiete der dynamischen Bildgebung und auf andere Bildgebungsmodalitäten neben MR werden am Ende der Dissertation skizziert.

Sogenannte Zeit-Intensitätskurven spezifizieren die Anreicherung eines Kontrastmittels für die Voxel in einem Perfusionsdatensatz. Parameter, welche von diesen Kurven abgeleitet werden, charakterisieren die Perfusion und müssen für die Diagnose integriert werden. Die diagnostische Auswertung solcher Multiparameter Daten ist anspruchsvoll und zeitintensiv aufgrund der Komplexität der Daten. In der klinischen Routine basiert die Auswertung auf einzelnen Parameterkarten, welche nebeneinander auf dem Bildschirm dargestellt werden. Die Interpretation einer derartigen Ansicht erfordert einen erheblichen kognitiven Aufwand, da der Arzt die einzelnen Karten immer wieder abwechselnd betrachten muss, um korrespondierende Regionen zu vergleichen. Fortgeschrittene Visualisierungstechniken sind daher notwendig, um eine integrierte Ansicht mehrerer Parameter zu generieren und dadurch die Auswertung zu beschleunigen. In dieser Dissertation werden Multiparameter Visualisierungen basierend auf Farbe, Textur und Glyphen für die integrierte Visualisierung mehrerer Perfusionsparameter vorgestellt.

Das Aufnahmeprotokoll für die MR-basierte Akquisition von Perfusionsdaten umfasst häufig die Aufnahme weiterer Bilddaten, welche unterschiedliche klinische Aspekte beschreiben. Zusammen vermitteln die Daten ein globales Bild des Patientenstatus. Die Diagnostik der KHK ist ein prominentes Beispiel. Sie umfasst sowohl Aufnahmen welche die Anatomie des Herzens und der Herzkranzgefäße charakterisieren, als auch Aufnahmen welche eine Beurteilung der Perfusion, Viabilität und Funktion des Myokards (Herzmuskel) gestatten. Innerhalb der Dissertation wird eine Glyphen-basierte 3D Visualisierung der Myokardperfusion vorgestellt. Diese ist in den anatomischen Kontext eingebettet und wird durch Informationen angereichert, welche die Viabilität und Funktion des Myokards beschreiben.

Die rein visuelle Exploration von Perfusionsdaten und den zugehörigen Perfusionsparametern ist vorherrschend im engen Zeitplan der klinischen Routine. Sie ist jedoch eine vom Betrachter abhängige und kaum reproduzierbare Aufgabe, die keine quantitativen Ergebnisse liefert. Für eine geordnete und reproduzierbare Analyse von Perfusionsdaten ist eine Kombination aus visueller Exploration und aus Techniken der Datenanalyse notwendig. Die Dissertation trägt dazu einen interaktiven, merkmalsbasierten Ansatz für die geordnete visuelle Analyse von Perfusionsdaten bei. Dieser Ansatz stützt sich auf drei Komponenten, für die Vorverarbeitung der Daten, für eine statistische Analyse und für die Spezifikation von Merkmalen. Die Durchführbarkeit des Ansatzes wurde für mehrere Datensätze aus der Diagnostik des ischämischen Schlaganfalls, der KHK-Diagnostik und der Brustkrebsdiagnostik erfolgreich getestet. Weiterhin konnte sein Nutzen bei der Beantwortung wichtiger investigativer Fragen in der Perfusionsforschung am Beispiel des Vergleichs von daten- und modellbasierter Auswertung zerebraler Perfusion demonstriert werden.

Abstract

Perfusion data are dynamic medical image image data which characterize the regional blood flow in tissue. These data bear a great potential in medical diagnosis, since diseases can be better distinguished and detected at an earlier stage compared to static image data. The thesis at hand focuses on Magnetic Resonance (MR) perfusion data and their analysis in ischemic stroke diagnosis and in the early detection and diagnosis of Coronary Heart Disease (CHD). When appropriate, examples from breast tumor diagnosis are consulted to illustrate the flexibility of the developed visual exploration and analysis techniques. The transferability to further application fields of dynamic imaging and to imaging modalities other than MR are outlined at the end of the thesis.

For each voxel in a perfusion dataset, a time-intensity curve specifies the accumulation and washout of a contrast agent. Parameters derived from these curves characterize the perfusion and have to be integrated for diagnosis. The diagnostic evaluation of this multiparameter data is challenging and time-consuming due to its complexity. In clinical routine, the evaluation is based on a side-by-side display of single-parameter visualizations whose interpretation demands a considerable cognitive effort to scan back and forth for comparing corresponding regions. Hence, sophisticated visualization techniques are required that generate an integrated display of several parameters thereby accelerating the evaluation. In this thesis, color-, texture- and glyph-based multiparameter visualizations for the integrated display of several perfusion parameters are presented.

MR perfusion data are often acquired in a scanning protocol together with other image data describing different clinical aspects. Together, the data contribute to a global picture of the patient state. CHD diagnosis is a prominent example including scans that characterize the anatomy of the heart and the great vessels as well as scans depicting the perfusion, viability, and function of the myocardium (heart muscle). The thesis at hand introduces a 3D glyph-based visualization of myocardial perfusion which is embedded in the anatomical context of the myocardium and enhanced by adding viability and functional information.

The pure visual exploration of perfusion data and associated perfusion parameters is the prevailing method in the tight schedule of clinical routine. However, it is an observer-dependent and barely reproducible task delivering no quantitative results. An approach is required that merges visual exploration and data analysis techniques into visual analysis for a streamlined investigation of perfusion. The thesis contributes an interactive feature-based approach for the streamlined visual analysis of perfusion data which comprises components for data preprocessing, statistical analysis, and feature specification. The approach is applied to several datasets from ischemic stroke, CHD, and breast tumor diagnosis for a proof of concept. Furthermore, its benefit in answering crucial investigative questions in perfusion research is demonstrated by comparing *data-near* and *model-near* cerebral perfusion assessment.

Danksagung

Die Entstehung dieser Arbeit verdanke ich vielen Menschen, die mich während der Promotionszeit unterstützt haben. Mein tiefer Dank gilt meinem Doktorvater Bernhard Preim, der mir auf meinem wissenschaftlichen Weg stets mit Anregungen, Hilfestellungen, Kritik, Aufmunterungen und sowohl fachlicher als auch menschlicher Kompetenz zur Seite stand. Viele Fähigkeiten, die mir bei der Entstehung dieser Arbeit geholfen haben, verdanke ich ihm. Weiterhin möchte ich mich bei Anja Hennemuth und Caroline Kühnel von Frauenhofer MeVis für eine interessante und fruchtbare Zusammenarbeit über die Jahre bedanken. Einige gemeinsame Publikationen sind daraus erwachsen. Ein besonderer Dank gilt Helmut Doleisch und Philipp Muigg von der SimVis GmbH, sowohl für die produktive Kooperation, welche einen wichtigen Beitrag zu der vorliegenden Promotion geleistet hat, als auch für die Bereitstellung der Software SimVis. Helwig Hauser von der Universität Bergen, Norwegen danke ich für die fantastische Zusammenarbeit, für zahlreiche fruchtbare Diskussionen, für seine Inspiration und für die Möglichkeit zu einem bereichernden Forschungsaufenthalt in seiner Arbeitsgruppe. Bedanken möchte ich mich weiterhin bei Arvid Lundervold und Jarle Rørvik von der Universität Bergen, Norwegen für die Weitergabe ihres unerschöpflichen Wissens zur zerebralen Perfusion, für die inspirierende gemeinsame Auswertung zerebraler Perfusionsdaten und für die Bereitstellung klinischer Daten. Frank Grothues vom Universitätsklinikum Magdeburg danke ich für die wertvolle Zusammenarbeit, die Weitergabe seines profunden Wissens zur myokardialen Perfusion und für die Erlaubnis zur Beobachtung und Auswertung einer seiner klinischen Studien. Uta Preim vom Universitätsklinikum Magdeburg hat mich bei Fragen zur Brustkrebsdiagnostik kompetent beraten und klinische Daten für die Promotion zur Verfügung gestellt. Weitere Ärzte bei denen ich mich für die Bereitstellung von klinischen Daten, teils über Fraunhofer MeVis, bedanken möchte sind: Jonathan Wiener (Boca Raton Community Hospital, USA), Andreas Fessel, Frank Fischbach (Universitätsklinikum Magdeburg), Michael Fenchel, Stefan Miller und Achim Seeger (Universitätsklinikum Tübingen) und Stephan Achenbach (Universitätsklinikum Erlangen). Ein ganz besonderer Dank gilt den ehemaligen Diplomanden Christian Bendicks, Sylvia Glaßer, Anja Kuß, Arvid Malyszczyk, Lydia Paasche, Christian Schumann und Verena von Hintzenstern, die einen großen Anteil an dieser Arbeit haben und deren Tatendrang und Forschergeist mich immer inspiriert haben. Tief verbunden bin ich meinen Kollegen vom Institut für Simulation und Graphik, die mich während der gesamten Promotionszeit durch zahlreiche Anregungen und Kritik unterstützt und stets für ein angenehmes und produktives Arbeitsklima gesorgt haben.

Nicht zuletzt möchte ich den wichtigsten Personen in meinem Leben danken, die diese Arbeit erst möglich gemacht haben. Edith hat mir den Rücken stets frei gehalten, mir die Kraft zum Schreiben dieser Arbeit verliehen und dafür gesorgt, dass die Prokrastinationsphasen nicht zu lang wurden. Marlene hat mich durch ihr süßes Lächeln stets motiviert und mir den Blick für das Wesentliche geöffnet. Meine Eltern waren mein Leben lang immer für mich da und haben mir den Weg zu dieser Promotionsschrift geebnet. Ich widme diese Arbeit Edith, Marlene und meinen Eltern.

Contents

Kurzfassung **v**

Abstract **vii**

Danksagung **ix**

1 Introduction **1**

2 Background **5**
2.1 Cerebral Perfusion in Ischemic Stroke Diagnosis 5
2.1.1 Medical Background 6
2.1.2 Brain Perfusion Imaging 9
2.1.3 Data Processing 12
2.1.4 Visualization and Exploration 17
2.2 Myocardial Perfusion in the Diagnosis of Coronary Heart Disease 19
2.2.1 Medical Background 20
2.2.2 Cardiac Magnetic Resonance Imaging 26
2.2.3 Data Processing 33
2.2.4 Visualization and Exploration 40
2.3 Summary and Implications for the Thesis 42

3 Visual Exploration **45**
3.1 Related Work 45
3.1.1 Color- and Texture-based Multiparameter Visualization 46
3.1.2 Glyph-based Medical Visualization 48
3.1.3 Comprehensive Cardiac Visualization 51
3.2 Multiparameter Maps 54
3.2.1 Colored Height Fields 55
3.2.2 Flexible Lenses 56
3.2.3 Color Icons 57
3.2.4 Refined Bull's Eye Plot 58
3.3 Glyph-based Visualizations 59
3.3.1 Intuitive Perfusion Parameter Mapping to 2D Glyph Shapes 59
3.3.2 3D Glyph-based Visualization of Myocardial Perfusion 67
3.4 Comprehensive Cardiac Visualization 76
3.4.1 Integrating Myocardial Perfusion and Angiographic Data 77
3.4.2 Integrating Perfusion, Late Enhancement and Cine Data 81
3.5 Conclusion 83
3.6 Discussion 85

4 Visual Analysis **87**
4.1 Related Work . . . 87
4.1.1 Data Mining and Knowledge Discovery in Perfusion Data . . . 88
4.1.2 Interactive Visual Analysis of Medical Data . . . 89
4.2 Interactive Visual Analysis of Perfusion Data . . . 92
4.2.1 Approach for a Streamlined Analysis . . . 93
4.2.2 Case Study: Ischemic Stroke Diagnosis . . . 98
4.2.3 Case Study: Diagnosis of Coronary Heart Disease . . . 102
4.2.4 Case Study: Breast Tumor Diagnosis . . . 104
4.2.5 Function-based Feature Specification . . . 109
4.3 Four Interactive Visual Analysis Approaches and a Comparison . . . 111
4.3.1 Image Data and Data Preprocessing . . . 111
4.3.2 Four Interactive Approaches . . . 112
4.3.3 Comparison . . . 119
4.4 Conclusion . . . 123

5 Discussion and Outlook **125**
5.1 Guidelines for Visual Exploration . . . 126
5.2 Potential of an Interactive Visual Analysis . . . 128
5.3 Outlook . . . 131
5.4 Transferability to Different Fields . . . 133
5.4.1 Different Imaging Modalities . . . 133
5.4.2 Different Application Areas . . . 135

Bibliography **141**

Nomenclature **163**

Chapter 1

Introduction

Compared to static image data, where the morphology of anatomic and pathological structures is represented with high spatial resolution, dynamic image data characterizes functional processes, such as metabolism and blood flow, which is often essential to detect diseases at an early stage or to discriminate pathologies with very similar morphology. Important examples of dynamic medical imaging are functional Magnetic Resonance Imaging (fMRI), where activations of brain areas are imaged, dynamic Positron Emission Tomography (dPET) and dynamic Single-Photon Emission Computed Tomography (dSPECT), where the temporal distribution of a labeled glucose analog may be monitored to assess metabolic processes and perfusion imaging, where the the microcirculation of blood through tissue capillaries is measured. The thesis at hand focuses on MR perfusion data which are acquired to support essential diagnostic tasks, e.g., the differentiation of irreversibly damaged and salvageable tissue in ischemic stroke diagnosis, the early detection and diagnosis of coronary heart disease (CHD), the assessment of different types and stages of tumors, the evaluation of disorders of the lung blood supply, the modeling of renal perfusion, the early detection of hepatic malignancies and cirrhosis in the liver, and the assessment of articular cartilage dynamics. The two major application areas covered in the thesis are ischemic stroke diagnosis and CHD diagnosis. When appropriate, additional insight into breast tumor perfusion is provided.

A restricted blood supply of tissue generally caused by pathologies of the supplying vasculature is referred to as *ischemia*. In the diagnosis of acute ischemic stroke, affected tissue must be detected and salvageable tissue must be identified in order to suggest an appropriate therapy. In early CHD diagnosis, ischemic regions of the myocardium (heart muscle) shall be identified and correlated with the supplying coronary artery branches to support the detection of pathologic vessel narrowings. If the existence of a narrowing is a priori known, its hemodynamical relevance shall be evaluated. Cardiac MR perfusion data are often acquired in conjunction with other data describing the function and viability of the myocardium. Together, the data contribute to a global picture of the patient state. Their concurrent analysis facilitates a differentiation of myocardial tissue states thereby supporting therapeutic decisions.

In perfusion imaging, the distribution of a contrast agent (CA) is registered to assess blood flow and tissue kinetics. Signal intensities after CA administration are recorded. Plotting the intensities over time results in so-called time-intensity curves (TICs). Whether or not a CA is delivered and subsequently absorbed within a particular region, how long it takes until the maximum amount of CA is delivered, which overall amount of CA traverses the tissue of interest in a certain time interval as well as other *perfusion parameters* are derived from the TICs for medical diagnosis. These parameters are substitutes for physiological parameters such as regional blood flow, regional blood volume and capillary permeability.

The parameter-based evaluation of perfusion data is an active area of research in ischemic stroke as well as in CHD diagnosis. Although, particular clinical relevance could be documented for one parameter in assessing myocardial perfusion, no clinical guideline yet exists implementing this and results may have to be reviewed due to advances in imaging technology and CA design. The thesis at hand aims at supporting physicians in clinical routine as well as researchers working in the field of perfusion imaging. While the clinical routine poses high demands on both, diagnostic accuracy and speed, research work is less time-critical.

A physician evaluating a perfusion scan and the associated parameters should be provided with advanced visual exploration techniques that facilitate the integrated comparative exploration of several perfusion parameters. The generated visualizations should outperform the prevailing side-by-side presentation of color-coded *parameter maps*. The latter demands a considerable cognitive effort in scanning back and forth for comparing corresponding regions. An integrated visualization of several parameters may speed up the diagnosis, facilitate the detection of more subtle changes between corresponding regions and reveal features that are not visible in any one of the separate parameter maps. The visual exploration for CHD diagnosis is especially challenging since the integrated visualization of several perfusion parameters should be combined with parameters describing function and viability of myocardial tissue.

Researchers working in the field of perfusion imaging aim at identifying the perfusion parameter or the combination of parameters having the strongest impact in terms of accurately representing perfusion status and predicting tissue outcome. They are seeking for optimal method(s) for parameter derivation that are immune against differences in imaging parameters such as magnetic field strength, scan parameters, and CA type and dose. The following crucial investigative questions were collected in an extensive research literature review:

- Which perfusion parameters or which combination of parameters is crucial for a specific diagnostic task?
- How are individual perfusion parameters related?
- How do imaging parameters as well as different parameter computation methods influence the expressiveness of perfusion parameters?
- How do answers to the previous questions differ from patient to patient?

Answering these questions should be left to researchers and clinicians working in the respective application field. However, this thesis will contribute an interactive visual analysis approach that may assist them in finding answers. The approach combines the visual exploration of perfusion parameters with statistical analysis methods and a feature specification component thereby facilitating an inspection of inter-parameter relations and of changes due to varying imaging parameters. The interactive feature specification based on the original data, perfusion parameters, and statistical analysis results together with a rapid visual update of the feature specification result should provide the researcher with a deeper understanding of the inspected data space. For the non-standardized MR signal intensities, an interactive feature specification may provide an alternative to static tissue classification algorithms.

The invented visual exploration and analysis techniques shall be applicable to both, cerebral and myocardial perfusion. Despite the differences in imaging and data preprocessing, the resulting data base for a visual exploration and analysis is very similar. It consists of the original 4D data and of a separate 3D volume for each perfusion parameter. Since from a computational point of view, the overall amount of data is low in both application fields, even when perfusion parameters are derived by various algorithms, the performance of generating visualizations and of the analysis should not pose an issue.

The thesis at hand is organized as follows: In *Chapter 2*, background information on cerebral perfusion in the diagnosis of ischemic stroke and on myocardial perfusion in CHD diagnosis is provided. The medical background, prevailing imaging modalities, data processing aspects as well as common visualization and exploration facilities, and available

commercial software and research prototypes are covered. *Chapter 3* is dedicated to the visual exploration of perfusion data. Multiparameter visualizations, in particular, glyph-based visualizations, and a comprehensive cardiac visualization integrating myocardial perfusion, function and viability are discussed. An approach for the streamlined visual analysis of perfusion data comprising a preprocessing, a statistical, and a feature specification component is presented in *Chapter 4*. Further, the application of a function-based feature specification is documented as particularly suitable for perfusion data. Four different feature specification approaches based on the original perfusion data and derived data are closely illuminated and compared in the context of cerebral perfusion. The thesis is completed in *Chapter 5* by a discussion of the presented work including the specification of guidelines for a visual exploration of perfusion data. In addition, the potential of an interactive visual analysis in supporting future perfusion research is estimated. Improvement opportunities for the presented visual exploration and analysis techniques are identified and ideas which may guide future work are rendered. Finally, the transferability of the techniques to other application fields of dynamic imaging and to imaging modalities other than MR are outlined.

Chapter 2

Background

The aim of perfusion imaging is to measure the microcirculation of blood through tissue capillaries. Since the capillary diameter and length are below the resolution of today's scanning devices, macroscopic parameters that characterize the microcirculation are derived from the measured data. This is feasible despite the heterogeneity of capillary perfusion on a microscopic level due to the high quantity of capillaries per tissue mm^3. Assuming a uniform distribution of the 30-40 billion capillaries inside the human body, 600 vessels with an average diameter of 6 μm and an average length of 750 μm exist per 1 mm^3 [Busse, 2005]. Example macroscopic parameters derived from perfusion images are regional blood flow, regional blood volume and capillary permeability.

The PhD thesis at hand covers two major application areas of perfusion imaging. In the diagnosis of acute ischemic stroke, the goals of an imaging evaluation are to detect the affected tissue as fast as possible, to identify salvageable tissue, to suggest an appropriate therapy, and to monitor the therapy progress. In the diagnosis of Coronary Heart Disease, less perfused regions of the heart muscle shall be identified and correlated with the supplying coronary artery branches to support the detection of a pathologic vessel narrowing. If the existence of the narrowing is a priori known, its hemodynamical relevance shall be evaluated. After a heart attack, perfusion imaging is applied to differentiate between irreversibly damaged tissue and tissue that might benefit from a revascularization therapy.

The following Sections 2.1-2.2 are each dedicated to one of these application areas. Information on the medical background as well as on the most important imaging modalities are given. Since the focus of this thesis is on Magnetic Resonance Perfusion Imaging, the other modalities are only covered briefly. The sections further comprise data processing aspects, e.g., noise removal and motion correction, the segmentation of relevant structures, common visualization and exploration facilities as well as available commercial software and research prototypes. This chapter is concluded by an elaboration of open research questions and the resulting implications for the thesis at hand in Section 2.3.

2.1 Cerebral Perfusion in Ischemic Stroke Diagnosis

Cerebral perfusion data are acquired to characterize the regional blood supply of brain tissue. One of their major diagnostic applications is ischemic stroke assessment. In the acute phase of an ischemic stroke, the differentiation between healthy, irreversibly damaged and salvageable tissue is crucial. The location and extent of the latter type of tissue have a strong impact on therapeutic decisions. This section is structured as follows: Subsection 2.1.1 briefly reviews ischemic stroke from a medical point of view, including definition, symptoms and therapy strategies. Subsection 2.1.2 summarizes the prevailing imaging modalities with a focus on perfusion MRI. Relevant data processing aspects including the computation of perfusion parameters are explained in Subsection 2.1.3. The visualization and exploration of cerebral perfusion data is discussed in Subsection 2.1.4. The focus is here on the State of the art in commercial software and in research prototypes.

2.1.1 Medical Background

In the United States and in Germany, stroke ranks number three among all causes of death after Coronary Heart Disease and cancer [Lloyd-Jones et al., 2009], [Kolominsky-Rabas, 2004]. Of all strokes, 87% and 78% are ischemic in the U.S. and in Germany, respectively, the rest are hemorrhagic. The distinction of both types is one of the most important tasks in early stroke management [Donnan et al., 2008]. In the following, the focus is on ischemic strokes. An ischemic stroke is a medical emergency that requires immediate action in its acute phase (≈24h from symptom onset). When assessed during this phase, ischemic stroke is also referred to as acute ischemic stroke.

In the event of an ischemic stroke, an artery supplying the brain with blood is blocked by a blood clot (*thrombosis*) or a fatty deposit causing a vessel narrowing (*stenosis*). This eventually leads to a death of brain cells due to a sustained undersupply of oxygen and nutrients. The phrase "time is brain" illustrates the necessity of both, a fast therapeutic decision and an immediate clinical intervention [Gomez, 1993]. In case of a typical large vessel ischemic stroke, an average patient looses as many neurons per hour as in 3.6 years of normal brain aging [Saver, 2006].

In the following, the anatomy of the brain will be briefly described. The reader is encouraged to familiarize oneself with terms describing the position and direction of brain structures as well as typical section planes before (Fig. 2.1). At a macroscopic level, the human brain is organized in cerebrum, cerebellum and brain stem (Fig. 2.2(a)). The cerebrum may be further divided along the longitudinal fissure into the left and the right hemisphere (Fig. 2.2(b)). Each hemisphere consists of four different lobes, the frontal lobe, the parietal lobe, the temporal lobe, and the occipital lobe, processing different information and performing different tasks (Fig. 2.2(c)). The surface of each lobe is contoured by gyri and sulci.

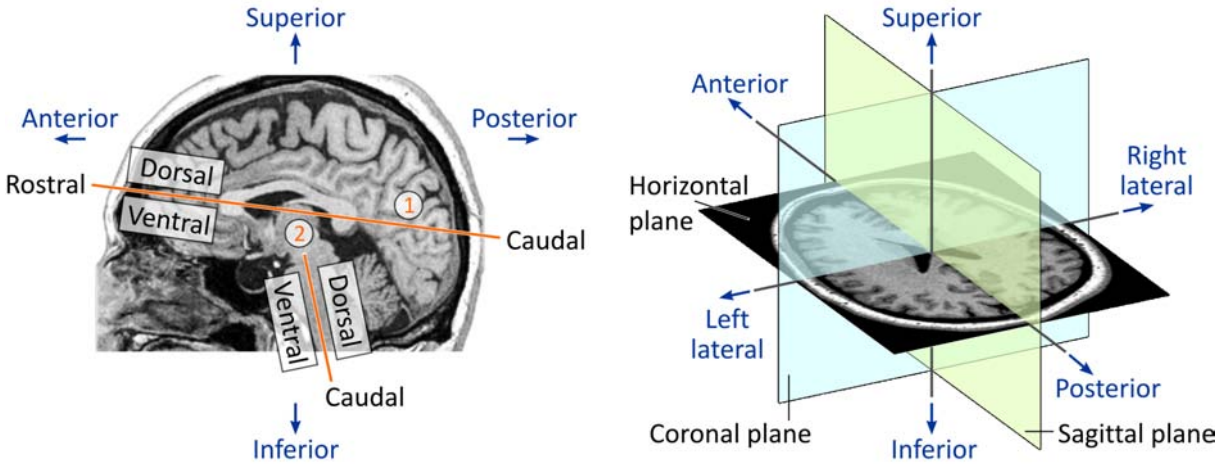

Figure 2.1: Brain: anatomical directions and section planes. (a) Mid-sagittal cut through the brain illustrating the anatomical directions with respect to the longitudinal axis of the forebrain (1), and the longitudinal axis of the brain stem and the spinal cord (2). (1) and (2) are also referred to as the *Forel-axis* and the *Meynert-axis*, respectively. (b) Typical section planes and anatomical directions. (Illustrations created using "Bruce Gooch's Brain" datasets.)

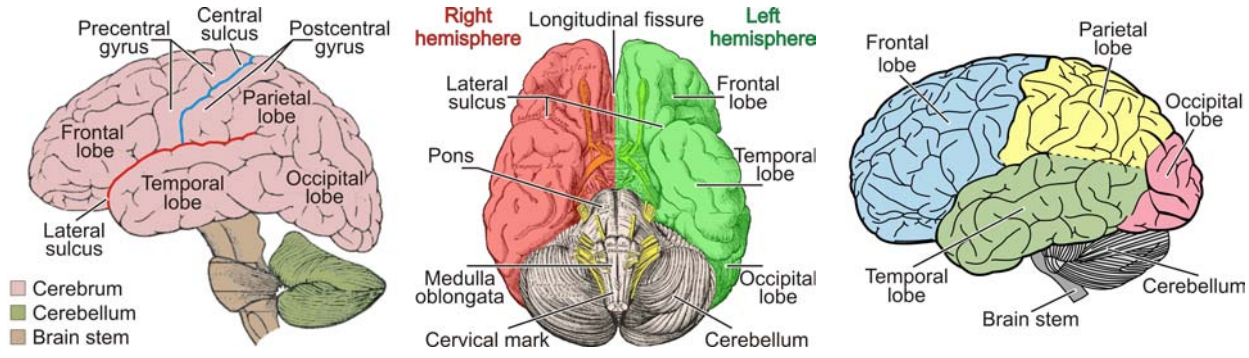

(a) (b) (c)

Figure 2.2: Macroscopic organization of the human brain. *(a)* Left lateral view showing a rough division of the brain into cerebrum, cerebellum and brain stem. *(b)* Inferior view illustrating the division of the cerebrum along the longitudinal fissure into left and right hemisphere. *(c)* Lateral view of the four major lobes of the left hemisphere. (Based on illustrations in [Gray, 1918].)

The two hemispheres are supplied with blood by two sets of paired arteries, the internal carotid arteries and the vertebral arteries (Fig. 2.3(a)). While the internal carotid arteries supply large parts of the anterior part of the cerebrum with blood, the vertebral arteries supply the posterior part. The right and the left vertebral artery join each other at the base of the brain forming the basilar artery. The basilar artery then joins the blood supply from the internal carotid arteries in the so called *Circle of Willis* located at the base of the brain. From the Circle of Willis, three sets of paired, large brain arteries originate and branch out up to the capillary level through all parts of the brain: the anterior, posterior, and middle cerebral arteries (Fig. 2.3(b)).

The anterior cerebral arteries supply the medial and superior aspects of the frontal lobes, and the medial aspects of the anterior parietal and the occipital lobes (Fig. 2.4). Also, four-fifths of the corpus callosum are drained by these arteries. The posterior cerebral arteries

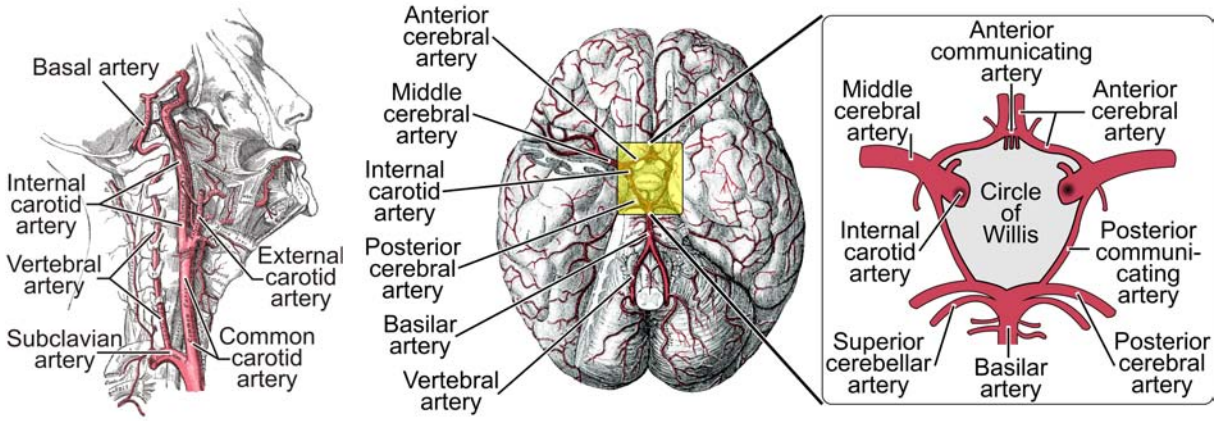

(a) (b)

Figure 2.3: Blood supply of the human brain. *(a)* Right lateral view of the major arteries in the deep neck. The brain hemispheres are supplied by the internal carotid and the vertebral arteries. *(b)* Basal view of the major brain arteries. The Circle of Willis is emphasized in the inset. (Based on illustrations in [Gray, 1918].)

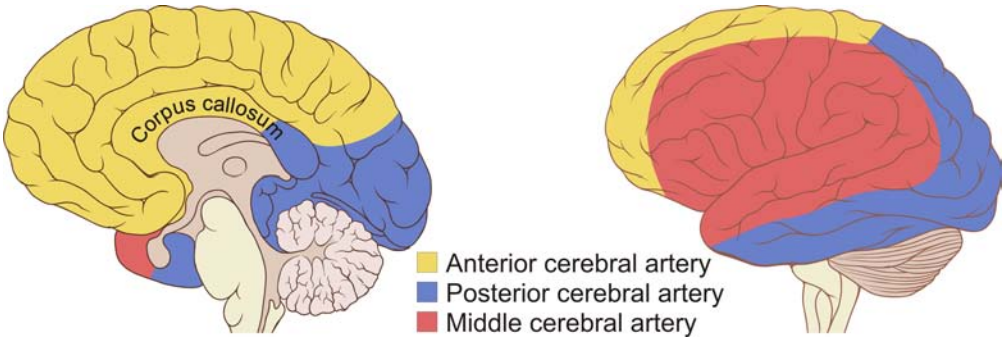

Figure 2.4: Vascular territories of the human brain. Both hemispheres are colored according to the territories of the three large brain arteries. (Based on a line drawing by Patrick J. Lynch, medical illustrator.)

supply the posterior medial parietal lobes and the remaining one-fifth of the corpus callosum. They further supply the inferior and medial aspects of the temporal lobes, including the hippocampus, and the medial and inferior surfaces of the occipital lobes. Finally, the middle cerebral arteries supply much of the lateral and inferior frontal lobes and the anterior lateral parts of the parietal lobes. Also, aspects of the posterior parietal lobes, much of the lateral occipital lobes, and the lateral temporal lobes, including their anterior tip, are drained by the middle cerebral arteries.

Depending on the location of an artery occlusion, different brain areas are affected resulting in different observable symptoms that may give a diagnostic hint on the location. A hemiplegia (paralysis of body parts causing a lack of control) for example of the face and arms indicates a stroke in the contralateral region of the middle cerebral artery. This artery is most often occluded in ischemic stroke [Schünke et al., 2006]. In Germany, the majority of ischemic strokes (25-35%) is caused by a blood clot arising in the heart, breaking free and traveling to the brain (*embolic strokes*) [Ringelstein and Nabavi, 2007]. Small vessel occlusions (20-25%) and occlusions of the large brain arteries (15-20%, Fig. 2.3(b)) due to a locally formed blood clot or a significant stenosis provide the second highest and third highest cause, respectively, followed by other causes (5%). For about 20-30% of ischemic strokes no cause is verifiable.

The tissue affected by an ischemic stroke can be classified in the infarction core and the penumbra (also called *tissue-at-risk*) which surrounds the core [Astrup et al., 1981] (Fig. 2.5). While the perfusion in the core is severely depleted, brain cells in the penumbra may remain viable for several hours. This is due to the collateral blood supply of this region which compensates for the restricted supply by the blocked branch. However, collateral perfusion can only delay the death of brain cells. The penumbra has been reported as a predicator for the final infarction size [Baron, 1999]. Its transformation into irreversibly damaged tissue is dependent on a variety of hemodynamic and metabolic factors and does not follow a fixed time schedule. At the best, the penumbra will survive 9-12 hours while at the worst, it will be completely transformed after 2-3 hours [Ringelstein and Nabavi, 2007]. Hence, a recanalization therapy must be carried out during the early hours after symptom onset to salvage the penumbra. The most promising therapy at the moment is the intravenous administration of a thrombolytic agent (*thrombolysis*) within the first 3 hours (6 hours when applied intra-arterial) that resolves the blood clot and restores the blood supply [Adams et al., 2007]. A good practical description of pathophysiology, diagnostic and therapy of ischemic stroke is given in [Ringelstein and Nabavi, 2007].

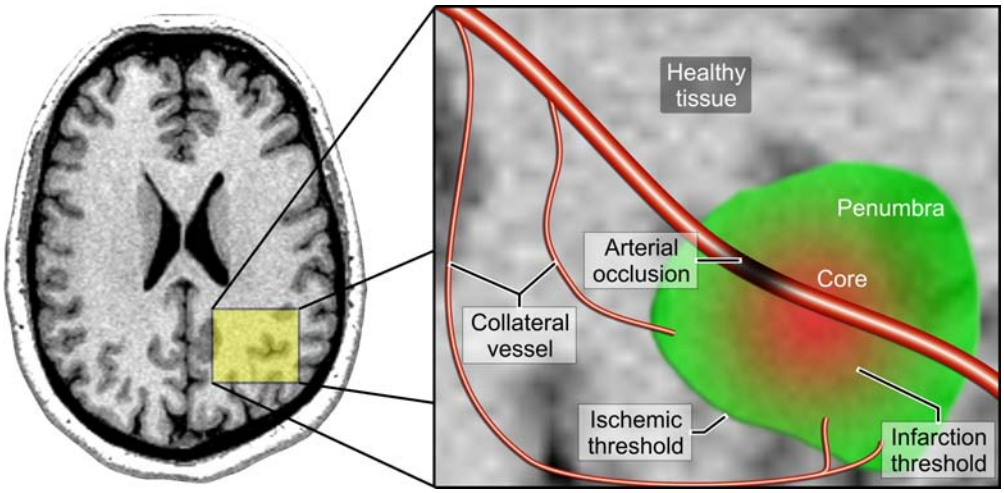

Figure 2.5: Tissue affected by an ischemic stroke which has been caused by an arterial occlusion. The infarction core is irreversibly damaged while the penumbra remains viable for a certain time due to collateral blood supply.

Successful stroke treatment requires a fast diagnosis and immediate therapeutic decisions. Once typical symptoms occur, the patient or relatives should act fast and call the emergency number. In hospital, the first step is to confirm that the patient is suffering from an ischemic stroke and to exclude other illness, especially intracranial hemorrhage [Donnan et al., 2008]. The latter is crucial since thrombolysis must not be applied in this case. For more information on guidelines for the early management of adults with ischemic stroke including prehospital management, emergency evaluation and diagnosis, brain imaging, general supportive care and treatment, as well as various therapeutic strategies ranging from drug administration to surgical interventions consult [Adams et al., 2007].

2.1.2 Brain Perfusion Imaging

Brain imaging is playing an important role in the initial phase after symptom onset and directly affects both acute and long-term treatment decisions. It can help to exclude intracranial hemorrhage and to assess the intracranial vessels. Furthermore, it can facilitate the assessment of the patient-individual risk for hemorrhagic transformation by thrombolytic agents thereby improving the patient selection for this kind of therapy. Brain perfusion imaging, as a special category of brain imaging, can help to detect the size, location and vascular distribution of the infarction and to identify salvageable brain tissue, i.e. the penumbra [Adams et al., 2007].

2.1.2.1 Clinical Aspects

In today's clinical research literature related to brain perfusion imaging, the different modalities available are often discussed in the context of thrombolytic therapy. The current recommendations for imaging of acute ischemic stroke as published by the *American Stroke Organization* (ASO) support this observation [Latchaw et al., 2009]. This priority is understandable against the background of thrombolysis being the most promising therapy for treating an acute ischemic stroke. Furthermore, the application of the different imaging modalities is frequently illuminated with respect to the elapsed time since symptom onset

[Latchaw et al., 2009]. This is mainly due to the fact that thrombolysis has only been approved in the first three hours after onset and must not be applied beyond this time window.

Within 3h after symptom onset, the most important tasks are to confirm the diagnosis of a stroke and to exclude cerebral hemorrhage. The imaging modalities recommended by the ASO for accomplishing these tasks are nonenhanced Computed Tomography and Magnetic Resonance Imaging (MRI). Brain perfusion imaging techniques do not play a significant role within this time window and would only delay the therapy [Ringelstein and Nabavi, 2007]. Their potential is the identification of salvageable tissue, i.e. the penumbra, whose existence however, is very likely in case of early patient presentation. The situation changes beyond the 3h time window. Here, the ASO suggests the application of perfusion imaging, particularly if intra-arterial thrombolytic therapy or mechanical blood clot removal are contemplated. Furthermore, recent clinical studies suggest that the time window for intravenous thrombolysis should be extended up to 6-9 hours or even longer [Latchaw et al., 2009]. The demand for an extension is based on the observation that penumbral tissue surviving longer than 3h can be correctly identified via brain perfusion imaging.

2.1.2.2 Prevailing Imaging Modalities

The imaging modalities perfusion Computed Tomography (CT) and perfusion Magnetic Resonance Imaging (MRI) are primarily used in clinical routine to assess cerebral perfusion. They have both proven to be useful in differentiating between infarction core and penumbra and in decision making for therapeutical interventions [Latchaw et al., 2009]. Major advantages of perfusion CT are its widespread availability, the fast applicability and the low cost. Furthermore, the feasibility of perfusion MRI studies is usually restricted due to the low availability of emergency settings in most clinical institutions and patient-specific difficulties with obtaining MRI, e.g., pace makers and claustrophobia [Wintermark et al., 2005b]. Major disadvantages of perfusion CT as compared to perfusion MRI are the exposition to radiation and the limited spatial coverage. While the entire brain can be scanned with perfusion MRI, in perfusion CT typically a thick slab of 2-4 cm is covered per scan which requires a good initial guess of the infarct location [Latchaw et al., 2009].

Another advantage of perfusion MRI is the intensively studied generation of an infarction core/penumbra mismatch representation being decisive already in some clinical centers [Hjort et al., 2005]. This generation is based on the so-called *perfusion-diffusion mismatch* as observed in combining results from perfusion MRI and MR Diffusion-Weighted Imaging (DWI) [Warach et al., 1996]. In DWI, the local characteristics of water diffusion are measured. During an ischemic stroke, the diffusion is restricted as extracellular water moves into the intracellular space. In addition, the cells are swelling and the extracellular spaces are narrowing [Latchaw et al., 2009]. Perfusion MRI facilitates the depiction of the entire affected tissue while DWI depicts the infarction core. The difference between the two regions, i.e. the mismatch, can be thought of as the penumbra. The precise identification of the penumbra by means of perfusion MRI or a combination of perfusion MRI and DWI is still part of ongoing research. Perfusion MRI data do not allow for a straightforward derivation of quantitative parameters describing the perfusion [Latchaw et al., 2009]. This hampers the definition of thresholds that accurately separate healthy from ischemic tissue and the core from the penumbra (Fig. 2.5). Furthermore, it is unclear on which of the common parameters the thresholds should be based. When combining perfusion MRI with DWI, it must be clarified which parameters should be used in perfusion MRI to identify the entire affected tissue [Ringelstein and Nabavi, 2007]. In addition, a threshold must be defined as from which

a significant mismatch size is present that legitimates a thrombolysis. In the following, the focus will be on perfusion MRI. A comparative overview on seven brain perfusion imaging modalities including perfusion CT and perfusion MRI is given in [Wintermark et al., 2005b].

2.1.2.3 Perfusion Magnetic Resonance Imaging

This subsection is based on [Brix et al., 1997] and [Petrella and Provenzale, 2000]. For a comprehensive introduction to cerebral perfusion MRI including specific MR-related technical details, e.g., on imaging sequences, the reader is referred to [Sorensen and Reimer, 2000]. perfusion MRI relies on the measurement of signal changes while and after the administration of a paramagnetic contrast agent (CA). The rapid intravenous injection is carried out by a specialized system such that a compact representation of the CA (*bolus*) is formed. The bolus travels with the blood and reaches the capillary bed after 5-10 seconds. The length of the first passage through the capillary bed is on the order of 18 seconds. Hence, very fast imaging sequences are necessary for a rapid acquisition of a series of images. Usually, only the first passage of the CA through the blood cycle is considered since it shows the most significant signal changes. With each further passage through the body, the bolus disperses and the CA eventually becomes excreted by the kidneys. The paramagnetic property of the CA has two different effects on the MR signal which are exploited by two different imaging techniques: Dynamic Susceptibility Contrast (DSC)-MRI and Dynamic Contrast-Enhanced (DCE)-MRI. DSC-MRI is based on the *susceptibility effect* which describes the development of local inhomogeneities in the magnetic field during the passage of an intravascular paramagnetic CA. It represents the prevailing imaging technique in the diagnosis of acute ischemic stroke and is used to assess the cerebral blood volume and the cerebral blood flow. DCE-MRI is based on the *relaxation effect* which describes the reduction of MR tissue relaxation times caused by a diffusible paramagnetic CA. It is applied alongside DSC-MRI in the diagnosis of brain tumors since it offers an investigation of the vascular permeability.

Before DSC-MRI will be discussed in more detail, the difference between an intravascular and a diffusible CA should be noted. While an intravascular CA stays inside the vessel lumen (as required for DSC-MRI), a diffusible CA passes the border between the intravascular and the extravascular space (as desired in DCE-MRI). At the moment, no intravascular CAs have been approved for measuring cerebral perfusion in clinical routine. However, in case of an intact blood-brain barrier diffusible CAs behave equal to intravascular ones. Hence, they are used in DSC-MRI as well. Gd-DTPA (gadolinium diethylenetriamine penta-acetic acid) is the most common diffusible CA. Since its susceptibility effect is much smaller than its relaxation effect, DSC-MRI requires a higher dose than DCE-MRI.

Dynamic Susceptibility Contrast MRI. In DSC-MRI, fast, heavily T2-weighted spin echo sequences, T2*-weighted gradient echo sequences or echo planar imaging sequences are used to exploit the susceptibility effect. Considerable differences in magnetic susceptibility between adjacent anatomic structures lead to local inhomogeneities in the magnetic field. These in turn lead to a signal decrease in T2-weighted spin echo and T2*-weighted gradient echo images. This effect is exploited by using a paramagnetic CA which has a much higher susceptibility than the surrounding tissue water. A crucial property of the effect is that it occurs not only inside the vessel lumen but extends far into the surrounding tissue leading there to a measurable signal reduction [Villringer et al., 1988]. The magnitude of reduction depends on the local cerebral blood volume and blood flow. Typical dataset parameters in DSC-MRI are: 128^2 matrix, 2 mm spatial resolution, 7 mm slice distance, 10-15 acquired

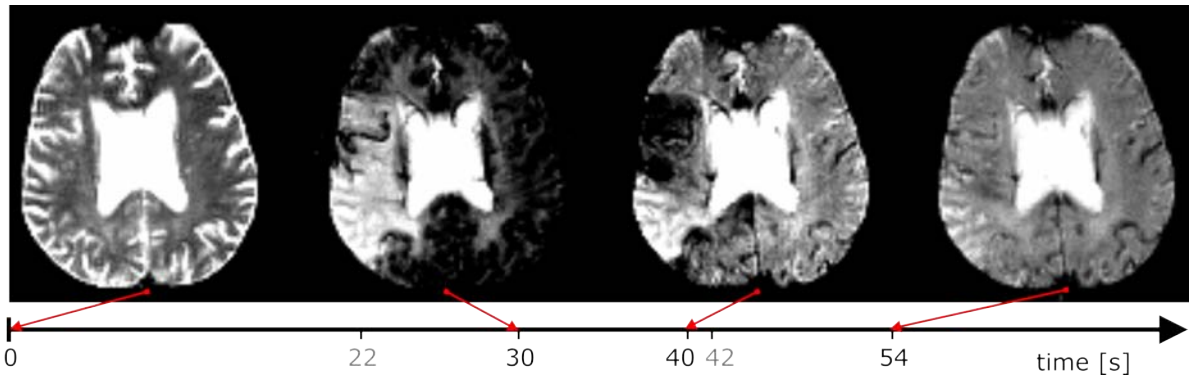

Figure 2.6: Extract from a DSC-MRI perfusion study. Four different points in time of the same image slice are displayed. At 0s, no contrast agent (CA) has arrived yet. At 22s, the first CA passage starts. At 30s, the CA accumulation reaches its maximum in the healthy tissue (dark areas) thereby visually exposing the infarcted tissue (bright areas). The ventricles (butterfly-shaped region) are not part of the infarction. At 40s, portions of the infarcted tissue show a delayed CA accumulation which is characteristic for the penumbra. The infarction core remains bright in the image. The first CA passage ends at 42s. At 54s, the maximum CA accumulation during the second passage is achieved. (Data is courtesy of Jonathan Wiener, Boca Raton Community Hospital.)

slices per point in time, 1-2 seconds temporal resolution, 40-80 points in time. As an example, an extract from a DSC-MRI perfusion study is presented in Figure 2.6. The patient suffered from an ischemic stroke due to a thrombosis of the middle cerebral artery mostly affecting the parietal lobe of the right hemisphere.

2.1.3 Data Processing

This subsection is dedicated to the data processing techniques commonly applied to DSC-MRI perfusion studies. These techniques may be classified into two categories. The first category contains techniques that either enhance or transform the original perfusion data, e.g., the correction for motion artifacts, the calibration of signal intensities and the removal of temporal noise. The second category contains techniques that derive additional data from the original perfusion scan characterizing the temporal course of the CA accumulation and washout, e.g., descriptive and quantitative perfusion parameters.

2.1.3.1 Motion Correction

The analysis and visualization of perfusion data relies on comparable image data. Comparability means that a precise anatomic location covered by a voxel with coordinates (x, y, z) at time $t1$ corresponds to exactly the same location covered by the voxel with the same coordinates at time $t2$. Often, a motion correction has to be carried out to achieve comparability. In brain perfusion imaging, motion artifacts may occur due to head movement during the scan. Motion artifacts might hide relevant signal changes, but also pretend signal changes that are actually not present. Hence, some vendor-supplied workstations for processing CT perfusion data, e.g., SIEMENS *syngo* `Volume Perfusion CT Neuro`, integrate a motion correction. Despite the significant impact of motion artifacts on analysis results, there has been no substantial investigation into the effects of patient motion and an appropriate motion correction scheme [Kosior et al., 2007]. In general, a rigid body registration should generate satisfying results since the shape of the brain changes very little with head

movement. In [Kosior et al., 2007], a six-parameter affine rigid-body registration using a least squares minimization and fourth-degree B-spline interpolation is applied. The authors reported an improved flow delineation between different tissues and a more clearly defined ischemic lesion after motion correction.

2.1.3.2 Calibration of Signal Intensities

In contrast to Single-Photon Emission CT (SPECT) and Positron Emission Tomography (PET), perfusion MRI does not facilitate a direct measurement of CA concentration. However, this is a prerequisite for the determination of quantitative hemodynamic parameters, such as cerebral blood volume and cerebral blood flow, or parameters that are at least proportional to those. The measured change in signal intensity is not even linearly related to the CA concentration. This would simplify quantification as could be shown for perfusion CT where the iodinated CT contrast concentration is linearly related to the resulting CT image density [Latchaw et al., 2009]. In perfusion MRI, a mathematical description is necessary that describes the complex relationship between signal intensity and CA concentration by taking into account the physical contrast mechanisms. The standard conversion formula applied here is [Rosen et al., 1990]:

$$C(t) = \frac{-\ln(S(t)/S_0)}{k_2 TE} \tag{2.1}$$

where $C(t)$ is the CA concentration at time t, S_0 is the baseline averaged signal intensity before CA arrival, $S(t)$ is the signal intensity at time t, TE is the echo time and k_2 is a constant which is specific to tissue type, field strength, and pulse sequence. Plotting $C(t)$ over time results in a so-called *concentration-time curve* (CTC) being the transformed version of an initial *time-intensity curve* (TIC). In Figure 2.7(a), a typical TIC in a single voxel of healthy brain tissue is presented. Figure 2.7(b) shows the result of converting the TIC to a CTC by means of Equation 2.1. Note that S_0 is close to zero after conversion. The TIC in Figure 2.7(a) is annotated with the four most important phases of CA traversal:

(I) Saturation During this phase, the MR signal achieves its steady-state condition.

(II) Baseline The change in signal intensity during the baseline phase is due to image noise. The phase ends with the arrival of the CA.

(III) First Pass The CA travels through the capillary bed for the first time resulting in a considerable signal drop.

(IV) Recirculation A reduced amount of CA arrives for the second time causing a significantly lower signal drop.

2.1.3.3 Temporal Denoising

As illustrated in Figure 2.7(a), the original perfusion data exhibits high-frequency noise which makes smoothing in the temporal dimension essential, especially, for a reliable voxel-wise analysis. In particular, the ability to accurately define the baseline phase and the first pass is crucial for converting signal intensity to CA concentration and for the computation of perfusion parameters (see Subsec. 2.1.3.4 - 2.1.3.5), respectively. An accurate definition would be simplified by a smoothed representation of the data.

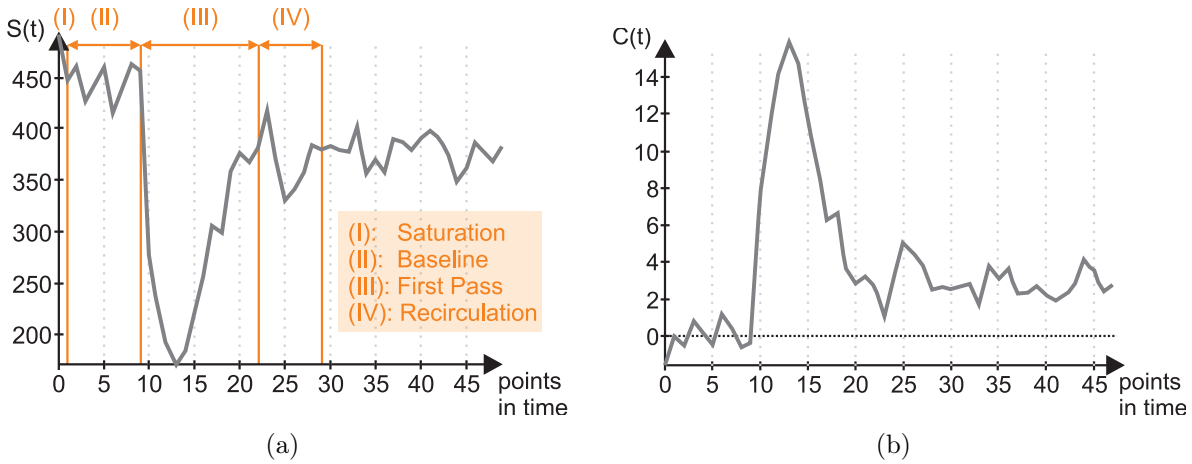

Figure 2.7: Typical time-intensity curve (TIC) in a single voxel of healthy brain tissue and the corresponding concentration-time curve (CTC). *(a)* The TIC is generated by plotting the signal intensities of the voxel over time. It is annotated with the four most important phases of contrast agent traversal. *(b)* The CTC has been generated by converting the TIC applying Equation 2.1. Note that the averaged signal intensity during the baseline phase is close to zero after conversion.

A straightforward approach is the application of a moving average or binomial filter with an appropriate kernel size to the TIC or CTC. This simple averaging however neglects the actual signal change caused by the CA as well as the recirculation effect (Fig. 2.7(a)). The most wide-spread denoising approach is the fitting of a *gamma-variate function* to the CTC (Fig. 2.8(a)). This asymmetric Gaussian function may describe the first pass in a CTC well under normal hemodynamical conditions. However, it may fail in areas with no distinctive CTC shape, i.e., abnormal hemodynamical conditions as prevalent in the infarction core. The gamma-variate fitting is also referred to as *parametric modeling*. It can compensate for noisy data and eliminate the effect of recirculation.

A more sophisticated solution that incorporates spatial as well as temporal smoothing has been introduced by [Lysaker et al., 2003] (Fig. 2.8(b)). The proposed filter scheme is based on fourth-order partial differential equations and has been successfully applied to a routine DSC-MRI perfusion study. In [Wirestam and Ståhlberg, 2005], noise reduction is accomplished by means of a wavelet transformation and Wiener-like filtering. The approach was successfully tested on simulated TICs and DSC-MRI data of healthy volunteers.

2.1.3.4 Descriptive Perfusion Parameters

In cerebral perfusion diagnosis, parameters describing the shape of the CTC are derived for a comparative analysis of the two hemispheres in a single scan study, for assessing the therapeutic benefit in a follow-up study and for an inter-patient comparison, e.g., in a clinical study. The parameters are either derived directly from the CTC or after an additional *deconvolution* step (Subsec. 2.1.3.5). The deconvolution step is crucial for obtaining real quantitative hemodynamic parameters. This subsection is dedicated to the parameters which are derived directly from the CTC. They are referred to here as *descriptive perfusion parameters*. In most studies, the differences between these parameters for the affected hemisphere and the contralateral side have been examined [Grandin et al., 2002]. The parameters are computed region- or voxel-wise from the first pass of the CTC. A CTC annotated with the essential parameters is shown in Figure 2.9.

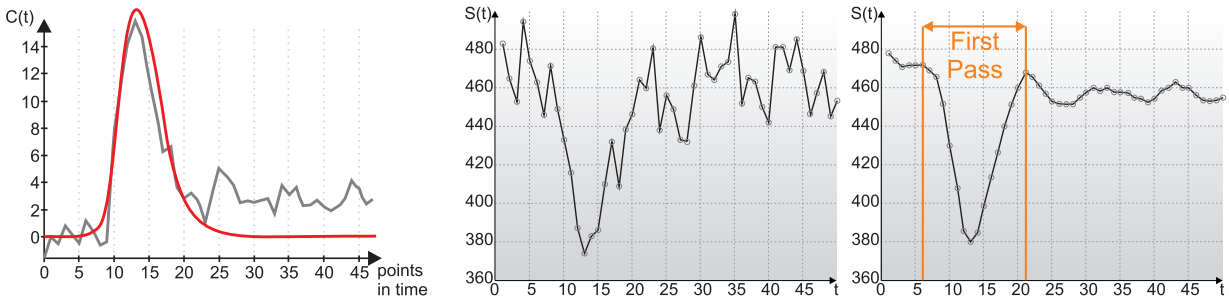

(a) (b)

Figure 2.8: Temporal denoising. *(a)*: A gamma-variate function has been fitted to the CTC from Figure 2.7(b) such that the first pass is approximated. *(b)*: The original CTC (left) has been smoothed (right) applying the filter scheme proposed by [Lysaker et al., 2003]. The smoothed version simplifies an identification of the phases of CA traversal, e.g., of the first pass (Fig. 2.7(a)). (Curve shape in *(b)* is adapted from [Lysaker et al., 2003].)

Before the descriptive parameters are described, four auxiliary variables necessary for a reliable derivation are introduced. The *CA arrival* represents the beginning of the first pass, whereas $Time_{End}$ refers to the end of the first pass. The *Baseline* is computed as the average intensity between $Base_{Start}$ and *CA arrival* and is applied for normalization. *CA arrival* and $Time_{End}$ are determined to focus the evaluation of the CTC on the relevant portion.

The most common descriptive parameters in cerebral perfusion are [Kane et al., 2007]:

- *Peak Enhancement (PE).* The maximum value normalized by subtracting the *Baseline*.
- *Time To Peak (TTP).* The point in time where *PE* occurs, normalized by subtracting the *CA arrival* time. This parameter allows assessing whether blood supply is delayed in a particular region. If *PE* is not a significant maximum or the temporal resolution is low, the *TTP* value is not expressive.
- *Integral.* For a certain time interval (often representing one cycle, or pass, of blood flow) the area between the curve and the *Baseline*, the approximated integral, is computed. The *Integral* is proportional to the quantitative hemodynamic parameter cerebral blood volume.
- *Mean Transit Time (MTT).* In the time interval used for the integral calculation, *MTT* represents the first moment of the curve. It is normalized by subtracting *CA arrival*.

Further typical descriptive parameters generated by a curve analysis are:

- *Slope.* The steepness of the ascending curve during the first pass. Depending on the temporal resolution, different regression methods, such as the gamma-variate and a linear fit are used to characterize the curve progression.
- *Maximum Intensity-Time Ratio (MITR).* The steepness of the ascending curve during the first pass computed as the ratio of *PE* and *TTP*.
- *DownSlope.* The steepness of the descending curve during the first pass which is computed similar to the *Slope*.

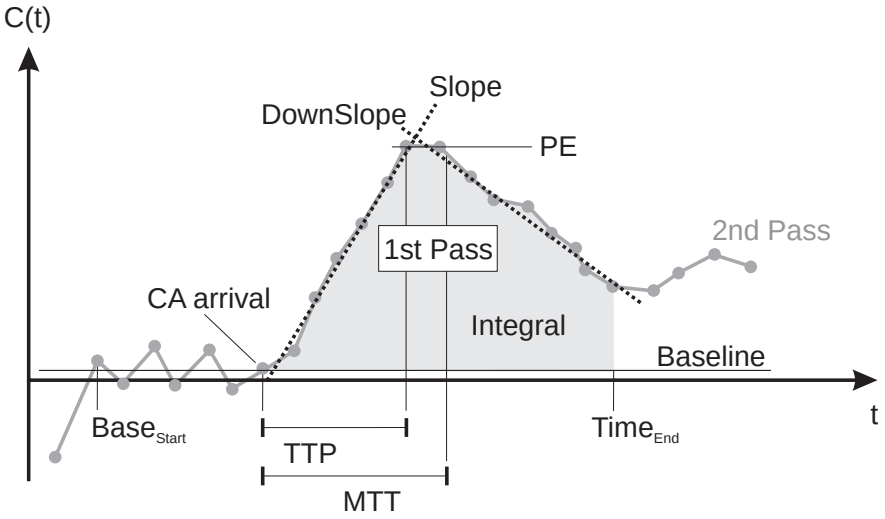

Figure 2.9: CTC annotated with the auxiliary variables and the descriptive perfusion parameters. The first pass is depicted artificially broadened to improve readability.

2.1.3.5 Quantitative Perfusion Parameters

The ultimate goal in MRI-based cerebral perfusion diagnosis is to derive quantitative hemodynamic parameters which facilitate a differentiation of infarction core, penumbra and healthy tissue with regard to established thresholds [Ringelstein and Nabavi, 2007]. The derivation of quantitative parameters requires an additional deconvolution step involving the determination of the so-called *Arterial Input Function (AIF)*. The AIF serves as a model of the vascular input and is usually measured in one of the major supplying arteries. Characteristics of the AIF as compared to curves measured in brain tissue are a significantly higher curve maximum that appears earlier in time and a more narrow curve shape. In the following, the purpose of deconvolution and the role of the AIF will be explained in the context of the typical quantitative hemodynamic parameters and their computation. The explanation is based on [Brix et al., 1997]. The following quantitative parameters are considered as essential in diagnosing ischemic stroke [Sorensen et al., 1999; Wittsack et al., 2002]:

- *regional Cerebral Blood Volume (rCBV)*: perfused vessel volume (in ml) of a voxel divided by the tissue mass (in g) inside this voxel.
- *regional Cerebral Blood Flow (rCBF)*: amount of blood (in ml) that travels through a voxel per time unit (in min) divided by the tissue mass (in g) inside this voxel.
- *regional Mean Transit Time (rMTT)*: average travel time of a tracer particle through the capillary bed.
- *TTP of the residue function (T_{max})*: indicates delay of the CA bolus between the site of AIF selection and the tissue.

The computation of these parameters is based on the indicator dilution theory for intravascular contrast agents [Zierler, 1962]. This theory describes the behavior of an indicator that is injected into a flowing stream in a one compartment circulation system. The single compartment here is the vessel lumen considering that a diffusible CA behaves as an intravascular CA in case of an intact blood-brain barrier. In such a system, the regional cerebral blood volume can be computed as [Axel, 1980]:

$$rCBV = \frac{k_H}{\varrho} * \frac{\int_0^\infty CTC(t)dt}{\int_0^\infty AIF(t)dt} \qquad [ml/100g] \tag{2.2}$$

where $CTC(t)$ is the observed tissue CTC, $AIF(t)$ is the arterial input function, ϱ is the density of brain tissue and k_H is a correction term that is dependent on the vessels hematocrit value. The regional cerebral blood flow is then computed by means of the central volume theorem [Axel, 1980; Zierler, 1962]:

$$rCBF = \frac{rCBV}{rMTT} \qquad [ml/min/100g]. \tag{2.3}$$

The $rMTT$ can be computed according to [Zierler, 1962] by means of the surface-to-height-relation as:

$$rMTT = \frac{\int_0^\infty R(t)dt}{R(t=0)} \tag{2.4}$$

where $R(t)$ is the so-called *residue-function*. This function is defined as the CTC that could be observed in case of an ideal, instantaneously injected CA bolus at time $t = 0$. In practice however, the injection takes a few seconds leading to a significantly broadened CTC. To account for this effect, the observed CTC can be expressed as a convolution of the AIF with the residue-function as:

$$CTC(t) = AIF(t) \otimes R(t). \tag{2.5}$$

Considering Equation 2.5, it is now possible to retrieve the residue-function applying a deconvolution of the observed CTC with the AIF. A comparison of several deconvolution methods including today's most commonly used one applying singular value decomposition (SVD) is given in [Ostergaard et al., 1996]. The manual determination of the AIF is a time-consuming and operator dependent task. Special care should be taken when selecting AIF candidate voxels in order to avoid the inclusion of severely damaged vessels. Several automatic approaches for AIF determination exist, e.g, based on a clustering algorithm [Mouridsen et al., 2006] and Independent Component Analysis [Calamante et al., 2004].

A crucial aspect in computing quantitative parameters is the restriction of all parameter derivations to the first pass of the CTC. This can either be achieved by carefully defining the auxiliary variables introduced in Subsection 2.1.3.4 (Fig. 2.9) or by fitting a gamma-variate function to the CTC and the AIF as described in Subsection 2.1.3.3. The parameter computation is then based on the fitted curves. The function fitting eliminates the effect of recirculation and furthermore, reduces temporal noise.

2.1.4 Visualization and Exploration

Cine-movies. The simplest way of inspecting perfusion data is the cinematic depiction of gray scale images in a movie loop. This technique is also referred to as *cine-movies*. Besides an initial evaluation of CA accumulation and washout, it is helpful to assess motion artifacts and image noise. However, it should be followed by a quantitative analysis since the inspection is user-dependent and small perfusion defects may remain undetected.

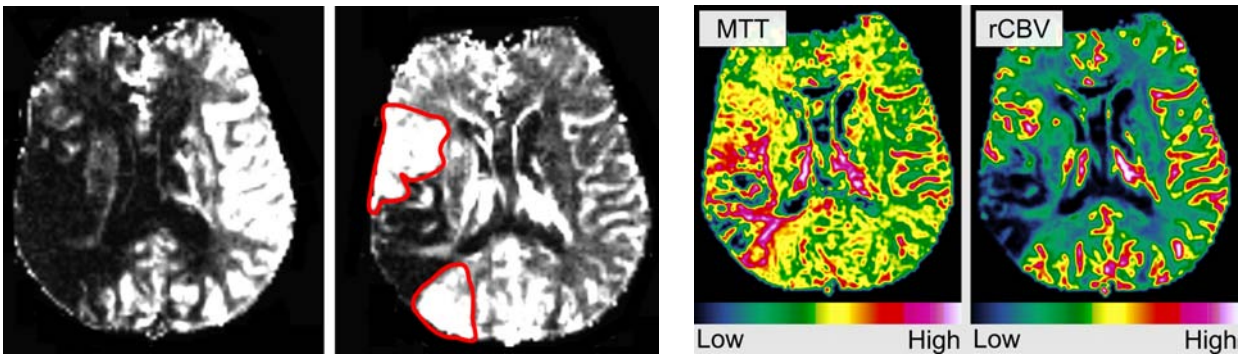

(a) (b)

Figure 2.10: Subtraction images and parameter maps of a cerebral MRI perfusion dataset. *(a)*: *Left*: difference between t_{16} and t_2. The low perfusion in a larger portion of the right hemisphere (left part in the images) characterizes the infarction zone. *Right*: difference between t_{21} and t_2. The late enhancement in a part of the right hemisphere is likely to represent the penumbra (bright, red encircled regions). The dark region surrounded by the penumbra then represents the infarction core. *(b)*: Parameter maps *MTT* and *rCBV* of the slice in *(a)*. The delayed and diminished blood supply becomes obvious. (Data is courtesy of Jonathan Wiener, Boca Raton Community Hospital.)

Subtraction images. Subtraction images are generated by subtracting a fixed precontrast image from an arbitrary image of the first CA passage. A gray scale representation of the subtraction result supports the identification of enhancement patterns. In Figure 2.10(a), two subtraction images are shown, which are used for the diagnosis of an ischemic stroke. Both images have been generated after converting the original signal intensities to CA concentration (see Subsec. 2.1.3.2). Both reveal a dark area in the right hemisphere (left part of the images). This is suspicious, since it does not occur in the corresponding region of the left hemisphere. The region, which is dark in both images, depicts the core of the ischemic stroke. Around this region, a larger area appears dark in the early subtraction image (left), but bright in the subtraction image which refers to a later time (right). This region is likely to represent the penumbra surrounding the core.

Subtraction images provide valuable diagnostic information. However, there is no assistance in choosing the "right" points in time for subtraction. Moreover, the 2D data are only used to visually detect abnormalities. Subtraction images do not provide quantitative temporal and spatial information, which would make the diagnostic results more reproducible.

Parameter maps. The perfusion parameters introduced in Subsections 2.1.3.4 - 2.1.3.5 may be derived voxel-wise and stored in parameter volumes. The color-coded visualization of a single slice of such a volume is referred to as a *parameter map* (see Fig. 2.10(b)). This technique has early been assessed as useful in the context of kidney perfusion by Hoehne et al. [1981]. It represents the standard visualization technique used for ischemic stroke diagnosis in today's vendor-supplied clinical workstations, such as SIEMENS `Neuro Perfusion` for MR examinations, SIEMENS *`syngo`* `Volume Perfusion CT Neuro`, PHILIPS `Brilliance Workspace CT` brain perfusion software, and the `CT Perfusion 4 Neuro-Package` by GE, as well as in other commercial software and research prototypes, such as `Jim V5.0` [1], `PerfTool`

[1]Product of Xinapse Systems; www.xinapse.com/Manual/index.html (01/16/2010)

[Kosior and Frayne, 2007], the *Perfusion/DCE* module of `nordicICE` [2], and the *DSC-MRI Perfusion Module* of `MIStar®` [3].

Advanced Visualizations. At the moment of writing this thesis, there are no advanced visualizations being used in clinical routine. Only a few research prototypes contain 3D visualizations as a "bonus feature". The software `DPTOOLS` [4] generates a 3D surface representation of a segmented infarction zone. This surface is registered to a standard brain for an atlas-based inspection and presented in the context of the entire brain or a volume slab. The software `Stroke Suite` [Nowinski et al., 2008] facilitates the semi-automatic segmentation of the infarction core and the penumbra from CT perfusion data. The segmentation results can then be converted to surface representations and viewed together with a user-controlled degree of blending. To support spatial orientation, the mid-sagittal cut as well as the brain's bounding box are visualized.

Exploration. Besides parameter maps, it is common to compute and display TICs or CTCs for user-selected regions of interest. The curve displays are often used to define or refine initially specified auxiliary variables necessary for perfusion parameter computation (Subsec. 2.1.3.4). Frequently, a parameter map is used first to detect interesting or suspicious regions, whereas the curves in selected regions are analyzed later. Another common strategy is to mirror a defined region on a vertical line of symmetry in horizontal views [Wintermark et al., 2005b]. This facilitates the comparison of the two hemispheres. Perfusion parameters computed for the defined regions are then presented in tabular views.

2.2 Myocardial Perfusion in the Diagnosis of Coronary Heart Disease

Myocardial perfusion data are acquired to characterize the regional blood supply of heart muscle (*myocardium*) tissue. They are crucial in the diagnosis of Coronary Heart Disease (CHD). At an early stage, CHD is characterized by a perfusion deficit caused by a severe stenosis of one ore more coronary arteries. The localization of less perfused myocardial tissue combined with anatomical knowledge about the supplying coronary arteries is essential in identifying CHD in an early, i.e. clinically silent, asymptomatic stage [Hunold et al., 2006]. This section is structured as follows: Subsection 2.2.1 will briefly review the anatomy and topology of the heart and the coronary arteries as well as familiarize the reader with the function of the cardiovascular system. Furthermore, CHD is introduced from a medical point of view, including definition, symptoms and therapy strategies. Subsection 2.2.2 summarizes the prevailing imaging modalities with a focus on MRI. Besides first-pass perfusion MRI, *Late Enhancement imaging* as well as *Cine imaging* are discussed. Relevant data processing aspects including motion correction and the computation of perfusion parameters are explained in Subsection 2.2.3. The visualization and exploration of myocardial perfusion data is discussed in Subsection 2.2.4. The focus is here on the State of the art in commercial software and in research prototypes.

[2] Product of NordicNeuroLab; www.nordicneurolab.com (01/16/2010)
[3] Product of Apollo Medical Imaging Technology; www.apollomit.com/mrstroke.htm (01/16/2010)
[4] ©Denis Ducreux; 193.55.58.11/DPTools/DPTools.htm (01/16/2010)

2.2.1 Medical Background

The human heart works as a pump sending oxygen-rich blood through all parts of the body. The pump mechanism is based on a regular and continuous process of contraction and relaxation of the myocardium establishing a blood circuit. Since the myocardium has a high demand on oxygen and nutrients which are delivered through the blood, a sufficient perfusion is a requirement for the functional efficiency of the heart.

2.2.1.1 Anatomy of the Heart

The following description of the heart anatomy is based on [Benninghoff, 2004], [Netter, 1990] and [Texas Heart Insitute, 2009]. The weight of the human heart is $\approx 250g$ in female and $\approx 300g$ in male which corresponds to $\approx 0.4 - 0.45\%$ of body weight. The heart size is approximately the size of the fist of the respective person. The heart is cone-shaped with a rounded apex. It is oriented with the apex facing downwards and slightly forward to the left. One third of the heart is located in the right part of the chest and two thirds are located in the left part. The heart is embedded in the pericardium between the left and the right lobe of the lung. It is attached to the diaphragm which adheres to the pericardium. The episternum covers the heart which in turn occludes the aorta and the esophagus.

The heart is divided by the interventricular septum into a left and a right half. The location of the septum is indicated on the surface of the heart by the anterior and posterior interventricular sulcus (Fig. 2.11). Both halves are divided into two chambers, a ventricle and an atrium. The left ventricle is the largest and strongest chamber since it needs enough force to push blood through the entire body. Several major blood vessels are attached to the heart chambers. The superior and inferior vena cava transporting deoxygenated blood empty into the right atrium. The pulmonary arteries transporting deoxygenated blood to the lung originate from the pulmonary trunk which is attached to right ventricle. The pulmonary veins which transport blood that has been oxygenated in the lung are attached to left atrium. The aorta which transports oxygen-rich blood is attached to the left ventricle.

The cardiac valves regulate the blood flow through the heart (Fig. 2.12(a)). Each valve allows only a one-way passage of the blood. The tricuspid valve is located between the right atrium and the right ventricle. The pulmonary valve is located between the right ventricle and the pulmonary trunk. The mitral valve is located between the left atrium and the left ventricle and the aortic valve is located between the left ventricle and the aorta. The tricuspid and the mitral valve are attached to the papillary muscles by means of branching cords. This construction hampers their resilience. The pulmonary and the aortic valve are constructed in a different way. Their parts are squeezed against each other in case of a reversed blood flow to prevent penetration.

The heart is a hollow organ. Its wall consists of three layers: endocardium, myocardium and epicardium (from interior to exterior). The endocardium separates chamber musculature and blood. Its major task is the prevention of thrombus development which is achieved by a very smooth surface and the production of coagulation-inhibiting substances. The epicardium mantles the heart and is part of the pericardium. It produces pericardial fluid which facilitates heart motion without friction and hence, works as a protective layer for the heart. The myocardium is the inner layer between endocardium and epicardium (Fig. 2.11(b)). The continuous contraction of the myocardium drives the entire blood circuit. The myocardium consists of specialized muscle fibers whose shape and arrangement facilitate a concentric contraction. The myocardial layer of the left ventricle is the thickest since strong forces are necessary to pump blood through the aortic valve to all parts of the body. It is thicker

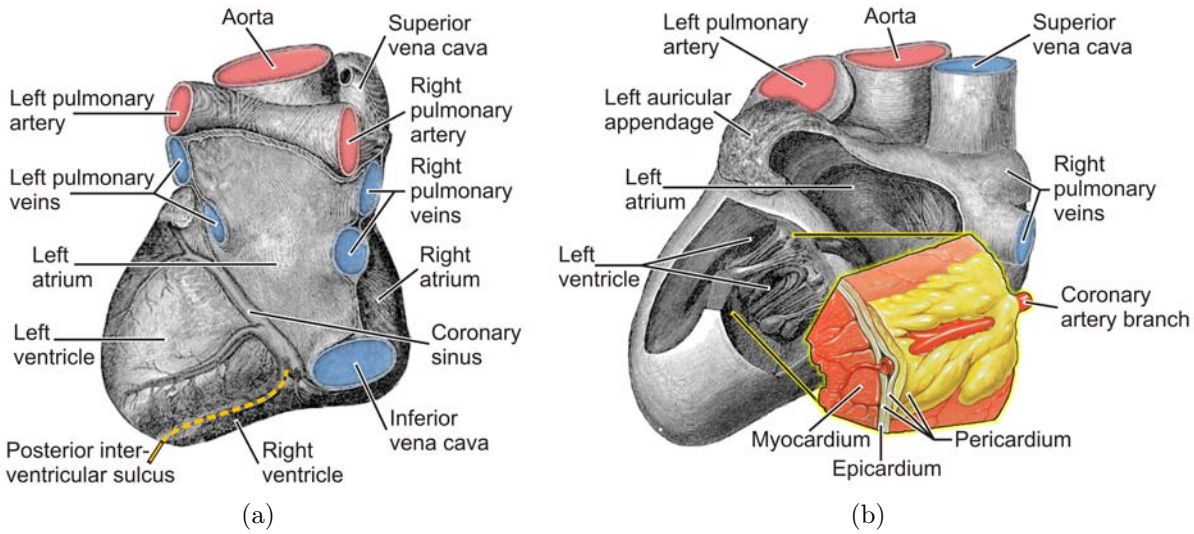

Figure 2.11: Anatomy of the human heart and the heart muscle. *(a)* Base and diaphragmatic surface of heart. The four heart chambers as well as the major blood vessels attached to the chambers are depicted. *(b)* Interior view of the left side of the heart. The inset depicts a part of the heart wall. The outer layer of the wall is formed by the epicardium which in turn represents the innermost layer of the pericardium. (Based on illustrations in [Gray, 1918]. The inset in *(b)* is based on an illustration by Patrick J. Lynch, medical illustrator, and C. Carl Jaffe, MD, cardiologist.)

than the layer of the right ventricle since the pressure in body circulation is higher than the pressure in pulmonary circulation. The thickness of the left ventricular myocardium varies between $10 - 14$mm [Leutert and Schmidt, 2000]. It is dependent on the status of contraction, i.e., it is thicker during contraction.

2.2.1.2 The Cardiac Cycle

The following explanation of the cardiac cycle is based on [Klabunde, 2005]. It has been simplified by omitting a discussion of the cardiac conduction system.

The heart beats ≈ 70 times per minute pumping 5 liters of blood at rest and up to $40-50$ liters under stress. The sequence of blood flow and blood pressure related events that occurs during one heart beat is referred to as the cardiac cycle. The cardiac cycle may be divided into four phases: relaxation and filling phase which together form the diastolic phase and contraction and ejection phase witch together form the systolic phase (Fig. 2.12(b)). The cardiac cycle begins with the filling phase (Fig. 2.12(b), left). The right atrium is filled with deoxygenated blood from the superior and inferior vena cava. Simultaneously, the pulmonary veins return oxygenated blood from the lungs to the left atrium. Next, both ventricles relax characterized by a decrease in myocardial wall thickness, the tricuspid and the mitral valve open, and the blood flows from the atria to the ventricles. This leads to an increase of pressure inside the ventricles. The tricuspid and the mitral valve close to prevent backward flow to the atria (Fig. 2.12(b), right). At the beginning of the systolic phase, the right and the left atrium contract and force the final volume of blood to the right and the left ventricle. Next, the right and the left ventricle contract characterized by an increase in myocardial wall thickness. The pulmonary and the aortic valve are opened shortly after the ventricles begin to contract. Then, the blood is rapidly ejected into the pulmonary and the body circulatory system through the pulmonary arteries and the aorta, respectively.

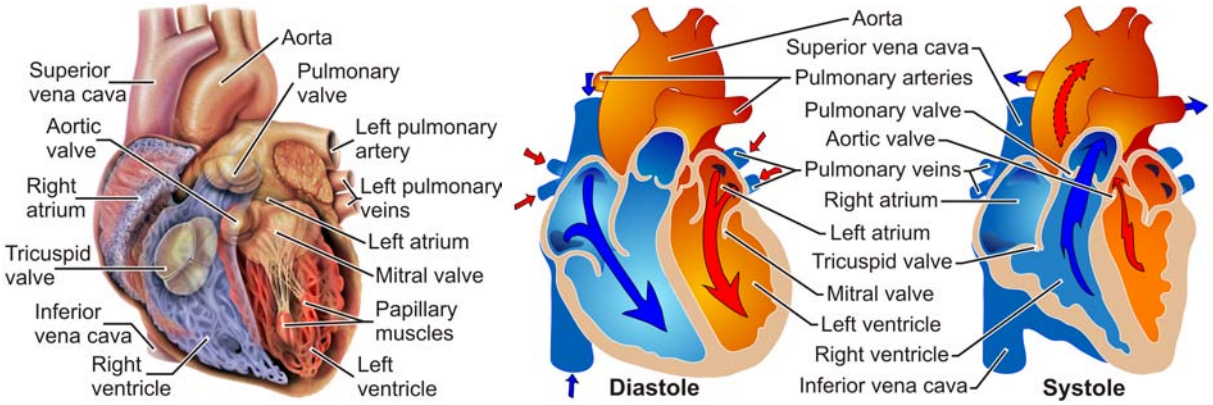

Figure 2.12: Cardiac valves and physiology of the cardiac cycle. *(a)* Four cardiac valves regulate the blood flow through the heart: the tricuspid, mitral, pulmonary, and aortic valve. For illustration purposes, the tricuspid valve is depicted as seen from the right atrium. *(b)* The four phases of the cardiac cycle. Relaxation and filling together form the Diastole whereas contraction and ejection together form the Systole. (*(a)* is based on an illustration by Patrick J. Lynch, medical illustrator, and C. Carl Jaffe, MD, cardiologist. *(b)* is based on an illustration by Mariana Ruiz Villarreal.)

As soon as the ventricular pressure falls below the pressure in the pulmonary arteries and the aorta, the pulmonary and the aortic valve are closed to prevent backward flow to the ventricles. After emptying, both ventricles signalize their receptivity to refilling which lowers atrial pressure and allows the atria to refill from their venous supply. At the beginning of atrial refilling, ventricular pressure exceeds atrial pressure. Hence, the tricuspid and mitral valve remain closed. The cardiac cycle ends when atrial pressure exceeds ventricular pressure and tricuspid and mitral valve open again to allow a rapid ventricular refilling.

2.2.1.3 The Coronary Arteries

The following description of the coronary anatomy is based on [Benninghoff, 2004], [Netter, 1990], and [Texas Heart Insitute, 2009]. The myocardium has a high demand on oxygen and nutrients. Hence, a sufficient perfusion is a prerequisite for its functional efficiency. The myocardium is supplied with blood through the left (LCA) and right coronary artery (RCA), both originating from the aorta (Fig. 2.13). Hence, the "freshly" oxygenated blood arrives early at the myocardium. The coronary branchings encircle the heart in an annular fashion. They are attached to the epicardium. Hence, a decreased blood flow and the associated lack of blood pressure first affect the subendocardial regions of the myocardium. The RCA supplies the wall of the right ventricle and the rear septum (Fig. 2.13(a)). The LCA splits into the left circumflex (LCX) and the left anterior descending coronary artery (LAD) about 1 cm after its separation from the aorta (Fig. 2.13(b)). The branchings of the LCA supply the wall of the left ventricle and the septum, except for its rear part.

It has been recognized early that there is a high variability of the human coronary artery system [Paulin, 1983]. Significant differences particularly exist in RCA and LCX distribution. Clinical studies, e.g. [Ortiz-Pérez et al., 2008], have shown that a standardized correspondence between myocardial regions and supplying coronary branches may only be valid for parts of the entire population. Figure 2.13 shows the prevailing, *right-dominant distribution* of coronary arteries.

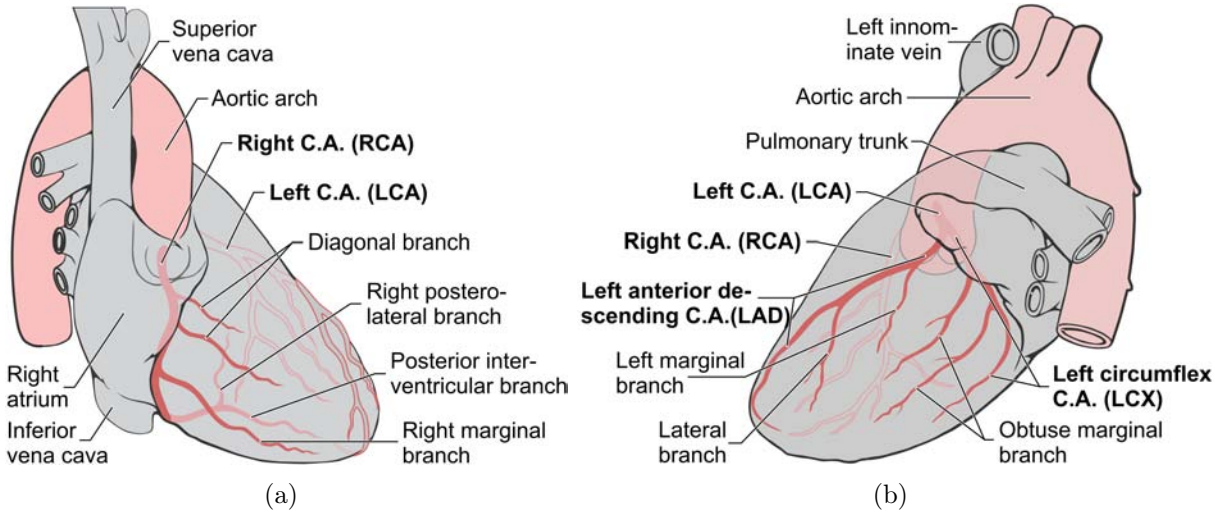

Figure 2.13: Right-dominant distribution of the coronary arteries. *(a)* Right anterior oblique view of the heart. The right coronary artery (RCA) originates at the aorta. Since the posterior interventricular branch is supplied solely by the RCA here, this distribution is classified as right-dominant which is present in $\approx 70\%$ of the population [Fuster et al., 2004]. *(b)* Left lateral view of the heart. The left coronary artery (LCA) originates at the aorta and splits into the left circumflex coronary artery (LCX) and the left anterior descending coronary artery (LAD). (Based on line drawings by Patrick J. Lynch, medical illustrator, and C. Carl Jaffe, MD, cardiologist.)

The oxygen demand of the myocardium is increased under physical or mental stress and may increase to a threefold of the demand at rest. The increased demand is satisfied by an increased coronary blood flow which in turn is achieved by *vasodilation* (vessel widening). The ability to increase coronary blood flow is also referred to as *coronary flow reserve*. It is defined as the ratio of blood flow under stress to blood flow at rest. The flow reserve is a matter of particular clinical interest in patients with suspected CHD.

2.2.1.4 Coronary Heart Disease

A severe stenosis or occlusion of one or more coronary arteries is referred to as Coronary Heart Disease. The CHD of a certain degree causes a perfusion defect of the myocardium restricting its pump function. In the United States and in Germany, CHD and its consequences, e.g., angina pectoris, cardiac arrhythmia and heart attack, are the leading causes of death [Lloyd-Jones et al., 2009], [Statistisches Bundesamt Deutschland, 2007]. The underlying cause of CHD is *atherosclerosis* of the coronaries. Fats and cell debris form plaques in the vessel wall that may become calcified in the further course. The so-called atherosclerotic plaque reduces the vessel diameter (stenosis) and hampers the elasticity of the vessels. A sufficient elasticity is crucial under stress conditions to account for the heart's increased demand on oxygen by vasodilation. Figure 2.14 illustrates the evolutionary path for plaque formation and provides the *American Heart Association Plaque Nomenclature*. The reader is referred to [Davies and Ho, 1998] for a detailed description of the different stages.

From a narrowing of the vessel diameter to approximately 30% (stenosis of 70%), the risk of a perfusion defect is significantly increased. In healthy humans, the maximum blood flow under stress is a three- to sixfold of the flow at rest. Due to the low oxygen demand of the myocardium at rest, a stenosis of up to 85%-90% can be compensated by collateral blood supply. The situation changes under stress. A stenosis of 50%-80% can induce a

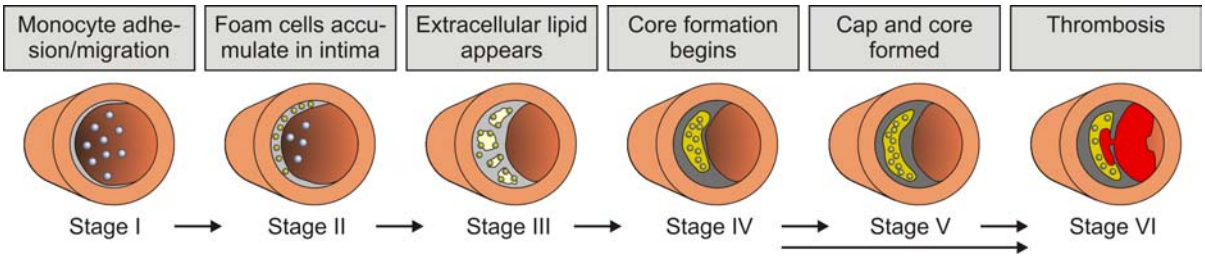

Figure 2.14: Evolutionary path for plaque formation and the American Heart Association Plaque Nomenclature. Thrombosis (*Stage VI*) may arise as early as the core begins to form (*Stage IV*) or later when the core and a cap of fibrous tissue have been formed with the latter separating core and vessel lumen (*Stage V*). (Based on an illustration in [Davies and Ho, 1998].)

perfusion defect of the corresponding myocardial region and can hence be considered as *hemodynamically relevant* [Bogaert et al., 2000].

All CHD therapies aim at restoring the blood flow through the clogged artery (*revascularization*). The most common revascularization therapies are bypass surgery and percutaneous coronary interventions. In bypass surgery, the blood is rerouted around clogged arteries by means of an artificial vessel piece, e.g., a long vein from the patients leg. The ends of the vein are then attached below and above the blocked area. Percutaneous coronary interventions comprise a variety of procedures with stenting being the most widely applied one [Kreitner and Horstick, 2007]. In stenting, a balloon-tip catheter is guided to the occluded area. There, the balloon is inflated thereby compressing the plaque and widening the artery. Next, an expandable wired mesh tube (*stent*) is inserted that props the artery open and stabilizes the vessel. Recently, drug coated stents are gaining in importance. They have been proven to reduce the risks of restenosis and the rate of reinterventions [Kreitner and Horstick, 2007].

The response of the myocardium to ischemia occurs in a determined order referred to as *ischemic cascade* [Nesto and Kowalchuk, 1987] (Fig. 2.15). The cascade starts with a perfusion disturbance in the affected myocardial region. The subsequent stage is characterized by a disturbance of the metabolism, in particular an abnormal Phosphocreatine-to-ATP Ratio (PCr/ATP). Disturbed perfusion and metabolism result in a hampered diastolic relaxation process and subsequent decrease of systolic contractility measured by reduced myocardial

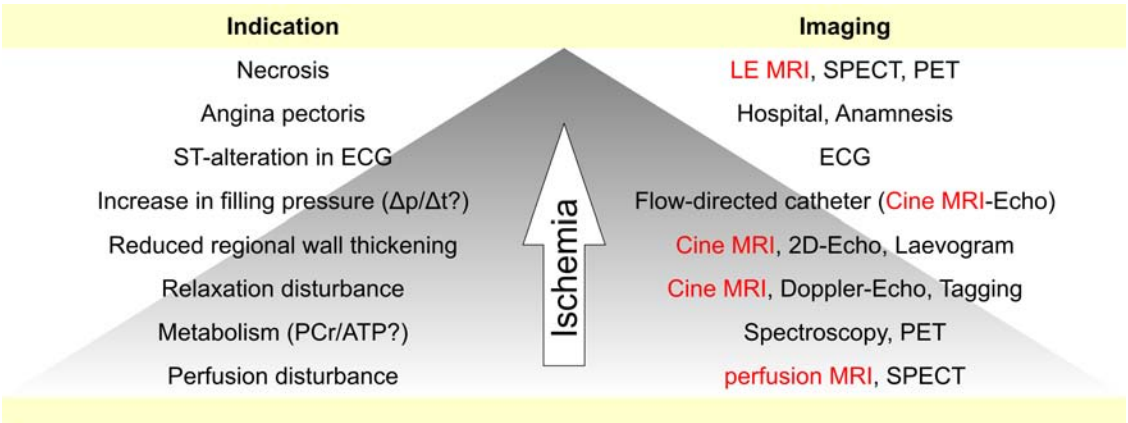

Figure 2.15: The ischemic cascade. In the beginning, perfusion disturbances occur which can already be detected by perfusion MRI. Furthermore, MRI has proven to be valuable in assessing myocardial function (Cine MRI) as well as in detecting necrotic (non-viable) tissue after an infarction (Late Enhancement (LE) MRI). (Based on an illustration in [Grebe, 2005].)

thickening and inward motion. Subsequently, the increase in filling pressure ($[dP/dt]$) of the heart chambers is affected. The myocardial ischemia may then be observed objectively as an alteration of the isoelectric period (ST segment) in the *electrocardiogram (ECG)* and subjectively as chest discomfort known as angina pectoris. When the blood supply of the myocardium is massively hampered or entirely absent for a period of 20 to 30 minutes, myocardial tissue is irreversibly damaged (necrosis) and eventually an infarct occurs.

Four different types of infarction may be distinguished [Davies and Ho, 1998] (Fig. 2.16):

(a) A *regional transmural infarction* is characterized by a single connected necrosis covering a limited part of the myocardial circumference and extending over the entire myocardial thickness (*transmural*).

(b) A *regional nontransmural infarction* is usually built up from one or several smaller foci of myocyte (muscle cell) necrosis.

(c) If subendocardial extensions are found at the margins of a regional transmural infarction, this type is referred to as *regional transmural infarction with extension.*

(d) In a *pure diffuse subendocardial necrosis*, necrotic tissue covers the whole circumference of the myocardium. This may be observed in patients suffering from widespread coronary artery stenosis causing a fall of overall myocardial perfusion.

A phenomenon that has been studied in the context of infarction is the so-called *microvascular obstruction.* In case of a profound and sustained perfusion defect, not only myocytes but also capillaries may undergo necrosis. Such a region may occur at the center of an infarction and is also referred to as infarction core. The core will not promptly reperfuse after revascularization. It could be shown that the existence of microvascular obstruction predicts more frequent cardiovascular complications [Wu et al., 1998].

Myocardial ischemia does not necessarily lead to necrosis of muscle tissue. If a coronary occlusion persisted only shortly, *stunned myocardium* may have formed. Stunned myocardium is characterized by a restored perfusion but a prolonged myocardial dysfunction (up to ≈ 2 weeks) that will gradually recover to normal contractility. Myocardial stunning requires no therapy unless large parts of the left ventricle are involved. Here, inotropic stimulation can reduce the extent of myocardial stunning. In case of a chronic perfusion

Figure 2.16: Different subtypes of myocardial infarction. Regional forms of infarction reflect a pathology of the supplying coronary branch. Diffuse forms usually occur due to an overall fall of perfusion. LV: left ventricle, RV: right ventricle. *(a)* Regional transmural infarction. *(b)* Regional nontransmural infarction. *(c)* Regional transmural infarction with extension. *(d)* Pure diffuse subendocardial necrosis. (Based on an illustration in [Davies and Ho, 1998].)

Viability	Term	Description
Viable	Normal	Healthy myocardium with normal perfusion and function
	Stunned	Normally perfused myocardium with a dysfunction that is persistent for max. 2 weeks after acute ischemia
	Hypoperfused	Reduced myocardial perfusion but normal function
	Hibernating	Reduced myocardial perfusion and dysfunction
Non-viable	Necrotic (Scarred)	Necrotic myocardium (infarction scar) which exhibits neither perfusion nor function

Table 2.1: Clinically Relevant States of Myocardial Tissue in CHD Patients

deficit due to high-grade stenosis, repetitive stunning or collateral occlusion, *hibernating myocardium* is formed which is characterized by a chronic myocardial dysfunction. Hibernating myocardium may functionally recover after revascularization [Grebe, 2005]. Table 2.1 summarizes the different states of myocardial tissue in CHD patients.

The differentiation between viable and non-viable myocardium as well as the subsequent differentiation between hypoperfused, stunned and hibernating viable myocardium are crucial in CHD diagnosis. Measures of perfusion, viability and function are necessary to differentiate between tissue states. Furthermore, the correlation of tissue that may benefit from a revascularization therapy and the supplying coronary branch is crucial for the decision on the best available therapy, e.g., percutaneous coronary interventions, bypass surgery as well as pharmacological therapy. Cardiac imaging should allow for differentiation of myocardial tissue states and an assessment of coronary anatomy. Perfusion imaging plays a crucial role since the reduced myocardial perfusion represents the beginning of the ischemic cascade and should hence be detected for early CHD diagnosis.

2.2.2 Cardiac Magnetic Resonance Imaging

The discussion of cardiac imaging modalities in this subsection is primarily based on [Thelen et al., 2007]. The MRI-specific parts are based on [Gerber et al., 2008; Thelen et al., 2007; Finn et al., 2006; Hunold et al., 2006; Breeuwer, 2005].

The gold standard for the diagnosis of coronary anatomy and atherosclerosis is conventional invasive Coronary X-ray Angiography (CXA) which facilitates interventional procedures albeit a certain amount of risk. CXA is a minimally invasive procedure where a catheter is guided through the large body arteries to a coronary artery. Then, an X-ray dye (radiocontrast agent) is injected and mixes with the blood. The blood flow is visible for 3-5 seconds. The angiographic view is stored as a movie and may be repetitively inspected by the physician. An advantage of CXA is that it can be coupled with an immediate revascularization therapy. Drawbacks of the technique are an associated risk of vessel wall injury by the catheter and the risk of injecting a thrombus or air causing an acute myocardial infarction. The 64-slice CT technology presents an alternative non-invasive technique. Computed Tomography Coronary Angiography (CTCA) provides a fast visualization of coronary anatomy and in clinical studies, a good sensitivity and specificity in the detection of coronary artery stenosis could be shown [Mollet et al., 2005]. Substantial research efforts are taken in Magnetic Resonance Coronary Angiography (MRCA). In [Sommer et al., 2002], a sensitivity and specificity of 88% and 91% in detecting coronary artery stenoses was reported for the proximal and middle main coronary arteries.

An alternative approach to the diagnosis of the coronary arteries is the inspection of myocardial perfusion which facilitates an assessment of the hemodynamic relevance of a stenosis. A stenosis detected by CXA or CTCA may not be hemodynamically relevant due to collateral flow which can only be confirmed by perfusion imaging. Furthermore, perfusion defects are not necessarily synonymous with stenoses of the coronary arteries. Myocardial ischemia exists in patients with syndrome X even though the arteries are in a perfect condition. Syndrome X describes angina pectoris in people who do not show signs of blockages in coronary arteries after an angiogram, or X-ray of these arteries.

The current reference standards in cardiac perfusion imaging are PET and SPECT. With these modalities, the regional distribution of a radioactive isotope, such as Rb-82 chloride, nitrogen 13 (N-13) ammonia, or oxygen 15 (O-15) water is represented [Iida et al., 1988; Kitsiou et al., 1999; Chua et al., 2006; Merhige et al., 2007]. PET is more specific than SPECT in discriminating vital and irreversibly damaged tissue after an infarction [Go et al., 1990]. However, high costs, limited availability and a higher logistical effort due to a lower radioactive half-life are derogatory for PET. Further difficulties and limitations of PET and SPECT are: attenuation artifacts, exposure to ionizing radiation, and a poor spatial resolution which does not allow for the reliable detection of subendocardial perfusion defects.

Perfusion CT and perfusion MRI provide a higher spatial resolution and less artifacts compared to PET and SPECT. While perfusion CT is in an early research stage, perfusion MRI has been recommended by the American Heart Association (AHA) and the American College of Cardiology (ACC) for detecting hypoperfused, viable, myocardial tissue and correlating this tissue with the supplying vessel. Perfusion MRI provides a noninvasive and radiation-free means to inspect the myocardium. Due to the increasing costs and the rising number of CHD patients, there is a major interest in a reliable non-invasive imaging technique to identify CHD in an early, i.e. clinically silent, asymptomatic stage. Perfusion MRI can reliably detect perfusion deficits which represent the first stage in the ischemic cascade (Fig. 2.15). It has been proven to have a high sensitivity and specificity in detecting significant stenosis [Nagel et al., 2003]. It is competitive with regard to CXA and PET [Schwitter et al., 2001] as well as thallium SPECT [Panting et al., 2001]. However, wide-spread use of perfusion MRI is still hampered by a variety of artifacts and the strong experience necessary to perform the examination and interpret the results. Recent technical advances in hardware, contrast agents and imaging sequences are described in [Hunold et al., 2006].

Measures of myocardial perfusion, viability, ventricular function (Fig. 2.15) as well as assessment of morphology and flow in the large coronary arteries can be integrated in a single MRI scanning protocol with a duration of $30 - 45$minutes. Therefore, cardiac MRI is often referred to as the *one-stop-shop* cardiac imaging modality [Breeuwer, 2005]. The focus of the remaining subsection will be on cardiac MRI, particularly on perfusion MRI in patients with suspected CHD. The application of perfusion MRI in patients with acute myocardial infarction will not be discussed. Here, perfusion MRI above all conduces to the detection of microvascular obstruction. A typical MRI scanning protocol for CHD diagnosis extended by an MRCA is illustrated by Figure 2.17.

At first, scout images are acquired (*scouting*) to ensure that the heart is centered in the imaging field of view and for planning of the typical cardiac imaging planes along the heart axes: horizontal long axis, vertical long axis, and short-axis (Fig. 2.18(a)). The images acquired along the major axes show all 4 heart chambers (4-chamber view), 2 selected chambers (2-chamber view, one ventricle and the associated atrium) or a frontal view of the myocardium (short-axis view). The latter views are most frequently used for assessing perfusion, viability and function (see Fig. 2.18(b) for an illustration of the different views).

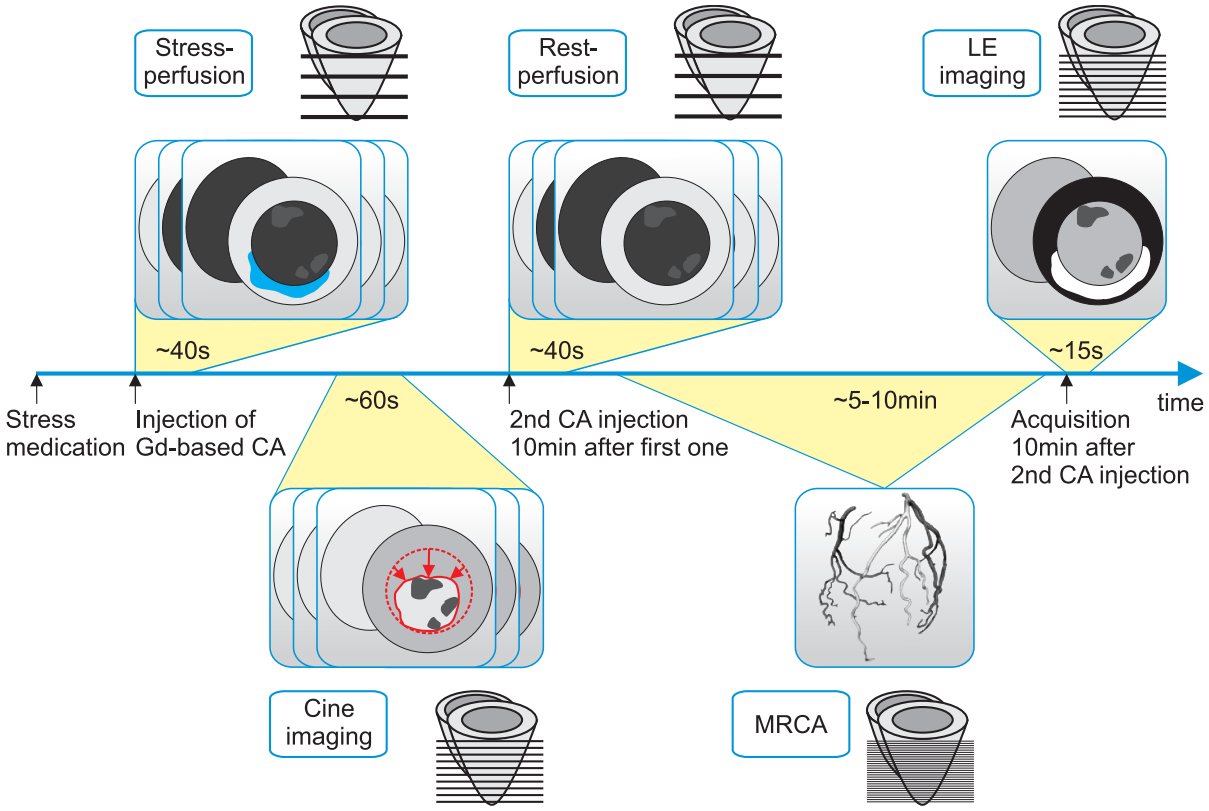

Figure 2.17: Typical MRI scanning protocol for CHD diagnosis extended by a Magnetic Resonance Coronary Angiography (MRCA). The acquisition of scout images being the very first step of the protocol is not illustrated. Note that the acquisition durations strongly depend on the applied imaging sequence. The timings here are related to an acquisition with parallel imaging (GRAPPA 2 [Griswold et al., 2002]). CA: contrast agent, Gd: Gadolinium, LE: Late Enhancement.

After scouting, stress and hence vasodilation are drug-induced. The drug is typically administered for 3-6 minutes. After the induction of vasodilation, a CA is injected very fast such that it forms a bolus. First-pass stress perfusion imaging is then performed during CA injection. The stress test is meant to detect perfusion defects. About 10min after the first CA injection, a second injection accompanied by first-pass rest perfusion imaging are performed. The comparison of rest and stress facilitates a determination of the coronary flow reserve and the distinction of perfusion defects versus image artifacts. Functional images are acquired in between the two perfusion scans (Cine imaging). However, special care must be taken in choosing an appropriate imaging sequence such that the image quality is not impaired by CA remaining in the blood circuit. About 10min after the second CA injection, Late Enhancement (LE) can be imaged. The objective of LE imaging is the identification of necrotic tissue indicating that the patient has a history of infarction. In between the rest perfusion scan and the LE imaging, a MRCA may be acquired depicting the heart and the coronary arteries [Hennemuth et al., 2008c]. The final data pool consists of three four-dimensional (space+time) datasets from perfusion and Cine imaging and several three-dimensional (space) datasets from scouting, LE imaging and MRCA.

A crucial aspect of the imaging are motion artifacts occurring due to proper motion of the heart and patient respiration. To reduce artifacts due to proper heart motion, the imaging is synchronized with the cardiac cycle by means of the patient ECG. The *R wave* of the ECG marking the beginning of systole is detected and forwarded to the sequence controlling unit

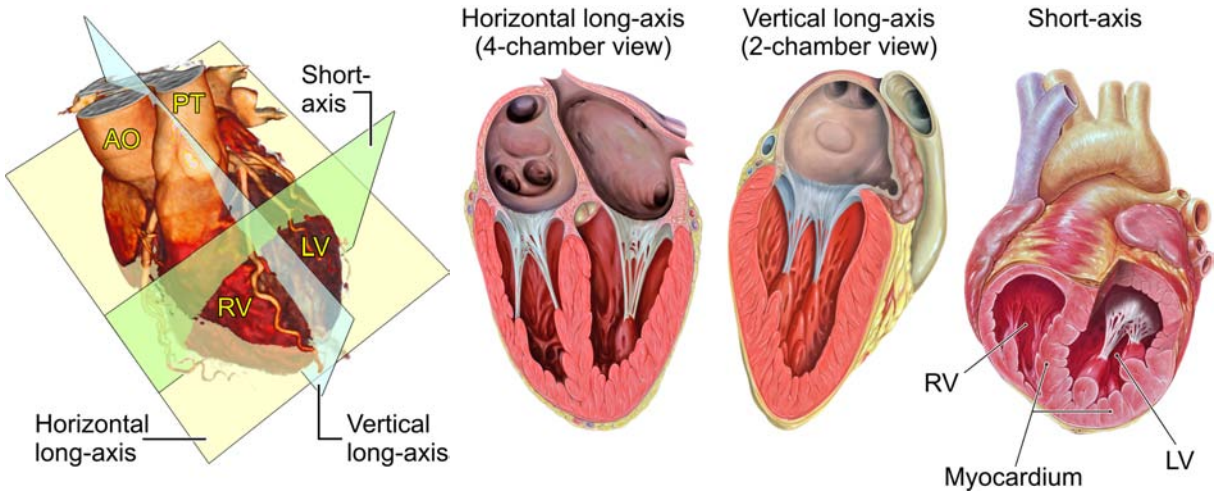

(a) (b)

Figure 2.18: Cardiac imaging planes and associated standard views. *(a)* The three standard cardiac imaging planes are located along the major axes of the heart: horizontal long-axis, vertical long-axis and short-axis. AO: aorta, PT: pulmonary trunk, LV: left ventricle, RV: right ventricle. *(b)* The images acquired along the major axes show all 4 heart chambers, 2 selected chambers (one ventricle and the associated atrium) or a frontal view of the myocardium (short-axis view). (Data in *(a)* is courtesy of Stephan Achenbach, University Hospital Erlangen. Illustrations in *(b)* by Patrick J. Lynch, medical illustrator, and C. Carl Jaffe, MD, cardiologist.)

which triggers the acquisition. The ECG-triggered imaging facilitates an acquisition of the heart always at the same point in time during the cardiac cycle. Since the heart is attached to the diaphragm, it is moving during patient respiration. To compensate for this effect, respiration-monitoring belts, navigator tracking of the diaphragm position or breath-hold maneuvers are applied. The latter is the standard technique for anatomical, perfusion, Cine and LE imaging. Special commands are first taught the patient. Then, the patient is asked to hold the breath several times for $10 - 15$s during acquisition [Strohm et al., 2006].

2.2.2.1 First-Pass Perfusion Imaging

Myocardial perfusion imaging by first-pass contrast-enhanced cardiovascular Magnetic Resonance was first presented in 1990 by Atkinson et al. [1990]. Due to technical advances in hardware, contrast agents and imaging sequences, perfusion MRI is gaining acceptance and competes well with standard nuclear imaging techniques [Gerber et al., 2008].

During the scan, the patient is connected to an ECG for triggering the acquisition. A CA is administered intravenously very fast by a specialized device such that a compact bolus is formed. Ultra-fast imaging sequences are applied during and after injection aiming at time-resolved heavily T1-weighted datasets. Most of the recent studies use fast gradient refocused echo (GRE) sequences with either inversion- or saturation-recovery techniques. Fast gradients warrant a high temporal resolution. Typically, 3-6 short-axis slices are acquired at end diastole once every heart beat (or interleaved once every other heart beat) over a period of 30-60s during the CA's entire first passage. The end diastole is chosen since it is a relatively stable cardiac phase having the advantage of reduced motion artifacts [Gerber et al., 2008]. The slice thickness is in the range of 5-10mm [Gerber et al., 2008]. Matrices of 128, 192 or 256 rows and columns provide a spatial resolution in the range of 1.5-3mm. However, only

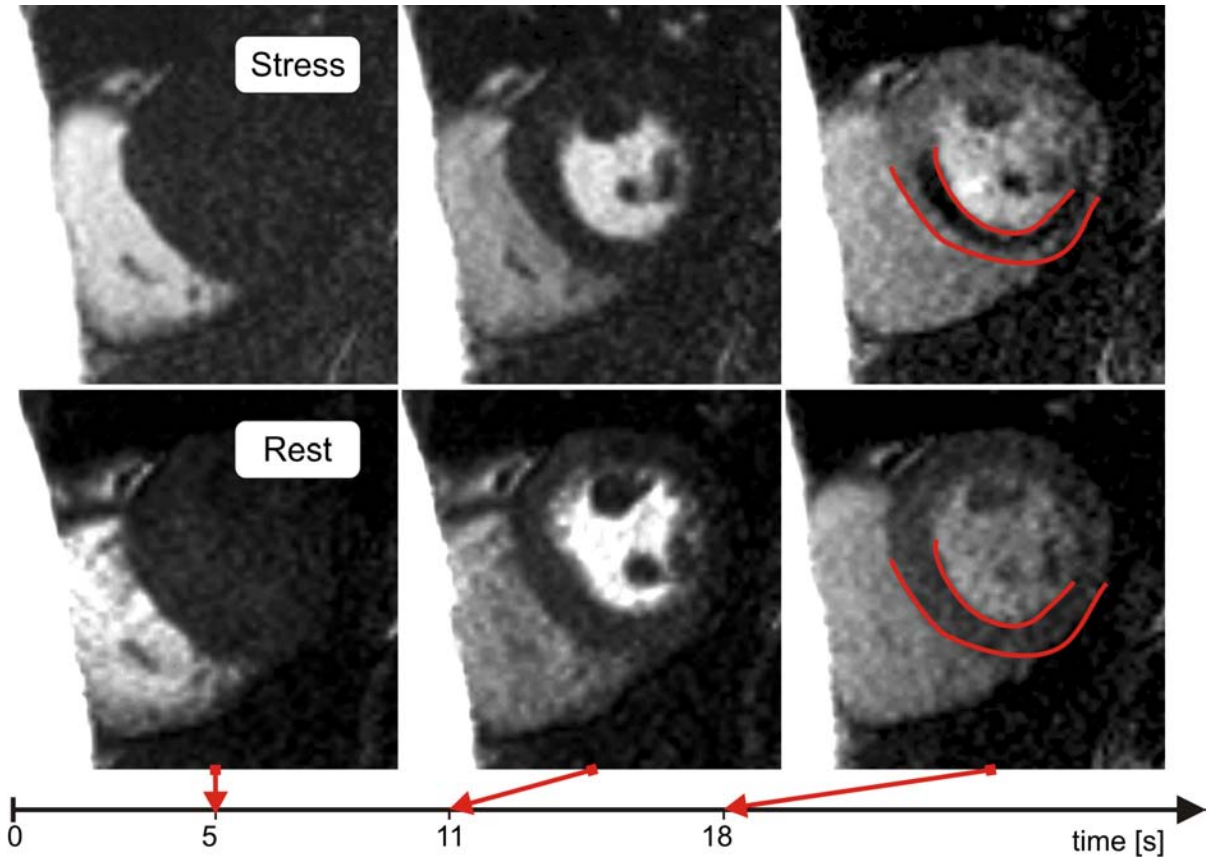

Figure 2.19: Extract from a MRI myocardial perfusion study. Three different points in time of the same image slice are displayed. The upper and the lower image row show an example slice from the stress and the rest test, respectively. At 5s, the contrast agent (CA) arrives in the right ventricle (bright half-moon shaped region). About 6s later, it accumulates in the lumen of the left ventricle (circular region). The dark spots inside the lumen represent the papillary muscles. At 18s, the CA reaches its accumulation peak in the myocardium (ring-shaped region surrounding the lumen). A subendocardially located perfusion deficit (dark region along the red delineated myocardial contours) which may not be recognized at rest, may be perceived under stress. (Data is courtesy of M. Fenchel, S. Miller and A. Seeger, Max Planck MR-center, University of Tübingen.)

a high spatial resolution (in-plane <2mm) enables subendocardial to be distinguished from transmural deficits [Hunold et al., 2006]. A minimum field strength of 1.5Tesla is required to achieve high signal- and contrast-to-noise ratios. A field strength of 3Tesla provides a higher intrinsic signal which may be used for higher resolution or larger volume coverage. Recently, Steady-State Free Precession (SSFP) sequences have gathered interest since they perform superior to GRE sequences in Cine imaging [Hunold et al., 2006].

At rest conditions, the restricted myocardial perfusion due to moderate to severe stenosis can be compensated by collateral blood supply. However, under stress conditions, the oxygen demand of the myocardium increases and must be satisfied by vasodilation. Stenosed arteries are not capable of this mechanism and cannot provide the coronary flow reserve. Perfusion MRI is usually accomplished at rest and under stress which facilitates a determination of the coronary flow reserve and hence, the detection of even mild to moderate stenosis becoming hemodynamically relevant only under stress (Fig. 2.19). Furthermore, the distinction of perfusion defects versus image artifacts, e.g. the dark rim artifact, is supported by rest/stress comparison. The stress is induced before the scan either pharmacologically or by physi-

cal exercise. Pharmacologic stress is preferred in order to prevent further complications. Either heart rate and contractility are increased with catecholamines, e.g., *dobutamine*, or vasodilation and coronary stealing effects are induced using *dipyridamol* or *adenosine*.

The same slice locations are used for rest and stress imaging to achieve comparable myocardial regions. However, the number of image slices that can be acquired must be adapted to the patient-specific heart rate. Since the heart rate may be increased by pharmacological stress medication, the application of the same imaging sequence results in image slices that show different contraction phases for perfusion at rest and under stress. Registration techniques to compensate for this effect are described in [Hennemuth et al., 2008c].

In cardiac perfusion MRI, paramagnetic, gadolinium (Gd)-based CAs are typically applied. They lead to an increase of myocardial signal intensities due to their T1-shortening effect. However, their additional $T2^*$ effects hamper the linear relationship between CA concentration and signal intensity. Extravascular CAs are the standard in cardiac perfusion MRI. For extravascular CAs, the signal intensity does not only depend on perfusion and tissue blood volume but also on diffusion since half of the CA leaks out into the interstitial space during the first pass. The missing linear relationship between CA concentration and signal intensity as well as the diffusion process complicate a quantification of myocardial perfusion.

2.2.2.2 Late Enhancement Imaging

In 1989, van Dijkman et al. [1989] were the first who observed myocardial infarction enhancement with extravascular CAs in a clinical context. The mechanism of CA enhancement in non-viable myocardium is not yet fully understood. However, necrotic tissue is associated with a larger extracellular fluid volume than viable myocardium which results in a higher concentration of Gd-based contrast agents than in healthy tissue. The worse the perfusion of tissue the longer it takes for Gd to accumulate. About 10-20min after CA injection, Gd accumulates in the infarction scar. The imaging of this effect is referred to as LE imaging. Necrotic tissue is characterized by higher signal intensities (bright areas) in the LE images (Fig. 2.20).

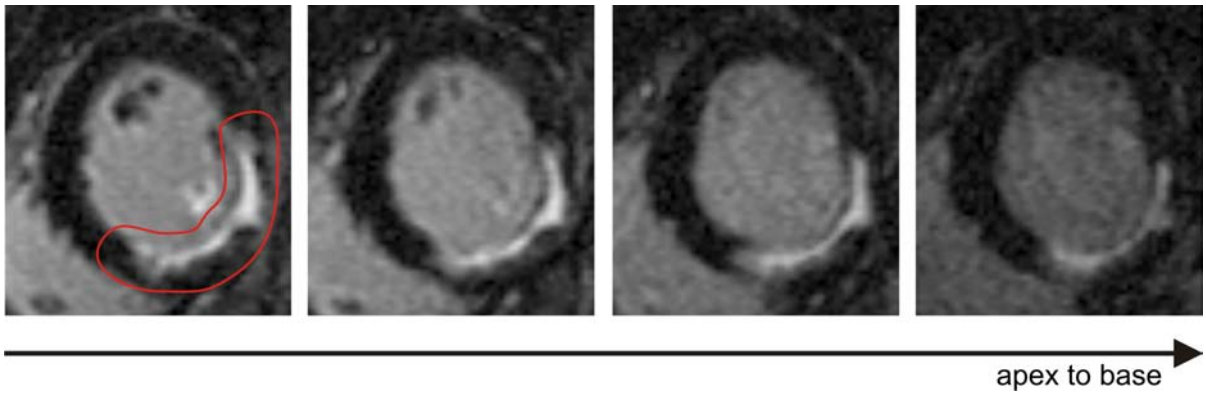

Figure 2.20: Extract from a MRI myocardial viability study acquired via Late Enhancement imaging. Four slices sorted from the apex of the heart to its base are displayed. About 10-20min after injection of a Gadolinium(Gd)-based contrast agent, the Gd accumulates in necrotic tissue (bright, red encircled region). The patient had previously suffered from an infarction. The necrosis hampers the contractility of the myocardium in this region (Fig. 2.21 shows Cine data acquired from the same patient). (Data is courtesy of Frank Grothues, University Hospital Magdeburg.)

Due to the improved spatial resolution of MR LE imaging, it facilitates the detection of even subendocardial infarctions thereby outperforming standard nuclear imaging [Finn et al., 2006]. The prospective functional recovery of a myocardial region correlates with the transmural extent (*transmurality*) of the infarction scar [Choi et al., 2001]. If the transmurality is $< 25\%$, the chances of recovery are high whereas the chances converge to zero if the transmurality is $> 75\%$. Together with stress perfusion imaging, LE imaging facilitates the differentiation of healthy, ischemic and necrotic tissue and hence, has a direct impact on therapy planning. Only in cases with ischemic tissue and no or smaller necrotic tissue (mismatch), revascularization may be performed [Strohm et al., 2006].

During the scan, the patient is connected to an ECG for triggering the acquisition. The standard sequence applied in LE imaging is an ECG-triggered, segmented inversion-recovery 2D turbo gradient echo sequence (Turbo-FLASH) aiming at T1-weighted datasets. The inversion pulse leads to an improved contrast between viable an non-viable myocardium after CA administration. Faster imaging is feasible by means of 3D Turbo-FLASH sequences. The scan is performed over several heart beats at end diastole. This cardiac phase is chosen since it is relatively stable having the advantage of reduced motion artifacts [Gerber et al., 2008]. Either one slice (2D Turbo-FLASH) or several slices (3D Turbo-FLASH) are acquired per heart beat. Several breath holds are necessary during the acquisition. Since the scan is spread over several heart beats, slice misalignment may occur. Techniques for misalignment correction are described in [Hennemuth et al., 2008c]. The slice locations of LE imaging may include slice locations of first-pass perfusion imaging which simplifies a comparative analysis of corresponding myocardial regions. The slice locations should be chosen such that myocardial regions are covered which showed a reduced contractility in Cine imaging since the likelihood of LE is higher here [Hunold, 2007] (recall that Cine imaging is part of a typical scanning protocol and is performed prior to LE imaging, Fig. 2.17). Up to 25 short-axis slices are acquired plus 2-chamber and 4-chamber views [Breeuwer, 2005]. A slice thickness of 6-8mm and a slice gap of 2-4mm (to equal 10mm) are recommended by the *Society for Cardiovascular Magnetic Resonance (SCMR)* [Kramer et al., 2008]. Typical matrix dimensions are 256×166 (2D Turbo-FLASH) [Hunold, 2007] and 256×192 (256×256 reconstructed) [Strohm et al., 2006]. The in-plane resolution should be in the range of 1.4-1.8mm [Kramer et al., 2008].

2.2.2.3 Cine Imaging

Early work on cardiac Cine imaging using spoiled GRE pulse sequences was presented in 1988 by Glover and Pelc [1988]. Today, MR Cine imaging is the gold standard of cardiac functional imaging [Ley and Kreitner, 2007]. In Cine imaging, the entire cardiac cycle is sampled at different phases. The acquired data facilitates the assessment of global (stroke volume, ejection fraction, and cardiac output) and local cardiac parameters (myocardial wall thickness and wall thickening) characterizing the function. An extract from a Cine series of slice stacks is presented in Figure 2.21. Stress Cine imaging may be applied for the detection of myocardial ischemia. The myocardial function decreases with an increasing stress-level in case of mild to moderate ischemia [Breeuwer, 2005]. The stress may be pharmacologically induced, e.g., by means of dobutamine. Cine imaging in combination with perfusion and LE imaging contributes to the detection of stunned and hibernating myocardium [Strohm et al., 2006] (Tab. 2.1).

During the scan, the patient is connected to an ECG for triggering the acquisition. SSFP sequences represent the standard in Cine imaging. The resulting image contrast is deter-

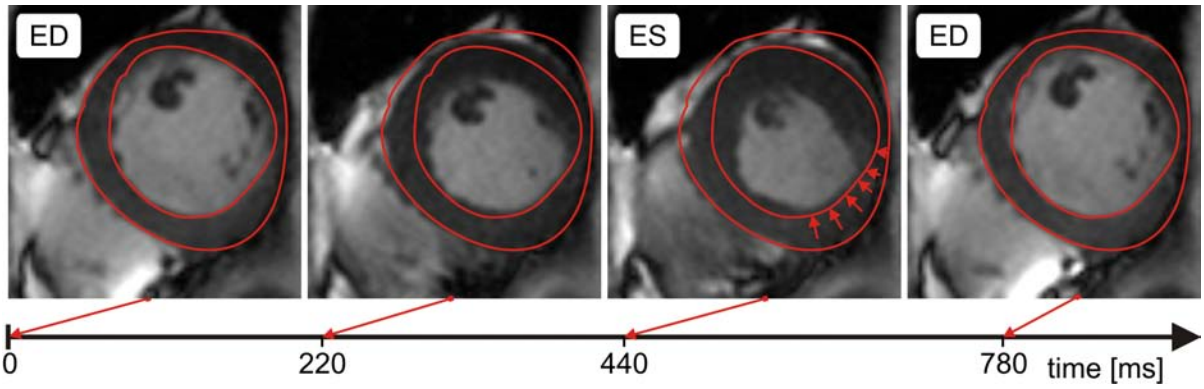

Figure 2.21: Extract from a MRI myocardial contractility study acquired by means of Cine imaging. Four different phases of the cardiac cycle are displayed for the same image slice. At end diastole (ED), the myocardium is fully relaxed. At end systole (ES), the maximum of contraction is achieved. The myocardial contours (red) have been delineated based on ED and then propagated to the other phases. At ES, a reduced contractility may be observed in the inferior and inferolateral regions (arrows). The patient had previously suffered from an infarction leading to tissue necrosis in this area. Figure 2.20 shows Late Enhancement data acquired from the same patient. (Data is courtesy of Frank Grothues, University Hospital Magdeburg.)

mined by the $T2/T1$ ratio of the tissue. Hence, the image quality is often not significantly impaired by CA administration previous to Cine imaging, e.g., for stress perfusion tests. Parallel imaging may be used to speed up the acquisition, to increase ventricular coverage or both [Finn et al., 2006]. It may also be used for perfusion MRI and LE imaging. In Cine imaging, up to 15 short-axis slices are acquired at 50 phases in the cardiac cycle [Breeuwer, 2005]. Often, additional 2-chamber and 4-chamber slices are acquired. Since the acquisition of the slices per phase is distributed over several cardiac cycles, ECG-triggering is necessary. As with LE imaging, a misalignment of slices may occur. The slice locations, as recommended by the Society for Cardiovascular Magnetic Resonance, should be distributed along the ventricular long-axis from the mitral valve plane through the apex. A slice thickness of 6-8mm and a slice gap of 2-4mm (to equal 10mm) should be applied [Kramer et al., 2008]. Typical matrix dimensions are 256×192 (256×256 reconstructed) [Strohm et al., 2006] with an in-plane resolution in the range of 1.4-1.8mm.

2.2.3 Data Processing

This subsection is dedicated to the data processing techniques commonly applied to cardiac MRI perfusion studies. LE imaging and Cine imaging studies are only covered briefly. A crucial step in data processing is the correction for motion artifacts. Motion correction may be followed by noise filtering to cope with the relatively low signal-to-noise-ratio (SNR). The approaches introduced for cerebral perfusion imaging in Subsection 2.1.3.3 may be applied here as well. In [Kholmovski et al., 2004], an image reconstruction scheme was presented which transforms the original data into images having spatially uniform noise distribution and image noise which is characterized by a Gaussian distribution. Therefore, post-reconstruction image noise filtering by means of anisotropic diffusion filters or total variation filters may be applied. While in cerebral perfusion a gamma-variate function may be fitted to the data to compensate for noise, a Fermi function is applied in myocardial perfusion since it adheres more closely to the typical TIC [Gerber et al., 2008].

Often, the myocardium is segmented in the data to restrict the computation of perfusion parameters to relevant tissue. Next, the signal intensities may be calibrated to correct for intensity inhomogeneities. Then, the myocardium may be divided into segments according to a standardized model which describes the relationship between myocardial regions and the supplying coronary branches. Finally, perfusion parameters are derived from the temporal course of the signal intensities either segment-wise or pixel-wise. Recently, an unsupervised analysis of myocardial perfusion MRI including motion and inhomogeneity correction as well as a robust computation of pixel-wise perfusion parameters has been proposed [Xue et al., 2009].

In data processing of LE images, the segmentation of the necrotic tissue and its transmurality play a crucial role. For the assessment of myocardial function, the parameters stroke volume, ejection fraction, cardiac output, myocardial wall thickness and wall thickening are computed based on Cine images.

2.2.3.1 Motion Correction

In cardiac perfusion MRI, motion artifacts may occur due to the proper motion of the heart, patient respiration and patient movement. Artifacts due to the first two causes are attenuated by ECG-triggering and breath-hold maneuvers but cannot be fully eliminated. However, a correction for motion artifacts is the prerequisite for a reliable perfusion analysis. Compared to cerebral perfusion (Subsec. 2.1.3.1), motion correction is a complex problem due to the proper motion of the heart and fewer well-defined anatomical landmarks [Mäkelä et al., 2002].

Xue et al. [2008] state that although motion correction has been intensively studied, no clinically accepted solution yet exists. They collected a large multi-center MR perfusion data pool (586 cases) and found motion correction to be a frequent requirement (67%). They proposed a registration method including rigid and non-rigid registration and quantitatively validated their approach. The proposed method proved to be highly robust to varying MR imaging parameters, myocardial anatomy and motion patterns. In [Milles et al., 2008], a fully automated motion correction approach based on Independent Component Analysis (ICA) is presented. The ICA is applied to extract relevant features together with their time-intensity behavior. From the ICA results, a reference dataset is computed that mimics intensity changes in the data of interest. This reference image is then incorporated in a two-pass registration framework which starts with a coarse registration on subsampled images and is subsequently executed on the full resolution data. The approach was successfully validated for 46 clinical datasets and turned out to be adequate in a clinical environment regarding accuracy, robustness and speed.

For a more detailed review of motion correction techniques, the reader is referred to [Mäkelä et al., 2002] and [Hennemuth et al., 2008c]. In [Hennemuth et al., 2008c], also the slice misalignment problem and possible solutions are discussed. The problem occurs when slice stacks are acquired over several heart beats as in Cine and LE imaging.

2.2.3.2 Segmentation of the Myocardium

To restrict the analysis of cardiac MRI perfusion, Cine and LE data to relevant tissue, the myocardium must be segmented. A comprehensive survey of existing segmentation approaches is beyond the scope of this thesis. Instead, individual problems in processing perfusion, Cine and LE data are discussed and one state-of-the-art approach as well as the methods applied in the thesis at hand are presented.

Assuming a faultless ECG-triggering, minimum respiratory motion and a successful motion correction, the segmentation of the myocardium in the perfusion scan is a straightforward task. A semi-automatic segmentation approach such as the *Live-wire* technique [Schenk et al., 2000] may be used to delineate the myocardium, i.e., the endocardial and the epicardial ring, in the $3-6$ short-axis slices at one point in time. A point in time should be chosen that facilitates a good visual distinction of the myocardium from the surrounding tissue, e.g., when the CA accumulates in the myocardium (Fig. 2.19, right column). The resulting contours may then be propagated to the remaining points in time. A visual inspection should follow the propagation and suitable assistance should be given to the user in interactively adapting the segmentation result.

The Live-wire technique may as well be applied in processing the LE data. However, in case of a maximum of 25 short-axis slices this is a time-consuming task which slows down the examination in clinical routine. In [Ciofolo et al., 2008], a fully automatic segmentation is presented. In a two-step workflow, a 2D geometric template is first deformed such that it roughly fits the myocardial contours in each slice. Next, a 3D geometric mesh of the left ventricle is registered to the LE data and deformed towards the contour stack. The deformation is carried out with respect to the contour stack, the image intensity as well as internal forces. The mesh was derived from previously acquired Cine data which facilitate an easier detection of myocardial contours.

Applying Live-wire for the segmentation of each phase (*no.* ≈ 50) in the Cine data is a prohibitively tedious task. Straightforward contour propagation as for the perfusion data is not possible since the myocardial wall changes due to relaxation and contraction. Hence, there is a strong demand for automatic methods. A new active contour model has been invented for this purpose which allows for an automatic adaptive contour propagation [Hautvast et al., 2006]. A clinical validation based on 107 datasets proved the propagation method to be fast, robust, and accurate. In [Dornheim et al., 2008], a 3D mass-spring model which has been extended by torsion forces and the capability of explicit rotation is applied for an automatic segmentation of the entire cardiac cycle. The model has been derived from a training set of segmentations based on an average patient population. Patient-specific details have been removed by extensive mesh smoothing. The model uses intensity information as well as the segmentation result from a previous phase for segmenting the current phase. It consists of an endocardial as well as an epicardial mesh.

Despite advances in research, manual segmentation is still the standard in clinical routine. However, it is often applied only at end systole and end diastole facilitating a computation of the common functional parameters (see Subsec. 2.2.3.6).

2.2.3.3 Calibration of Signal Intensities

The computation of perfusion parameters (Subsec. 2.2.3.5) requires the calibration of signal intensities to correct for intensity inhomogeneities. These inhomogeneities are due to the use of surface coils which may be attached to the patient during image acquisition. A surface coil is a loop of conducting material, e.g., copper tubing. It is placed on the chest of the patient over the heart to increase magnetic sensitivity in this region. Since the sensitivity decreases with increasing distance from the coil, signal inhomogeneities arise. To resolve this problem, the standard calibration formula divides the signal intensities after CA arrival by the baseline averaged signal intensity before CA arrival [Schmitt et al., 2002]:

$$S_N(t) = \frac{S(t) - S_0}{S_0} \tag{2.6}$$

where $S_N(t)$ is the the normalized signal intensity, S_0 is the baseline averaged signal intensity before CA arrival, and $S(t)$ is the signal intensity at time t. Plotting $S_N(t)$ over time results in a *time-intensity curve* (TIC). In Figure 2.23(a), a TIC in a single voxel of healthy myocardium is presented. The TIC represents an idealized version of TICs usually observed in clinical routine. In patients, a shorter scanning duration (fewer points in time) is often chosen covering only a small part of the CA washout. The TIC is annotated with three phases of CA traversal:

(I) Saturation During this phase, the MR signal achieves its steady-state condition.

(II) Baseline The change in signal intensity during the baseline phase is due to image noise. The phase ends with the arrival of the CA.

(III) First Pass The CA travels through the capillary bed for the first time resulting in a considerable signal increase.

2.2.3.4 AHA-conform Myocardial Division and Nomenclature

In 2002, the American Heart Association (AHA) developed a standardized myocardial division and nomenclature for tomographic imaging of the heart [Cerqueira et al., 2002]. The main purpose was to allow for accurate intra- and cross-modality comparisons for clinical patient management and research.

According to the AHA, the left ventricle should be divided into 17 segments (*17-segment model*) for an assessment of the myocardial state (Fig. 2.22). Parameters describing myocardial perfusion, function and viability may then be determined and communicated segment-wise. The number of segments is based on autopsy studies which provided data on myocardial mass and size. The acquisition of three short-axis slices is necessary to cover the first 16 segments. Segment 17 can either be covered by a fourth short-axis slice or it can be evaluated from vertical and horizontal long-axis slices. The location and thickness of the short-axis slices is as well standardized. They should be defined such that the basal, mid-cavity, and the apical part of the left ventricle are adequately sampled. The slice thickness is dependent on the modality-specific resolution but should be smaller than 1cm. In the basal and the mid-cavity slice, the ring-shaped myocardium should be divided into six 60° segments starting at the anterior junction of left and right ventricle. Since the left ventricle narrows towards the apex, the apical slice is divided into only four 90° segments following the same procedure. Then, the apical cap forms segment 17. The segments are labeled with respect to their locations relative to the long axis of the heart and their circumferential location. Each segment is finally associated with a supplying coronary branch based on the prevailing right-dominant distribution of the coronary arteries (Fig. 2.13). However, a warning is issued that the tremendous variability in coronary artery distribution should be recognized. Several studies, e.g. [Ortiz-Pérez et al., 2008], have shown that the standardized correspondence may only be valid for parts of the entire population.

The acquisition of myocardial perfusion data is often accomplished in 3-4 short-axis slices according to the 17-segment model. However, more slices are typically acquired in LE and Cine imaging. Hence, additional segments are often introduced when evaluating these data. If an adherence to the 17-segment model is crucial, each individual slice is assigned to its corresponding ventricular part (basal, mid-cavity, apical, apex) and the myocardium in each slice is divided into segments accordingly. Then, parameters describing the myocardial

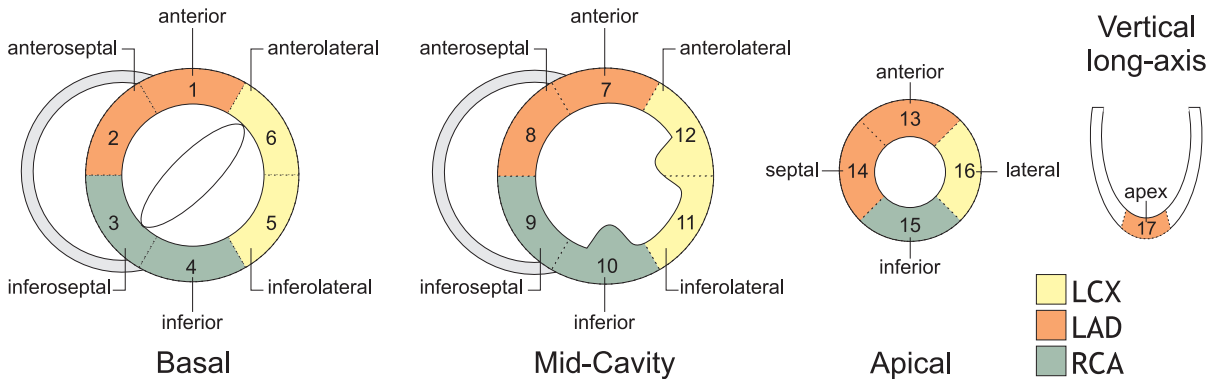

Figure 2.22: AHA-conform myocardial division and nomenclature in short-axis views. The basal and mid-cavity part of the left ventricle are each divided into 6 segments. The apical part is divided into 4 segments. The apex forms a segment itself and is often evaluated from a vertical long-axis slice. Each segment is colored with respect to the associated coronary branch. LCX: left circumflex coronary artery, LAD: left anterior descending coronary artery, RCA: right coronary artery. The right ventricle is indicated as filled semi-circle. (Line drawings are courtesy of Anja Kuß.)

viability and function are computed and averaged over all equally labeled segments, e.g., all inferior segments in slices which have been assigned to the basal part.

The 17-segment model provides a rather rough division of the myocardium which may hamper the detection and precise assessment of subtle perfusion disturbances. Hence, the definition of an arbitrary number of segments is commonly offered in existing software. Furthermore, each segment may be bisected by the myocardial centerline thereby generating inner and outer segments which represent the subendocardial and subepicardial regions, respectively. This approach is particularly suitable for analyzing MRI data which provides a sufficiently high spatial resolution. Also a voxel-wise myocardial assessment was proven to be reliable in detecting ischemia [Panting et al., 2001]. However, it poses the highest demands on the accuracy of the prior motion correction.

2.2.3.5 Perfusion Parameters

In myocardial perfusion diagnosis, parameters describing the shape of the TIC are derived for diagnosing ischemia in a single scan study, for assessing the benefit of a revascularization therapy in a follow-up study and for an inter-patient comparison, e.g., in a clinical study. In [Schmitt et al., 2002], three different approaches in assessing myocardial perfusion based on perfusion parameters are discussed. The first approach relies on a derivation of shape parameters from the TIC by means of simple mathematics. It is equal to the computation of descriptive perfusion parameters in cerebral perfusion (Subsec. 2.1.3.4 and Fig. 2.9). The second and the third approach both extend the first one by incorporating the AIF thereby accounting for the effect of variations in rate, amount and timing of CA delivery to the myocardium. In the second approach, the effect is only approximately corrected for by normalizing the TIC parameters with the corresponding parameters of the AIF. Since the approach does not facilitate a full calculation of tissue transit effects or extravascular CA exchange, it is referred to as *semi-quantitative analysis*. The third approach aims at real quantitative parameters, e.g., myocardial blood flow in $[ml/min/100g]$. It is based on the deconvolution of the TIC with the AIF and can be compared to the computation of quantitative perfusion parameters in cerebral perfusion (Subsec. 2.1.3.5). A major issue involved in the quantification is the lack of linearity between the CA concentration and the signal

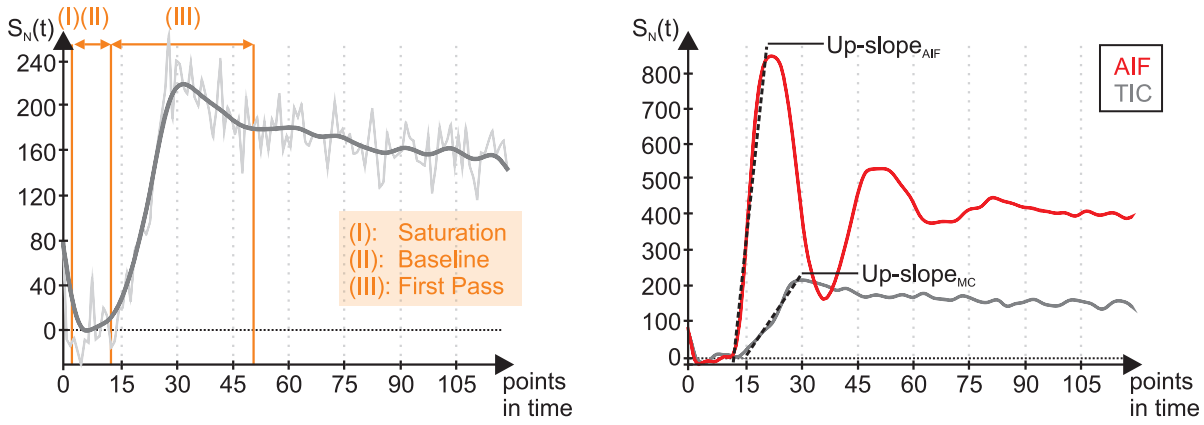

Figure 2.23: Idealized time-intensity curve (TIC) and arterial input function (AIF) in a single voxel of healthy myocardium (MC) and the lumen of the left ventricle (LV), respectively. In clinical routine, a shorter scanning duration (fewer points in time) is often chosen covering only a small part of the CA washout in the MC. *(a)* The TIC (bright gray curve) is generated by calibrating the signal intensities according to Equation 2.6 and plotting them over time. It has been smoothed by a binomial filter (dark gray curve) to improve readability and annotated with three phases of CA traversal. *(b)* The AIF is superimposed on the TIC from *(a)*. It has a higher curve maximum appearing earlier in time. A second, more flattened pass of CA traversal may be observed. To correct the perfusion parameter values for the effect of the AIF, they are divided by the corresponding AIF parameter values as illustrated for *Up-slope*.

intensities. Since only low-doses of CA provide this linearity and since the quantification involves time consuming and operator dependent calculations, it does not yet play a role in clinical settings [Hunold et al., 2006]. In the following, the focus will be on the first two approaches.

The perfusion parameters, which have been investigated in assessing myocardial perfusion, are *Slope*, *PE*, *TTP* [Al-Saadi et al., 2001; Panting et al., 2001], *Integral* [Klocke et al., 2001] and *MTT* [Lombardi et al., 1999] (Fig. 2.9). In this context, the *Slope* is also referred to as *Up-slope* and has proven to be a particularly useful clinical parameter in detecting ischemia [Al-Saadi et al., 2000]. The reader is referred to Subsection 2.1.3.4 for a detailed description of the approved parameters and other typical parameters generated by a curve analysis. The parameter derivation is either based on the TIC itself or on a fitted Fermi function. The function fitting eliminates the effect of temporal noise. The parameters may be computed per myocardial segment from an averaged TIC (SubSec. 2.2.3.4) or voxel-wise.

In order to approximately correct the perfusion parameter values for the effect of the AIF on the TIC, they are divided by the corresponding values of the AIF [Gerber et al., 2008]. The AIF is determined from the lumen of the left ventricle by defining a region of interest and computing the average TIC. A point in time is selected from the perfusion sequence at which the CA accumulates in the lumen (Fig. 2.19, middle column). Special care must be taken to avoid an inclusion of the papillary muscles. Characteristics of the AIF as compared to curves measured in myocardial tissue are a significantly higher curve maximum that appears earlier in time and a more narrow curve shape (Fig. 2.23(b)).

In the concurrent evaluation of stress and rest perfusion, the computation of the *Myocardial Perfusion Reserve Index (MPRI)*, which expresses the capability of coronary va-

sodilation, has been proven to be valuable. The MPRI is computed as [Al-Saadi et al., 2000]:

$$MPRI = \frac{Up - slope_{MC}^{stress} / Up - slope_{LV}^{stress}}{Up - slope_{MC}^{rest} / Up - slope_{LV}^{rest}} \tag{2.7}$$

being the ratio of normalized slopes measured in the myocardium (MC) and in the lumen of the left ventricle (LV). While a cut-off value of 1.5 was determined in [Al-Saadi et al., 2000] for the differentiation between healthy and ischemic myocardium, there is an ongoing debate on the generality of this value [Gerber et al., 2008]. The MPRI may be computed and communicated segment- or voxel-wise.

2.2.3.6 Processing of LE and Cine Data

A comprehensive survey of existing approaches for processing LE and Cine data is beyond the scope of this thesis. Instead, the respective standard approach as well as state-of-the-art methods applied in the thesis at hand are presented. The reader is referred to [Hennemuth et al., 2008a] for an overview of viability analysis techniques based on LE data.

Processing of LE data. The main goal in processing LE data is an automatic segmentation of the infarction scar and the determination of its transmurality. In a first step, myocardial tissue is segmented by identifying the myocardial contours in the LE data (Subsec. 2.2.3.2). The standard approach then performs a thresholding of two or three standard deviations above the average intensity value of a healthy myocardial region to identify necrotic tissue [Kim et al., 1999]. A prerequisite is the often user-defined delineation of a healthy tissue portion. The transmurality is then commonly determined as the portion of segmented voxels per radial myocardial segment [Noble et al., 2004].

A fully automatic detection of necrotic tissue is presented in [Hennemuth et al., 2008b]. The infarction scar is segmented with a histogram analysis method. The intensity distribution within the segmented myocardium is analyzed by fitting the mixture model of a Rayleigh distribution and a Gauss distribution. The determined threshold is then fed to a watershed segmentation with automatically determined seed points which identifies myocardial regions showing late enhancement. Determining the transmurality as the portion of segmented voxels per segment does not consider the position of the voxels relative to epi- and endocardium. However, as the supplying coronary arteries are attached to the epicardium, a decreased blood flow initially affects the subendocardial regions of the myocardium and infarctions occur here first and then, propagate towards the epicardium [Reimer and Jennings, 1979]. Hence, transmurality may be computed as the distance between the outer rim of necrotic tissue facing the epicardium and the epicardium itself [Hennemuth et al., 2008c]. Small distance values then indicate a high transmurality while larger distances indicate a low penetration of the myocardial tissue. In case of several focii of necrotic tissue (Fig. 2.16(b)), the outer rim of each individual focus may be employed for distance computations.

Processing of Cine data. The main goal in processing Cine data is to assess the left ventricular function. For this purpose, global (stroke volume, ejection fraction, and cardiac output) and local cardiac parameters (myocardial wall thickness and wall thickening) are derived from the data. In a first step, the end-diastolic and the end-systolic phase, which are characterized by a minimum and maximum in myocardial wall thickness, respectively, are extracted from the data. Then, the myocardial contours are delineated (Subsec. 2.2.3.2).

Based on the contours, the volume of the ventricle at ED (V_{ED}) and ES (V_{ES}) and the global cardiac parameters may be computed [Kochs et al., 2005]:

$$SV[ml] = V_{ED} - V_{ES} \tag{2.8}$$
$$EF[\%] = SV/V_{ED} \times 100\% \tag{2.9}$$
$$CO[ml/min] = SV \times HR \tag{2.10}$$

where SV is the stroke volume, EF the ejection fraction, CO the cardiac output, and HR is the patient-individual heart rate.

More detailed information about the myocardial contraction is provided by the local cardiac parameters. The wall thickness is typically computed by means of the *centerline method* [Kochs et al., 2005]. Here, the myocardial centerline located between endo- and epicardium is first computed. Next, it is sampled at equidistant locations and cords are drawn perpendicular to the centerline. The wall thickness is then defined for each sample point as the distance between the cord intersections with endo- and epicardium. It is computed per sample point and optionally averaged per myocardial segment. The sampling always starts at at the inferior connection of the right and the left ventricle. To compensate for the rotational movement of the heart, the starting point must be recomputed for each cardiac phase. The wall thickening (WT) represents the difference in wall thickness between end diastole W_{ED} and end systole W_{ES}. It is computed per sample point as:

$$WT[\%] = \frac{W_{ES} - W_{ED}}{W_{ED}} \times 100\% \tag{2.11}$$

2.2.4 Visualization and Exploration

Cine movies, parameter maps as well as the exploration by means of curve displays for user-defined regions of interest (Subsec. 2.1.4) have also been approved for the assessment of myocardial perfusion [Hunold et al., 2006; Panting et al., 2001]. The qualitative interpretation of the data by means of cine movies remains the clinical standard [Gerber et al., 2008]. In the cardiac context, the purely visual inspection is also referred to as *eye balling*. Special care is necessary since the signal intensities may vary considerably between the septum and the inferolateral wall due to the use of surface coils (Subsec. 2.2.3.3). Furthermore, perfusion defects must be differentiated from typical dark artifacts due to $T2^*$ susceptibility effects, low resolution, or cardiac motion [Hunold et al., 2006].

Bull's Eye Plot. The standard technique in cardiology for visualizing the perfusion parameters (Subsec. 2.2.3.5) as well as transmurality and myocardial wall thickness and thickening is the Bull's Eye Plot (BEP, also referred to as polar plot). The BEP is related to the division of the myocardium into segments and hence, is applied to communicate the results of a segment-wise analysis (Subsec. 2.2.3.4). The BEP is constructed by fictitiously projecting all myocardial segments onto a plane (Fig. 2.24(a)). If the myocardium has been divided according to the 17-segment model (Fig. 2.22), the rings of the plot from exterior to interior represent the basal, the mid-cavity and the apical part of the left ventricle, as well as the apex itself (Fig. 2.24(b)). The analysis results are computed segment-wise and then color-coded in the BEP. The coloring facilitates a detection of suspicious tissue and the correspondence between segments and coronary branches indicates the source of the defect.

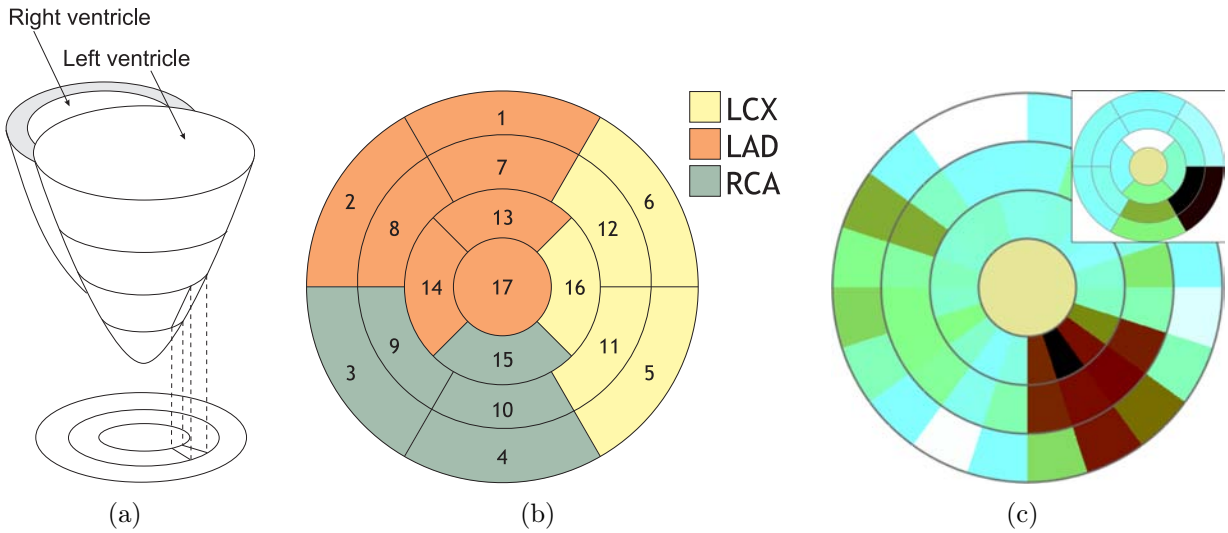

Figure 2.24: The Bull's Eye Plot (BEP). *(a)* Construction of the BEP by fictitiously projecting all myocardial segments onto a plane. *(b)* BEP corresponding to the 17-segment model (Fig. 2.22). Each segment is colored according to the associated coronary branch. LCX: left circumflex coronary artery, LAD: left anterior descending coronary artery, RCA: right coronary artery. *(c)* BEP representing the parameter *PE*. The segments of the 17-segment model (inset) have been subdivided to facilitate a more accurate assessment of the perfusion disturbance (dark segments). Segment 17 is missing since no slice was acquired at the apex. (Line drawings are courtesy of Anja Kuß.)

Based on the discussion in Subsection 2.2.3.4, the segments of the BEP may be subdivided radially for a more subtle analysis (Fig. 2.24(c)) and/or bisected by a circular arc for depicting differences between subendocardial and subepicardial regions. The BEP can be adapted to the acquired number of slices by adding as many rings as necessary. An exploration facility often associated with the BEP is the selection of individual segments. The BEP is then linked with a curve display and a tabular view of the corresponding TICs and perfusion parameters, respectively. The BEP, a curve and a tabular view represent the standard visualizations in today's vendor-supplied clinical workstations, such as SIEMENS `Argus Dynamic Signal` and PHILIPS `Cardiac Specialist` for MR examinations, and PHILIPS `Comprehensive Cardiac Analysis` application for CT examinations, as well as in packages for nuclear medicine, such as the `Emory Cardiac Toolbox` (ECT) and `Cedars-Sinai's Quantitative Perfusion SPECT (QPS)` software. They are also standard in other commercial software, such as the *PerfusionTools* plug-in of `CMRtools`[5] and `QMass® CT/MR`[6].

Advanced Visualizations. At the time of writing this thesis, there are no advanced visualizations of myocardial perfusion MRI data being used in clinical routine. Packages for nuclear medicine (ECT, QPS) offer a surface reconstruction of the left ventricle colored according to perfusion and functional parameters. ECT further merges the visualization with surfaces of generic coronary arteries illustrating the standard correspondence between myocardial territories and coronary branches (Subsec. 2.2.3.4). See [Lin et al., 2006] for a detailed description of visualizations offered by traditional packages for nuclear medicine. Surface reconstructions of the left ventricle which are colored by wall thickening and transmurality are included in commercial software (`CMRtools`) as well as in research prototypes

[5]Product of CMRtools; www.cmrtools.com (01/16/2010)
[6]Products of Medis; www.medis.nl/Products/Cardiology.htm (01/16/2010)

[Wesarg and Nowak, 2006; Wald et al., 2007]. In [Wald et al., 2007], necrotic tissue is segmented in the LE data, rendered as a surface, and presented together with the ventricle. A 3D visualization of the beating heart based on Cine data is included in the research prototypes `Segment` [Heiberg et al., 2005] and `HeAT` (Heart Analysis Tool) [Säring et al., 2009]. It requires a delineation of the myocardial contours at each phase of the cardiac cycle which is accomplished automatically in `Segment`.

2.3 Summary and Implications for the Thesis

MR perfusion imaging has been used to assess cerebral perfusion for more than 20 years now [Villringer et al., 1988]. "Despite this lengthy history of use, perfusion MR imaging remains a boutique method in many neuroimaging practices, used only occasionally. [...] Until clear data indicating how perfusion MR imaging can affect patient care are available, perfusion MR imaging will remain academically interesting but unproved." [Sorensen, 2008] Though it has been shown that perfusion imaging in combination with diffusion-weighted imaging can help to identify the penumbra, definite data is missing indicating that such imaging findings can be used to guide therapy [Sorensen, 2008]. One of the major issues in generating such data has been identified by the recently published *Acute Stroke Imaging Research Roadmap* [Wintermark et al., 2008]. A systematic comparison is missing that will "determine which [perfusion] parameters have, or do not have, a significant impact in terms of accurately representing acute perfusion status and predicting subsequent tissue outcome." The roadmap further elucidates that the optimal method(s) for parameter derivation should be immune against differences in imaging parameters such as magnetic field strength, scan parameters, and CA type and dose.

The history of MR perfusion imaging in the diagnosis of Coronary Heart Disease covers almost 20 years now [Atkinson et al., 1990]. Perfusion MRI has proven to be competitive with regard to Coronary X-ray Angiography as well as the prevailing nuclear imaging methods [Schwitter et al., 2001; Panting et al., 2001]. The American Heart Association and the American College of Cardiology recommend perfusion MRI for the detection of hypoperfused viable myocardial tissue and the correlation between this tissue and the supplying vessel. A standardized perfusion MRI imaging protocol has been suggested [Kramer et al., 2008]. However, wide-spread use of perfusion MRI is still hampered by a variety of artifacts and the strong experience necessary to perform the examination and interpret the results. Furthermore, large clinical trials are missing which define the impact of perfusion MRI on patient management [Hunold et al., 2006]. Eye balling is still the prevailing method for analyzing perfusion MRI data in clinical routine. Semi-quantitative approaches are time-consuming since the applied software often requires a manual delineation of myocardial contours [Hunold et al., 2006]. In contrast to cerebral perfusion, researchers in myocardial perfusion seem to agree on one particularly useful clinical parameter in detecting ischemia which is *Up-slope* [Gerber et al., 2008]. However, there is no official guideline supporting this agreement and results might have to be reviewed with respect to improved imaging sequences, the advent of 3Tesla and 7Tesla scanning, and the application of intravascular CAs. As in cerebral perfusion, the perfusion quantification is an active research area. A variety of approaches exists enforcing a correction of perfusion parameters for effects of the AIF ranging from simple scaling with the AIF parameters up to complex compartment models and deconvolution techniques [Gerber et al., 2008]. A comparison of the different approaches and their results, as well as a comparison with purely qualitative data assessment is crucial.

Cardiac Magnetic Resonance Imaging facilitates a comprehensive investigation of the state of the heart. Myocardial perfusion, viability and function may be assessed based on datasets acquired in a single scanning protocol. The standardized cardiovascular Magnetic Resonance imaging protocol recommends as a postprocessing step the side-by-side visual inspection of cine views, stress and rest perfusion, and LE images [Kramer et al., 2008]. The purely visual evaluation of this complex data pool is barely reproducible and time-consuming since it requires scanning back and forth for comparing corresponding regions.

Briefly summarized, four crucial problems, which motivate the major goals of the thesis at hand, arise in the diagnostic evaluation of perfusion data from ischemic stroke and CHD diagnosis:

1. It is unclear which perfusion parameter(s) derived by which computational method(s) best identify ischemic tissue. Hence, the entire set of parameters may be consulted.

2. A pure visual exploration is the prevailing method of evaluating perfusion data and the associated parameters in clinical routine. It is observer-dependent, barely reproducible and does not deliver quantitative results.

3. Varying imaging parameters and a varying parametrization of preprocessing methods affect the reliability of perfusion parameters and computational methods. Such effects have not yet been satisfactorily investigated.

4. The concurrent evaluation of perfusion, viability and function for CHD diagnosis is insufficiently supported in clinical routine.

Goal 1. Physicians shall be supported in visually exploring a set of perfusion parameters. Attaining this goal will be tackled by providing advanced visual exploration techniques that facilitate the integrated comparative exploration of several perfusion parameters. The generated visualizations should outperform the side-by-side presentation of parameter maps whose mental integration demands a considerable cognitive effort [Levkowitz, 1997].

Goals 2 and 3. Physicians shall be supported in a streamlined investigation of perfusion. Researchers in the field of perfusion shall be supported in gaining a better understanding of which perfusion parameters or which combination of parameters is crucial (1. problem), how individual parameters are related, and how imaging parameters, different parameterizations of preprocessing methods as well as different parameter computation methods influence their expressiveness.

For achieving these aims, an interactive visual analysis approach will be suggested. The approach comprises preprocessing methods, data analysis techniques and feature specification methods and arranges them in a proper order for a streamlined investigation of perfusion. The approach facilitates an inspection of inter-parameter relations and of changes due to varying imaging parameters. The interactive feature specification reduces the amount of data for a visual exploration and directs the user to suspicious regions. The specification based on the original perfusion data, perfusion parameters, and data analysis results in conjunction with a rapid visual update of the specification result provide the user with a deeper understanding of the inspected data space. For the non-standardized MR signal intensities, an interactive feature specification may provide an alternative to static tissue classification algorithms.

The techniques which are invented to attain the first three goals shall be applicable to both, cerebral and myocardial perfusion. Despite the differences in imaging as well as in data preprocessing, the resulting data base for subsequent visual exploration and analysis is very similar. It consists of the original 4D data as well as a separate 3D volume for each perfusion parameter. However, the number of slices differs since in myocardial perfusion, stacks of 3-4 slices are usually acquired while in cerebral perfusion, a stack consists of 10-15 slices. Furthermore, different matrix sizes in the range of 128 to 256 might have been used. Both aspects should be considered and should have no effect on the generality of the techniques. Since the overall amount of data is low in both cases, even when perfusion parameters are derived by various computational methods, performance of generating visualizations, exploration and analysis should not pose an issue. The diagnostic meaning of the different parameters is similar in both applications. For example, a small *Integral* together with a small *Slope* (*Up-slope*) and a long *TTP* indicate a perfusion disturbance. In other application areas, e.g., in breast tumor perfusion, such a scenario might be assessed as positive indicating a benign lesion.

Goal 4. To reduce the cognitive effort involved in a mental integration of corresponding regions in perfusion, LE and Cine data and to allow for a more reproducible analysis, the thesis at hand is aiming at the development of integrated visualizations based on the acquired datasets. The visualizations shall facilitate a concurrent analysis of parameters describing perfusion, viability and function. They are to accurately reflect the spatial relations between cardiac anatomy and the derived parameters which are strongly hampered by the standard parameter visualization in a BEP. They shall allow for a differentiation between healthy, hypoperfused, stunned, hibernating, and necrotic myocardial tissue. Only in cases with hibernating tissue or hypoperfused and no or smaller necrotic tissue (mismatch), revascularization may be performed [Strohm et al., 2006].

Chapter 3

Visual Exploration

The diagnostic evaluation of perfusion data and associated perfusion parameters is a challenging and time-consuming task. Perfusion parameters represent a special instance of multiparameter data since they are derived over a multidimensional observation space (n-dimensional data with n=3) and a multidimensional feature space (multivariate data, n=number of parameters). Existent visual exploration techniques are based on a side-by-side display of single-parameter visualizations whose interpretation demands a considerable cognitive effort for comparing corresponding regions. Hence, sophisticated visualization techniques are required that generate an integrated display of several parameters thereby accelerating the exploration.

Perfusion data are often acquired in a scanning protocol together with other data describing different clinical aspects. Together, the data contribute to a global picture of the patient state. The diagnosis of Coronary Heart Disease is a prominent example including scans that characterize the anatomy of the heart and the great vessels as well as scans depicting myocardial perfusion, viability and function. Multiparameter visualizations of perfusion should be integrated with visualizations of information extracted from the other scans thereby supporting a concurrent analysis.

The remainder of this chapter is organized as follows: Section 3.1 is dedicated to work which is related to multiparameter and comprehensive cardiac visualization. Section 3.2 discusses color- and texture-based multiparameter maps for the integrated display of several perfusion parameters. The proposed techniques have been published in [Bendicks, 2004; Oeltze et al., 2005, 2006]. 2D glyph-based visualizations for various application areas and 3D glyph-based visualizations specific to myocardial perfusion are presented in Section 3.3. This work has been published in [Malyszczyk, 2007; Oeltze et al., 2008a,b]. A comprehensive cardiac visualization based on the integration of vascular anatomy, perfusion, viability, and function is described in Section 3.4 and has been published in [Paasche, 2007; Paasche et al., 2007; Oeltze et al., 2006, 2008a]. In Section 3.5, the chapter is summarized and conclusions are drawn. The chapter is completed in Section 3.6 by a review of the glyph-based visualizations with respect to usage guidelines for the integration of glyph-based techniques in medical visualization [Ropinski and Preim, 2008].

3.1 Related Work

This section summarizes relevant work related to the visualization of multiple parameters and a comprehensive cardiac visualization. It is beyond the scope of the thesis to give a complete survey of multiparameter visualization techniques. Instead, the focus is on the exploitation of color and texture, both being applied in the few existing visualization approaches for visually exploring perfusion data, as well as on glyphs representing a standard approach for visualizing multivariate data. The discussion of glyph-based techniques is restricted to the medical domain, in particular, cardiac diagnosis. For an overview of multiparameter visualizations, the reader is referred to [Schumann and Müller, 1999]. A detailed survey on multivariate visualization is is given in [Chen et al., 2008]. State-of-the-art techniques are

found in the proceedings of the IEEE Visualization conference[1] which have been published since 2006 as a special issue of IEEE Transactions on Visualization and Computer Graphics[2]. Parts of this section are based on a recently published survey of the visual exploration and analysis of perfusion data [Preim et al., 2009].

3.1.1 Color- and Texture-based Multiparameter Visualization

The need for an integrated visualization of several parameters has been early recognized also in the medical domain [Levkowitz et al., 1990]. The cognitive effort necessary to scan back and forth for comparing corresponding regions in a side-by-side representation of conventional images is avoided by multiparameter visualizations [Levkowitz, 1997]. They facilitate the detection of more subtle changes between corresponding regions and might reveal features that are not visible in any one of the separate parameter maps [Levkowitz, 1991].

In principle, color may be employed for the integrated visualization of two or three parameters. A straightforward coding would be the mapping by means of the RGB color model which is applied in display monitors. However, this model lacks perceptual linearity since uniform changes in parameter values are not perceived as uniform changes in color [Levkowitz, 1997]. Among the wide-spread color spaces, the HSV space (describing a color by its Hue, Saturation, and Value component) is the best choice since it is perceptually roughly linearized [Ware, 2000]. To direct the attention of the viewer to suspicious regions, conspicuous parameter combinations may be mapped to a red color (Hue) with high saturation and high intensity (Value) [Preim and Bartz, 2007].

In [Levkowitz et al., 1990], T1- and T2-weighted MR images of a patient with a malignant glioma (brain tumor) have been integrated by means of different color models and varying color channels. It could be observed that each visualization emphasized different features in the data. Colored isosurfaces and volume renderings are employed in [Tory et al., 2001] for visualizing renal perfusion based on dynamic SPECT data. Multiple isosurfaces from different points in time are extracted, colored according to the original signal intensities and displayed together. Volume renderings are as well colored with respect to the signal intensities and updated in an animated fashion over time.

Kohle et al. [2002] suggest to apply a colorized temporal Maximum Intensity Projection (MIP) for the exploration of DCE-MRI mammography data. The maximum value is chosen here along the temporal scale. With this approach, voxels characterized by strong dynamics (either in the accumulation or washout phase) are represented by a color which incorporates the accumulation as well as the washout behavior by mapping these values to Value and Hue. As an improvement to MIP, the Closest Vessel Projection (CVP) also known as local MIP, was developed to add depth information to MIP images [Napel et al., 1993]. The most intense voxel along the projection ray is no longer selected; rather, the voxel which represents the first local maximum above a certain threshold is taken. The threshold has to be adjusted to display only the interesting structures. A threshold of 20% relative enhancement has been empirically determined as appropriate for restricting the visualization to the interesting structures of the data. Figure 3.1(a) shows a colored CVP of DCE-MRI mammography data. Both, MIP and CVP are offered as whole-volume visualization techniques and as slab rendering—restricted to a portion of the data characterized by two parallel clipping planes.

A long-term effort on visualizing DCE-MRI mammography data has also been accomplished by Hellwig et al. [2002]. They investigated virtual reality input and output technology

[1] ieeexplore.ieee.org/Xplore/guesthome.jsp (01/16/2010)
[2] www.computer.org/portal/web/tvcg (01/16/2010)

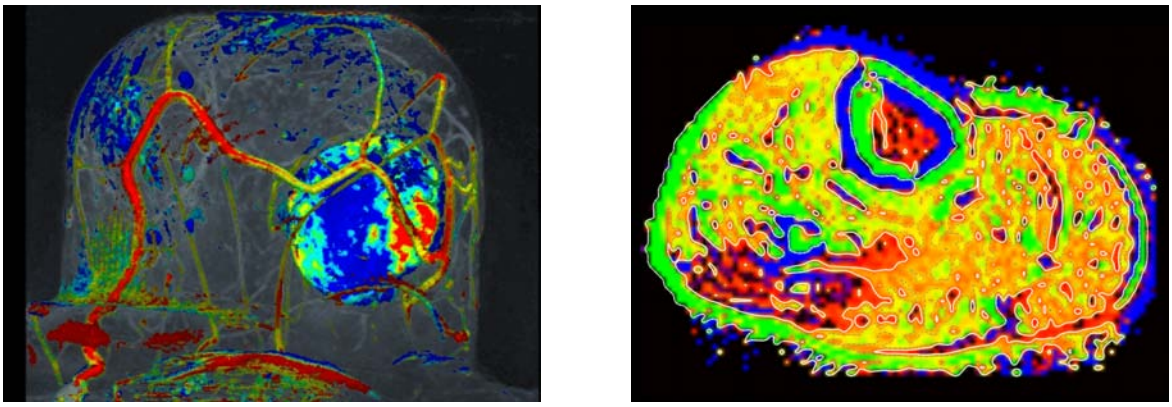

(a) (b)

Figure 3.1: Multiparameter visualization of breast tumor and lower leg perfusion. *(a)*: Breast tumor perfusion. A gray scale MIP of the subtraction volume of two early points in time is combined with a color-coded CVP. The color encodes the dynamical behavior: bright voxels show a strong enhancement for an early period, less intense voxels show less enhancement. A blue color indicates a continuous enhancement for a later period in time, and a green color indicates a plateau in the TIC. Yellow and red colors indicate a rapid washout. *(b)*: Lower leg perfusion. The parameter *Integral* is color-coded and additionally visualized by isolines. (Image *(a)* is courtesy of Sven Kohle, SIEMENS Healthcare. Data in *(b)* is courtesy of Ronald Leppek, Philipps University of Marburg.)

for exploring integrated stereoscopic 3D visualizations of morphologic data and two kinetic perfusion parameters. While the parameters were derived from the DCE-MRI mammography data, a separate scan was acquired providing morphologic information. The integrated visualization of the two aspects has been accomplished based on a 3D texture-based volume rendering. The texture elements encode the morphologic data as well as the perfusion parameters. A predefined 4×4 RGB color matrix is then applied for mapping a rapid and strong accumulation to a bright color and a slow and weak accumulation to a dark color. It was concluded that the integrated stereoscopic display facilitates an improved localization and differentiation of lesions in space. This is further supported by virtual input devices to adjust, e.g., orientation and transparency of the display.

The value of combining color and isolines for inspecting cerebral perfusion and perfusion of the lower leg and pelvic region has been documented in [Preim et al., 2003]. Color is applied to encode one perfusion parameter. Then, isolines connect regions where the investigated perfusion parameter has a certain value (Fig. 3.1(b)). Noise removal is important in order to prevent that many irrelevant small and distracting isolines or relevant but jagged lines result. In contrast to color-coding, isolines are not interpreted at a glance but allow a more quantitative interpretation.

The mapping of signal intensities to color in an animated fashion over time for the analysis of myocardial perfusion has been discussed in [Breeuwer, 2002]. Two new visualization concepts were presented: the *uptake movie* and the *perfusogram*. For generating an uptake movie, the myocardial signal intensities are either color-coded voxel-wise or segment-wise after computing the average intensity. The successive images in the movie then indicate the passage of the contrast agent. The perfusogram maps the averaged signal intensity per segment to color and plots the resulting colors segment-wise over time. Up-take and perfusogram are linked such that the user may navigate through the movie by means of the perfusogram.

The interaction with movable viewing lenses (*Magic Lenses*) has been assessed as useful for exploring multidimensional data [Bier et al., 1993]. In conventional images, digital lenses work as pixel magnifiers facilitating the analysis of small scale phenomena within enlarged visualizations. *Magic lenses* may not only magnify information but also show different information in the lens region. Different color scales may be applied for the lens region and the remaining image part.

The value of color for generating multiparameter visualizations is limited since only two or three parameters may be integrated [Levkowitz, 1997]. Furthermore, the correct interpretation of two or even three perfusion parameters by means of one color cannot be achieved by preattentive vision. To overcome these limitations, the combination of color and texture has been investigated by Levkowitz [1991]. He developed *color icons* which merge different parameters by using color, shape and texture. A color icon is an arbitrarily shaped area that is defined by its boundary, area subdividers, and the areas resulting from the subdivision. These components are associated with attributes such as orientation, size, shape, and color. For generating a multiparameter visualization, the pixel of an image may be replaced by a color icon whose attributes are then modified according to the values of different parameters. The perception of the resulting texture conveys the global distribution of certain parameter combinations.

In [Healey and Enns, 1999], the visualization of multivariate data on an underlying height field is presented. Simple texture patterns are combined with perceptually linearized color scales to increase the number of parameters which may be displayed simultaneously. Perceptual texture elements with varying height and color are arranged with different regularity and density. The approach is demonstrated for the tracking of typhoon conditions based on weather data. To incorporate the geo-spatial reference of the data, the texture elements are placed on a height field representing the land mass. The parameters windspeed, pressure, and precipitation are mapped to the texture element's height, density, and color.

The visualization of multiple fields on the same surface is discussed in [Tayler, 2002]. Color, isolines, height fields as well as orientations of textures might be employed to integrate several parameters in a multiparameter visualization. Height is identified as an attribute that seems to combine well with many other attributes. Applying the orientation of textures was originally presented as *oriented sliver textures* in [Weigle et al., 2000]. Here, the final image is composed by a set of individual layers each of them showing slivers with a specific orientation. The intensity of all slivers in one layer is modified according to one parameter image. Hence, orientation is not used to encode a parameter but to allow for a differentiation of the layers.

3.1.2 Glyph-based Medical Visualization

Glyphs represent a standard technique in the visualization of multivariate data. A glyph is a simple geometric primitive which is positioned with respect to the original data points in space and whose attributes, e.g., color, extent, size, and orientation, are modified according to some represented values. Ropinski and Preim proposed a glyph taxonomy for medical visualization which is based on the two-phase information processing as described in semiotic theory [Ropinski and Preim, 2008]. They distinguish between a preattentive and an attentive processing phase. Preattentive stimuli can be exploited in the first phase only in order to extract basic features of objects in the display, which include, e.g., colors, contrast, and size. Attentive stimuli facilitate a quantitative analysis during the second phase. The preattentive stimuli are glyph shape, glyph placement, and glyph appearance, including color, transparency and texture. Attentive stimuli are glyph legends, the interaction

with glyphs, e.g., repositioning, and composite glyph shapes being composed of several basic glyph shapes. The glyph taxonomy is completed by usage guidelines for the integration of glyph-based techniques in medical visualization. Ropinski and Preim review existing glyph-based medical visualizations with respect to the taxonomy. In the following, relevant parts of this review are summarized and an extended survey of glyph-based visualizations in the cardiac domain is presented.

Kindlmann proposed superquadric tensor glyphs for the visualization of a diffusion tensor [Kindlmann, 2004]. Superquadrics outperform the prevailing ellipsoids by being unambiguously perceivable independent of viewing parameters. Since superquadrics do not allow the visualization of arbitrary diffusion directions, [Domin et al., 2007] propose deformable spheres. Glyph placement has a crucial impact on the perception of glyph aggregations. Kindlmann and Westin propose a glyph packing strategy based on a particle system which distributes the glyphs such that the undue visual emphasis of the regular sampling grid of the data is removed [Kindlmann and Westin, 2006].

Several glyph-based visualizations have been presented in the cardiac domain. Choi et al. [2003] apply glyphs for visualizing ventricular function parameters obtained by fitting a heart model throughout the cardiac cycle in cine data. Their visualization supports a quantitative parameter analysis. They attach great importance to a perceptually easy interface for diagnostic and patient monitoring applications.

The reconstruction of heart muscle fibers from MR-Diffusion Tensor Imaging (DTI) data is discussed in [Zhukov and Barr, 2003]. Colored cubes are applied for visualizing the tensors. The cubes are scaled and oriented according to the three eigenvalues and the corresponding eigenvectors, respectively. The glyph color is represented as RGB triple with the components encoding the x-, y-, and z-value of the largest eigenvector. The glyphs are visualized voxel-wise and slice-based for axial slices of the MR-DTI data. They are integrated in slice-based visualizations of the anisotropy measure. A fiber tracking algorithm is presented reconstructing myocardial fibers which are then rendered applying illuminated streamlines.

In [Wünsche et al., 2004], glyphs are employed for visualizing the myocardial strain which has been computed based on a model and finite element simulations. The myocardial deformation is here characterized by a strain tensor. The myocardial displacement between end diastole and end systole may be visualized by employing vector arrows. Color-coded ellipsoids facilitate an encoding of the full tensor information (Fig. 3.2(a)). Multiple regions of the glyph are colored depending on the sign of the eigenvalues thereby giving information on the present contraction or relaxation. The visualization of eigenvector fields is achieved by means of streamlines, hyperstreamlines, Line Integral Convolution, and isosurface rendering each of them revealing certain features in the data.

The superquadric glyphs introduced in [Kindlmann, 2004] have been applied to canine myocardial MR-DTI data and high-resolution myocardial DENSE strain data [Ennis et al., 2005]. The glyph visualization is not embedded in the anatomic context but presented either next to a short-axis or a long-axis slice of the original data or next to a combination of short- and long-axis slices (Fig. 3.2(b)). It is restricted to a user-defined region of interest. The orientation of the glyphs reflects the arrangement of myocardial fibers. The glyphs are colored by means of a color scheme that highlights orthotropy (three distinct eigenvalues).

Mlejnek et al. [Mlejnek et al., 2005] proposed the *Profile Flag*, an intuitive glyph-based tool for browsing and annotating of temporal data. It enables the visualization of spatial or temporal curves closely connected to the rendering of the anatomic structure of the data without removing any parts thereof. The probed curve data is visualized on the banner of the glyph. The Profile Flag can be positioned on and dragged along the surface or inside

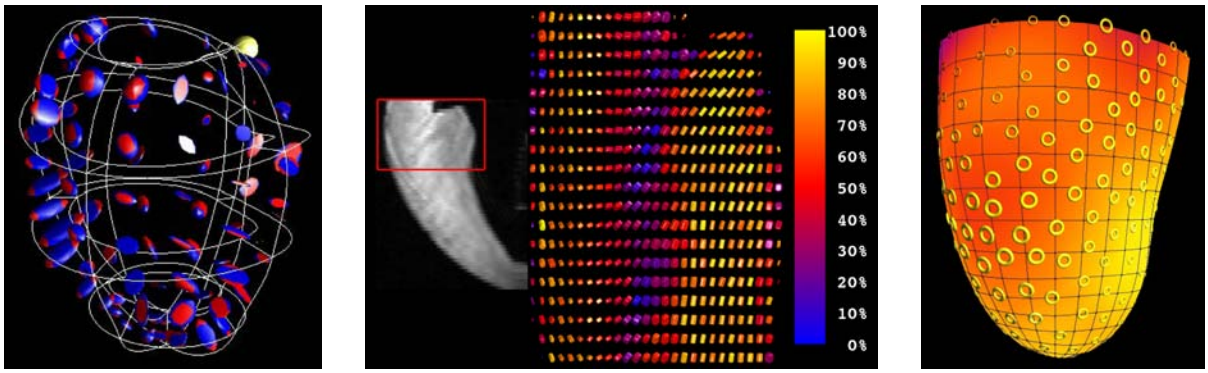

(a) (b) (c)

Figure 3.2: Glyph-based visualization for cardiac analysis. *(a)*: Visualization of myocardial strain. The strain tensors in the left ventricle are visualized by means of colored ellipsoids. The color encodes contraction and relaxation. *(b)*: Superquadrics are employed for visualizing myocardial structure. The visualization is restricted to a region around the anterior papillary muscle. The region has been defined in a gray-scale representation of a long-axis slice (left). The glyphs encode fiber direction and orthotropy (color). *(c)*: Glyph visualization of myocardial perfusion and function based on SPECT data. The left ventricular surface is colored according to *Up-slope* under stress. The supertorii encode *Up-slope* at rest (color), the difference of both *Up-slopes* (size), myocardial wall thickening (roundness) and a self-defined level of conspicuousness (opacity). (*(a)* is adapted from [Wünsche et al., 2004] and used with permission of Burkhard Wünsche, University of Auckland. Image *(b)* is courtesy of Daniel B. Ennis, University of California, Los Angeles. Image *(c)* is courtesy of Timo Ropinski, University of Münster.)

of the inspected anatomical object causing an update of the displayed information. For 3D dynamic perfusion data, the probed information is taken along the time axis (TICs). The Profile flag has been proven to be useful for annotating DCE-MRI mammography data [Mlejnek et al., 2006].

The glyph-based visualization of two-dimensional myocardial strain rate using MR velocity mapping is presented in [Haraldsson et al., 2008]. Myocardial strain tensors were derived from myocardial velocity measured using phase contrast velocity mapping. They are visualized by means of ellipses encoding the two eigenvectors and the two eigenvalues via orientation and size, respectively. The ellipses are positioned voxel-wise in a short-axis view of the original data. They are superimposed onto unit circles which facilitates the detection of expansion (outside the circle) and compression (inside the circle) for both, the x- and the y-direction.

Ropinski et al. [2007] apply superquadrics for a hybrid visualization of PET and CT data. They put special emphasis on avoiding visual clutter by means of dedicated placement strategies, on a user-interface for easily adjusting the glyph configuration, and on glyph legends. They extend their approach and apply it to SPECT data for CHD diagnosis [Meyer-Spradow et al., 2008]. Supertorii are employed which encode rest/stress perfusion parameters as well as myocardial wall thickness and thickening. The torii are positioned in 3D on the surface of the left ventricle (Fig. 3.2(c)). The view is linked with slice views of the original data. Once a glyph is picked in 3D, the corresponding slices as well as the glyph position are highlighted in 2D. A tooltip provides access to quantitative data associated with the glyph.

In a recent publication, Peeters et al. [2009] apply line segments and ellipsoids with a fixed shape for visualizing myocardial fiber orientation based on MR-DTI data. They integrate

a cross-sectional view of fiber orientations with fiber tracking results visualized by means of colored thin tubes. Also original slices may be integrated as textured planes. The focus of their work is on a real-time exploration of the data by dragging the cross-sectional view through the dataset. Interactive frame rates are achieved using a dedicated local ray casting which avoids expensive data preprocessing.

3.1.3 Comprehensive Cardiac Visualization

This subsection is dedicated to visualization approaches which facilitate a concurrent analysis of at least two separate scans characterizing different aspects of the heart state. The focus is on scans typically acquired in a cardiac MRI scanning protocol (Fig. 2.17). Besides being based on SPECT data, the previously discussed glyph-based visualization of perfusion and function (Fig. 3.2(c)) belongs to this category [Meyer-Spradow et al., 2008].

Perfusion and Viability. Breeuwer et al. [2003] suggest a combination of rest/stress perfusion and LE data supporting the differentiation between healthy, hypoperfused and necrotic tissue. At first, the myocardium is divided into user-defined segments. Next, the myocardial perfusion is analyzed and the MPRI is derived segment-wise from the stress and rest *Up-slope*. Thresholding is applied on the MPRI to detect hypoperfused tissue. Then, the necrotic tissue is segmented in the LE data and each myocardial segment is tested for the inclusion of necrotic tissue. Finally, all results are concurrently visualized in a Bull's Eye Plot (BEP) or superimposed on the myocardium in original short-axis slices. The MPRI is color-coded for each segment. Segments containing necrotic tissue are shown in gray and a strip pattern is superimposed on segments which have been classified as hypoperfused.

The software assistant `MeVisCardioPerfusion` has been introduced in [Kühnel et al., 2006]. It facilitates the threshold-based segmentation of suspicious regions in parameter maps and subtraction images. A curve view shows the TIC corresponding either to the segmented tissue, to a single voxel or to segments obtained from a division of the myocardium. Furthermore, a BEP communicates segment-wise analysis results. A 3D BEP is generated by extracting the left-ventricular surface from the LE data and coloring it according to the BEP segments. A prerequisite is the registration of the LE and the perfusion data. Necrotic tissue may be segmented in the LE data, reconstructed as a surface and superimposed on a transparent visualization of the 3D BEP. The 3D visualization opportunities have been extended in [Hennemuth et al., 2007]. A texture representation of a parameter map may be integrated in the visualization of ventricle and scar. This approach allows for a fine-granular analysis of the perfusion in the scar region as well as in the immediate vicinity (*peri-infarct zone*).

Viability and Function. The identification of hibernating myocardium is presented in [Noble et al., 2004]. At first, LE and Cine data are aligned by a rigid registration of the end-diastolic Cine images to the epicardial contours in the LE images. Normalized mutual information is employed as a similarity measure. Next, necrotic tissue is segmented manually and its percentage transmurality is computed segment-wise. Finally, the percentage wall thickening is derived from end diastole and end systole in the Cine data. To combine the information, a function is defined that weights transmurality and wall thickening. It exhibits a maximum (high chance of hibernating tissue) in case of no transmurality and strongly reduced thickening. Finally, the function results are color-coded on a surface representation of the left ventricle.

The software assistant HeAT for the analysis of left ventricular remodeling after myocardial infarction in 4D MR follow-up studies is introduced in [Säring et al., 2006]. To combine information from LE and Cine data, both datasets are registered by means of semi-automatic rigid registration based on mutual information as a similarity measure. Then, necrotic tissue including areas of microvascular obstruction is segmented in the LE data using a data-driven approach. Myocardial wall thickening is computed by means of the centerline method (Subsec. 2.2.3.6). Next, the myocardium is divided radially in each slice of the registered data into 100 segments and the percentage of necrotic tissue, microvascular obstruction, as well as wall thickening is computed for each segment. Finally, a diagram plot is presented to the user showing curves which have been generated by plotting the percentage values over segments. In an extension of HeAT, a transformation field describing the heart motion in the Cine data over all cardiac phases is computed and applied to the necrotic tissue thereby generating a beating LE sequence [Säring et al., 2009].

Morphology and Perfusion. The 3D fusion of SPECT perfusion and CXA data is presented in [Schindler et al., 1999]. The coronary tree is reconstructed from biplane projections and the left ventricular surface is extracted from interpolated SPECT data. The 3D-representation of the coronary arteries together with a mapping of the perfusion data to the ventricle allow for an accurate assignment of particular myocardial regions to the supplying vessels. Since the reconstruction of the coronaries from CXA data induces spatial distortion and CXA is an expensive and invasive procedure, [Nakajo et al., 2005] studied the fusion of CTCA and SPECT. After the coronary arteries and the left ventricle are segmented and visualized in 3D, the SPECT data are mapped to the ventricle.

Termeer et al. [2008] do not apply perfusion scans but derive the myocardial perfusion from the coronary anatomy in a computational simulation. The coronary arteries as well as both ventricles are extracted from a whole-heart CT scan. Color, isolines and texture are then used to map the simulation results onto the surface of the left and the right ventricle. Dedicated exploration facilities are provided to explore the result. The user may select a region on the ventricular surface causing the display of arrows which originate at the supplying coronary branches and point at the region. The arrow width encodes the relative supply by or the likelihood of being supplied by each of the branches. Furthermore, the user may induce a stenosis of an arbitrary degree by picking a branch at the desired location. The perfusion simulation is then recomputed and the visualization is updated such that the affected territories are highlighted. While the visualization was rated as very useful by clinical experts they cast doubts on the sufficient realism of the simulation. The effects of vasodilation and collateral blood supply are neglected by the simulation.

Morphology and Viability. The combination of whole-heart MRI data depicting the cardiac anatomy and LE data has been studied in [Termeer et al., 2007]. Termeer et al. introduced a volumetric extension of the BEP (VBEP), which preserves continuity and the volumetric nature of the left ventricular wall thereby improving a transmurality analysis. The coronary arteries, which have been extracted from the whole-heart data, are superimposed on the VBEP in a centerline rendering. The VBEP is integrated in a 3D view showing the ventricles and the coronaries. The ventricles have also been segmented in the whole-heart data. The left ventricle is rendered as a highly transparent surface. The left ventricle extracted from the LE data is superimposed as a volume rendering with an opacity modulation according to the scar classification function. The coronary arteries as well as the right ventricle are rendered in an opaque mode and hence, may occlude scarred tissue.

Selective masking of the ventricle depending on the viewpoint as well as semi-transparent vessel rendering with outline highlighting resolves occlusion issues. The VBEP is linked with the 3D view such that the user may select a region in the VBEP which is then emphasized in the anatomical view.

In [Hennemuth et al., 2008a], a new segmentation method is proposed for extracting necrotic tissue from CT LE images. A 3D view shows the left ventricle and the necrotic tissue rendered as surfaces. The color and opacity of the left ventricular surface are modified according to its distance to the scar. A red solid color indicates that no necrotic tissue exists between endocardial and epicardial layer while transparent blue indicates a very small distance, i.e. high transmurality. The result is then fused in a software prototype with the coronary anatomy from CTCA data. The arteries are volume rendered and superimposed on the ventricle. The user may define a starting point and an endpoint along a branch causing the computation of a curved multiplanar reformation (CMPR). The reformatted view facilitates an assessment of the vessel course which cannot be achieved by simple axial slices. The user may define cross MPRs in the CMPR view to analyze the vessel diameter at a specific position as well as the course of the diameter.

Integrating Three Scans and More. A comprehensive analysis of MR rest/stress perfusion, LE data and a whole-heart MRCA is presented in [Hennemuth et al., 2008c]. A detailed discussion of dedicated image registration methods and algorithms for image analysis, e.g., for coronary tree segmentation, the automatic segmentation of necrotic tissue and the semi-automatic delineation of hypoperfused tissue, are included. For visualization purposes, the left ventricle is extracted from the LE data and shown as highly transparent surface (Fig. 3.3(a)). It is colored with respect to the distance to the infarction scar which is superimposed as opaque surface. The vasculature is segmented in the MRCA data and included by means of a surface rendering. The hypoperfused regions which have been delineated by thresholding a perfusion parameter are included as contours. A texture representation of an original image slice of any of the datasets may be included and provide further spatial reference, e.g., the location of the right ventricle. The benefit of a comprehensive analysis could be documented for 21 datasets of healthy volunteers and diseased patients.

The integrated analysis of morphology and myocardial function based on CT data as well as perfusion and viability based on MR data in a software assistant is discussed in [Kühnel et al., 2008]. In a 3D view, the coronary arteries are volume rendered and superimposed on a surface rendering of the left ventricle extracted either from Cine or LE data. The surface may be colored according to myocardial wall thickening, the existence of necrotic tissue or transmurality. The infarction scar may be rendered as an opaque surface inside the transparent ventricle. The 3D view is linked with 2D slice views of the original data. In order to establish a correspondence, the 2D views may be overlaid with segmentation masks and color-coded analysis results also applied for surface coloring in 3D. An interactive BEP is applied for visualizing perfusion parameters, wall thickening or transmurality. It is linked with the 3D view by exploiting the AHA correspondence between coronary branches and supplied myocardial segments (Fig. 2.22). The linkage has been introduced in [Oeltze et al., 2006] and will be discussed in more detail in Subsection 3.4.1.2. The vasculature may be analyzed in CMPRs and MPRs.

Termeer combined the integrated visualization of morphology and viability [Termeer et al., 2007], and of morphology and perfusion [Termeer et al., 2008] and added function as a further cardiac parameter [Termeer, 2009]. The left ventricle and the coronary arteries are segmented in whole-heart MR data. The ventricular surface is colored according to

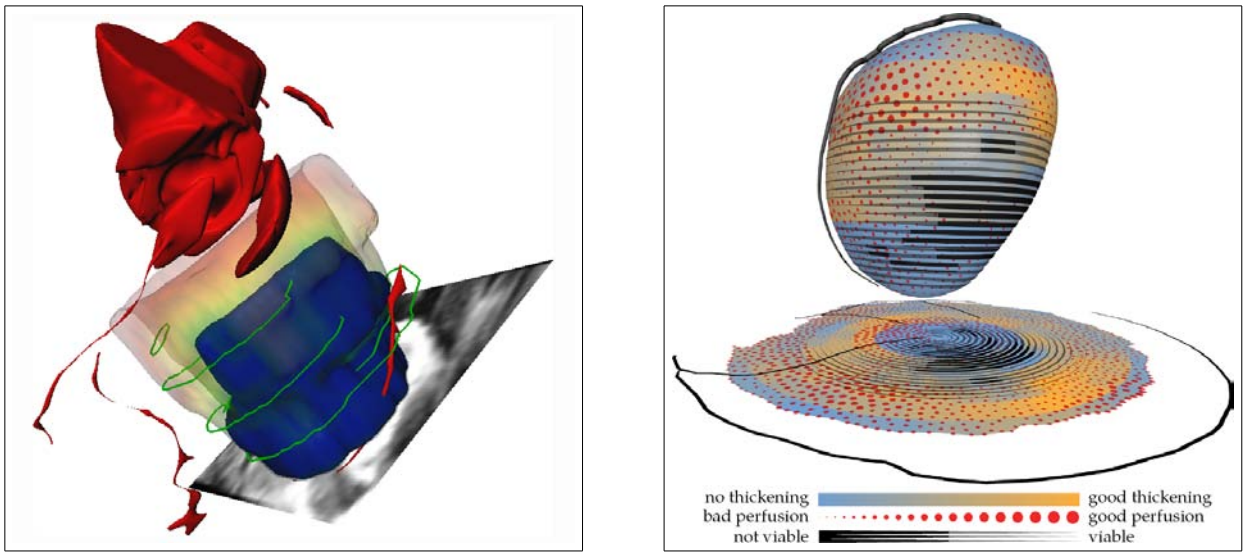

(a) (b)

Figure 3.3: Integrated visualization for comprehensive cardiac analysis. *(a)*: Integrated visualization of vasculature, the left ventricle (transparent surface), necrotic tissue (blue, opaque surface), hypoperfused regions (green contours), and a texture representation of an original slice from the Late Enhancement data. The color of the left ventricle encodes its distance to the infarction scar. *(b)*: Integrated visualization of vasculature (black vessel centerlines), wall thickening (surface color), perfusion parameter *Up-slope* (size of dots), necrotic tissue (striped pattern overlay), and transmurality (stripe width). The left ventricle has been unfolded and projected onto a plane below. (Image *(a)* is courtesy of Anja Hennemuth, Fraunhofer MeVis. Image *(b)* is from [Termeer, 2009] and is used with permission of Maurice Termeer, Philips Healthcare.)

myocardial wall thickening (Fig. 3.3(b)). One perfusion parameter is encoded by dots of varying size which are placed on the surface. The location of the scar and its transmurality are indicated by a uniformly colored stripe pattern. The width of the stripes is modified according to the transmurality. The ventricle is unfolded and projected onto a plane below establishing an extended BEP view. The centerlines of the coronaries are rendered as tubes and superimposed on the ventricle as well as on the projection.

3.2 Multiparameter Maps

Multiparameter maps are an extension of the conventional parameter maps introduced in Subsection 2.1.4. They represent an integrated visualization of several perfusion parameters which supports a comparative analysis in a suspicious region. Bendicks [2004] and Oeltze et al. [2005, 2006] investigated methods where color (for one perfusion parameter) is combined with another visualization attribute for displaying a second parameter. In particular, height fields, flexible lenses and color icons were employed to combine several parameters within a single image. Multiparameter maps were created based on precomputed parameter volumes, where the respective perfusion parameter is represented for each voxel of the original dataset. The design of the maps was inspired by related work summarized in Subsection 3.1.1.

3.2.1 Colored Height Fields

According to Tayler [2002], height combines well with other visualization attributes in a multiparameter visualization. Colored height fields enable the integrated visualization of two parameter maps. A 3D elevation profile is generated based on the pixel-values of the first parameter map. In a next step, the resulting profile is colored according to the pixel-values of the second parameter map and an arbitrary color look-up-table (Fig. 3.4(a)). The profile may be freely rotated such that initially occluded parts become visible. The mapping to height is scalable. It is initially adapted to the domain of the first parameter. A local illumination simplifies the detection of small differences in height (Fig. 3.4(b)). The isometric projection and a linear interpolation of the parameter values guarantee the non-ambiguous relation between visualization and underlying data. As a natural mapping, the parameters *PE* or *Integral* should be mapped to the height parameter since they convey the magnitude of CA accumulation.

An issue in using height fields is the occlusion of interesting parts by high elevations. This may be partially solved by rotating the height field. Further support is provided by a contour plot based on the parameter that is mapped to height. This plot may be superimposed on an original slice of the parameter volume and positioned beneath the height field (Fig. 3.5(a)). However, special care must be taken by the user for specifying expressive isovalues. In an initial setting, a fixed number of values is equally distributed within the parameter domain. The contour plot may as well be used to convey a third perfusion parameter.

The visualization of myocardial perfusion by means of height fields poses an intrinsic problem. The circular shape of the myocardium hampers the user's spatial orientation. However, physicians are used to communicate their findings with respect to anatomic landmarks, such as the septum. To improve the orientation, an original slice of the perfusion dataset may be presented together with the height field (Fig. 3.5(b)). The right ventricle

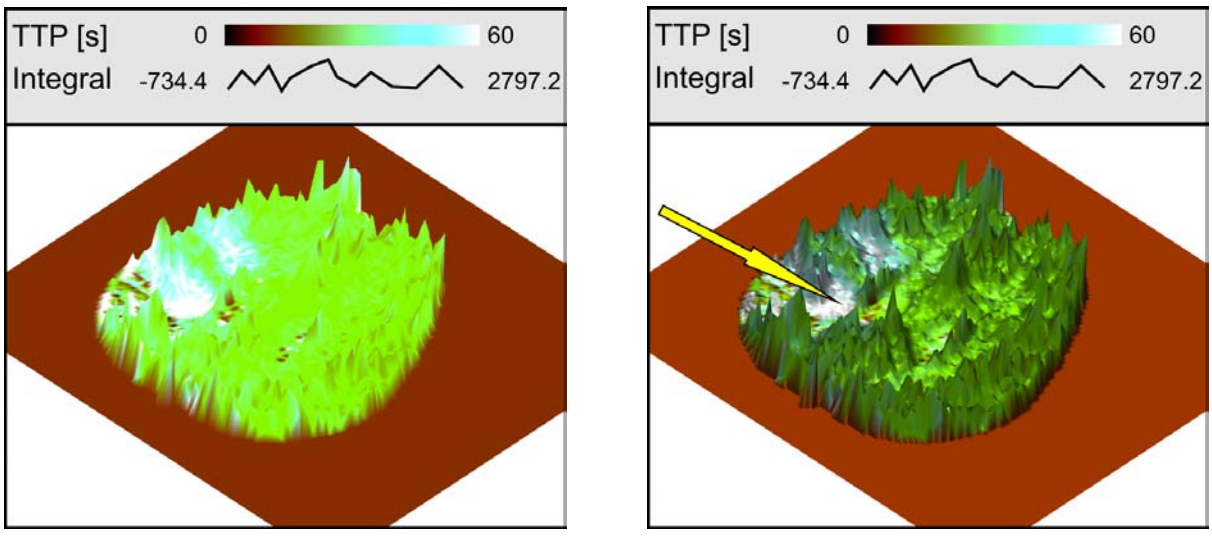

(a) (b)

Figure 3.4: Colored height field for analyzing cerebral perfusion. *(a)*: The parameters *Integral* and *TTP* are mapped to height and color, respectively. *(b)*: A local illumination simplifies the detection of small differences in height. The infarction core appears as a whitish valley (arrow). Tissue with a depleted perfusion surrounds the core and is represented by small elevations in white to light blue. (Data is courtesy of Jonathan Wiener, Boca Raton Community Hospital.)

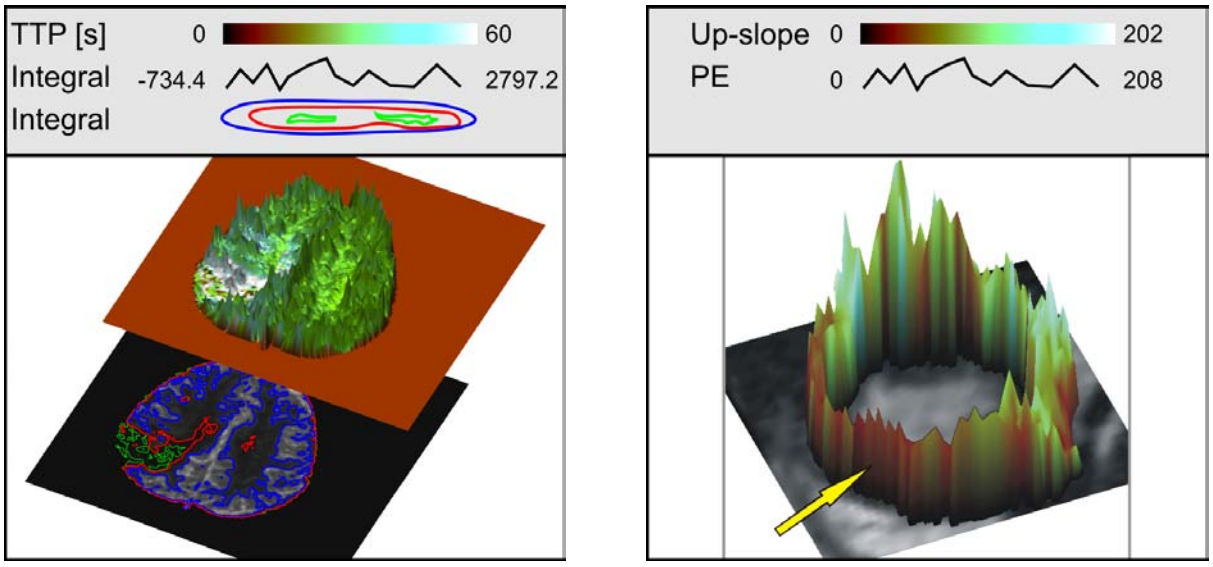

(a) (b)

Figure 3.5: Improving readability and spatial orientation in using colored height fields. *(a)*: A contour plot based on the parameter *Integral* is superimposed on the corresponding slice of the parameter volume and positioned beneath the height field. The contours support the assessment of regions that are occluded by high elevations in the height field. *(b)*: Assessment of myocardial perfusion. The parameters *PE* and *Up-slope* are mapped to height and color, respectively. Small elevations (diminished perfusion) and dark colors (delayed perfusion) represent ischemic territories (arrow). The corresponding original slice at an adjustable point in time serves as context information. (Data in *(a)* is courtesy of Jonathan Wiener, Boca Raton Community Hospital. Data in *(b)* is courtesy of Stefan Miller, University Hospital Tübingen.)

and hence, the septum may be easily identified in such a slice. The user may browse through the individual points in time to observe the CA accumulating in the right ventricle or the left ventricular lumen.

3.2.2 Flexible Lenses

The interaction with movable viewing lenses has been rated as useful for exploring multidimensional data [Bier et al., 1993]. For parameter maps, lenses may show information relating to one parameter either in the context of the original perfusion data (Fig. 3.6, 3.7(a)), in the context of a map of another parameter, or both (Fig. 3.7(b)). In cerebral perfusion diagnosis, synchronized lenses may be used to exploit the symmetry of the brain in axial views [Wintermark et al., 2005b]. A lens is mirrored on a relocatable, vertical line of symmetry to detect differences between both hemispheres (Fig. 3.6(b)). Moving either of the lenses causes an automatic repositioning of the other one.

When applying flexible lenses, the user starts by selecting a foreground and a background parameter (for example *Integral* and *MTT*) and then moves a lens (a rectangle or an ellipse) to select either of the parameter set. Inside the lens region, displays of the foreground and background parameter are combined by means of alpha-blending thus combining an opaque background and translucent foreground to imitate transparency (Fig. 3.6). With an alpha value equal to 1, only the foreground parameter is represented (Fig. 3.7).

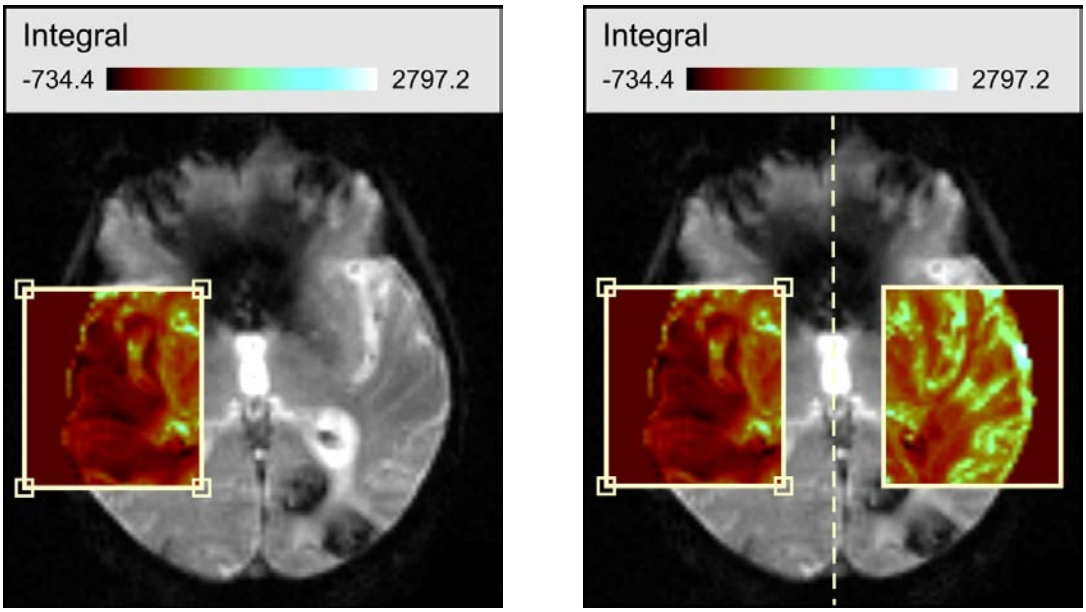

(a) (b)

Figure 3.6: Flexible lenses for analyzing cerebral perfusion. *(a)*: A flexible lens is positioned over parts of the right hemisphere (appears left in the image). The parameter *Integral* is projected through the lens and displayed in the context of the original perfusion data. Within the lens, the information from both entities is combined via alpha-blending. *(b)*: Synchronized lenses support the comparison of both hemispheres. The initially defined lens is mirrored on a relocatable, vertical line of symmetry. The infarction core is revealed in the right hemisphere. It is characterized by significantly lower *Integral* values as compared to the contralateral side. (Data is courtesy of Jonathan Wiener, Boca Raton Community Hospital.)

3.2.3 Color Icons

The application of color icons is inspired by [Levkowitz, 1991]. This technique harnesses color and texture perception to create images that convey multiparameter distributions. A color icon is a generalization of a pixel having a multitude of attributes and features. In theory, an arbitrarily high number of parameter maps can be integrated into one visualization by means of color icons. However, to establish an initial controllable testing scenario, their number has been limited here to four. Each pixel of the original map is replaced by a color icon consisting of four new, quadratically arranged pixels (inset of Fig. 3.8). The boundary of the icon (black square) as well as the two area subdividers (white lines) are neglected for the parameter mapping. A mapping to a user-defined color is defined for each pixel of the icon. Finally, the parameter values of the corresponding pixels in up to four parameter maps are color-coded and assigned to the newly generated pixels (Fig. 3.8). The perception of the resulting texture conveys the global distribution of certain parameter combinations. The user may zoom in on an interesting structure for better recognition of the underlying texture. The integrated visualization in Figure 3.8 facilitates the inspection of areas exhibiting a delayed perfusion (visible in the TTP and MTT maps) in the context of the major blood vessels (visible, e.g., in the *Integral* map as dark, tubular regions). Furthermore, it supports a differentiation of white and gray matter which is not feasible solely based on the TTP or the MTT map. A drawback of the integrated visualization is the worse separation of penumbral tissue as compared to the TTP map (red encircled region).

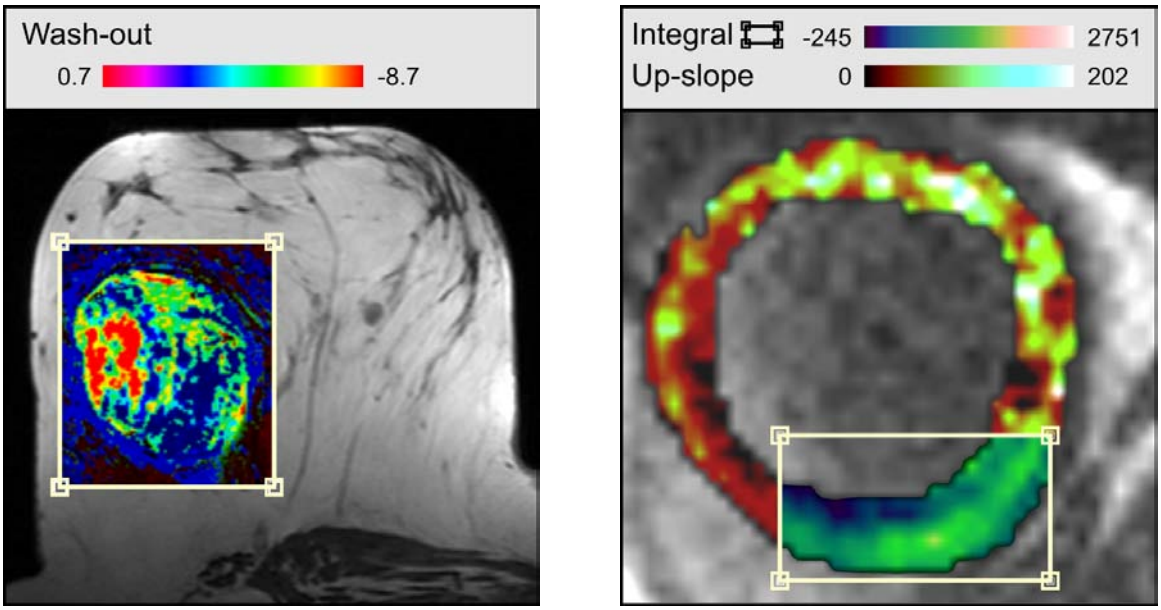

(a) (b)

Figure 3.7: Flexible lenses for analyzing breast tumor and myocardial perfusion. *(a)*: Exploration of DCE-MRI mammography data with a lens. The parameter *Wash-out* is projected through the lens and displayed in the context of the original perfusion data. A blue color indicates a continuous enhancement for a later period in time, a green color indicates a plateau in the time intensity curve. A yellow and in particular a red color indicate a strong CA washout. The latter is characteristic for malignant lesions. *(b)*: Analysis of myocardial perfusion. The parameter *Up-slope* is displayed for the myocardium in the context of the original perfusion data. The parameter *Integral* is projected through a user-defined lens. Dark inferior and septal regions indicate a perfusion defect. (Data in *(a)* is courtesy of Jonathan Wiener, Boca Raton Community Hospital. Data in *(b)* is courtesy of Stefan Miller, University Hospital Tübingen.)

3.2.4 Refined Bull's Eye Plot

A BEP can be considered as an abstract parameter map communicating results from a segment-wise analysis of the myocardium (Subsec. 2.2.4). In a rest/stress comparison, two BEPs showing the same perfusion parameter at rest and under stress may be displayed side-by-side to identify segments where perfusion defects first appear or become worse with stress. In order to simplify a mental integration of rest and stress perfusion in one myocardial region, a refined BEP was introduced in [Kuß, 2006; Oeltze et al., 2006]. Each segment ring is bisected by a circular arc, thus, doubling the number of segments. The resulting outer and inner rings represent the stress and the rest state, respectively (Fig. 3.9). This circular bisection ensures that neighboring segments in the plot are adjacent in the myocardium as well and that they show the same state. Compared to the original variant in [Oeltze et al., 2006], the segments may be visually separated by a gap (gray ring) for better recognizability. A reliable rest/stress comparison requires an accurate registration of the two datasets prior to the analysis. The refined plot may also be used for comparing two different perfusion parameters of either rest or stress perfusion.

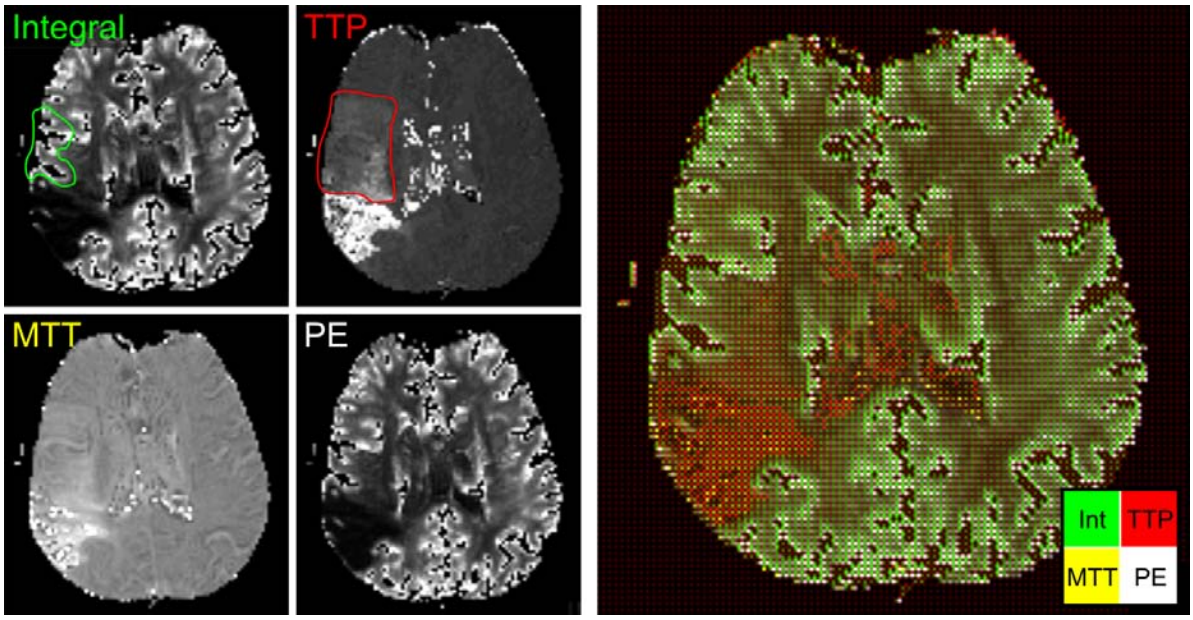

Figure 3.8: Color icons for analyzing cerebral perfusion. The four leftmost images show parameter maps based on *Integral*, *TTP*, *MTT*, and *PE*. All maps correspond to the same slice. In the *Integral* and *PE* map, major blood vessels can be observed (green encircled, dark, tubular regions). Penumbral tissue is revealed in the *TTP* map (red encircled region). The rightmost image represents an integrated visualization of the four maps by means of color icons. The color icon template is shown as an inset. The infarction core appears as a reddish yellow region characterized by a delayed (high *TTP* and *MTT* values) and depleted (small *Integral* and *PE* values) perfusion. The ventricles (butterfly-shaped region in the middle) are not part of the ischemic tissue. However, they show perfusion characteristics similar to the core since no contrast agent arrives in the cerebrospinal fluid filled ventricular system. (Data is courtesy of Jonathan Wiener, Boca Raton Community Hospital.)

3.3 Glyph-based Visualizations

Ropinski and Preim proposed 8 usage guidelines for the integration of glyph-based techniques in medical visualization [Ropinski and Preim, 2008]. The third guideline stresses the importance of an intuitive parameter mapping. In cases of a semantic correspondence between a parameter and a glyph attribute, the parameter should be mapped to this attribute. The following Subsection 3.3.1 is dedicated to the definition of such an intuitive parameter mapping for 2D glyph-based visualizations of perfusion parameters. The 3D glyph-based visualization of myocardial perfusion is presented in Subsection 3.3.2. It is embedded in an anatomical representation of the left ventricle following the eighth guideline which recommends a hybrid visualization including the spatial context.

3.3.1 Intuitive Perfusion Parameter Mapping to 2D Glyph Shapes

The integrated glyph-based visualization of multiple perfusion parameters has been presented in [Malyszczyk, 2007; Oeltze et al., 2008b] with a focus on an intuitive mapping of perfusion parameter values to glyph shape. Intuitive mapping here refers to the generation of an easy to learn glyph coding of CTC shape, e.g., by mapping parameter *Integral* (area below the curve) to glyph size, and *Slope* (steepness of the ascending curve) to glyph orientation (Fig. 3.10). Medical users should benefit from such a mapping since they are trained to infer tissue characteristics from the shape of the CTC.

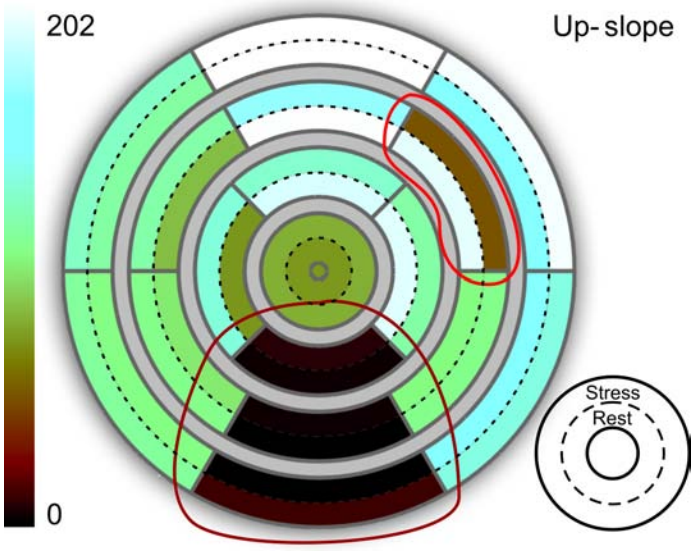

Figure 3.9: Integrated visualization of the parameter *Up-slope* for the rest and stress state in a refined Bull's Eye Plot. Dark regions mark the diminished perfusion. An area with significantly reduced perfusion is revealed that spans all inferior segments (lower encircled region). The corresponding Late Enhancement scan shows necrotic tissue in this area. In the anterolateral segment of the mid-cavity (upper encircled region), a perfusion defect is revealed that may have remained unnoticed if perfusion was only examined at rest.

3.3.1.1 Glyph Design and Placement

Glyph design and placement are non-trivial tasks. Dimensionality of the representation, glyph layout, glyph shape, as well as the number of glyphs have to be carefully chosen. Considering that medical scientists are used to a slice-based exploration in clinical routine, a 2D slice-based glyph placement has been favored. The 2D glyph shapes are presented within the context of a slice of the original perfusion dataset. The slice is rendered as a texture on a 2D plane and scaled such that a single texel (texture element similar to a pixel in an image) covers more than one pixel on the screen. The glyphs are laid out following a dataset-driven placement. They are placed texel-wise in a regular fashion for each slice (Fig. 3.11(a)). To avoid visual irritations caused by resulting grid patterns, the glyph positions are slightly jittered about the texel centers [Laidlaw et al., 1998] (Fig. 3.11(b)). For testing purposes, several simple glyph shapes with different degrees of freedom (in parentheses) were implemented: circular discs (color, size), rectangles (color, horizontal and vertical extent), ellipses (color, size, orientation), toroids (color, size, roundness, thickness), and oriented toroids (equal to toroids plus orientation). Most of the attributes allow an intuitive mapping as illustrated by Figure 3.10. The parameters *TTP* and *MTT* should be mapped to the horizontal extent of a glyph thereby imitating the length of a time bar. Parameter *PE* should be mapped to the vertical extent since it characterizes the maximum of CA accumulation. Since *Integral* represents the overall amount of accumulated CA, it should be mapped to glyph size. The different slope parameters, *Slope*, *DownSlope*, and *MITR*, should be mapped to a glyph's orientation. Besides facilitating an intuitive mapping, the attributes horizontal extent, size, and orientation have been identified as preattentive visual features [Treisman and Gormican, 1988; Treisman and Gelade, 1980; Julész and Bergen, 1983]. The preattentive phase is the initial phase of perception where stimuli are perceived rapidly and

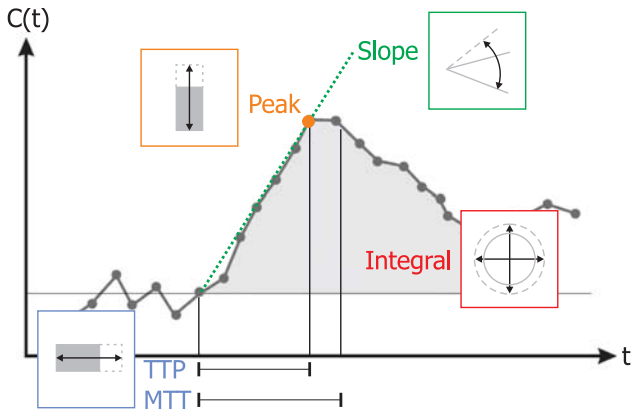

Figure 3.10: A typical concentration-time curve in cerebral perfusion annotated with the essential parameters. Guidelines for an intuitive mapping of parameters to glyph attributes are indicated, e.g., *TTP* should be mapped to horizontal extent, *Slope* to orientation and *Integral* to size.

in parallel. Another preattentive feature that will be exploited in the following is color, more precisely, the hue component [Nagy and Sanchez, 1990].

A simple yet promising alternative glyph shape for assessing cerebral perfusion is the triangle. Its application is inspired by the observation that in a CTC, the first pass of the CA may be well represented by a triangular shape (Fig. 2.7(b)). This observation is not necessarily transferable to myocardial perfusion since the scanning duration is often too short to cover the entire CA washout. However, if the focus is not on a correct depiction of the parameter *DownSlope*, triangles may be applied here as well. The *DownSlope* has not been reported in clinical literature as one of the essential parameters neither in cerebral nor in myocardial perfusion. The parameters *PE* and *TTP* are sufficient for constructing the triangle. The remaining perfusion parameters are inherently coded by the construction result. The vertical distance from the base of the triangle to its apex is determined by *PE*. The horizontal location of the apex with respect to the base is determined by *TTP*. The length of the base corresponds to the length of the first pass in healthy tissue. Though this may lead to an incorrect depiction of the *DownSlope* in infarcted tissue, it visually emphasizes the differences in *TTP* between healthy tissue, penumbra and core. The length of the base has been derived from the CTC of a user-defined region of interest. The triangle provides an almost complete coding of the perfusion parameters and the cognitive effort in inferring the CTC shape from the glyph should be minimal. It is consistent with the request for an intuitive glyph shape as formulated in the sixth guideline for the integration of glyph-based techniques in medical visualizations [Ropinski and Preim, 2008].

3.3.1.2 Multi-resolution Glyph Display

Initial tests of the glyph-based visualizations showed that a texel-wise glyph placement results in very small glyphs due to the limited space per texel (Fig. 3.11). For example, a screen area of 512×512 pixels reserved for the texture display of a dataset matrix $M = 128 \times 128$ would lead to an upper glyph size bound B of 4×4 pixels. This glyph size prevents the readability of subtle changes in glyph shape and color (*small size color blindness*). It strongly hampers a legible coding of a large parameter domain while complying with a minimally perceivable glyph size and the upper bound. A straightforward uniform scaling of glyph size leads to overlapping and z-fighting artifacts. Hence, a multi-resolution glyph-display incorporating different resolution layers has been implemented (Fig. 3.12). The bottommost

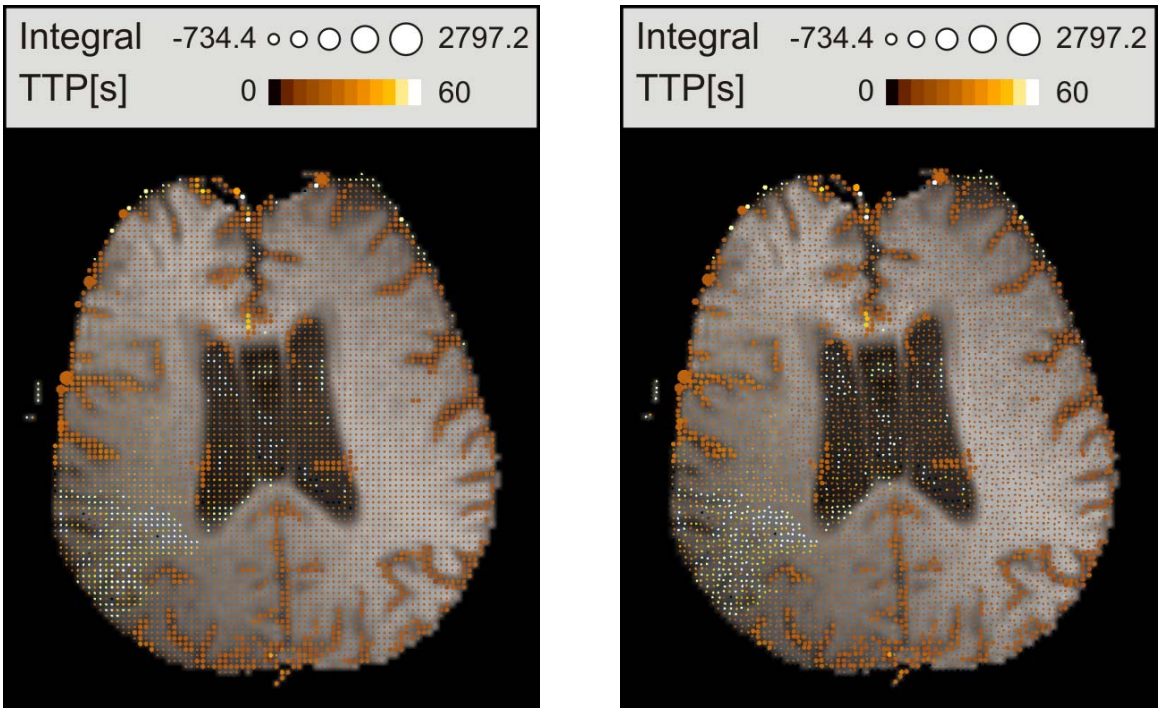

(a) (b)

Figure 3.11: Texel-wise glyph placement and the effect of jittering. *(a)*: One circular disc is placed per texel. The parameters *Integral* and *TTP* are mapped to glyph size and color, respectively. The resulting glyphs are very small due to the limited screen space per texel. Hence, changes in size are very hard to perceive. Due to the regular glyph placement, visually irritating grid patterns are generated. *(b)*: A slight jittering of the glyph positions about the texel centers resolves the visual artifacts. (Data is courtesy of Jonathan Wiener, Boca Raton Community Hospital.)

layer L_0 represents the highest possible resolution of one glyph per texel. For the above mentioned example, B_0 is then equal to 4×4 pixels. In each following layer $L_i, i \in [1, n]$, a glyph covers the area of four quadratically arranged neighboring texels in L_{i-1}. A useful maximum number of layers n has been determined empirically so far. For the discussed example, n has been set to three. With $B_i, i \in [1, n] = 2^i \cdot 4 \times 2^i \cdot 4$ pixels, this results in the upper glyph size bounds $B_1 = 8 \times 8$ pixels, $B_2 = 16 \times 16$ pixels, and $B_3 = 32 \times 32$ pixels. The user may interactively drill down the layers starting with the initially displayed topmost layer and focusing on regions which appear suspicious here. The reader is referred to [Malyszczyk, 2007] for detailed information on the implementation of the multi-resolution display.

An open question is how to compute the parameter values which determine the glyph attributes in lower resolution layers. Simple averaging of data values may suppress pathologies. Instead, the minimum or maximum value, dependent on the particular parameter and the application, are computed. In cerebral perfusion, e.g., high *TTP* and low *Integral* values indicate suspicious tissue. Hence, the maximum value for *TTP* and the minimum value for *Integral* are coded in the next lower resolution layer. This strategy ensures that no pathologies are suppressed though, it is prone to outliers values.

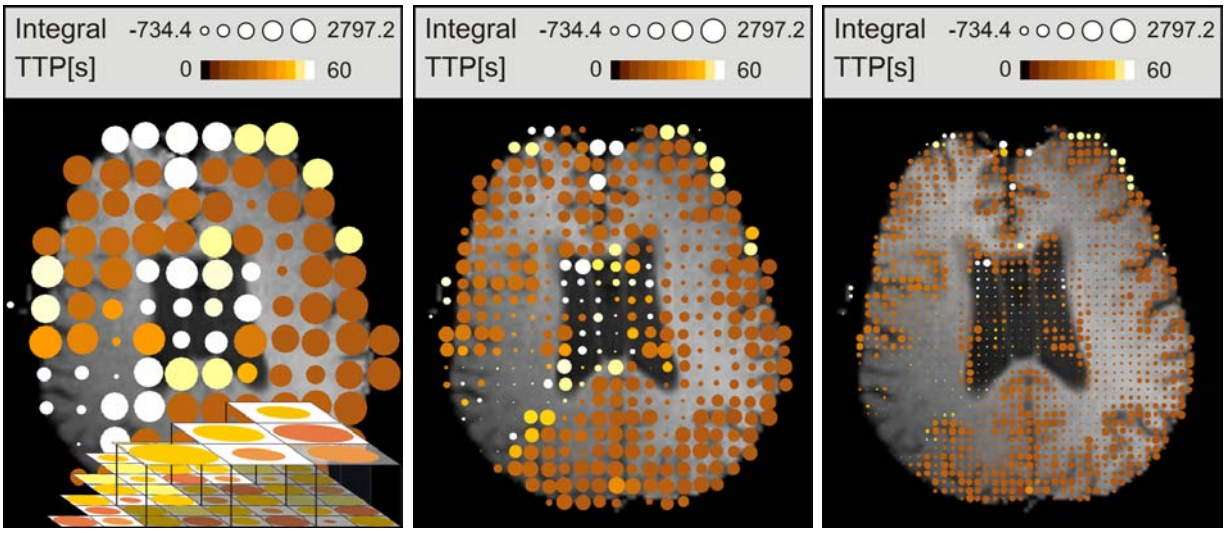

(a) (b) (c)

Figure 3.12: Multi-resolution glyph display. The parameters *Integral* and *TTP* are mapped to glyph size and color, respectively. *(a)*: The resolution layer $B3 = 32 \times 32$ pixels is presented, i.e. a glyph represents 8×8 voxels. Since small *Integral* values are of special interest in cerebral perfusion, the minimum of all voxel values is mapped to size. The inset illustrates the voxel aggregation. *(b)*: The resolution layer $B2 = 16 \times 16$ pixels is presented, i.e. a glyph represents 4×4 voxels. The infarction core is characterized by tiny, bright glyphs. *(c)*: The resolution layer $B1 = 8 \times 8$ pixels is presented, i.e. a glyph represents 2×2 voxels. (Data is courtesy of Jonathan Wiener, Boca Raton Community Hospital.)

3.3.1.3 Coupling Glyph Display and Feature Specification

The diagnostic evaluation of the multivariate parameter data is challenging and time-consuming due to its complexity. To reduce the amount of data and to direct the user to suspicious areas, a feature specification component has been integrated. This component implements the concept of *linking & brushing* and has been motivated by the work of Doleisch et al. [2003]. A scatterplot opposing two perfusion parameters is linked to the glyph display. Once an interesting subset of the parameter data is interactively brushed in the plot, the glyph visualization is updated and restricted to this subset. To account for the uncertainty involved in the definition of the interesting subset, *smooth brushing* is supported [Doleisch and Hauser, 2002]. In contrast to a binary decision, this allows a gradual transition from less interesting (*context*) to definitely interesting (*focus*). This transition (*near-focus*) may be integrated in the glyph display by mapping the so-called *degree of interest (DOI)* to one of the glyph attributes (compare to Furnas [1986]). Figure 3.13(a) illustrates the definition of a feature based on the parameters *TTP* and *Integral*. In the scatterplot, both parameters are opposed. The purple rectangle specifies the focus region. It includes high *TTP* and very small *Integral* values. Such values are characteristic for the infarction core. The surrounding bluish rectangle specifies the near-focus region. It has been extended from the focus region such that tissue is included whose perfusion is indeed delayed though, a considerable amount of CA arrives over time as compared to the core. Such behavior is characteristic for the penumbra. The resulting DOI map (pointed at by the arrow) is integrated with the glyph display such that the glyph visualization is restricted to the defined feature (Fig. 3.13(b)). The glyphs then encode the parameter subdomain of the feature. This

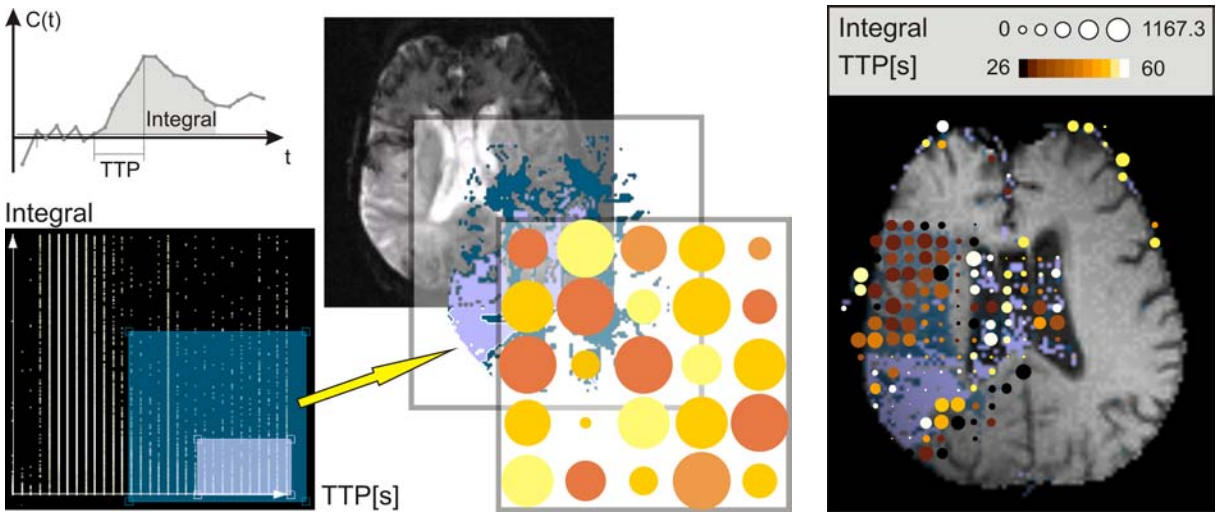

(a) (b)

Figure 3.13: 2D glyph display coupled with a feature specification component. *(a)*: The parameters *TTP* and *Integral* are opposed in the scatterplot. A focus region (purple rectangle) and a near-focus region (bluish rectangle) are defined for localizing infarction core and penumbral tissue. The resulting degrees of interest are then integrated with the glyph display. *(b)*: The glyph display is restricted to the focus and the near-focus region. The glyphs encode the parameter subdomain of the feature. The core (small, bright glyphs) and the surrounding penumbra (large, dark glyphs) are well differentiable. (Data is courtesy of Jonathan Wiener, Boca Raton Community Hospital.)

leads to a better differentiation of core and penumbra as compared to Figure 3.12(b). While the glyphs in the core region are bright (high *TTP* values) and small (very small *Integral* values), the glyphs in the surrounding penumbral region are dark (smaller *TTP* values) and large (higher *Integral* values).

3.3.1.4 Selected Visualization Examples

The results presented in this subsection have been achieved in performing three different diagnostic tasks. In cerebral perfusion, the localization of infarction core and penumbra has been aimed at (Fig. 3.14, 3.15(a)). In breast tumor perfusion, a tumor in the right mamma has been examined in order to confirm or reject the hypothesis of the tumor being malignant (Fig. 3.15(b)). In myocardial perfusion, the localization of tissue characterized by a delayed and diminished perfusion has been aimed at (Fig. 3.15(c)). The visualization examples in Figure 3.14 and Figure 3.15 illustrate a sample of glyph shapes that have been implemented.

In Figure 3.14(a), toroids have been applied. Their empty inner space reveals more of the anatomical context information as compared to circular discs or rectangles. The parameters *Integral* and *TTP* have been mapped to glyph size and color, respectively. An assignment of parameters to glyph thickness and roundness has been omitted since experiments showed that changes of these two attributes are hard to perceive. Their perceivability is heavily dependent on the overall glyph size. The resolution layer $B2 = 16 \times 16$ pixels is presented, i.e. a glyph represents 4×4 voxels. A discrete color scale has been applied for coding *TTP* since the parameter domain is small and in whole numbers (seconds). The infarction core is characterized by small, bright glyphs. A differentiation of the penumbra is not possible. For this purpose however, the visualization could be coupled with the feature specification component as illustrated in Figure 3.13(b).

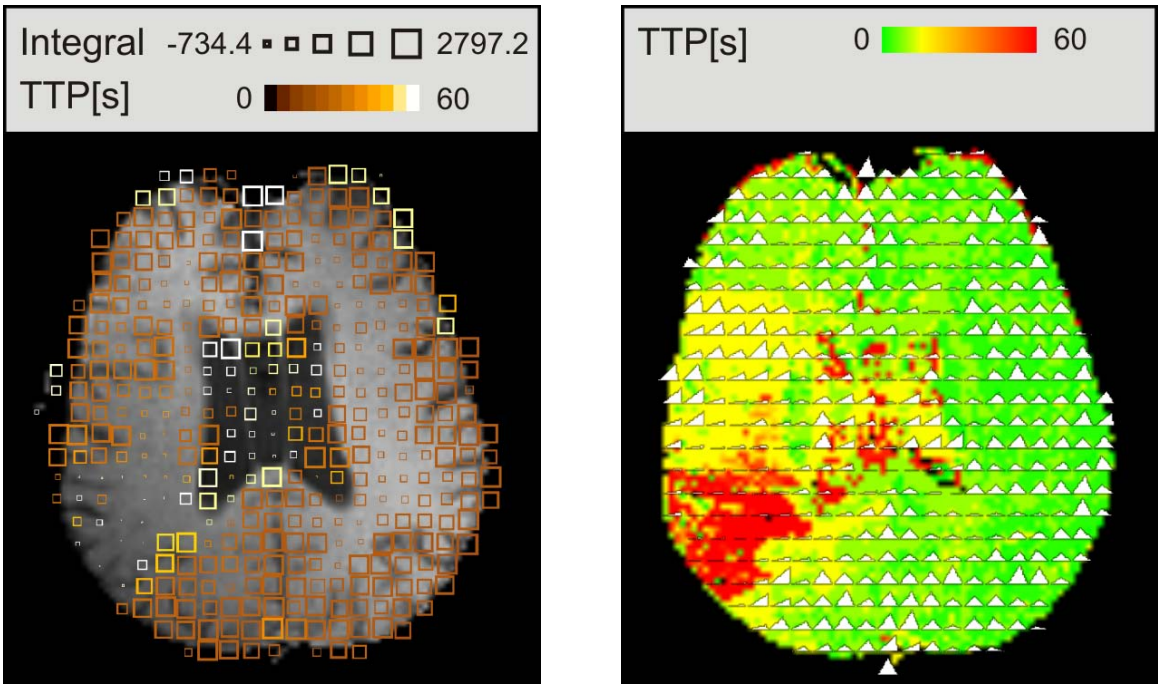

(a) (b)

Figure 3.14: Toroids and triangles for visually encoding cerebral perfusion parameters. *(a)*: The parameters *Integral* and *TTP* have been mapped to toroid size and color, respectively. The infarction core is characterized by small, bright glyphs. The resolution layer $B2 = 16 \times 16$ pixels is presented, i.e. a glyph represents 4×4 voxels. *(b)*: The triangular glyphs have been constructed based on *PE* (height of apex) and *TTP* (horizontal location of apex). The resolution layer $B2$ is presented. The glyphs are superimposed on a colored *TTP* parameter map. In the infarction core (red regions), no distinctive triangle shapes exist. The triangles in healthy tissue (greenish regions) are close to being isosceles triangles while the triangles in penumbral tissue (yellow regions) exhibit an apex that is shifted from the center of the base to the right. The latter indicates a delayed perfusion. (Data is courtesy of Jonathan Wiener, Boca Raton Community Hospital.)

Triangular glyphs have been applied in Figure 3.14(b). Their contours are emphasized to improve the visual separation from the background. Parameters *PE* and *TTP* have been used to construct the triangles as described in Subsection 3.3.1.1. The resolution layer $B2$ is presented. Since small *PE* and large *TTP* values are of special interest in cerebral perfusion, the minimum and maximum data value of all aggregated voxels are mapped to apex height and horizontal location, respectively. The glyphs are superimposed on a colored *TTP* parameter map for validation purposes. The color scale has been defined such that the infarction core and the penumbra appear as red and yellow regions, respectively. The triangles in the core region appear as straight lines due to very small *PE* values. This well resembles the lack of a distinctive CTC shape during the first pass of the CA. The triangles in the penumbral region are quite distinctive due to significantly higher *PE* values. However, a comparison with the corresponding primitives in the contralateral region shows that their apex is shifted further to the right than in healthy tissue. This is due to the delayed perfusion, i.e. the higher TTP *values*.

An advantage of triangles over the other tested glyph shapes is their ability to encode all perfusion parameters by shape attributes leaving color open, e.g., for encoding an additionally derived parameter. If cerebral perfusion research eventually identifies one parameter

as particularly clinically relevant, it may be color-coded such that suspicious regions can be identified rapidly by preattentive vision. A subsequent closer examination of the glyph shape in the attentive phase then provides more detail on the local perfusion. A drawback of triangles is that their declining part suggests a signal decrease back to the level of *CA arrival* which is not a valid assumption (Fig. 2.9).

Rectangles have been applied in Figure 3.15(a). The parameters *PE* and *TTP* are mapped to vertical and horizontal extent, respectively. The glyph display has been restricted to suspicious tissue by means of a feature specification similar to the one illustrated in Figure 3.13(a). However, instead of integrating the DOI map in the visualization as in Figure 3.13(b), the glyphs are colored according to the DOI value. The resolution layer $B2$ is presented. The mapping of *PE* to vertical extent has been inverted in order to visually emphasize the infarction core (high and wide glyphs). The surrounding penumbra is characterized by flattened, narrow glyphs. Such an inverse mapping may be useful for a detailed inspection of the core which is otherwise represented by barely perceivable glyphs (Fig. 3.14). Rectangles might have the advantage over circular discs that their shape better matches the shape of the represented voxel region thereby simplifying a mental assignment.

In Figure 3.15(b), ellipses are used to code the two most important parameters in tumor perfusion. The *Slope* (also called *Wash-in* in tumor diagnosis) is mapped to size while the *DownSlope* (also called *Wash-out*) is mapped to orientation. The resolution layer with $B_3 = 32 \times 32$ pixels is presented, i.e. a glyph represents 8×8 voxels. Since the glyph size is modified according to *Wash-in*, whose large values are of special interest in tumor perfusion, the maximum data value of all aggregated voxels is mapped to size. The glyph placement has been restricted by means of the feature definition component (inset). A focus region (purple rectangle) has been defined such that large *Wash-In* and negative *Wash-out* values are included. A steep ascending time-intensity curve followed by a declining part is characteristic for malignant tissue. A near-focus region (bluish rectangle) has been extended such that values indicating a continuous enhancement for a later period in time (positive *Wash-out* values) or a plateau (*Wash-out* values close to zero) in the time-intensity curve are included. The tumor region appears as circular region filled with ellipses. The glyphs are colored with respect to the DOI values. The whitish ellipses are part of the focus region. Potentially malignant tissue is indicated by large, slanted ellipses which represent strong perfusion and a high permeability of vessels. The broad variety in glyph size and orientation within the tumor region illustrates the heterogeneity of tumor tissue.

Ellipses have been successfully applied also for exploring myocardial perfusion as illustrated by Figure 3.15(c). *Up-slope* being the most important parameter is mapped to orientation and the resulting ellipses are colored according to *PE*. Since the myocardium has a low spatial extent in the original perfusion data and the number of voxels covered by myocardial tissue is small (250-500 per slice), a texel-wise glyph placement is appropriate. The coloring of *PE* has been chosen such that regions characterized by a sufficient oxygen supply are colored red and regions with a diminished supply are colored blue. This coloring scheme is wide-spread in cardiology. A large myocardial region (blue, horizontally oriented glyphs) has been affected by an infarction. Both perfusion parameters seem to correlate quite well. Neither red, horizontally oriented glyphs nor blue vertically oriented glyphs exist.

A further improvement of the 2D glyph-based visualizations is discussed in detail in [Malyszczyk, 2007]. Extending the brushing facilities from perfusion parameter space to object space (original perfusion data) facilitates the inclusion or exclusion of certain anatomical regions from the visualization. As can be seen, e.g., in Figures 3.12 and 3.13(b), it would be helpful to exclude the ventricles from the visualization since no CA accumulates there.

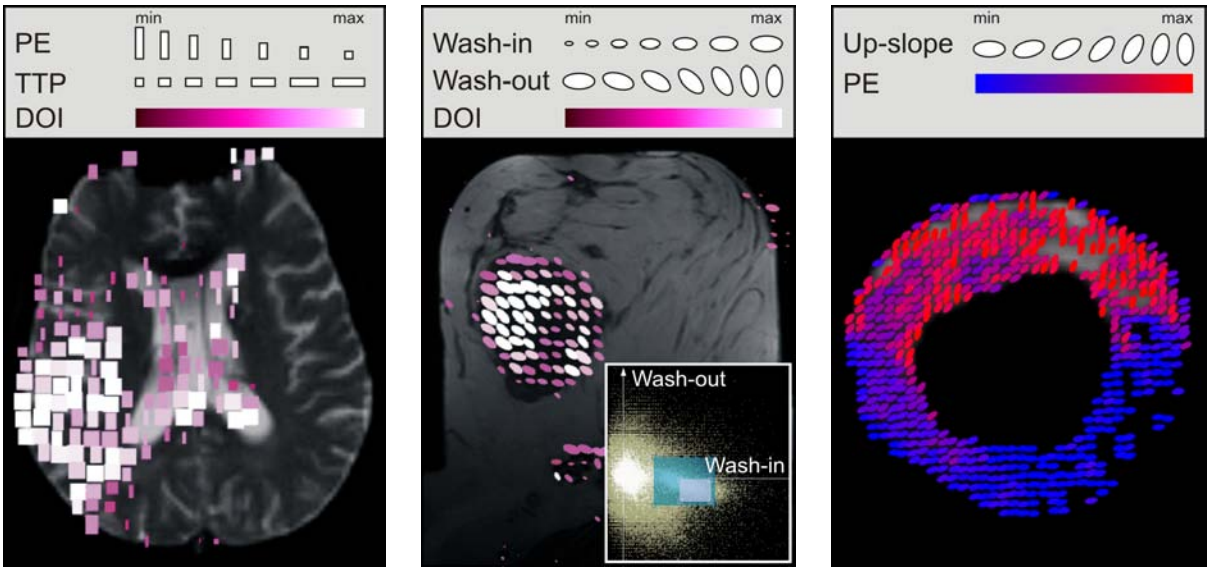

(a) (b) (c)

Figure 3.15: Rectangles and ellipses for encoding cerebral, tumor and myocardial perfusion parameters. *(a)*: The parameters *PE* and *TTP* are mapped to vertical and horizontal extent. The degree of interest (DOI) values are mapped to glyph color. The resolution layer $B2$ is presented. The mapping of *PE* has been inverted in order to visually emphasize the infarction core (high and wide glyphs). *(b)*: The parameters *Wash-in* and *Wash-out* are mapped to size and orientation, respectively. The visualization is coupled with a feature definition component (inset). The degree of interest values are mapped to glyph color. The resolution layer B_3 is presented. Potentially malignant tissue is indicated by large, slanted ellipses. *(c)*: The parameters *Up-slope* and *PE* are mapped to orientation and color, respectively. One glyph is placed per texel. A large myocardial region is revealed (blue, horizontally oriented glyphs) that has been affected by an infarction. Here, the perfusion is diminished and the speed of CA accumulation is decreased. (Data in *(a-b)* is courtesy of Jonathan Wiener, Boca Raton Community Hospital. Data in *(c)* is courtesy of Stefan Miller, University Hospital Tübingen.)

3.3.2 3D Glyph-based Visualization of Myocardial Perfusion

Discussions with a cardiologist showed that a visual representation of the perfusion in 3D space embedded in the anatomical context could help to assess the global myocardial perfusion. It may accurately reflect the spatial relations between anatomy and perfusion parameters which is strongly hampered by a standard BEP visualization. Indicating the localization of the imaging planes defined for the perfusion scan together with the applied slice thickness would illustrate the ventricular coverage. The visualization in 3D could serve as an overview and provide the basis for a more fine-granular slice-based analysis. It could be helpful for the communication between the cardiologist and the referring physician or a surgeon.

The application of direct or indirect volume rendering techniques is not suitable for the visualization of MRI myocardial perfusion data and the associated perfusion parameters due to the low number of slices that is usually acquired $(3-4)$. This observation may have to be reviewed with increased availability of parallel imaging techniques offering a greater spatial coverage [Finn et al., 2006]. Perfusion parameter data represent a special instance of multivariate data requiring dedicated visualization approaches. Glyphs have been tested for the integrated 3D display of perfusion parameters embedded in the anatomical context [Paasche, 2007; Paasche et al., 2007; Oeltze et al., 2008a]. As context information, the left

and the right ventricular surface have been extracted from additional cardiac data which was acquired during the same scanning protocol.

Besides the assessment of myocardial perfusion, current cardiac imaging technology allows for the investigation of myocardial function and viability. The combined inspection of these data supports diagnosis finding and therapy planning by allowing for the discrimination of different myocardial tissue states. To facilitate such an inspection, registration methods have to be applied that cope with differences in orientation and coverage between the datasets. Then, the glyph-based visualization of perfusion parameters may be enhanced by integrating parameters describing the myocardial function and viability. The acquired data as well as the applied registration methods will be discussed in Subsections 3.3.2.1 and 3.3.2.2, respectively. Aiming at a clearly structured thesis, the remainder of this subsection (Subsec. 3.3.2.3-3.3.2.4) is focused on the glyph-based visualization of perfusion parameters. The integration of function and viability by means of other visualization techniques will be presented later in Subsection 3.4.2.

3.3.2.1 Image Data

The image data applied in the following has been acquired in a low-dose CA study by Dr. Frank Grothues (University Hospital Magdeburg). 15 patients participated in the study which had all suffered from an infarction within one year prior to the study. The glyph-based visualizations illustrating Subsections 3.3.2.3 and 3.4.2 have been generated based on the two representative cases $case_1$ and $case_2$, respectively. In $case_1$, the infarction affected the inferior and inferolateral wall whereas in $case_2$, it had an effect on the anterolateral and inferolateral wall. Data acquisition was carried out on a SIEMENS TRIO (3Tesla) MR scanner. The characteristics of the corresponding datasets are:

Perfusion Data 4 short-axis slices with 8 mm thickness, an in-plane-resolution of 1.875 mm × 1.875 mm, and a gap of 10 mm were imaged per heart beat at end diastole using a Turbo-FLASH (TF) sequence and ECG-triggering. The acquisition was carried out at rest over 40 consecutive heart beats.

Cine Data The Cine data was acquired prior to the perfusion data with an inversion-recovery TF sequence. 10 short-axis slices with 6 mm thickness, a gap of 4 mm and an in-plane-resolution of 1.4 mm x 1.4 mm represent one contraction cycle in 30 phases.

Late Enhancement Data 10 to 15 minutes after CA injection, 3D LE data was acquired at end diastole applying the same image plane location, orientation and in-plane-resolution as for the Cine data. A TF 3D sequence was used for acquisition.

3.3.2.2 Image Data Preprocessing

Patient breathing and contractile heart motion can influence the acquisition, such that an image slice at one spatial position can show the heart at different positions or in a different shape if it is acquired at different points in time. Therefore, the combined inspection of the given cardiac image data demands methods that compensate for the movement. The end-diastolic image of the Cine data is used as a reference image for the alignment of the perfusion, Cine, and LE data.

The LE data is registered slice-wise with the reference image using rigid transformations. The transformation parameters are optimized with the so-called *Simplex algorithm* [Nelder and Mead, 1965] and *Normalized Cross Correlation* as similarity measure.

The perfusion data are acquired with ECG-triggering, so that every time frame shows the same contraction phase as its temporal predecessor. However, displacement due to breathing motion frequently occurs within the image sequence. Thus, motion correction has to be performed for the whole sequence (Subsec. 2.2.3.1). The slices of a reference time frame, which shows CA in the left ventricular lumen but not yet in the myocardium, are registered with the reference image of the Cine data as described above. Then, the consecutive time frames are registered with their corrected predecessors as described in [Hennemuth et al., 2007].

To analyze the spatially aligned images, the myocardium is segmented with the Live Wire algorithm [Schenk et al., 2000] in all datasets (Subsec. 2.2.3.2). After the motion correction of the perfusion data, only one point in time needs to be segmented. The resulting contours are then propagated over time. For the Cine data, the segmentation is limited to the end-diastolic and end-systolic phase. The infarction scar is segmented with the histogram analysis method proposed in [Hennemuth et al., 2008b] (see Subsec. 2.2.3.6 for a brief discussion). The result of all segmentations is a binary mask.

To visualize the segmented structures in 3D, they are represented as surfaces generated by means of the *Marching Cubes* algorithm [Lorensen and Cline, 1987]. Due to the discrete nature of the data, the resulting surfaces exhibit so-called *stair-case artifacts*. Those artifacts hamper a reliable computation of inter-surface distances which will be applied for the computation of wall thickening and transmurality. Hence, as a preprocessing step, the surfaces are smoothed applying the λ/μ Filter [Taubin, 1995].

After a calibration of signal intensities (Subsec. 2.2.3.3), descriptive perfusion parameters (Subsec. 2.1.3.4 and Subsec. 2.2.3.5) are calculated for all myocardial voxels and stored in parameter volumes. Based on the binary mask of the perfusion data, myocardial properties are calculated which are required for the glyph placement. For each slice s, $s \in [1, number\ of\ slices]$, the center of gravity of myocardial voxels ($COGmyo_s$) is computed. Further, the minimum, maximum and average Euclidean distances from ($COGmyo_s$) to myocardial voxels in s are determined in voxel as well as in world space.

A final preprocessing step is related to the segment-wise parameter analysis of the perfusion data (Subsec. 2.2.3.4). It has to be repeated whenever the user switches from the 17-segment model to a user-defined division or changes the number of segments in the latter case. For each segment, the corresponding myocardial voxels are determined. Based on that information, the average parameter values as well as $COGseg_{ID}$ of the segment with the unique identification ID are computed. This is needed later on for modifying glyph attributes and for glyph placement, respectively. To support and improve the readability of the next subsection, the following abbreviations are defined:

- $BMmyo_{perf}$: Binary mask from perfusion data showing the segmented myocardium,
- $COGmyo_s$: Center of gravity of myocardial voxels in the slice s of $BMmyo_{perf}$,
- $COGseg_{ID}$: Center of gravity of all myocardial voxels in $BMmyo_{perf}$ which belong to the segment labeled with ID,
- $SF\{lv, rv\}_{LE}$: Left (lv) and right (rv) ventricular surface from LE data

3.3.2.3 Glyph Placement and Glyph Design

The glyph-based visualizations illustrating this subsection have been generated based on $case_1$. In each image, $SFlv_{LE}$ serves as context information and is rendered semi-

transparently. The lack of perceivable surface texture and object boundaries is compensated in Figure 3.16 and 3.18 by a superimposition of feature lines and in Figures 3.19–3.20 by a silhouette rendering [Gooch et al., 1999]. While the silhouette describes the outer contour of an object, feature lines represent ridge lines and creases on the object surface carrying the visually most prominent characteristics. The infarction scar is rendered as a brownish surface inside the ventricle. Glyph legends illustrate the mapping of perfusion parameters to glyph attributes.

The two crucial aspects of glyph design are glyph placement and the design of a meaningful glyph shape. The proposed selection of a placement strategy directly influences the range of feasible glyph shapes. If the original perfusion data exhibit a high SNR and could be reliably motion-corrected, the user may consider a voxel-wise perfusion analysis. For that purpose, a glyph is generated and centered at each voxel midpoint of the original perfusion data slices. The midpoint coordinates in 3D are computed by means of a matrix M that describes the transformation from voxel to world space. M is retrieved from the DICOM-header. Often, cardiac perfusion data exhibit a low SNR and the user will carry out a segment-wise analysis, e.g., based on the 17-segment model. Then, a glyph is generated for each segment and centered at $COGseg_{ID}$. To enable a more subtle division of the myocardium, the user may select an arbitrary number of segments per slice. The glyph placement is then updated accordingly.

Simple Glyph Shapes. Initial tests have been carried out following a voxel-wise glyph placement strategy and utilizing simple shapes, e.g., cubes and spheres, thereby employing two degrees of freedom, color and size. Both are modified according to the assigned parameter values and the corresponding minimum and maximum values. The real color is derived from a color look-up-table. As a default look-up-table, a blue (low in oxygen) to red (oxygen rich) scale is applied which is borrowed from other systems in use in Cardiology. The maximum size of a glyph is initially restricted to the in-plane size of a voxel. An arbitrary number of coloring and scaling steps can be chosen by the user. Instead of a step-wise function which visually classifies the data into a few categories, a continuous scaling can be selected.

For a voxel-wise placement, cubes delivered the best results since a cube optimally fills in the voxel area it represents. In Figure 3.16(a), *PE* and *Up-slope* are mapped to cube color and size, respectively. In the infarction zone, small bluish glyphs display the expected perfusion defect. For illustration purposes, the glyph size has been slightly scaled up. Since the size now exceeds the in-plane size of a voxel, overlapping and z-fighting occur in a few regions.

Often, the user may wish to examine the perfusion segment-wise. In Figure 3.16(b), the myocardium has been divided according to the 17-segment model and a cube has been placed per segment. This visualization suffers from two major problems. First, the spatial location of a glyph is difficult to assess due to a lack of depth information. Second, the full extent of the region represented by a glyph may not be inferred since the glyph covers only a part of this region. The first problem may be addressed by creating thick dots at voxel midpoints, thereby generating a spatial reference that indicates the myocardial shape (Fig. 3.16(c)). The second problem is mitigated by superimposing line segments that originate at $COGmyo_s$ and indicate the myocardial segment borders.

3D BEP Segments. In order to completely resolve the problems induced by a segment-wise placement of simple glyph shapes, a new shape has been designed that resembles a planar BEP segment extruded in 3D space (Fig. 3.17(a)–(b)). This new shape far better

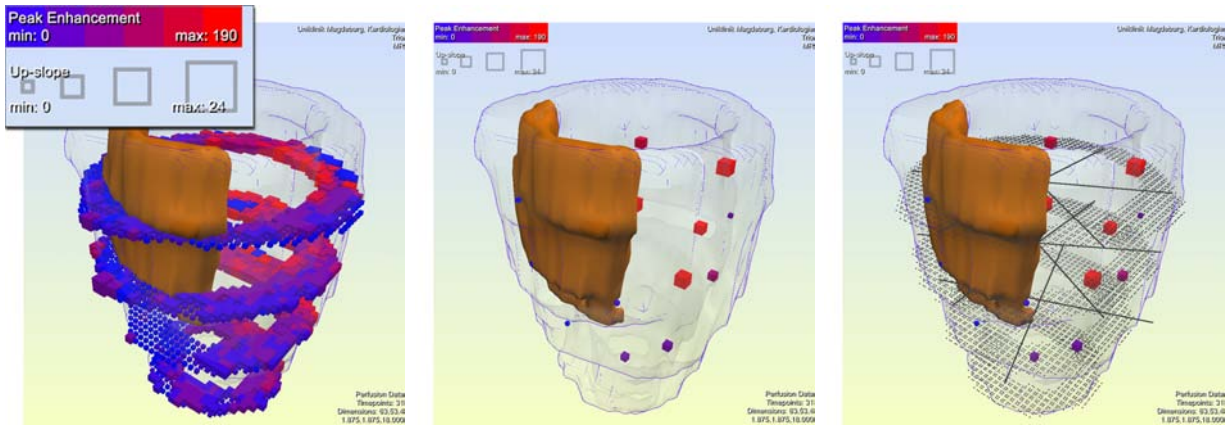

(a) (b) (c)

Figure 3.16: Simple glyph shapes for voxel- and segment-wise encoding of myocardial perfusion which has been sampled by four short-axis slices. Glyph color and size encode perfusion parameters *PE* and *Up-slope*, respectively. *(a)*: Cubes are placed voxel-wise. The perfusion disturbance is characterized by small, bluish glyphs. *(b)*: Cubes are placed segment-wise according to the 17-segment model. The spatial location of a glyph is difficult to assess. Since a glyph covers only part of the region it represents, the full extent of the this region may not be inferred. *(c)*: These problems are partially resolved by creating thick dots at voxel midpoints and superimposing the segment borders. (Data is courtesy of Frank Grothues, University Hospital Magdeburg.)

fills in the region it represents. The spatial location of the ring formed by all glyphs lying in the same plane may be easier to assess than the location of a loose set of cubes. Three degrees of freedom are employed: color, difference between the radius of the outer (r_{out}) and inner (r_{in}) circular arc (thickness) and height (h). The radii r_{in} and r_{out} are defined with respect to $COGmyo_s$. The segments are aligned along r_{in} which equals the average distance of myocardial voxels in s to $COGmyo_s$. The radius r_{out} of each glyph is set individually with respect to the average perfusion parameter value assigned to the corresponding segment. The upper limit of r_{out} is set to the maximum distance of a myocardial voxel in s to $COGmyo_s$. The angle α is set with regard to the radial position of the segment represented by the glyph. The angle β depends on the number n of segments in s and equals $360°/n$.

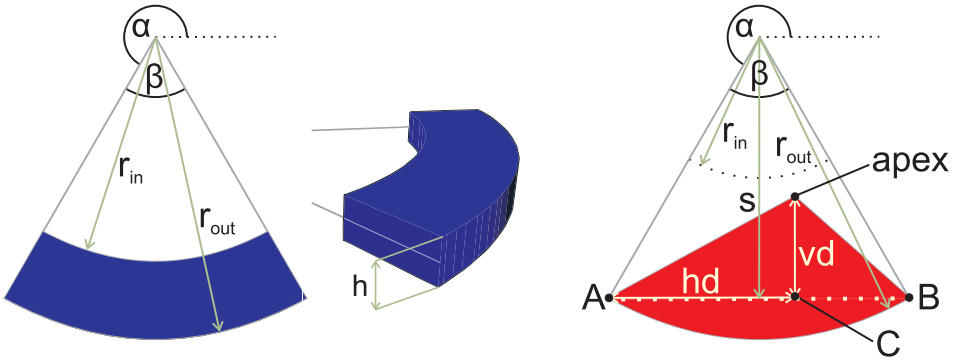

(a) (b) (c)

Figure 3.17: Construction of advanced 3D glyph shapes for coding perfusion parameters. *(a-b)* 3D Bull's Eye Plot Segment. *(c)* 3D Time Intensity Curve (TIC) Miniature.

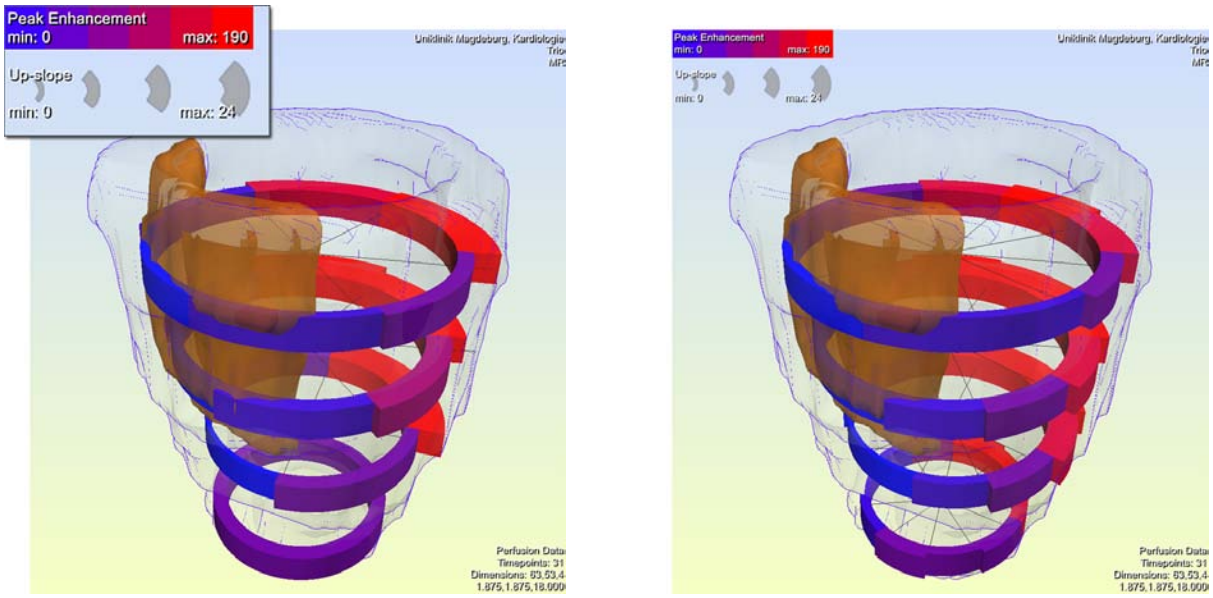

(a) (b)

Figure 3.18: 3D BEP segments for segment-wise coding of myocardial perfusion. The glyph color represents *PE*. Glyph height and thickness are adjusted with respect to the slice thickness of the original perfusion data and the perfusion parameter *Up-slope*, respectively. *(a)*: Glyphs are placed segment-wise. The myocardium has been divided according to the 17-segment model. *(b)*: A more subtle assessment of perfusion is enabled by a fine-granular user-defined division (10 segments per slice). (Data is courtesy of Frank Grothues, University Hospital Magdeburg.)

In Figure 3.18(a), *PE* and *Up-slope* are mapped to color and thickness. Thin bluish segments indicate a perfusion deficit. The myocardium has been divided according to the 17-segment model. The glyph height encodes the thickness of the original perfusion data slices. In contrast to other visualizations that interpolate between the slices pretending a comprehensive ventricular coverage, this approach conveys the considerable inter-slice gap. To enable a more subtle perfusion assessment, 40 segments have been defined by the user (10 per slice) in Figure 3.18(b). Particularly, for the most apical slice (bottom ring), the precise extent of the perfusion disturbance becomes apparent.

3D TIC Miniatures. It could be observed in designing 2D glyph shapes for visualizing cerebral perfusion that the first pass of the CA may be well resembled by a triangular shape (Subsec. 3.3.1.1, Fig. 3.14(b)). In [Oeltze et al., 2008a], this observation has been reviewed in the context of myocardial perfusion. As shown in Figure 2.23(a), the observation cannot be directly transferred since the signal intensity does not return to the precontrast level after the peak. Furthermore, the scanning duration in diseased patients is often too short to cover the entire CA washout. However, since the *DownSlope* has not been reported by clinical literature as one of the essential parameters in myocardial perfusion, triangles may be applied here as well. They facilitate an intuitive encoding of the perfusion parameters *Up-slope*, *PE*, *TTP*, *Integral*, and *MTT* which have been approved in cardiac diagnosis (Subsec. 2.2.3.5). Hence, a new glyph shape has been designed that represents a simplified miniature of a TIC extruded in 3D. Since physicians are trained to infer tissue characteristics from TIC shape, this glyph should facilitate an easy decoding of perfusion parameters.

The construction of the new glyph is illustrated in Figure 3.17(c). As explained in Subsection 3.3.1.1, PE and TTP are sufficient for constructing the base triangle. First, to form a visually pleasing 3D representation, the rectilinear base of the triangle (dotted line) is replaced by a circular arc. Then, the resulting shape is extruded perpendicular to its construction plane by an extrusion factor h, as illustrated for the 3D BEP segments in Figure 3.17(b). While the replacement step results in a visually more pleasing representation, the construction of the glyph continuous to be based on the rectilinear base. The position of the apex relative to the base is computed as:

$$apex = C + (s - r_{in}) * vd * \hat{v}_{aux} \tag{3.1}$$

with:

$$\begin{aligned} C &= A + hd * \overrightarrow{AB} \\ hd &= \frac{TTPseg_{ID} - TTP_{min}}{TTP_{max} - TTP_{min}} \\ s &= \cos(\beta/2) * r_{out} \\ vd &= \frac{PEseg_{ID} - PE_{min}}{PE_{max} - PE_{min}} \\ \hat{v}_{aux} &= crossProd((0,0,1)^T, \hat{AB}) \end{aligned}$$

A and B are explained by Figure 3.17(c). The computation of hd and vd for the segment with identification ID is based on the corresponding averaged parameter values ($TTPseg_{ID}$ and $PEseg_{ID}$) and the minimum and maximum for TTP and PE. The minimum of TTP (TTP_{min}) is zero and the maximum (TTP_{max}) equals the duration of the CA's first pass. The duration is determined based on an averaged TIC in healthy tissue as the time from *CA arrival* to $Time_{End}$ (Fig. 2.9). For PE, both extremes (PE_{min} and PE_{max}) are simply set to the extreme values of the corresponding parameter volume. The radial orientation and extent of the glyph are defined as described for the 3D BEP segments (Fig. 3.17(a)).

In Figure 3.19(a), the new triangular glyphs are presented with a coloring according to PE. The grayish glyphs, partly visible in the infarction zone, represent the averaged TIC of the entire myocardium and serve as a reference. In healthy tissue, none or just a small part of the reference TIC is visible. The utilization of a reference shape is inspired by [Haraldsson et al., 2008] (Subsec. 3.1.2). In contrast to the previously discussed glyphs, the new glyphs are not positioned inside the ventricle. Instead, they are pulled away from the ventricle to provide more space for glyph construction. A pulling factor pf, which is determined empirically so far, is multiplied with r_{in} of the glyphs: $r'_{in} = pf \times r_{in}$. The initial value of r_{in} is determined as described for the 3D BEP segments. The radius r_{out} is updated accordingly and set to a multiple of r'_{in}. The magnitude of this multiple has also been determined empirically so far. Since the glyphs are positioned outside the ventricle, the extrusion factor h is set to a reasonable small value in order to minimize occlusions of the anatomy.

An interesting view results from rotating the ventricle such that the view direction points down from the ventricular base along its long-axis to the apex of the ventricle (Fig. 3.19(b)). The resulting view imitates a BEP and hence, gives an overview of the perfusion in all segments. This provides a reasonable default setting for an initial view when analyzing a new dataset.

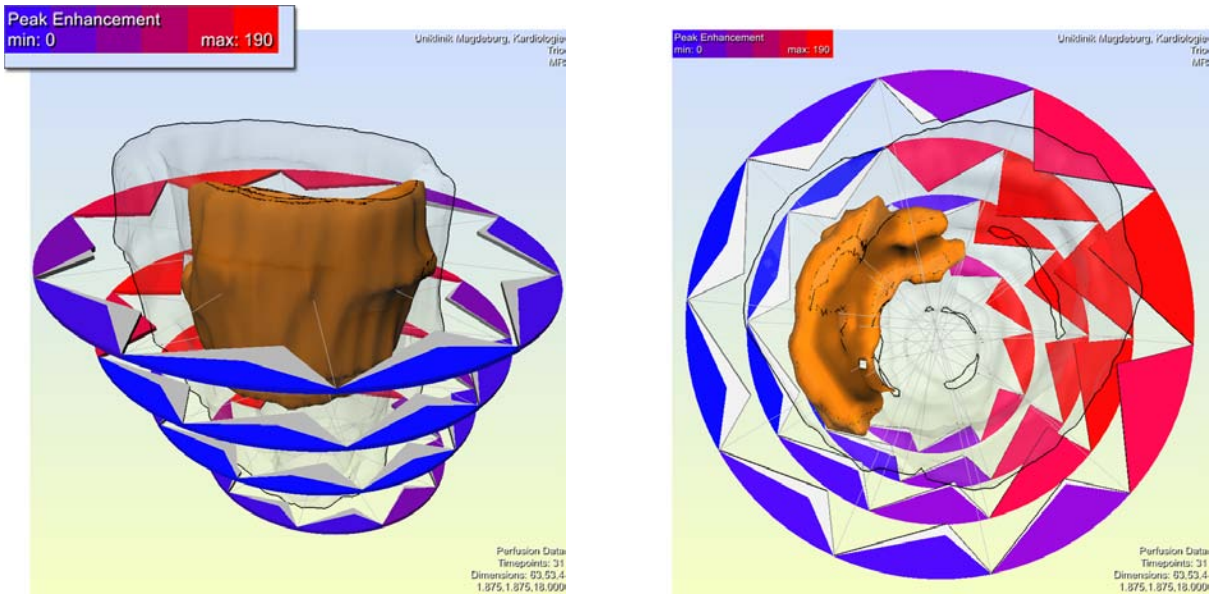

(a) (b)

Figure 3.19: 3D time-intensity curve (TIC) miniatures for segment-wise encoding of myocardial perfusion. The glyph color represents *PE*. *(a)*: For each segment, a 3D TIC miniature resembles the averaged TIC shape. The TIC of the entire myocardium is superimposed (gray glyphs) and serves as a reference. *(b)*: The view along the ventricular long-axis resembles a BEP view. (Data is courtesy of Frank Grothues, University Hospital Magdeburg.)

Improvement of Spatial Orientation. A drawback of the visualizations discussed so far (Fig. 3.16, 3.18, 3.19) is a lack of spatial orientation due to the symmetry of the ventricle around its long-axis. However, physicians are used to systematically inspect the ventricle and communicate findings related to anatomical orientation cues. In 2D slices, the right ventricle serves as an orientation cue. For example, the division of the myocardium into segments and their labeling, start from the anterior connection of the left and the right ventricle. Hence, $SFrv_{LE}$ is included in the visualization as a semi-transparent surface with highlighted silhouette (Fig. 3.20(a)).

Another information that is not clearly conveyed due to the transparency of $SFlv_{LE}$, is the thickness of the ventricular wall, i.e. the distance between endocardial and epicardial surface. Furthermore, if the glyphs are located outside the ventricle, such as in Figure 3.19(a), the distance between glyph and surface as well as the surface part that corresponds to a glyph, are difficult to assess. To address this problem, the intersection contours of the original perfusion data imaging planes and $SFlv_{LE}$ are computed in 3D and emphasized by coloring them according to the corresponding glyph (Fig. 3.20(a)).

Further simple techniques that support a spatial orientation are illustrated in Figure 3.20(b). An orientation cube labeled with common abbreviations for anatomical viewing directions is integrated. In addition, a textured plane may be integrated which, e.g., shows a slice view of the original perfusion data. The user can interactively browse through the slices as well as through the points in time of a single slice, thereby examining the perfusion parameters in the anatomical context. To support the identification of a glyph and a segment, respectively, and to simplify the correlation with a BEP, each glyph may be labeled with its unique segment number. In Figure 3.20(b), the myocardium has been divided according to the 17-segment model. The corresponding BEP is presented in the inset.

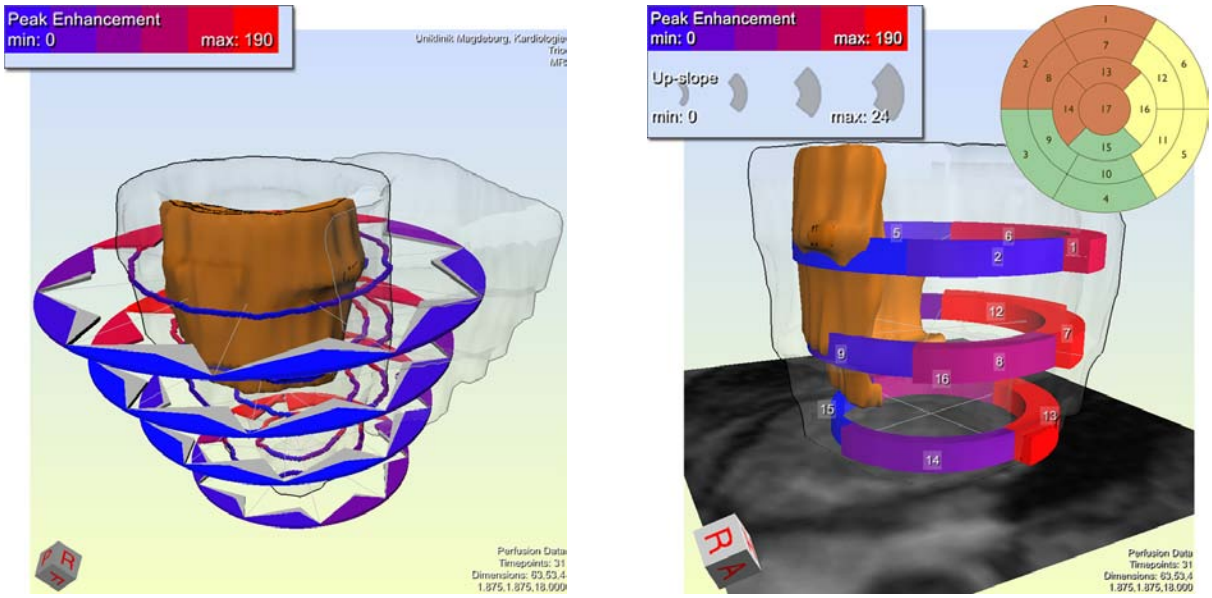

(a) (b)

Figure 3.20: Improving spatial orientation in 3D glyph-based visualizations of myocardial perfusion. *(a)*: The right ventricle is provided as context information. The left ventricular wall is emphasized at intersections with the perfusion imaging planes. The intersection contours are colored according to the corresponding glyph. *(b)*: The glyphs are labeled to indicate the correspondence with the BEP (inset). A textured plane is integrated showing a slice view of the original perfusion data. An orientation cube labeled with common abbreviations for anatomical viewing directions is integrated. (Data is courtesy of Frank Grothues, University Hospital Magdeburg.)

Glyph Animation. An interesting feature that is inspired by the *uptake movie* [Breeuwer, 2002] is the animated depiction of the original signal intensities in a movie loop. The glyph color is changed with respect to the intensity at the respective point in time. It is computed based on the current intensity and normalized by the overall range of intensities occurring in the dataset. Besides a direct visualization of the intensity, the percentage enhancement, the difference in enhancement as well as the ratio with respect to a user-defined precontrast point in time may be shown. The user may stop the animation and may manually browse back and forth through the points in time. A limited range of possible color values should be defined in order to reduce flickering artifacts.

3.3.2.4 User Feedback

The glyph visualizations have been used for the examination of datasets from 14 patients who suffered from an infarction. A representative subset of the generated visualizations was presented to three collaborating physicians for informal comments.

All physicians appreciated the possibility of globally assessing the myocardial perfusion in 3D. They evaluated the integration of context information, i.e. of ventricles and infarction scar, as important and successfully accomplished. The invention of advanced glyph shapes for a segment-wise analysis was confirmed as necessary. The possibility of encoding the slice thickness and thereby illustrating the inter-slice gap, was seen as an advantage of 3D BEP Segments over 3D TIC miniatures. However, a benefit of the latter is the encoding of all important perfusion parameters in a single glyph. The reference 3D TICs were rated as

useful. An overview representation as generated in Figure 3.19(b) serves as a good starting point for an examination. All physicians appreciated the application of a voxel-wise glyph placement in cases of high SNR and low motion artifacts thereby facilitating a fine-granular perfusion analysis across the entire ventricular wall.

A few drawbacks were identified for the visualizations based on 3D TICs. For example, a perspective view as in Figure 3.19(a) may hamper the readability of the glyphs. It is difficult to assess whether the PE of the reference curve occurs earlier in time or later than the one of the segment's curve for glyphs facing away from the viewer. Furthermore, the glyph size is not readable once the viewing direction is perpendicular to the long axis of the ventricle. The 3D TIC miniatures may occlude quite large parts of the surface which is disadvantageous if the surface is colored according to another parameter, e.g., myocardial wall thickening. Another drawback of these glyphs is their variation in shape depending on the number of segments per slice. For a small number (< 6), they are considerably stretched and flattened and for a larger number, they may become too small for a reliable interpretation. A general problem of the visualizations is that the comparison of individual glyphs requires a mental integration of glyph shapes and colors.

3.4 Comprehensive Cardiac Visualization

Today, clinical examinations often result in a variety of datasets acquired from the same patient using different imaging modalities and different imaging sequences of the same modality. Each individual scan is dedicated to a specific problem and all scans together convey a global picture of the patient state. In cardiac MRI, perfusion, viability and function of the myocardium may be assessed based on datasets acquired in a single scanning protocol. The protocol may be completed by an MRCA or a separate high resolution CTCA may be acquired, both depicting the coronary arteries and the ventricles (Fig. 2.17). An integrated visualization of angiographic and perfusion data will be discussed in Subsection 3.4.1. It facilitates the detection of myocardial perfusion disturbances and the correlation between affected tissue and the supplying coronary branch. A fusion of perfusion, LE and Cine data will be presented in Subsection 3.4.2. It allows for a differentiation of several myocardial tissue states (Tab. 2.1) and has an impact on therapeutic decisions.

Prior to the discussion of fusing different datasets, the simple integration of a restricted perfusion display and spatial reference information which is obtained from the same dataset is presented. Relevant perfusion parameters are often only extracted and visualized for a restricted region in the entire dataset, e.g., the myocardium, suspicious brain tissue or a tumor. However, other constituents such as the right ventricle, healthy brain tissue or the outer breast skin might provide substantial information for displaying the diagnostically relevant regions in their anatomic environment. Also other surrounding tissues that are not enhancing, can be of indispensable diagnostic value. Therefore, it is useful to add spatial reference information in the regions not containing relevant dynamic information. As a simple example, the display of an original slice from the perfusion scan together with the height field in Figure 3.21(a) supports the spatial orientation which is hampered by the circular shape of the myocardium. The user may browse through the points in time thereby observing the CA accumulation in the right ventricle and in the left ventricular lumen. In Figure 3.21(b), the synchronized flexible lens display is enhanced by a slab volume rendering of the original perfusion scan at an arbitrary point in time. The visualization in 3D communicates the slice location with respect to the overall brain extent thereby contributing to the infarction local-

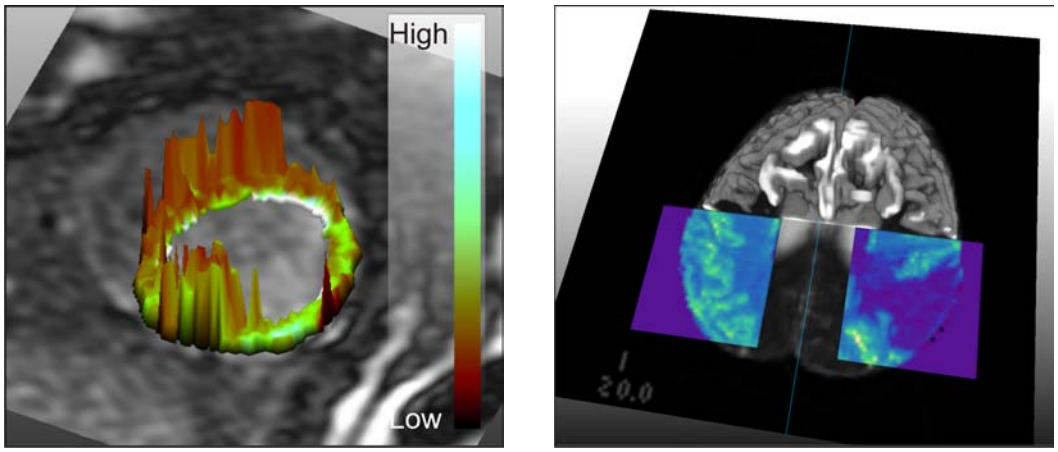

(a) (b)

Figure 3.21: Restricted perfusion display and added spatial reference information. *(a)* The colored height field is restricted to the myocardium. Surrounding tissue is indicated by an original slice from the perfusion scan thereby improving spatial orientation. *(b)* A synchronized flexible lens display is enhanced by a slab volume rendering of the original perfusion scan at an arbitrary point in time. (Data in *(a)* is courtesy of Stefan Miller, University Hospital, Tübingen. Data in *(b)* is courtesy of Jonathan Wiener, Boca Raton Community Hospital.)

ization. The user may adjust the point in time as well as the transfer function. A reasonable strategy to add spatial reference information is to color-code dynamic information and to display the reference data in the background using a gray scale. Depending on the resolution of the image data, the integration of perfusion and spatial reference information should be carried out in 2D slice visualizations or 3D renderings.

3.4.1 Integrating Myocardial Perfusion and Angiographic Data

In this subsection, the integrated visualization of perfusion analysis results and vasculature, which has been extracted from CTCA images, is presented. The patient whose data is applied in the following suffered from atherosclerosis of the RCA and the LAD. Besides the coronary arteries, the epicardial left ventricle and the aorta ascendens are extracted from the CTCA data and visualized in 3D. The integration of perfusion and morphology is implemented by a bidirectional link between a BEP representing perfusion analysis results and a 3D view showing the coronary arteries, the ventricle and the aorta. This approach does not require an accurate registration of perfusion and angiographic data. However, it demands an accurate, patient-specific assignment of coronary branches to myocardial segments which in turn requires a detailed analysis of the coronary tree and its distribution around the ventricle. For simplification, the standard correspondence according to the 17-segment model (Subsec. 2.2.3.4) is applied in the following. Coincidentally, this correspondence is valid for the patient mentioned above. However, since it is only valid for $\approx 70\%$ of the population, it is recognized by the author that the concurrent analysis of perfusion and vasculature would strongly benefit from the patient-specific assignment of coronary branches to myocardial segments or a fusion of perfusion and angiographic data. The fusion would facilitate a subsequent examination of a specific coronary branch for possible stenosis once a perfusion disturbance has been detected. Fusing perfusion data and less cost-intensive patient-specific MRCA data is discussed in [Hennemuth et al., 2008c]. While first promis-

ing results could be achieved, a reliable concurrent analysis is hampered by the poor image quality of MRCA data resulting in fragmented segmentations of the coronary tree. The computation of patient-individual vascular supply territories based on the coronary artery distribution and a corresponding refinement of the BEP have been introduced in [Termeer et al., 2009] and are subject to further clinical validation.

3.4.1.1 Preprocessing of the Angiographic Data

In a first step, the epicardial left ventricle is segmented from the CTCA data using Live-wire as an edge-based segmentation method [Schenk et al., 2000]. Hereby, the Live-wire algorithm is applied on a user-selected subset of slices. An intelligent cost function is employed which refines its immanent parameters after each contour delineation leading to a reduced number of required seedpoints for subsequent slices. Once the user has processed the subset of slices, intermediate contours are computed utilizing shape-based interpolation. The contours are then optimized according to the learned Live-wire cost function. The resulting binary ventricle mask is resampled and then smoothed by a Gaussian kernel to improve the visual appearance of the epicardial surface which is reconstructed by Marching Cubes [Lorensen and Cline, 1987]. Accuracy is not a critical issue here since the ventricle only serves as context information. In a next step, the coronary tree is segmented from the original CTCA data (no preprocessing) by means of an advanced 3d region growing algorithm [Hennemuth et al., 2005]. The aorta ascendens is manually separated from the vessel segmentation result, stored in an extra data set and preprocessed and visualized similar to the left ventricle. For the coronary arteries, the vessel skeleton and associated radius information is extracted with the help of a thinning algorithm presented in [Selle et al., 2002]. The three main branches of the coronaries, LAD, LCX and RCA, are identified manually according to their splitting pattern proximal to the aorta (Subsec. 2.2.1.3) and assigned a unique color. The skeleton as well as the coloring serve as an input for the visualization of the coronaries by means of *Convolution Surfaces* [Oeltze and Preim, 2005]. Polygonal models of the left ventricle, the aorta ascendens and the coronary arteries are eventually combined in a single 3D view (Fig. 3.22 (e)).

3.4.1.2 Interactive Bull's Eye Plot

The link between the BEP and the 3D view, in particular the coronary arteries, is established by assigning a unique ID to the polygonal models of the three main branches. The same ID is assigned to each segment of the plot which is supplied by the respective branch according to the standardized correspondence. Furthermore, picking facilities are implemented for both, the plot and the 3D view. A segment of the plot exhibiting a suspicious parameter value may now be selected by the user via mouse interaction (Fig. 3.22 (c)). The previously assigned ID is retrieved and the corresponding vessel branch is focused in the 3D view (Fig. 3.22 (e)).

Focusing of objects benefits from animations since the user is guided through the scene instead of being confronted with the final interaction results only. For focusing purposes, animation scripts are applied which are based on a script language independent of the underlying data [Mühler et al., 2006]. The script language allows to define appropriate viewpoints for each object of interest which serve as an input for computing animations in-between.

To focus on the coronary branches, the animation script requires a predefined appropriate viewpoint for each branch. This definition is accomplished by the user so far. However, the process is supported based on computing a sphere S enclosing the entire scene. As the center

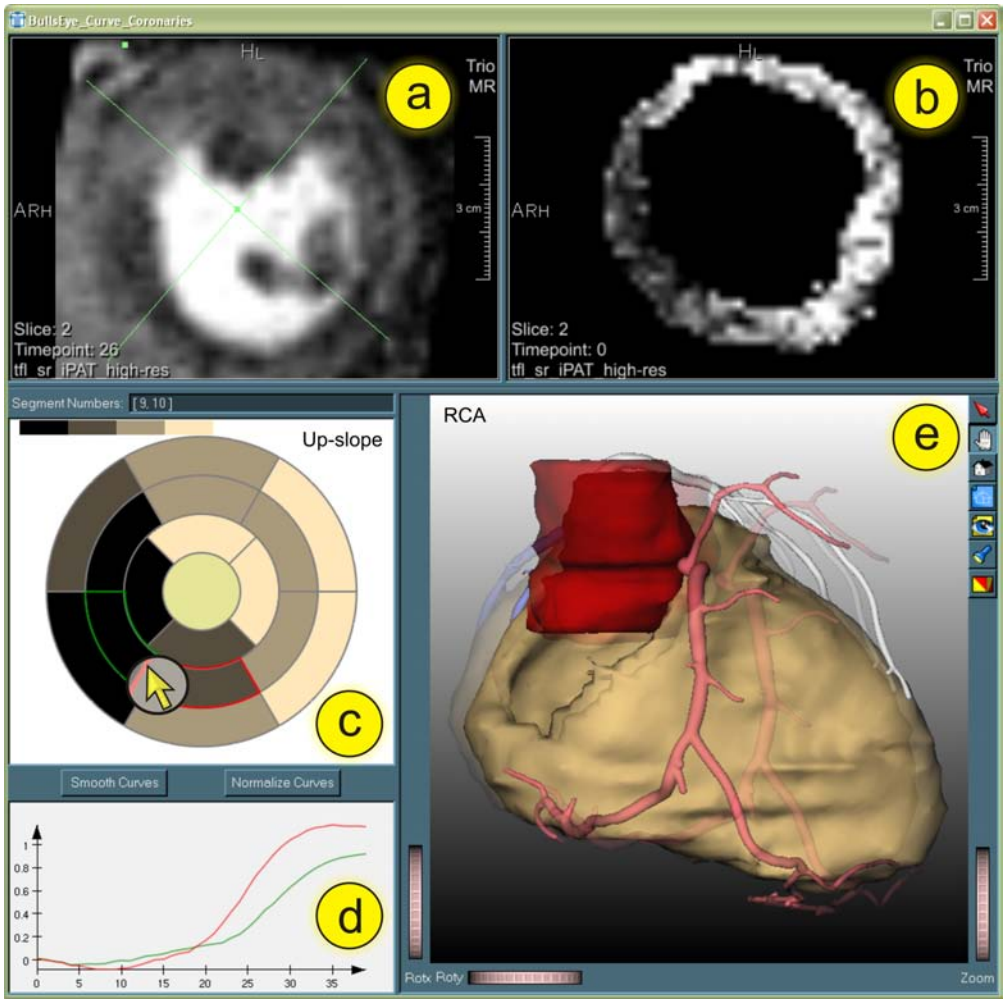

Figure 3.22: Integrated Visualization of perfusion and angiographic data. *a*: Apical slice of the original perfusion dataset and the AHA-consistent segmentation of the myocardium overlaid. *b*: Apical slice of the parameter volume computed for *Up-slope*. *c*: Selection of 2 segments in the Bull's Eye Plot which color-codes the parameter *Up-slope*. Segment 17 is missing since no slice has been acquired at the apex itself. *d*: Time-intensity curves corresponding to the selected segments. *e*: Coronary branch (RCA) supplying the selected segments is focused. The animated focusing process is illustrated by a semitransparent overlay of a previous point in time. (Data is courtesy of M. Fenchel, S. Miller and A. Seeger, Max Planck MR-center, University of Tübingen, S. Achenbach, University Hospital Erlangen, and SIEMENS Healthcare.)

c of S, the center of the scene's axis-aligned bounding box BB is determined. To include the whole scene, the radius r of S is computed as the distance between the furthermost vertex of BB and c. Next, the viewpoint is determined manually for each branch by moving the camera along a trajectory on S. The camera position is modified via the script language by applying the trigonometric description of a sphere and varying azimuth and elevation angles. Zooming in and out is supported as well. Once ideal viewpoints were determined, the corresponding angle values and zooming factors are stored in a separate file for each branch. When the user selects a segment in the BEP, the corresponding file is fed into the script interpreter. The interpreter then performs the animated motion from the current camera position to the stored ideal viewpoint and lets the camera orbit the ventricle.

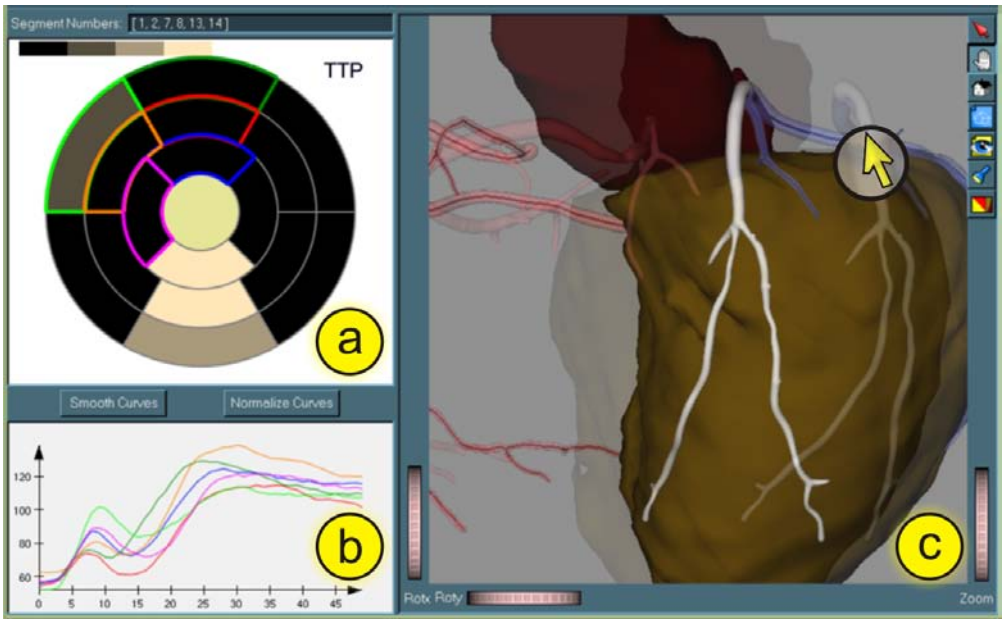

Figure 3.23: Selection and focus of a coronary branch (LAD) in the 3D view (c). The course of the animation is illustrated by a superimposition of a previous point in time. The other branches are rendered semi-transparently with the vessel skeleton overlaid to enhance spatial comprehensibility. The segments of the Bull's Eye Plot which correspond to myocardial regions supplied by the selected branch are highlighted (a). The respective time-intensity curves are visualized (b). (Data is courtesy of M. Fenchel, S. Miller and A. Seeger, Max Planck MR-center, University of Tübingen, S. Achenbach, University Hospital Erlangen, and SIEMENS Healthcare.)

As mentioned above, the link between the BEP and the 3D view is bidirectional. The user may select a coronary branch in the 3D view by picking via mouse interaction as well. Based on the correspondence between coronary branches and supplied myocardial regions, the respective segments of the BEP are highlighted and the associated TICs are displayed (Fig. 3.23). Regarding the 3D view, the camera moves to the ideal viewpoint defined for the selected branch. For further emphasizing the selection, the other branches are rendered semi-transparently while the selected branch is rendered opaque. In addition, the saturation of the surface colors of the left ventricle and the ascending aorta is strongly reduced. The change in material properties is animated as well over a predefined period of time.

3.4.1.3 Analysis of Vasculature

In cases, where patient-specific angiographic data is available, the application shown in Figure 3.22 might be extended by a 2D view and a diagram view for the analysis of vasculature. The user could specify a position along the vessel tree and the system could compute a multiplanar reformation orthogonal to the vessel skeleton through the angiographic data. The resulting image would be displayed in the additional 2D view. If a CTCA was applied, an analysis of the Hounsfield units may support the detection of plaque. Furthermore, a radii profile along the vessel skeleton for a selected range about the user-specified position could be displayed in the diagram view. The cross sectional view of the vessel in the MPR together with the radii profile may indicate stenosis. Different radius information, e.g. minimum and maximum radius, as well as the ring of voxels sampling the vessel wall are available from the thinning algorithm applied for skeletonizing the vessel tree [Selle et al., 2002].

3.4.2 Integrating Perfusion, Late Enhancement and Cine Data

To facilitate a joint inspection of myocardial perfusion, function and viability, the 3D glyph-based visualization of perfusion parameters presented in Subsection 3.3.2 is enhanced by integrating the parameters wall thickening and transmurality. See Subsection 2.2.3.6 for a detailed description of these parameters and their computation. The patient studies $case_1$ and $case_2$, which are utilized in the following, have been described in Subsection 3.3.2.1. A few abbreviations are used in this subsection to improve the readability:

- $SFepi_{LE}$: Left ventricular epicardial surface from LE data,
- $SF\{epi, endo\}_{cine\{ED,ES\}}$: Left ventricular endocardial (endo) and epicardial (epi) surface from Cine data at end diastole (ED) and end systole (ES), respectively,
- $SFrv_{cineED}$: Right ventricular surface from cine data at ED,
- $SFscar_{LE}$: Surface of the scar from LE data.

3.4.2.1 Perfusion and Viability

Since the coronary arteries are attached to the epicardium, perfusion deficits and infarctions occur here first and then, propagate towards the endocardium. Therefore, also scarred tissue mostly adjoins the endocardium and the transmurality may be measured indirectly by computing the minimum distance from the scar to the epicardium. A short distance then corresponds to a high transmurality. In order to assess the transmurality, the distance from each vertex of $SFscar_{LE}$ to $SFepi_{LE}$ is computed and stored in a field associated to the vertex. The distances are then color-coded on $SFscar_{LE}$. As an example, the transmurality has been determined and visualized for $case_1$ in Figure 3.24(a). The transmurality in this particular example is quite low over the entire scar (greenish regions). Only close to the right ventricle and at the basis, small distance values indicating a higher transmurality are revealed (dark regions). The small values at the basis can be neglected since $SFscar_{LE}$ and $SFepi_{LE}$ overlap in this region. The overlapping results from the surface generation algorithm that produces closed surfaces and caps the epicardium and the scar in the first and last slice of their occurrence (Subsec. 3.3.2.2). In a more advanced solution, the caps should be removed before distance computation. They are kept here for illustrating this discussion.

3.4.2.2 Perfusion, Function and Viability

The parameter wall thickening is retrieved based on three passes of minimum distance computations. Before the distances are computed, the caps of $SFendo_{cineED}$, $SFepi_{cineED}$, $SFendo_{cineES}$ and $SFepi_{cineES}$ are removed to avoid invalid computations. In a first pass, the distances between $SFendo_{cineED}$ and $SFepi_{cineED}$ are computed and stored in fields associated to the vertices of $SFendo_{cineED}$. Next, the process is repeated for $SFendo_{cineES}$ and $SFepi_{cineES}$. After that, the wall thickness has been computed at end diastole and end systole and is stored with the endocardial surfaces. The latter has been chosen to allow for an occlusion-free integration of the viability information later on. In the last pass, a copy of $SFendo_{cineED}$ is generated ($SFendo'_{cineED}$) and for each vertex in this copy, the closest vertex in $SFendo_{cineES}$ is determined. Based on the field values FV_{ED} and FV_{ES} of a vertex pair, the wall thickening is calculated such that it describes the percentage increase of wall

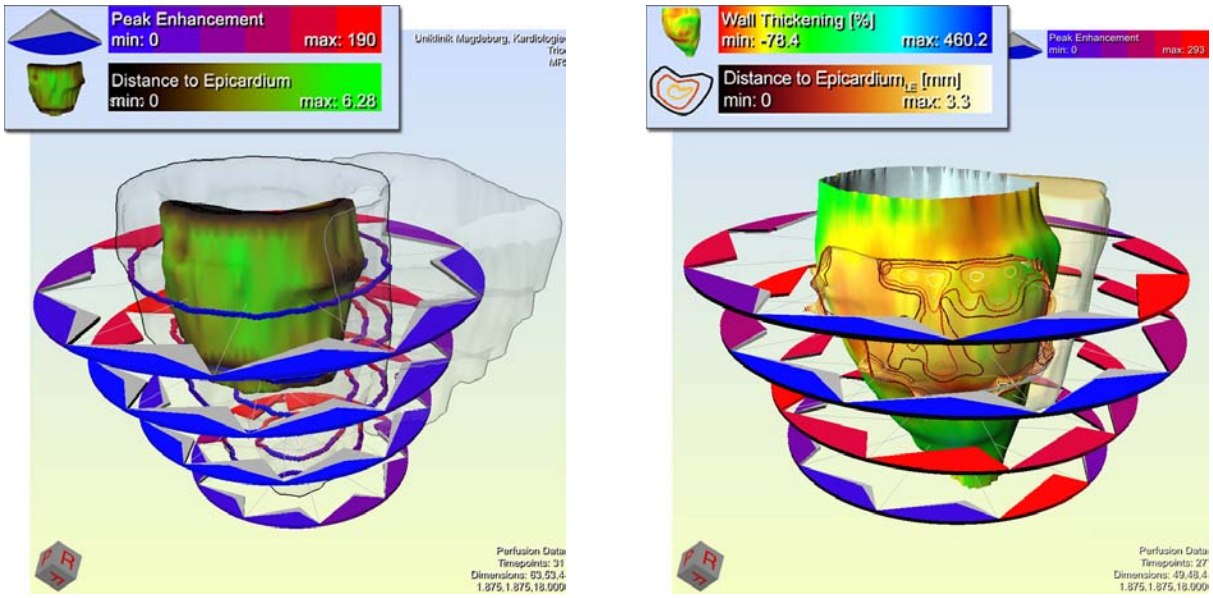

(a) (b)

Figure 3.24: Integrated visualization of myocardial perfusion, viability and function. The perfusion is encoded as in Figure 3.19. *(a)*: Integrating perfusion and viability. The infarction scar (opaque surface inside the ventricle) is colored with respect to its distance to the epicardium. Dark parts exhibit small distances, i.e. a high transmurality. *(b)*: Integrating perfusion, viability and function. Isolines encode the surface distance of the scar to the epicardium. The overall transmurality is high, indicated by dark isolines (small distance values) enclosing large surface parts. The wall thickening is color-coded on the endocardium. Red regions exhibit a decreased contractility. (Data is courtesy of Frank Grothues, University Hospital Magdeburg.)

thickness from end diastole to end systole according to Equation 2.11. The field values of the vertices in $SFendo'_{cineED}$ are replaced by the computed wall thickening values.

As an example, the wall thickening has been determined and visualized for $case_2$ by coloring $SFendo'_{cineED}$ according to the vertex' field values (Fig. 3.24(b)). With the applied color look-up-table, small values are mapped to red, values around 100% to green and very high values to blue. The interpolation in between is carried out in the perceptually roughly linearized HSV color space. Before discussing the visualization in more detail, adding the transmurality to this exemplary representation will be explained.

In first experiments, the transmurality was color-coded on $SFscar_{LE}$ as in Figure 3.24(a). This of course would lead to an undesired occlusion of the wall thickening information in the infarction zone. Though increasing the transparency of $SFscar_{LE}$ would reveal the occluded parts of $SFendo'_{cineED}$, color blending would mislead the viewer. To solve the occlusion problem, 3D isolines are computed on $SFscar_{LE}$ by considering the stored distances to $SFepi_{LE}$. The isolines are then superimposed on a highly transparent, colorless version of $SFscar_{LE}$ (Fig. 3.24(b)). The number of isolines has been chosen empirically so far and the corresponding isovalues are uniformly distributed in the range of measured distances. While all previously discussed visualization techniques have been implemented in the software platform `MeVisLab`[3], the isolines were generated using `AMIRA`[4].

[3]Product of Fraunhofer MeVis; www.mevislab.de (01/16/2010)
[4]Product of Visage Imaging GmbH;www.amiravis.com (01/16/2010)

The comprehensive cardiac visualization in Figure 3.24(b), facilitates a joint assessment of perfusion, function and viability. In the region of the scar, the perfusion is hampered as indicated by flat bluish TICs revealing parts of the reference TICs. The red regions on the endocardium imply a loss of wall thickening in the infarction zone. Close to the base, a region with a decreased wall thickening appears that does not belong to the infarction zone. This might be a hint on hibernating myocardium. To review this assumption, the perfusion in this region must be assessed. However, the perfusion scan did not cover the top basal part of the myocardium. A perfusion deficit in this region would confirm the existence of hibernating myocardium. The overall transmurality of the scar is high as indicated by dark isolines (small distance values) enclosing large surface parts. Unfortunately, this must be interpreted as a negative prediction for long-term improvement of cardiac performance.

3.5 Conclusion

Multiparameter maps enable the simultaneous visualization of two (colored height field, flexible lens) or more perfusion parameters (color icon). Height fields are visually attractive and might be used to present diagnostic results, e.g., in educational settings. However, the use of height fields poses interaction problems due to occlusion and is probably not an optimal choice for efficient routine diagnosis. The use of lenses is based on ideas of clinical users and was considered useful in informal discussions with a neuroradiologist and a cardiologist from the medical faculty of the University of Magdeburg. Both appreciated that they can explore two parameter maps simultaneously instead of having to mentally integrate the information from spatially separated visualizations. The neuroradiologist valued the synchronized lenses for comparing the two hemispheres and suggested the extension to arbitrarily shaped lenses as well as an automatic computation of the vertical symmetry axis. Color icons are useful for integrating more than two parameters. As documented in Subsection 3.2.3, the resulting texture may facilitate the concurrent inspection of features which are otherwise depicted separately in different parameter maps. However, it was also shown that features which are clearly perceivable in a single map may be suppressed in the multiparameter visualization. Hence, color icon-based multiparameter maps should not replace conventional maps but add to the diagnosis by providing new insight.

The presented 2D glyph-based visualization was successfully applied for detecting and analyzing pathologies in datasets from three different application areas so far. The visualization is coupled with a feature specification component. By brushing interesting parameter combinations, visual clutter is reduced and the user gains a deeper insight into the data. In order to improve the discrimination of glyph attributes, the screen space for glyph display is increased by glyph aggregation. Different resolution layers are generated and the user may interactively drill down the layers while focusing on a suspicious region. A clinical evaluation should clarify which glyph shapes perform best regarding accuracy and speed of detecting perfusion disturbances. Furthermore, the winning glyph-based visualization should be compared to side-by-side presentations of conventional parameter maps. Also the usefulness of the feature specification component and the multi-resolution glyph display should be tested.

The 3D glyph-based visualization was applied to a low-dose CA myocardial perfusion study with 15 participating patients. The analysis results could be validated by means of the study report. For a voxel-wise perfusion analysis, cubes outperform other simple primitives since they optimally cover the space they represent. Furthermore, their size is easier to perceive from different viewing angles than for elongated shapes, e.g., ellipsoids. To resolve

spatial orientation problems in a segment-wise analysis and to provide a good spatial match of myocardial segments and corresponding glyphs, advanced glyph types have been introduced, namely the 3D BEP segment and the 3D TIC miniature. 3D BEP segments are inspired by the well established BEP. The 3D TIC miniatures provide a concurrent, intuitive mapping of all important parameters in cardiac diagnosis. They exploit the familiarity of physicians with TIC shapes. A drawback of the TIC miniatures is their variation in shape depending on the number of segments per slice. For a small number (< 6) they are considerably stretched and flattened. A further problem is that the declining part of the glyph suggests a signal decrease back to the level of *CA arrival* which is not a valid assumption (Fig. 2.23(a)) and in fact, the scanning duration is often too short to cover the entire CA washout. For the joint inspection of perfusion, function and viability, the glyph-based visualization has been combined with a color encoding of wall thickening on the endocardial surface extracted from Cine data and with isolines depicting the transmurality along the scar's surface.

While the 3D glyph-based visualization of myocardial perfusion was new in 2008 when it was published [Oeltze et al., 2008a], in the same year and one year later Meyer-Spradow et al. [2008] and Termeer [2009] presented comparable approaches. Both are discussed in detail at the end of Subsection 3.1.2 and 3.1.3, respectively. Meyer-Spradow et al. investigated their approach for SPECT data, whereas Termeer employed MRI data. SPECT does not facilitate the direct imaging of necrotic tissue. The supertorii applied in [Meyer-Spradow et al., 2008] encode perfusion and wall thickening. Rest/stress scans are considered and the respective tracer *uptake* is used for parameter mapping. Termeer focuses on the *Upslope* and employs uniformly colored dots whose size encode the parameter values. In both approaches, the glyphs are placed on the surface of the left ventricle representing a region that is indicated by a grid pattern in [Meyer-Spradow et al., 2008] but remains unclear in [Termeer, 2009]. A voxel-wise glyph placement facilitating a detailed inspection of perfusion across the myocardial wall is not included in either of the approaches. Since SPECT data offer a more comprehensive coverage of the left ventricle along it long-axis, the perfusion is more densely sampled. In [Termeer, 2009], perfusion is derived by a numerical method and may thus be computed across the entire ventricle. Hence, the initial situation is different for glyph placement and design as compared MR myocardial perfusion where only a sparse ventricular coverage is achieved. From a visualization point of view, the most comprehensive cardiac visualization is achieved in [Termeer, 2009] by integrating perfusion, viability and function as well as the vascular anatomy. A particularly interesting aspect in [Meyer-Spradow et al., 2008] is the computation of a level of conspicuousness based on perfusion and function which controls the glyph opacity (high opacity indicates high conspicuousness).

The refined Bull's Eye Plot and the linking to angiographic data have been considered useful in informal discussions with a cardiologist from the medical faculty of the University of Magdeburg. He explained that supporting the simultaneous examination of rest and stress perfusion has been widely neglected so far. He suggested that the 3D view would benefit from mapping the perfusion analysis results to the ventricular surface hereby facilitating an exact assignment of the perfused territories to the supplying coronary branches. The picking facilities implemented for the BEP and the 3D view as well as the animated focusing of coronary branches might contribute to patient education.

3.6 Discussion

A substantial clinical evaluation of the presented 2D and 3D glyph-based visualizations is still outstanding, though some anecdotic feedback could be collected regarding the latter (Subsec. 3.3.2.4). From the visualization point of view, both approaches should be reviewed with respect to the 8 usage guidelines for the integration of glyph-based techniques in medical visualization [Ropinski and Preim, 2008]:

Guideline 1: Parameter mapping functions should visually emphasize important variables. (*2D*) For cerebral perfusion, there is no agreement yet on the most important parameter. In breast tumor and myocardial perfusion, particular clinically relevant parameters have been identified. In Figure 3.15(b), only these parameters are encoded. In Figure 3.15(c), *PE* is added by color coding. *Up-slope* being the most accredited parameter is mapped to orientation since the perception of quantities depicted by orientation is more accurate than by color [Cleveland and McGill, 1984]. Furthermore, the mapping to orientation adheres to an intuitive mapping. (*3D*) The visualizations based on 3D TIC miniatures, e.g., in Figure 3.19, could be improved by mapping *Up-slope* to color instead of *PE*. All other visualizations illustrating Subsection 3.3.2.3 adhere to the guideline.

Guideline 2: Parameter mapping functions should guide the user's focus of attention. (*2D*) Figure 3.12 violates this guideline since regions represented by very small glyphs are of special interest. On the other hand, small glyphs represent a low blood supply while large glyphs represent a normal supply. In Figure 3.15(a), the mapping to *PE* has been inverted such that large glyphs (small *PE*) guide the user's attention to the suspicious tissue. Hence, a trade-off between conspicuity and intuitiveness may be required. In Figure 3.15(c), the viewers attention is guided to reddish regions though the bluish regions characterize the perfusion disturbance. Since cardiologists are used to the encoding of oxygen-rich by red and oxygen-low by blue this might not pose an issue for them. (*3D*) In order to follow this guideline, the mapping of *Up-slope*, e.g., in Figure 3.16, should be inverted since small values are of special interest. However, intuitiveness was favored in this case. The issue of the blue-to-red color scale has been discussed above. In Figure 3.19, visible parts of the reference TICs may be highlighted in order to guide the user's focus of attention to less perfused regions.

Guideline 3: Parameter mapping functions should incorporate semantics of the data. (*2D*) The visualizations adhere to this guideline by following the rules illustrated in Figure 3.10. (*3D*) *Up-slope* should be mapped to glyph orientation according to the guideline. However, in a voxel-wise glyph placement (Fig. 3.16(a)), occlusion problems would hamper the differentiability of orientation. Apart from that, the differentiability is dependent on the viewpoint, also in segment-wise placements (Fig. 3.16(b)).

Guideline 4: Parameter mapping functions should be mentally reconstructable based on the visualization. (*2D*) One way to achieve this is to apply perceptually linearized color scales where the perceptive distance between color matches the represented range of values [Ropinski and Preim, 2008]. Figure 3.14(b) provides a good example since the perceptually roughly linearized HSV color space is applied for color coding. Furthermore, triangles probably facilitate the easiest mental reconstruction of the parameter mapping since

they are symbolic miniatures of the represented information (TIC). The heated object color scale and the magenta scale, applied, e.g., in Figure 3.14(a) and 3.15(a), should be replaced by perceptually linearized versions as presented in [Levkowitz, 1997]. (*3D*) Similar to triangles, TIC miniatures facilitate the easiest mental reconstruction of the parameter mapping (Fig. 3.19). The blue-to-red color scale could be replaced by a perceptually linearized version.

Guideline 5: Glyph placement should avoid unwanted glyph aggregations in image space. (*2D*) Jittering has been applied to the glyph positions in oder to avoid visual irritations caused by undue grid patterns. (*3D*) The glyph positions have been jittered for a voxel-wise glyph placement (Fig. 3.16(a)). No unwanted glyph-aggregation occurs for the segment-wise placement.

Guideline 6: Glyph shapes should be unambiguously perceivable. (*2D*) Since the glyphs are presented in 2D only and this guideline is related to the viewing direction, it can be neglected here. However, in the context of this guideline, Ropinski and Preim [2008] also mention the importance of intuitive glyph shapes which express the semantics of the parameters to be shown. The most intuitive glyph shape in the context of perfusion parameters is the triangle due to the reasons mentioned in Guideline 4. (*3D*) TIC miniatures clearly express the semantics of the shown parameters. However, the perspective viewing mode should be switched to orthogonal projection in order to facilitate a comparison of glyphs with varying distance from the camera (Fig. 3.19(a)). Furthermore, the glyphs should be realigned with respect to the viewing direction such that their readability is maintained.

Guideline 7: Glyph visualizations should support quantitative analysis in the attentive phase. (*2D*) The glyphs may be picked by the user and the corresponding TIC is displayed in a curve view. Tooltips which give an overview on the corresponding parameter values would contribute to a quantitative analysis and may be added in future work. (*3D*) No support has been integrated for a quantitative analysis so far.

Guideline 8: Hybrid visualization should be exploited to provide the spatial context. (*2D*) The glyphs are superimposed on a slice of the original perfusion scan. The slice number as well as the point in time may be adjusted. As illustrated in Figure 3.12(c), this facilitates the inspection of the glyphs in the context of anatomical features, e.g., ventricles and major blood vessels in cerebral perfusion. (*3D*) The glyph visualization is embedded in a spatial context consisting of surface representations of both ventricles and the infarction scar (Fig. 3.20(a)).

Chapter 4

Visual Analysis

The pure visual assessment of perfusion data and associated perfusion parameters is an observer-dependent and barely reproducible task delivering no quantitative results. An approach is required that merges visual exploration and data analysis techniques into visual analysis for a streamlined investigation of perfusion. Such an approach may integrate statistical methods for dimension reduction, the detection of trends, and the exposure of inter-parameter relations. To reduce the amount of data for visual exploration, a feature-based approach is appropriate since it directs the user to suspicious areas. Features may either be specified automatically by data mining or knowledge discovery algorithms or interactively by the user. A benefit of the latter is that the user gains a deeper insight into the data by interactively changing the feature specification and simultaneously observing the updated specification result, i.e., the tissue selection. The feature specification should account for the involved uncertainty due to the non-standardized domains of MR signal intensity and perfusion parameter values.

The visual analysis may be based on different kinds of data, such as the original perfusion data, descriptive perfusion parameters, derived statistical analysis results, or quantitative perfusion parameters. The way of specifying a feature as well as the complexity of the specification process vary with respect to the underlying data. Furthermore, the specification result is likely to differ. Hence, a comparison is required which contributes to a discussion between *data-near* and *model-near* (quantitative perfusion) assessment strategies and their respective opportunities.

The remainder of this chapter is organized as follows: Section 4.1 is dedicated to work which is related to data mining and knowledge discovery in perfusion data as well as to the interactive visual analysis of medical (multiparameter) data. Section 4.2 presents an interactive approach for the streamlined visual analysis of perfusion data which has been published in [Oeltze et al., 2007]. The approach consists of three components for data preprocessing, statistical analysis, and feature specification. It is applied to several datasets from ischemic stroke, CHD, and breast tumor diagnosis as a proof of concept. In Section 4.3, the feasibility of the approach for answering crucial investigative questions in perfusion research is demonstrated by comparing *data-near* and *model-near* perfusion assessment. Four variants of the approach based on four different kinds of input data are presented in the context of cerebral perfusion. The different approaches are compared regarding the complexity of the interactive visual analysis. The focus is on the involved data preprocessing as well as the feature specification. Furthermore, the respective tissue selections are compared quantitatively. This work has been published in [Oeltze et al., 2009]. The chapter is completed in Section 4.4 by a summary and a brief discussion of the presented work.

4.1 Related Work

This section summarizes relevant work related to data mining and knowledge discovery in perfusion data as well as to an interactive visual analysis of medical data. The second part is focused on the application of multiple linked views showing the data and derived variables such as statistical analysis results from multiple perspectives. It comprises related work documenting the value of an interactive visual analysis for evaluating medical multiparameter

data. Both parts make no claim to be complete but present a relevant subset of existing work which has inspired the thesis and additionally include highly topical publications. Portions of this section are based on a recently published survey of the visual exploration and analysis of perfusion data [Preim et al., 2009].

4.1.1 Data Mining and Knowledge Discovery in Perfusion Data

This subsection is structured according to the main application areas of perfusion data.

Cerebral Perfusion. Wismüller et al. [2006] propose clustering as a promising extension to parameter maps in assessing ischemic stroke. They apply a minimal-free-energy vector quantization, self-organizing maps, and fuzzy c-means clustering to achieve a segmentation of ischemic tissue in DSC-MRI images. Their approach was successfully applied to two patients with and two patients without a history of stroke, respectively. The clustering results added to an analysis by means of parameter maps through unveiling additional subtle side asymmetries.

In [Wu and Liu, 2007], independent component analysis (ICA) is performed on DCE-CT perfusion images of nine patients with ischemia and/or a brain tumor. First, the minimum description length criterion is applied to determine the number of independent components. Next, a principal component analysis (PCA) is carried out based on this criterion for dimension reduction. Finally, the ICA is applied resulting in component maps which support the identification of arterial and venous structure and improve the demarcation of tumor territories.

Kao et al. [2008] investigated the ICA for classification of brain tissue in DSC-MRI images of 12 patients suffering from a unilateral carotid stenosis. The classification results were exploited as regions of interest for which the mean CTC as well as the perfusion parameters were subsequently computed. It could be concluded from the derived variables that the ICA provides useful information about the blood supply to arteries and the local perfusion of brain tissue. In addition, AIFs could be automatically modeled as the mean CTCs of normal and stenotic arteries which were represented as distinct components.

Myocardial Perfusion. Di Bella and Sitek [Bella and Sitek, 2001] present the application of a factor analysis and an extended k-means clustering for blood pool detection in myocardial perfusion MRI data. They find the clustering approach to be less sensitive to starting estimates. With their approach, both ventricles and the left ventricular lumen (blood pool) are identified. No further classification of myocardial tissue is achieved.

In [Hansen et al., 2007], myocardial perfusion MR images were analyzed by an extension of the Support Vector Domain Description. The images were first motion-corrected and the myocardium was segmented using an active appearance model. Then, myocardial tissue was classified into ischemic and healthy tissue. Finally, the results were compared to a common pixel-wise analysis in parameter maps and were found to correspond well.

Blekas et al. [2008] propose a regression mixture model with spatial constraints for clustering spatiotemporal data and apply the model in a case study to myocardial perfusion MR images obtained from an instrumented pig. The spatial constraints are defined such that spatially adjacent voxels have a higher probability of belonging to the same cluster. A successful identification of both ventricles, the lumen and coronary arteries could be documented. However, the results must be reviewed with respect to real patient data where less slices are acquired at fewer points in time administering a lower CA dose.

Breast Tumor Perfusion. In particular, the classification of DCE-MRI mammography data by means of artificial neural networks and clustering techniques is an active research area [Chen et al., 2006; Nattkemper and Wismüller, 2005; Twellmann et al., 2005; Schlossbauer et al., 2008; Glaßer et al., 2009]. As an example, Twellmann et al. [2005] applied an artificial neural network architecture which combines unsupervised and supervised techniques for voxel-by-voxel classification of temporal kinetic signals derived from the data. Chen et al. [2006] developed a fuzzy c-means clustering-based technique to automatically identify characteristic kinetic curves from segmented breast lesions in the data. Nattkemper and Wismüller [2005] described the application of self-organizing maps to time curve features of the data and discussed how the results may be visually represented as color-coded cross-sections. Schlossbauer et al. [2008] focus on the classification of small enhancing breast lesions in DCE-MRI mammography data. They apply a combination of morphological criteria and dynamic analysis based on unsupervised vector-quantization for assessing the dignity (benign/malignant) of a lesion. Recently, Glaßer et al. [2009] presented a region-wise qualitative and quantitative analysis of lesion enhancement kinetics. The regions are generated by a region merging approach that aggregates voxels with similar perfusion characteristics. The analysis is combined with a glyph-based representation for a fast overview of the entire lesion.

A broad variety of data analysis techniques has been applied to perfusion data from different application areas. A common approach is to utilize the original time dependent data and to neglect perfusion parameters. This is motivated by two observations: (1) perfusion parameters only partially represent the available temporal information, and (2) their computation may involve error-prone sub-steps such as the determination of an arterial input function in cerebral perfusion. While each individual technique was proven to be successful in a particular application field and for a subset of datasets, a substantial comparison is lacking which identifies the technique that performs best in a certain application field or even across fields. If no gold standard can be determined, it should be investigated whether hypotheses may be derived from data properties that influence the choice of a particular technique and its parametrization. Furthermore, an evaluation of the techniques with respect to varying imaging parameters is desirable especially, while standardized imaging protocols are missing.

4.1.2 Interactive Visual Analysis of Medical Data

The interactive detection and visualization of breast lesions from DCE-MRI mammography data is presented in [Subramanian et al., 2004]. The applied view setup consists of a curve view for feature specification which is linked to conventional slice views and a 3D view. In the curve view, a reference curve may be interactively specified reflecting the desired TIC shape. Alternatively, the mean curve of voxels selected by the user in the 3D view is used. Additionally, a confidence interval as well as a lower and an upper threshold may be specified by the user for each point in time. All voxels exhibiting curves that fall into the confidence interval are assigned a confidence value of 1. All voxels exhibiting curves that fall outside the threshold curves are are assigned a confidence value of 0. In between, the confidence value is linearly interpolated. The 2D texture-based slice views and the 3D texture-based volume rendering of the data is updated whenever the user adjusts the desired TIC shape in the curve view. The color of the 3D volume rendering is computed as a mix of intensity and confidence value such that voxels with high confidence are assigned a bright red color while voxels with a low confidence are represented in shades of gray.

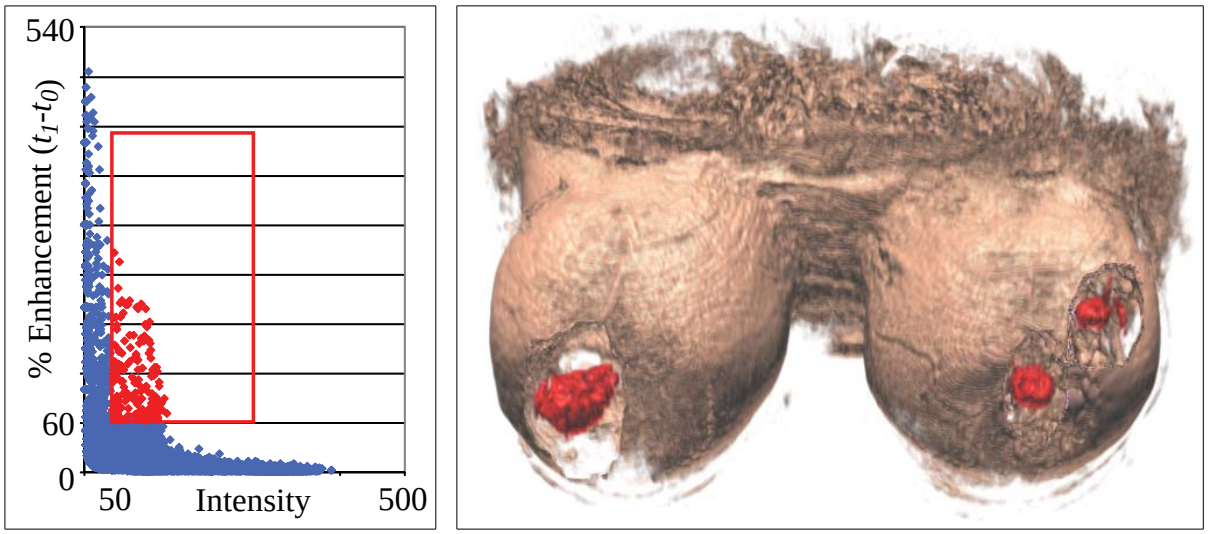

(a) (b)

Figure 4.1: Visual analysis of DCE-MRI mammography data. *(a)*: An enhancement scatterplot computed for the scan at t_1 is applied for feature specification (red rectangular brush). *(b)*: The importance-driven volume rendering shows regions (red) defined by brushing on a set of enhancement scatterplots. The lesions otherwise covered by the skin are revealed by assigning them an importance higher than the one of the spatial context. (Images are courtesy of Ernesto Coto, Central University of Venezuela.)

Coto et al. [Coto et al., 2005] presented several investigation tools, e.g., scatterplots and volume rendering for the classification and visualization of DCE-MRI mammography data. Their approach combines linking & brushing interaction with effective visualization of the selected suspicious areas. For the conversion of the TICs, the precontrast scan (t_0) is subtracted from all postcontrast scans (t_i). This step emphasizes the gradient in the temporal dimension of the analyzed curve and highlights suspicious areas. An enhancement scatterplot is calculated for each postcontrast scan (Fig. 4.1(a)). It shows the relative enhancement of the postcontrast scan with respect to the precontrast scan t_0. In the interaction step, brushing is performed on one of the scatterplots, while the selected set is emphasized on all remaining scatterplots. If the brushing is performed on multiple scatterplots, the result of the selection is calculated by a logical "and" operation. The selection set and the way of interaction with the scatterplots depends on the specific application. The result of the interaction can be displayed in a 2D slice view by highlighting the selected areas, or in a 3D view employing importance-driven volume rendering [Viola et al., 2004] (Fig. 4.1(b)).

Janoos et al. [2009] developed a system for the visual analysis of brain activity from functional MRI (fMRI) data. fMRI data represent a special kind of spatiotemporal scalar data with a time-series associated at every voxel. A hierarchical clustering algorithm performed in the wavelet domain is applied for the aggregation of voxels showing similar activity patterns. The resulting clusters are shown as a tree-like representation in a special view which is linked to conventional axial slice views and a 3D view showing the brain as a volumetric, cortical surface or by orthogonal cutting planes. Once clusters are selected in the tree, the corresponding voxels are highlighted in the 2D and 3D views by colored blobs.

The exploration of 3D DTI fiber tracts by combining traditional 3D views and lower dimensional representations is presented in [Jianu et al., 2009]. The 3D visualization based on streamtubes is linked to an embedding in the plane and a hierarchical clustering tree.

The linkage is represented by means of interaction and coloring. Special emphasis is on a perceptually uniform coloring. At first, similar fiber tracts are hierarchically clustered according to a pair-wise distance measure. The result is a similarity matrix. Then, the tract similarity is visualized by a dendrogram view as a hierarchical clustering tree. Furthermore, a planar embedding of the fiber tracts is generated by treating each tract as a point in 2D. The 2D coordinates reflect the distances stored in the similarity matrix. The authors gathered expert feedback indicating that their approach can accelerate tract bundle selection and improve the exploration of the connectivity in the brain.

Medical Multiparameter Data. Gresh and Rogowitz [Gresh et al., 2000] presented the system `WEAVE` for visually linking 3D and statistical visualizations applied to cardiac simulation and measurement data. Linking is implemented by means of color brushing, i.e., the user may interactively select a region in the 3D view or one of the statistical views and assign a color to this region. As a result, the corresponding regions in all other views are colored accordingly. The presented system for analyzing cardiac data comprises histogram views, scatterplot views, parallel coordinates views and a 3D view showing the cardiac anatomy as a surface representation. However, due to the underlying flexible architecture containing over 20 different representations of data, e.g., for the sophisticated visualization of correlations between variables, other systems may be rapidly prototyped. Inspired by the `WEAVE` system, Doleisch and Hauser [2002]; Doleisch et al. [2003] developed the `SimVis` framework for interactive feature specification in computational fluid dynamics data. `SimVis` will be discussed in more detail in Subsection 4.2.1.3 since it has been utilized also in the thesis at hand.

The exploration of higher dimensional histograms for differentiating tissue in ischemic stroke diagnosis was described by Grzesik et al. [2000]. They incorporate MR cerebral perfusion and diffusion-weighted imaging (DWI) data for an integrated analysis of stroke lesions. Histogram and scatterplot views are combined with a slice-based visualization of the original datasets or parameter maps. Perfusion parameters as well as parameters derived from the DWI data are computed and presented in the statistical views. The user may brush a region of interest in these views and the corresponding region in the slice view is emphasized by coloring.

In [Blaas et al., 2007], the concepts of Gresh et al. [2000] have been optimized for the interactive work with very large medical multi-field datasets and extended by the integration of analysis techniques from pattern classification. A framework of multiple coordinated views is presented consisting of a theoretically arbitrary number of histogram views, scatterplot views, slice views and pseudo-color slice views. The latter shows the same slice as the slice-viewer but colored according to features defined in the histogram or scatterplot view. The features may be defined interactively by the user or by means of pattern classification algorithms, such as clustering. Particularly interesting is the possibility of interactively creating and modifying scatterplots with arbitrary projections of the high-dimensional feature space. Blaas et al. successfully applied their framework for material classification in CT virtual colonoscopy and for a concurrent analysis of brain fMRI and structural MRI data.

Keefe et al. [2009] propose an interactive coordinated multiple-view visualization of biomechanical motion data. They employ a small multiples view [Tufte, 1990] of motion sequences, a parallel coordinates view, simple 2D plots and a 3D view showing a surface representation of the inspected anatomy. The small multiple overview presentation facilitates a concurrent visualization of hundreds of motion cycles. Zooming, filtering, and exploration is supported in all views thereby causing an update of the linked views. The presented

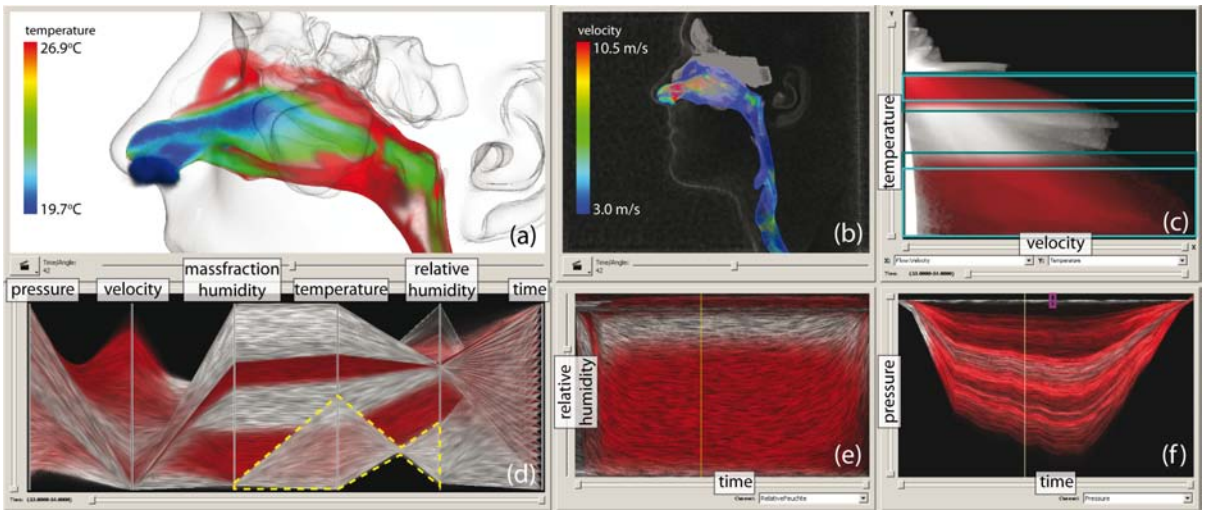

Figure 4.2: Visual analysis of nasal air flow. A parallel coordinates view *(d)*, a scatterplot view *(c)*, and two curve views *(e-f)* are linked with each other and brushing is applied for feature specification. The specification result is visualized in its spatial context in linked 3D views *(a-b)*. (Image is courtesy of Stefan Zachow, Zuse-Institut-Berlin.)

approach could be successfully validated in studying the mechanics of chewing motions in pigs.

Zachow et al. [2009] discuss a visual analysis approach for the investigation of nasal airflow. They exploit the `SimVis` framework [Doleisch and Hauser, 2002; Doleisch et al., 2003] for the analysis of modeling and simulation results based on data acquired in rhinomanometry (the investigation of nasal airflow and pressure). Several attribute views from Information Visualization such as parallel coordinates views, curve views for time-series visualization, histograms and scatterplots are linked with each other and to an unstructured grid multi-volume rendering showing the spatial context (Fig. 4.2). Brushing is facilitated in each attribute view causing a colored emphasis of the corresponding regions in all other views. Sophisticated point-based and ray-casting techniques have been integrated for rendering the spatial context and adapted in order to cope with large dataset size and severe occlusion problems. The in-depth analysis of nasal airflow with multiple-coordinated views led to a variety of interesting observations and new hypotheses.

4.2 Interactive Visual Analysis of Perfusion Data

This section is dedicated to an interactive visual analysis approach for the streamlined evaluation of perfusion data which has been published in [Oeltze et al., 2007]. The approach extends ideas from systems composed of multiple linked views for analyzing and exploring medical (multiparameter) data such as [Gresh et al., 2000; Coto et al., 2005]. It integrates preprocessing and statistical analysis methods as well as feature specification techniques. Motion correction and denoising are fundamental preprocessing steps to achieve a reliable correspondence of voxels over time. Since the different perfusion parameters are derived from the same curve, it is likely that some parameters correlate with each other. Hence, a correlation analysis and a PCA are applied in order to achieve a better understanding of the inter-parameter relations, to extract relevant parameter subsets, and to detect trends

in the data. The non-standardized domains of MR signal intensity and perfusion parameters complicate the diagnostic evaluation. For the visual analysis of such data, feature-based approaches allow to direct the user to suspicious regions and to reduce the amount of data. The presented approach integrates methods for an interactive feature specification of high-dimensional complex features in multiparameter data. Multiple, linked attribute views facilitate the definition of features which can be complex and/or hierarchically described by brushing multiple dimensions. Non-binary brushes account for the uncertainty involved in the inspection of a non-standardized parameter domain. Furthermore, they represent a natural mapping of irreversibly damaged/malignant tissue, reversibly damaged/suspicious tissue, and healthy tissue to focus, near-focus and context. The specification result from all attribute views is linked to a 3D view, establishing a focus+context style of visualization. The 3D visualization of perfusion parameters embedded in spatial reference information improves the comprehension of spatial relations between suspicious tissue and other anatomical constituents.

The presented visual analysis approach primarily addresses medical researchers seeking for a better understanding of, e.g., which perfusion parameters are crucial for specific diagnostic tasks and how imaging parameters influence the expressiveness of perfusion parameters. It is discussed with respect to clinical datasets from three major application areas: ischemic stroke, CHD, and breast tumor diagnosis.

4.2.1 Approach for a Streamlined Analysis

In the following, the interactive visual analysis approach is described independent of a specific application area. However, the included figures have been generated based on cerebral perfusion data to illustrate the approach by means of a real-world example.

The streamlined analysis consists of three major components (Fig. 4.3): a preprocessing component, a component for statistical analysis, and a component for interactive feature specification in multiparameter data. For the thesis, these components have each been implemented in `MeVisLab`[1], a platform for medical image processing and visualization, `MATLAB`[2], and the visual data analysis software `SimVis`[3].

4.2.1.1 Data Preprocessing

The original 4D perfusion data serves as input for the preprocessing component. Here, a motion correction algorithm is applied, the signal intensities are calibrated, and spatial as well as temporal noise may be reduced. The separate points in time (3D data) are exported and may, e.g., serve as context information during the visual analysis. For some applications, such as ischemic stroke or CHD diagnosis, it is useful to restrict the computation of perfusion parameters to relevant structures such as brain tissue or the ventricles of the heart. However, the segmentation part may be skipped if the entire dataset must be analyzed. At the end of the preprocessing, descriptive and/or quantitative perfusion parameters are derived voxel-wise for the segmented regions and exported separately as *parameter volumes*. These volumes serve as input for the feature specification as well as for the statistical component. The eligible algorithms for preprocessing of cerebral and myocardial perfusion data were discussed in Subsection 2.1.3 and 2.2.3.

[1]Product of Fraunhofer MeVis; www.mevislab.de (01/16/2010)
[2]Product of the MathWorks, Inc.; www.mathworks.com (01/16/2010)
[3]Product of the SimVis GmbH; www.simvis.at (01/16/2010)

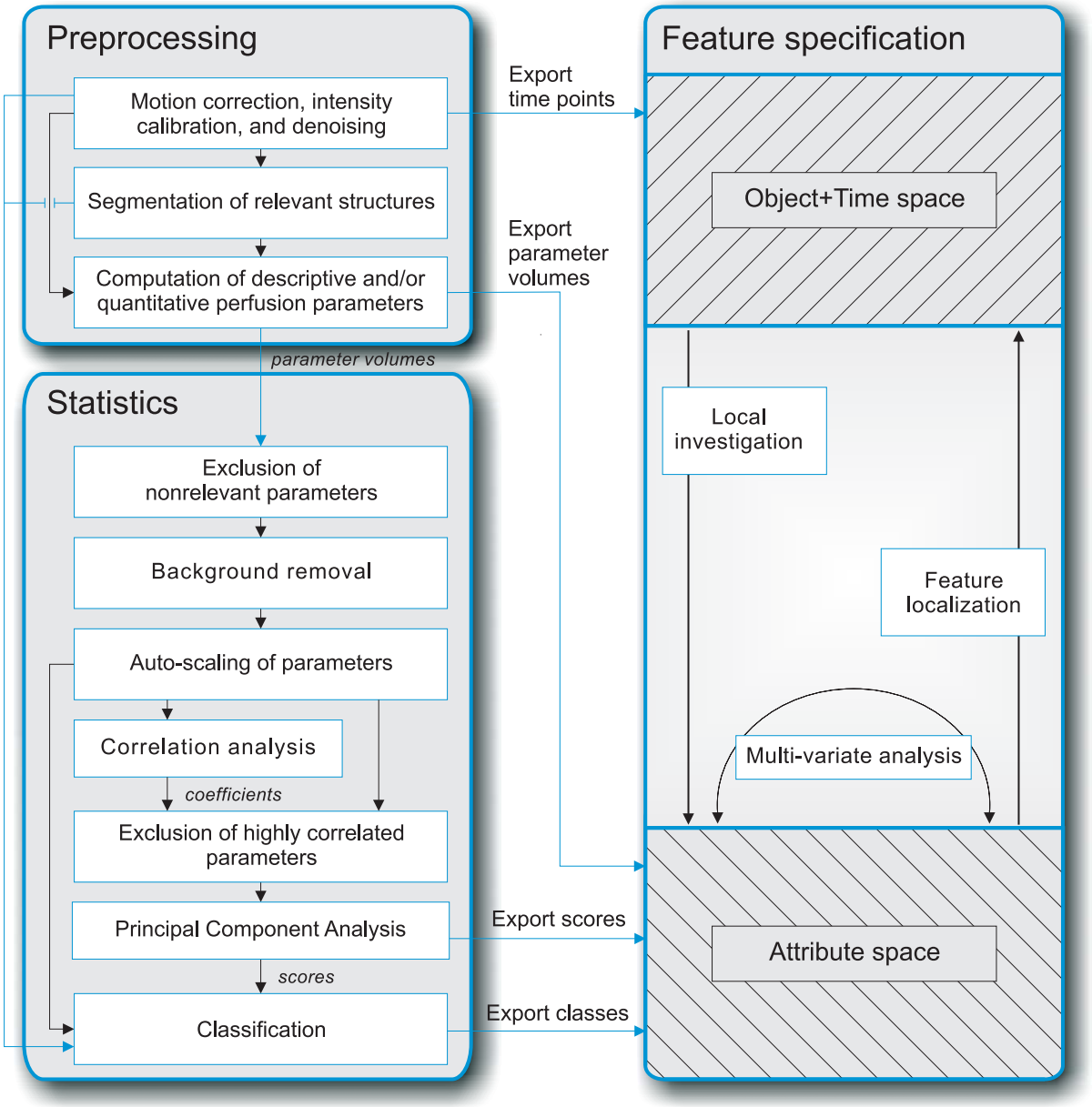

Figure 4.3: Schematic representation of the perfusion data analysis approach consisting of a preprocessing component, a component for statistical analysis, and a component for interactive feature specification.

4.2.1.2 Statistical Analysis

Before an application of the statistical analysis component is described in detail, the background of correlation analysis and PCA is reviewed briefly. For an in-depth discussion of PCA, the reader is referred to [Jolliffe, 2002].

Correlation Analysis. Correlation analysis reveals whether variables vary independently of each other or are (inversely) proportional. The amount of correlation is represented by the so-called *correlation coefficient (r)*. Let $A^{m \times n}$ be a matrix representing n variables (perfusion parameters) and m observations (number of voxels in a parameter volume). The symmetric matrix $R^{n \times n}$ of correlation coefficients is then computed based on the covariance matrix C

of A. A value of $r_{ij} = -1$ indicates a perfect inversely proportional relationship, whereas a value of $r_{ij} = 1$ corresponds to a perfect proportional relationship. A value of $r_{ij} = 0$ relates to non-correlated variables. Besides R, an equally-sized symmetric matrix P of p-values is computed for testing the hypothesis of no correlation. If a particular p-value is < 0.05, the correlation is considered significant. Müller et al. [2006] suggest that the user may exclude variables from a PCA that strongly correlate with each other. Otherwise, these variables might misleadingly strengthen certain trends.

Principal Component Analysis. The PCA is a technique from multivariate statistics to detect variables from multi-dimensional data that may be redundant. For dimension reduction, these variables may be grouped together. Furthermore, PCA explains the structure of relationships between variables and thus provides additional insight into the data. The PCA results in new variables, the so-called *principal components*. Each principal component (pc) represents a single axis in a new orthogonal coordinate space (*pc-space*)—generated by a variance maximum rotation of the original data space. The first pc (pc_1) explains most of the variance in the original data, the second pc (pc_2) most of the remaining variance, etc.

It is often required to standardize the data before applying a PCA, in particular, if the variables have not been measured in the same units or if their variance is substantial. For standardization, A is centered around its mean and then each column of A is divided by its standard deviation. This step is often referred to as *Auto-scaling*. One way to compute the pcs is to apply a *Singular Value Decomposition (SVD)*. As a result, the SVD returns matrices $PCS^{n \times n}$, $scores^{m \times n}$ and a vector containing the eigenvalues $\lambda^{1 \times n}$ of C. Each column of PCS consists of n *loadings* representing the weights for the linear combination of the n original variables. The *scores* are the coordinates of the original data transformed into *pc-space*. The vector λ represents the variances explained by the n pcs.

According to Müller et al. [2006], the PCA results may be exploited in several ways, e.g., for detecting prominent trends in the data. These trends are represented by the pcs. The *loadings* indicate how individual variables correlate with these trends. The eigenvalues of C may be applied to neglect less significant trends (low values correspond to a low variance explained by the corresponding pc). A major problem involved in interpreting PCA results is the difficulty to relate trends to the original variables. Therefore, Müller et al. suggest to oppose the *scores* and the original variables in a scatterplot. Another approach, they recommend, is to present the *scores* in their spatial frame of reference (the original perfusion data). Furthermore, linking & brushing should be applied to relate the *scores* to the original variables.

Applying the statistical analysis component. At the beginning of the statistical analysis, the user is presented a list containing the set of perfusion parameters which have been derived in the curve analysis. The user may refine this initial set resulting in a new set $\{P_k\}$ of k parameters. In the example from cerebral perfusion, which is used for illustrating this section, the descriptive perfusion parameters introduced in Subsection 2.1.3.4 have been selected for further analysis. In a next step, the background voxels within the parameter volumes corresponding to $\{P_k\}$ are identified to restrict further computations to the anatomic structures. If relevant structures have already been segmented in the preprocessing component, the segmentation mask may be used for identification. Otherwise, the histogram of one of the parameter volumes is generated where the highest peak is likely to represent the background voxels and a simple thresholding is applied. Once the background voxels have been identified, they are excluded from further analysis (*Background removal*). The indices of the

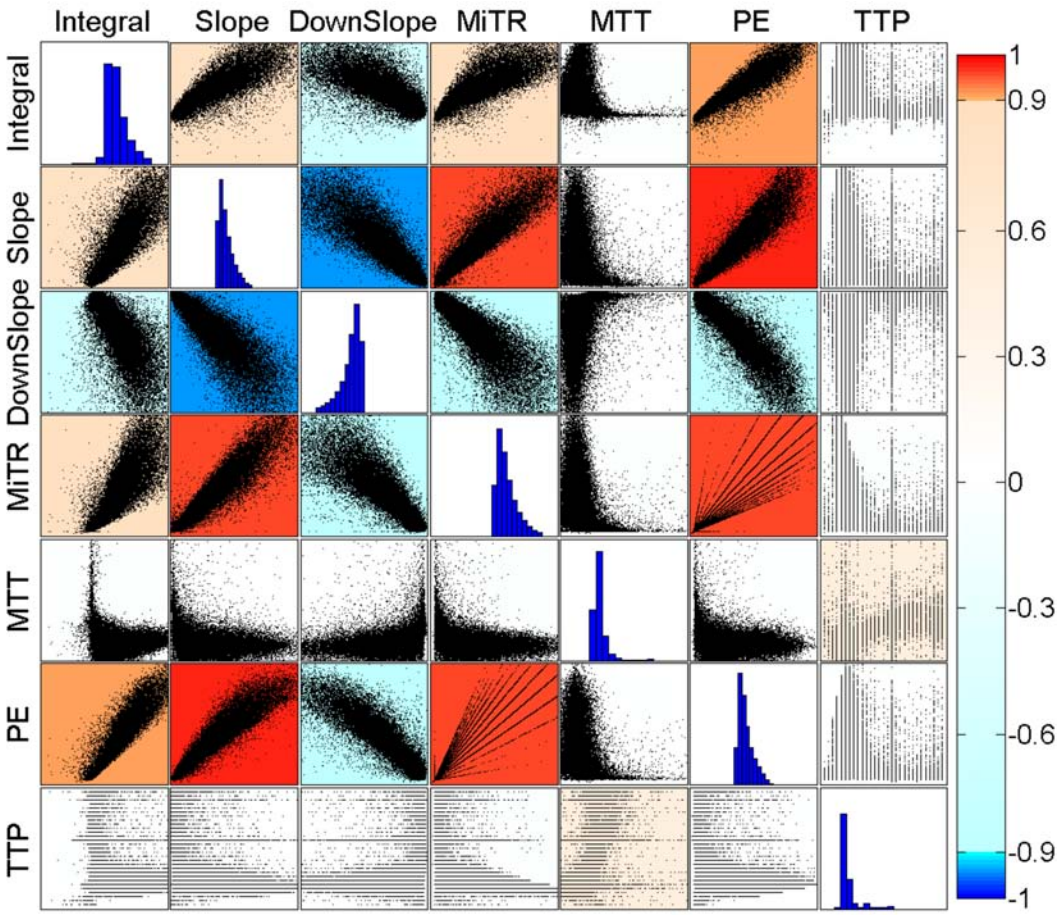

Figure 4.4: Scatterplot matrix for inspecting inter-parameter relations. The background color of each plot is chosen according to the respective correlation coefficient. The color scale is designed such that strong correlations (< -0.9 or > 0.9) are emphasized. To improve readability, all axes limits are based on the respective inner quartile range ($25\% - 75\%$) such that the primary orientation of the scatter becomes evident. The diagonal of the matrix shows a histogram for each parameter.

remaining m voxels VOX_{relev} are stored in a vector ID_{relev}. Then, the perfusion parameter matrix $A^{m \times k}$ is constructed considering only the voxels referred to by ID_{relev}. As discussed above, the PCA may require a standardization of its input to deliver meaningful results. Since the perfusion parameters have not been measured in the same units, *Auto-scaling* is applied to A resulting in $A_{std}^{m \times k}$.

To evaluate the relationships between several parameters, a correlation analysis may be carried out resulting in matrices R and P. In order to consider only significant correlations, P is examined for values < 0.05. The correlation coefficients in R corresponding to the remaining values are set to 0 (no correlation). A visual representation of R now enables the user to identify parameters that are highly correlated (Fig. 4.4). A scatterplot matrix is generated by plotting all columns in A_{std} against each other. The background color of each plot has been chosen according to the respective value in R. A color scale has been designed that visually separates negative and positive coefficients. Furthermore, it emphasizes strong correlations (coefficients < -0.9 or > 0.9). To improve readability, all axes limits are set based on the respective inner quartile range ($25\% - 75\%$) such that the primary orientation of the scatter becomes evident. The diagonal of the scatterplot matrix shows a histogram for each parameter.

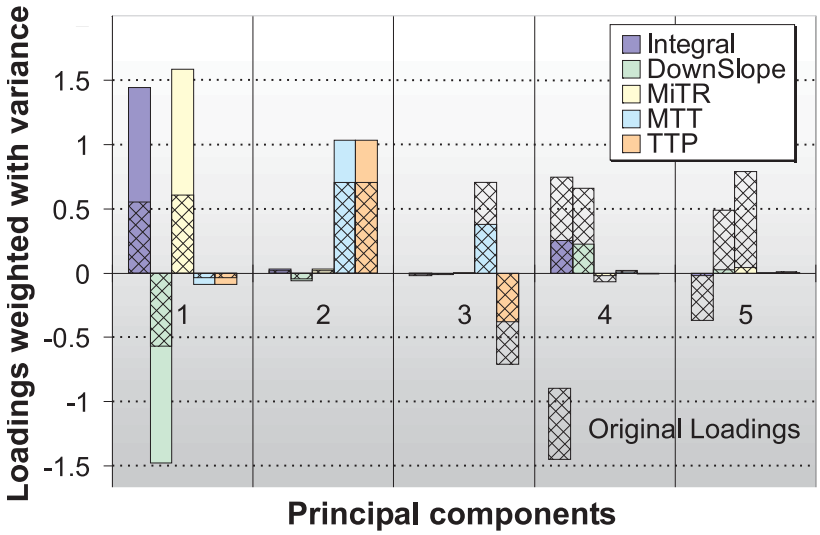

Figure 4.5: Bar chart for inspecting PCA results. The principal components and their *loadings* for the perfusion parameters are displayed. The original loadings are visualized as crosshatched bars. Trends are characterized per pc by dominant loadings, e.g., *Integral*, *DownSlope*, and *MiTR* for pc_1. To incorporate the significance of each trend, the loadings are weighted with the variance explained by the corresponding pc (filled bars).

The visualization of R in Figure 4.4 shows the following strong correlations: $Integral \leftrightarrow PE$, $PE \leftrightarrow MiTR$, $PE \leftrightarrow Slope$, $Slope \leftrightarrow MiTR$ *and* $Slope \leftrightarrow DownSlope$ (inversely proportional). Since parameters PE and $Slope$ each strongly correlate with three other parameters, they are excluded from further processing. This results in the Matrix $A_{corr}^{m \times l}$, where l is the number of the remaining parameters.

In a next step, a PCA is carried out based on A_{corr} resulting in the matrices $PCS^{l \times l}$, $scores^{m \times l}$ and a vector $\lambda^{1 \times l}$. To detect trends in the data, the *loadings* in PCS are visualized in a bar chart (Fig. 4.5, crosshatched bars). However, the PCA does not only reveal the trends but it orders them by their significance—expressed by the variances in λ. To incorporate this significance in the visualization, the *loadings* in column $i, i \in [1, l]$ of PCS are weighted with $\lambda(1, i)$ according to [Müller et al., 2006] (filled bars). The plot reveals a major trend represented by pc_1. This trend is determined by the parameters $Integral$, $DownSlope$ and $MiTR$. The positive *loadings* of $Integral$ and $MiTR$ indicate a direct proportional relationship, whereas the negative *loading* of $DownSlope$ indicates an inversely proportional relationship. To relate the trends to the original perfusion parameters, the user may select individual pcs and export their associated *scores* for a later processing within the feature specification component.

The end of the statistical analysis constitutes a classification step which has not been implemented in the thesis. However, related work indicates that techniques to classify perfusion data are promising in detecting suspicious regions (Subsec. 4.1.1).

4.2.1.3 Feature Specification

The interactive feature specification based on data arising in the preprocessing as well as in the statistical analysis stage is carried out in a framework employing the `SimVis` technology [Doleisch et al., 2003; Doleisch and Hauser, 2002]. `SimVis` has been originally developed for the analysis of 3D time-dependent flow simulation data, but has been extended to cope also with multiple other data types, e.g., 3D weather radar data and 3D medical data.

A data converter has been implemented to transform medical RAW data into the SimVis data-format.

In SimVis, multiple linked views are used to concurrently show, explore, and analyze different aspects of multiparameter data. 3D views of the volume (also over time) can be used next to several types of attribute views, e.g., scatterplots, parallel coordinates or histograms. Interactive feature specification is usually performed in these attribute views. The user chooses to visually represent selected data attributes in such a view, thereby gaining insight into the selected relations within the data. Then, the interesting subsets of the data are interactively brushed directly on the screen (Fig. 4.2). The result of such a brushing operation is reintegrated into the data in form of a synthetic data attribute $DOI_j \in [0,1]$ (*degree of interest (DOI) attribution* of the data, compare to Furnas [1986]). This DOI attribution is used in the 3D views of the analysis setup to visually discriminate the interactively specified features from the rest of the data in a focus+context visualization style which is consistent in all (linked) views [Hauser, 2005].

In the SimVis system, *smooth brushing* [Doleisch and Hauser, 2002] (enabling fractional DOI values) as well as the logical combination of brushes for the specification of *complex features* [Doleisch et al., 2003] are supported. A smooth brush results in a trapezoidal DOI function around the main region of interest in the attribute views. The corresponding fractional DOI values may be employed for modulating opacity and/or color of the feature specification result. To enable the integration of a flexible derived data concept, a data calculator module with a respective graphical user interface has been added. New attributes can be derived from existing ones and thereafter are available for investigation in all linked views.

The interactive feature specification process and the associated exploration and analysis steps serve several different tasks, of which the most important are:

- *Feature localization*: to search for places in the 3D domain of the data where certain feature characteristics are present. In the SimVis approach, the user can brush features in attribute views and concurrently localize the respective feature in the 4D (3D+time) volume domain.

- *Multi-variate analysis*: to investigate multi-variate data properties by specifying a feature in one attribute view and at the same time analyzing the DOI distribution with respect to other data attributes in other attribute views (through view linking).

- *Local investigation*: to inspect the values of selected data attributes with respect to certain spatiotemporal subsets of the 3D volume domain. In the SimVis system, the user can also load spatial as well as temporal data references into attribute views—brushing these kinds of data attributes then yields features which are specified according to their spatiotemporal extents.

4.2.2 Case Study: Ischemic Stroke Diagnosis

The presented perfusion data analysis approach has been applied to a variety of datasets from ischemic stroke, CHD, and breast tumor diagnosis. In the following, four representative cases covering all application fields are discussed in more detail starting with an example from ischemic stroke diagnosis. In case of an ischemic stroke, the existence and the extent of the penumbra surrounding the core of the stroke have to be evaluated. Pharmaceutical and surgical interventions may salvage at least parts of the penumbra.

Case Description. The patient suffered from an acute stroke caused by a thrombosis of the middle cerebral artery affecting the parietal lobe of the right hemisphere. Characteristic imaging parameters of the acquired DSC-MRI perfusion study are: gradient echo planar imaging with TR = 2000ms, TE = 53.7ms and flip angle = 90°, matrix =128×128, slice thickness = 6mm, slice gap = 1.02mm, in-plane resolution = 1.7×1.7mm^2, number of slices = 12, number of acquisitions = 40, and total acquisition time = 78s.

Preprocessing. A careful inspection of the dataset by cine movies and random TIC probing showed no motion artifacts. The signal intensities have been calibrated according to Equation 2.1. A Gaussian with kernel size 3×3 has been applied to reduce spatial noise. Temporal denoising has been carried out in one iteration by means of a binomial filter of size 1×3. Then, the brain tissue has been separated from the background applying a 3D watershed transform [Hahn and Peitgen, 2000]. Finally, the descriptive perfusion parameters described in Subsection 2.1.3.4 have been derived for the segmented tissue in a curve analysis.

Statistical analysis. The results of the statistical analysis are illustrated in Figure 4.4 and 4.5. All perfusion parameters were considered for the analysis. The segmentation mask from the preprocessing stage was used to exclude the background voxels and autoscaling was applied to the values of the remaining voxels. Then, a correlation analysis has been carried out indicating strong correlations between parameters describing the amount of the CA enhancement ($Integral \leftrightarrow PE$), between parameters describing the velocity of the enhancement ($Slope \leftrightarrow MiTR$, $Slope \leftrightarrow DownSlope$), and in between these types ($PE \leftrightarrow MiTR$, $PE \leftrightarrow Slope$). The correlation between *Slope* and *DownSlope* is inversely proportional. Since the *DownSlope* is measured in negative values, this indicates that a fast CA accumulation (high *Slope* values) is likely to be followed by a fast washout (high negative *DownSlope* values). Since *PE* and *Slope* strongly correlate with three other parameters respectively, they have been excluded from further processing.

The PCA showed four major trends (pc_1-pc_4) which account for 52%+29%+11%+7% = 99% of the variance in the data. A problem when interpreting PCA results is to assign a meaning to the newly generated coordinate axes. According to Müller et al. [2006], the axes are labeled with respect to the parameter loadings that determine the trend in the respective pc. More meaningful labels could be "Amount and Velocity" for pc_1 and "Time to Enhancement" for pc_2. Interestingly, the trends represented by pc_3 and pc_4 characterize atypical enhancement patterns in cerebral perfusion and conflict with pc_2 and pc_1, respectively. An increased *TTP* indicating a shift of the enhancement to a later time point should involve an increasing *MTT* which is contradictory to the trend represented by pc_3. Furthermore, an increased *Integral* is associated with a steep *Slope* which again involves a steep *DownSlope* (high negative values). However, a contradictory trend is represented by pc_4. Both, the typical as well as the atypical enhancement patterns will be closely investigated by means of the feature specification component.

Visual analysis. Before the visual analysis will be discussed in detail, the generation of spatial reference information for embedding the feature specification result is described. Such an embedding improves the localization of suspicious tissue with respect to other anatomical constituents thereby supporting diagnostic and therapeutic decisions. A simple approach for generating a spatial reference exploits gradient information. The gradient characterizes the

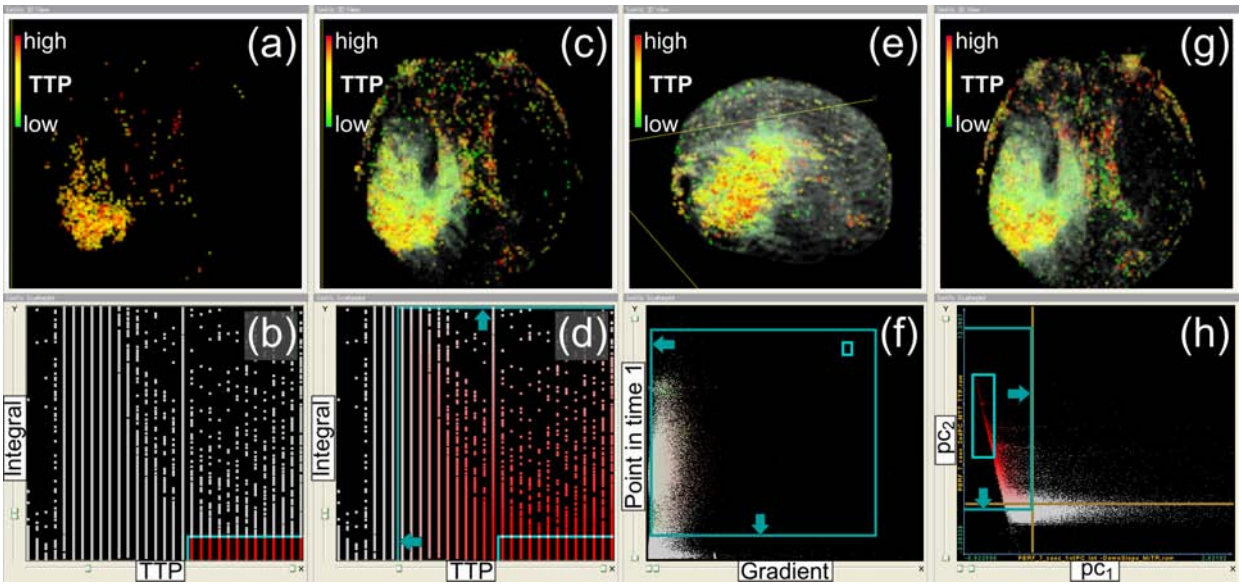

Figure 4.6: Ischemic stroke diagnosis. High TTP and low $Integral$ values have been brushed in a scatterplot *(b)*. As a result, the infarction core is revealed in *(a)*. In *(d)*, a near-focus region (arrows point at its borders) is additionally defined. The updated visualization in *(c)* gives a hint on the location of the penumbra (greenish area). In *(e)*, the brain is rotated to gain a better impression of the overall extension of the infarction. Furthermore, the shape of the brain is indicated by a concurrent smooth brushing of signal intensities and derived gradient magnitude *(f)*. Interestingly, a smooth brushing of the *scores* of pc_1 and pc_2 *(h)* yields a very similar result *(g)* as compared to *(c)*. The brown lines in *(h)* represent the zero-axes. (Data is courtesy of Jonathan Wiener, Boca Raton Community Hospital.)

strength of local variation and may be computed based on the intensity values from a single point in time of the original perfusion data. High gradient values occur here at the transition from background to tissue and at the transition of tissues with significant differences in signal intensity. The point in time should be chosen such that the structures of interest are visually well separable. For example, the lumen of the left and the right ventricle may serve as spatial reference information when examining myocardial tissue. They are visually well separable once the CA accumulates in the left ventricular lumen (Fig. 2.19, middle column).

The gradient magnitude is computed by the data calculator module of the feature specification component and integrated as a new attribute. A concurrent smooth brushing of high gradient magnitudes and signal intensities then reveals the shape, e.g., of the brain, the left and right ventricular lumen or the outer breast skin. The smooth brushing is defined such that the shape is only gently indicated by assigning low opacity values. This enables a visual separation of spatial reference information and suspicious tissue which is assigned a high opacity. Furthermore, the shape is treated within the feature specification component as a separate feature being independent of the specification of suspicious tissue. The previously described approach to generating spatial reference information will be used throughout this section.

How visual analysis may guide the process of localizing infarction core and penumbra is illustrated in Figure 4.6. In a scatterplot, TTP and $Integral$ are opposed and a region is brushed that indicates delayed and diminished perfusion (Fig. 4.6 (b)). As a result of this *feature localization*, the infarction core appears as a bright region in the right hemisphere (Fig. 4.6 (a), the right hemisphere is located on the left in all images). High TTP values are

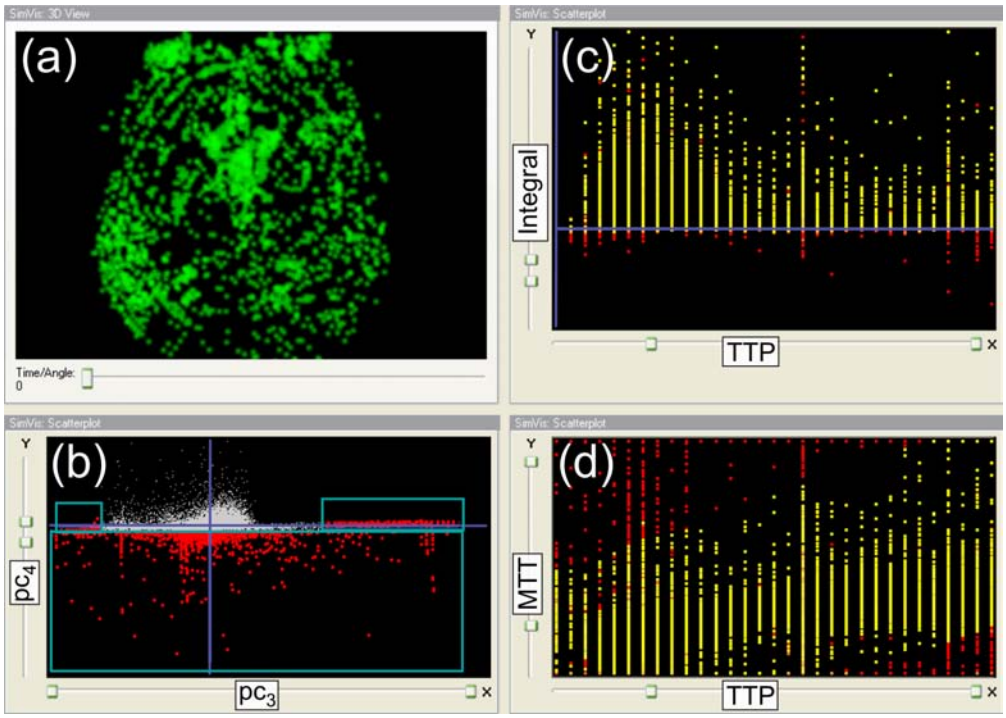

Figure 4.7: Examination of the atypical enhancement patterns represented by pc_3 and pc_4 (Fig. 4.5). Negative Integral values (red dots below the blue zero-axis in *(c)*) are revealed by brushing the scores of pc_3 and pc_4 *(b)*. In the corresponding brain tissue *(a)*, no contrast agent arrives at all. Hence, the results of the parameter derivation are not reliable. In *(d)*, the selection from *(b)* is shown in *TTP*-*MTT* space (red dots). Combinations of low *TTP* and high *MTT* values (upper left) as well as high *TTP* and low *MTT* values (lower right) are revealed. This trend is expressed by pc_3. (Data is courtesy of Jonathan Wiener, Boca Raton Community Hospital.)

mapped to colors from yellow to red. Smooth brushing now gives a hint on the penumbra (Fig. 4.6 (d)). A near-focus region is defined (arrows point at its borders) incorporating areas where the perfusion is delayed as well, however, a considerable amount of blood arrives over time. Candidate areas for the penumbra appear greenish (medium *TTP* values) in Figure 4.6 (c). This observation could be successfully validated with [Kohle et al., 2002] where the same dataset has been examined. In Figure 4.6 (e), the brain has been rotated to illustrate the overall extension of the infarction. Furthermore, the shape of the brain is indicated as spatial reference information by means of smooth gradient magnitude and signal intensity brushing (Fig. 4.6 (f)). In Figure 4.6 (h), the scores of pc_1 and pc_2 have been opposed. As discussed above, meaningful axes labels could be "Amount and Velocity" and "Time to Enhancement". Hence, small values on the x-axis and high values on the y-axis are brushed. The near-focus region is selected accordingly. A comparison of Figure 4.6 (g) and Figure 4.6 (c) shows that the revealed areas match closely. Hence, the trends expressed by pc_1 and pc_2 together facilitate the detection of core and penumbra.

As discussed above, pc_3 and pc_4 represent atypical enhancement patterns which should be investigated. For this purpose, the scores of pc_3 (x-axis) and pc_4 (y-axis) have been opposed in a scatterplot and explored via brushing (Fig. 4.7 (b)). Composite brushes which form a selection of extreme values in pc_3 and high negative values in pc_4 reveal an interesting detail about the data: negative *Integral* values have been computed. These values are emphasized in a scatterplot opposing *TTP* (x-axis) and *Integral* (y-axis) (Fig. 4.7 (c), red dots below the blue zero-axis). Examination of the CTCs of the corresponding brain tissue (Fig. 4.7 (a))

showed that at these regions no CA accumulates at all. Here, the curve never significantly exceeds the *Baseline* but instead, at some points in time, the CA concentrations were even lower resulting in a negative *Integral*. This hampered the computation of the MTT at which the *Integral* is bisected. The TTP values are not reliable here either. It always exists a PE over time, no matter how small the concentration values are. Therefore, at some brain regions, high MTT values together with low TTP values (and vice versa) were computed as indicated by the inversely proportional relationship in pc_3. This is further illustrated by transferring the selection (red dots) from Figure 4.7 (b) to a scatterplot opposing TTP (x-axis) and MTT (y-axis) (Fig. 4.7 (d)). The negative *Integral* values also explain the proportional relationship of *Integral* and *DownSlope* in pc_4. Since the *DownSlope* values are negative by definition, they are directly proportional to the negative *Integral* values.

4.2.3 Case Study: Diagnosis of Coronary Heart Disease

In CHD diagnosis, less perfused regions of the myocardium shall be identified and correlated with the supplying coronary artery branches to support stenosis detection. If the existence of a stenosis is a priori known, its hemodynamical relevance shall be evaluated.

Case Description. Both patients, whose datasets will be investigated in the following, suffered from an infarction. For the first patient, a two-vessel CHD has been diagnosed pertaining to RCA and LCX. The affected tissue spans the entire inferior and inferolateral wall of the myocardium. Also for the second patient, a two-vessel CHD has been diagnosed pertaining to RCA and LAD. The affected tissue spans the inferoseptal and parts of the anteroseptal wall of the basal and mid-cavity myocardium. For both patients, a diagnostic report was available. However, the data was first analyzed blindfolded and then, the analysis results were compared with the report. In the following, tissue with a depleted perfusion will be referred to as ischemic tissue though parts of it or the entire tissue may be necrotic as a consequence of the infarction. However, the available LE data, which would facilitate a differentiation, has not been integrated in the visual analysis so far.

Characteristic imaging parameters of the acquired DCE-MRI perfusion studies $Heart_1$ and $Heart_2$ (in parentheses if different) are: gradient recalled echo imaging with inversion-recovery and with TR = 158ms (160ms), TE = 1.01ms, TI = 95ms, and flip angle = 12°, matrix =144×192, slice thickness = 6mm (8mm), slice gap = 12mm (10mm), in-plane resolution = 1.875×1.875mm^2 (1.82×1.82mm^2), number of slices = 4 (3), number of acquisitions = 40, and total acquisition time = 40.2s (23.35s). Both datasets were acquired with a magnetic field strength of 3 Tesla and ECG-triggering.

Preprocessing. Both datasets showed slight motion artifacts which have been reduced by a combination of rigid and elastic registration employing mutual information as the similarity measure and a gradient descent method for optimization purposes [Rueckert et al., 1999]. Then, the signal intensities have been calibrated according to Equation 2.6. A Gaussian with kernel size 3×3 has been applied to reduce spatial noise. Temporal denoising has been carried out in one iteration by means of a binomial filter of size 1×3. Next, the epicardial and endocardial contours have been delineated for one point in time by means of the Live-wire technique [Schenk et al., 2000]. The resulting contours have then been propagated to the remaining points in time. Finally, the descriptive perfusion parameters described in Subsection 2.1.3.4 have been derived for the myocardial tissue in a curve analysis.

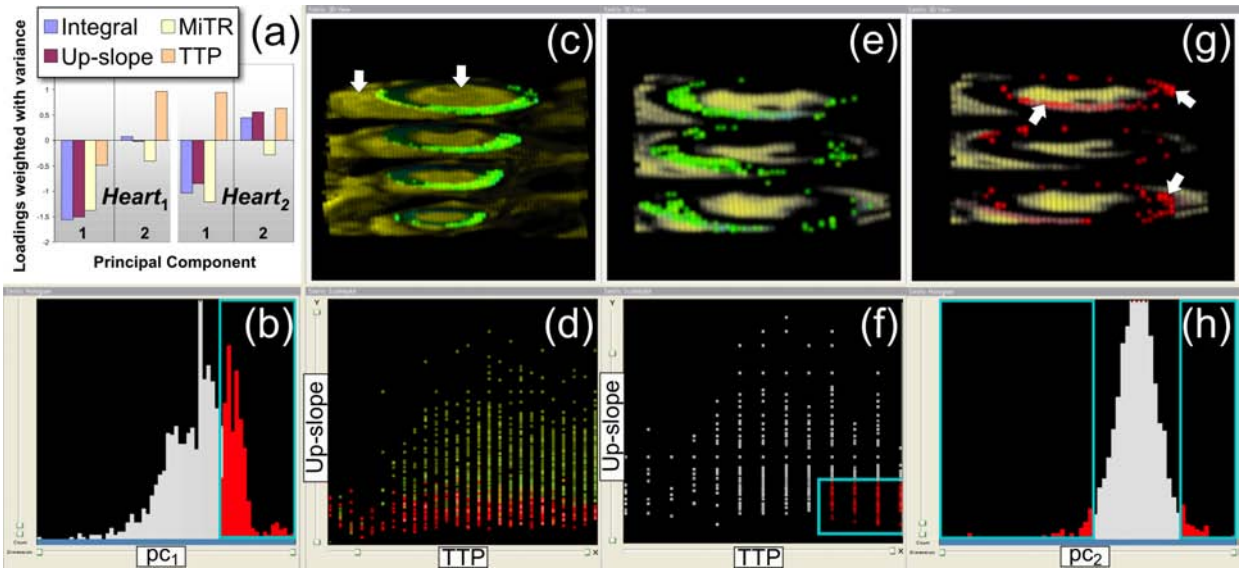

Figure 4.8: Diagnosis of Coronary Heart Disease based on the datasets $Heart_1$ *(a-d)* and $Heart_2$ *(a, e-h)*. An excerpt from the PCA results is shown in *(a)*. Brushing the scores of pc_1 *(b)* reveals ischemic tissue (green area in *(c)*). The right ventricle (left arrow) and the lumen of the left ventricle (right arrow) are incorporated as spatial reference information. The selection from *(b)* is transferred to a scatterplot opposing TTP and *Up-slope (d)*. In $Heart_1$, TTP is not a reliable parameter to detect ischemic tissue since the selection is spread over its entire codomain (red dots). However, the situation is different in $Heart_2$. A selection of high TTP values and small *Up-slope* values *(f)* reveals the ischemic tissue (green area in *(e)*). Brushing the scores of pc_2 *(h)* exhibits areas where the motion correction and thus the segmentation of the myocardium have partially failed *(g)*. ($Heart_1$ is courtesy of Frank Grothues, University Hospital Magdeburg. $Heart_2$ is courtesy of Stefan Miller, University Hospital Tübingen.)

Statistical analysis. All perfusion parameters were considered for the analysis. The segmentation mask from the preprocessing stage was used to exclude the background voxels and auto-scaling was applied to the values of the remaining voxels. Then, a correlation analysis has been carried out. The correlation coefficients indicated a strong correlation between $Integral$ and PE for both $Heart_1$ and $Heart_2$. Due to the higher variance of the $Integral$ values in both cases, PE was excluded from the PCA. The PCA of $Heart_1$ showed two major trends in pc_1 and pc_2, respectively (Fig. 4.8 (a)). Both pcs together explain $\approx 91\%$ of the variance in the data. However, pc_1 describes an atypical enhancement pattern. In ischemic tissue, low $Integral$ and high TTP values may be expected due to a diminished and delayed blood supply, respectively. In healthy tissue, high $Integral$ and low TTP values may be observed. The contradictory trend indicated by pc_1 describes a directly proportional relationship of $Integral$ and TTP and will hence be investigated.

The PCA of $Heart_2$ showed three major trends expressed by pc_1 to pc_3. All together account for $51\% + 25\% + 17\% = 93\%$ of the variance in the data. For the sake of brevity, only the first two pcs are examined here (Fig. 4.8 (a)). A typical enhancement pattern is represented by pc_1. However, pc_2 shows an atypical pattern. As in pc_1 of $Heart_1$, TTP is proportional to $Integral$ and *Up-slope*. Furthermore, $MiTR$ is inversely proportional to *Up-slope* though both parameters describe the steepness of the curve during CA accumulation. Hence, the trend represented by pc_2 will be further investigated.

Visual analysis. To examine the atypical enhancement pattern, represented by pc_1 of $Heart_1$, the scores of pc_1 have been brushed in a histogram (Fig. 4.8 (b)). A selection of high values reveals the ischemic tissue (green region in Fig. 4.8 (c)) within the ring-shaped myocardium. Since the circular shape of the myocardium hampers the orientation, spatial reference information has been added. The right ventricular lumen (left arrow) as well as the lumen of the left ventricle (right arrow) are unveiled thereby shedding light on the anatomical location of the ischemic tissue. It spans the entire inferior and inferolateral wall of the myocardium which could be validated by means of the diagnostic report. The selection in Figure 4.8 (b) has been transferred for a *multi-variate analysis* to a scatterplot opposing TTP and *Up-slope* (Fig. 4.8 (d), red dots). Interestingly, the selection is spread over all points in time indicating that a feature specification solely based on TTP would fail. The reason is that only very few or no CA accumulates in ischemic tissue. However, PE and therefore TTP may always be computed—no matter if the TIC represents CA enhancement or noise. A solution to this problem would be to restrict the perfusion parameter derivation to TICs with a significant peak and to assign a unique identifier to the remaining TICs. After all, it seems that in spite of the unreliable TTP values, a brushing of the scores of pc_1 still delivers meaningful results. This might be due to the low loading of TTP (Fig. 4.8 (a)).

An issue in analyzing perfusion data is that the reliability of a parameter may vary from dataset to dataset. As illustrated in Figure 4.8 (e-f), TTP might be a reliable parameter for *feature localization* in $Heart_2$. Brushing of high TTP and small *Up-slope* values reveals the ischemic region (green). It spans the inferoseptal and parts of the anteroseptal wall of the basal and mid-cavity myocardium which could be validated by means of the diagnostic report. For $Heart_1$, pc_1 describes a typical enhancement pattern. In contrast, pc_2 describes an atypical pattern: TTP and $Integral$ are directly proportional, and *Up-slope* and $MiTR$ are inverse proportionally related. Brushing of extreme values of pc_2 (Fig. 4.8 (h)) reveals areas located close to the endocardial and epicardial contours (Fig. 4.8 (g), left and right arrows). A review of the myocardial segmentation showed that the propagation of the segmented myocardial contours did not match the myocardium at all points in time. Hence, tissue with different enhancement characteristics as compared to the myocardium has been included in the segmentation result. Eventually, it turned out that the motion correction had partially failed.

4.2.4 Case Study: Breast Tumor Diagnosis

The major diagnostic task in breast tumor diagnosis is to assess the dignity of a tumor, i.e. to rate the tumor as benign or malignant. In the following, the terms tumor and *lesion* will be used interchangeably since the latter is often found in related literature. Evaluating the shape of the TICs has proven to be effective in the differentiation of enhancing lesions [Kuhl et al., 1999]. The perfusion parameters *Slope* and *DownSlope* have been identified as particularly clinically relevant. In the context of breast tumor diagnosis they are referred to as *Wash-in* and *Wash-out*. TICs—which show a rapid *Wash-in* followed by a rapid *Wash-out*—are especially suspicious because they indicate strong tumor angiogenesis (growth of new vessels from existing ones) and high vessel permeability. Less suspicious are TICs showing a plateau later on, or regions which continue to enhance. For more details on tumor perfusion, see Heywang-Köbrunner et al. [1997].

Case Description. Both patients, whose datasets will be examined in the following, were referred to an MRI examination since a suspicious lesion had been detected in the right

mamma during conventional mammography. Two different visual analysis strategies based on these datasets will be described later on. The first strategy focuses on the previously detected lesion aiming at a characterization of the tumor tissue. The second strategy considers the entire dataset aiming at a detection and subsequent characterization of suspicious tissue.

For the first patient, the MRI scan revealed very heterogeneous tissue in the relatively large lesion exhibiting both benign and malignant characteristics. Hence, a biopsy was inevitable yet it confirmed the benignity of the lesion. For the second patient, the MRI scan indicated malignant characteristics of the investigated lesion. Furthermore, a satellite lesion was discovered which is probably connected to the larger lesion. A diagnostic report has been available for both cases. However, the data was first analyzed blindfolded and then, the analysis results were compared with the reports. For the sake of brevity, the statistical analysis of the second case will only be discussed briefly. However, a feasible diagnostic workflow based on the preprocessing and the feature specification component will be demonstrated.

Characteristic imaging parameters of the acquired DCE-MRI mammography studies $Mamma_1$ and $Mamma_2$ (in parentheses if different) are: gradient recalled echo imaging with TR=10ms (8.15ms), TE = 4.5ms (4.02ms), and flip angle = 25°, matrix =512×256 (512×512), slice thickness = 2.5mm (3mm), slice gap = 0mm, in-plane resolution = 0.664×0.664mm^2 (0.684×0.684mm^2), number of slices = 80 (40), number of acquisitions = 5 (6), and total acquisition time = 11min4s (7min8s). Both datasets were acquired with a magnetic field strength of 1.5 Tesla.

Preprocessing. Both datasets showed motion artifacts due to respiration and patient movement. The same approach as for the cardiac data has been applied for motion correction (Subsec. 4.2.3). Next, the left mamma has been cropped off the datasets to improve the performance of subsequent steps. Then, the signal intensities have been normalized by subtracting the *Baseline*. A Gaussian with kernel size 3×3 has been applied to reduce spatial noise. Temporal denoising has been omitted due to the low number of acquisitions. In $Mamma_1$, the lesion has been segmented by means of region-growing and a simple gap-closing algorithm in subtraction images. The significant differences in signal values between tumor and normal breast tissue facilitated this step. No segmentation was carried out in $Mamma_2$. Finally, the descriptive perfusion parameters described in Subsection 2.1.3.4 have been derived for the lesion in $Mamma_1$ and for the entire dataset in $Mamma_2$. The set of parameters has been extended by two additionally derived parameters: *3TP-Slope1* and *3TP-Slope2*. Their computation is inspired by [Degani et al., 1997] where an optimal number of three acquisitions is recommended for DCE-MRI mammography in order to increase the spatial resolution. The points in time should be chosen carefully such that *3TP-Slope1* can be computed between t_1 and t_2 and *3TP-Slope2* can be computed between t_2 and t_3. If the data has been acquired at > 3 points in time, the user may define t_1-t_3 to simulate the acquisition according to [Degani et al., 1997].

Statistical analysis. The entire set of perfusion parameters has been considered for the analysis. The segmentation mask from the preprocessing of $Mamma_1$ was used to exclude the background (non tumor) voxels and auto-scaling was applied to the parameter values of the remaining voxels. In $Mamma_2$, a simple thresholding was applied prior to auto-scaling in order to separate the mamma from the background. Next, a correlation analysis has been carried out.

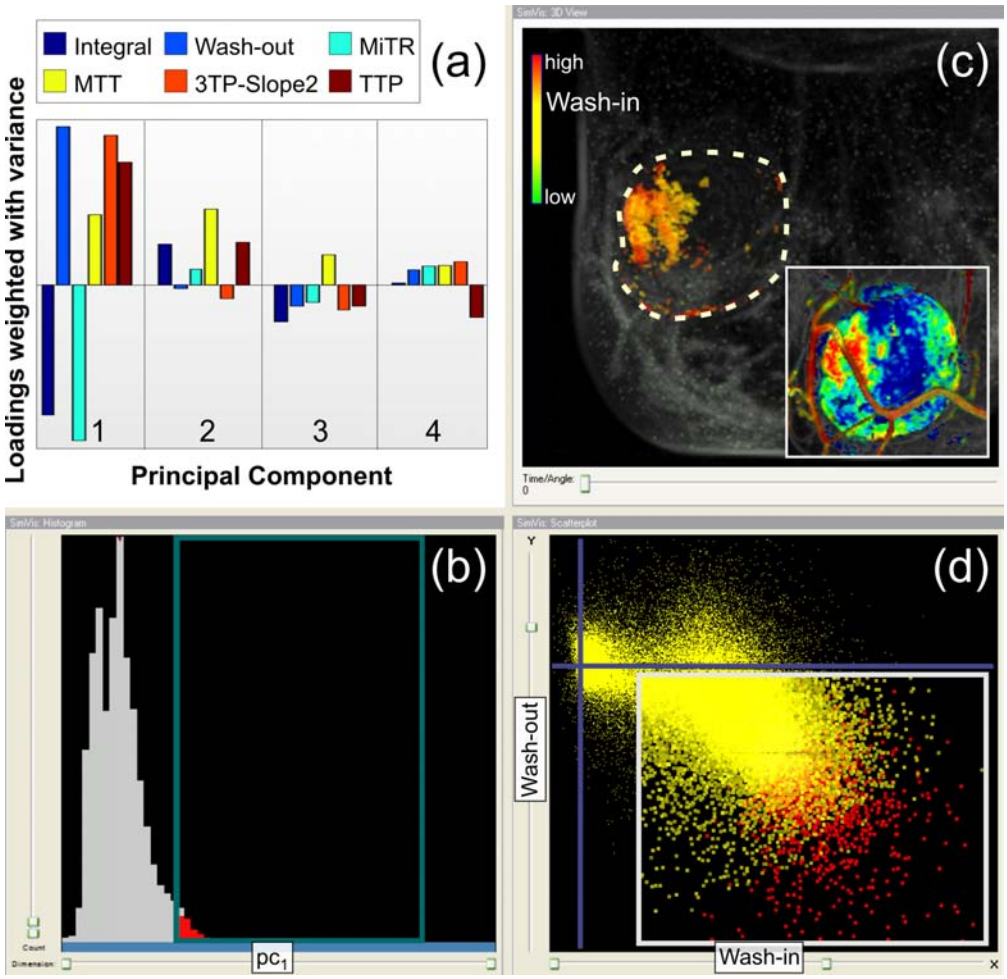

Figure 4.9: Visual analysis for the characterization of a priori known suspicious breast lesion. The bar chart in *(a)* depicts the first four principal components computed in a PCA from the perfusion parameters of the lesion. High scores in pc_1 have been brushed in *(b)* and the selection is visualized within the context of the right mamma in *(c)*. The selection has been colored according to *Wash-in*. Yellow and red regions indicate a fast CA accumulation. The boundary of the tumor has been delineated. The selection in *(b)* is transferred to a scatterplot *(d)* opposing *Wash-in* (x-axis) and *Wash-out* (y-axis). Zooming in on the plot reveals that regions exhibiting a fast CA accumulation as well as a fast washout have been detected (red dots). Location and extent of these regions could be successfully checked against results achieved in [Kohle et al., 2002] (red colored tissue parts in the inset of *(c)*). (Data is courtesy of Jonathan Wiener, Boca Raton Community Hospital.)

For $Mamma_1$, strong correlations between parameters describing the amount of the CA enhancement ($Integral \leftrightarrow PE$), between parameters describing the velocity of the enhancement ($Wash\text{-}in \leftrightarrow 3TP\text{-}Slope1$), and in between these types ($Integral \leftrightarrow Wash\text{-}in$, $Integral \leftrightarrow 3TP\text{-}Slope1$, $PE \leftrightarrow Wash\text{-}in$, $PE \leftrightarrow 3TP\text{-}Slope1$) were observed. Each of the four involved parameters is highly correlated with the respective remaining three parameters. Hence, only one of them should remain in the parameter set which serves as an input for PCA. *Integral* has been chosen since its values showed the highest variance. The PCA showed four major trends represented by the first four principal components (pc_1-pc_4) which account for $58\% + 17\% + 11\% + 9\% = 95\%$ of the variance in the data (Fig. 4.9 (a)).

So far, a meaning could only be assigned to the most prominent trend represented by pc_1. It describes parameter relationships which are typical in breast tissue enhancement: *Integral*

(overall amount of blood) is directly proportional to *MiTR* (speed of accumulation). Both are inversely proportional to *Wash-out* and *3TP-Slope2* (speed of washout; high negative values indicate a fast washout) as well as to TTP and MTT (time to enhancement). The scores of the first pc have been analyzed by means of the feature specification component. The analysis results will be described later on.

For $Mamma_2$, strong correlations between *Integral* and PE as well as between PE and *Wash-in* were found. Since PE strongly correlated with two other parameters, it has been excluded from further processing. The PCA showed four major trends expressed by pc_1-pc_4. All together account for $\approx$ 91% of the variance in the data. An interesting aspect could be observed when comparing the correlation patterns of $Mamma_1$ and $Mamma_2$. Decreasing the upper threshold for a significantly strong proportional relationship from 0.9 to 0.8 for $Mamma_2$ and modifying the color scale shown in Figure 4.4 accordingly lead to the same pattern of highly correlated perfusion parameters as for $Mamma_1$. It would be interesting to examine the generality of this observation. However, in the following, the visual analysis of $Mamma_2$ will be focused on a streamlined localization and separation of suspicious structures for *local investigation*.

Visual analysis. The visual analysis of the lesion in $Mamma_1$ is illustrated by Figure 4.9. At first, a histogram of the scores of pc_1 has been generated (Fig. 4.9 (b)). High scores have been brushed and the selection is visualized within the context of the entire mamma (Fig. 4.9 (c)). The tumor boundary has been derived from the segmentation mask and is indicated as dotted line. Transferring the selection in Figure 4.9 (b) to a scatterplot opposing *Wash-in* (x-axis) and *Wash-out* (y-axis), reveals that regions exhibiting a fast CA accumulation as well as a fast washout have been selected (Fig. 4.9(d)). This is characteristic for malignant tumors. However, the remaining parts of the lesion exhibit different enhancement characteristics ranging from suspicious to benign. Hence, a biopsy was finally recommended which rated the tumor as benign. In a visual comparison, the location and extent of the malignant tissue parts could be successfully checked against the results achieved by Kohle et al. [2002] who analyzed the same dataset (Fig. 4.9 (c), yellowish and reddish colored tissue parts in the inset).

Subtraction images emphasize regions where the CA is accumulated (Subsec. 2.1.4). They represent a standard way of analyzing DCE-MRI mammography data. Hence, additional attributes have been derived from the normalized signal intensities at each point in time for $Mamma_2$. Each attribute describes the intensity difference between two subsequent time steps t_j and t_i, where $j > i$. In Figure 4.10 (b), high differences in intensity between time points t_2 and t_0 have been selected. The corresponding tissue is visualized in Figure 4.10 (a) (green region). The structure S_{large} had already been detected in conventional mammography. Furthermore, a smaller structure S_{small} is revealed close to the outer breast skin. Besides these structures, major vessels and the acromastium are emphasized. The outer breast skin has been added as spatial reference information. To focus the analysis on a region around S_{large} for *local investigation*, Euclidean distances between its center and the surrounding tissue have been computed. Then, a range of distance values is brushed such that the local region LR around S_{large} includes S_{small}. The definition of a local region around S_{large} is illustrated in Figure 4.10 (c,d). In Figure 4.10 (f), the selection (red bars) including high differences in intensity within a limited distance to the center of S_{large} is transferred to a histogram of parameter *Wash-out* for *multi-variate analysis*. High negative values indicating a rapid washout are typical for malignant tumors. Hence, this range has been selected by excluding positive and small negative values with the help of a negative brush (purple box).

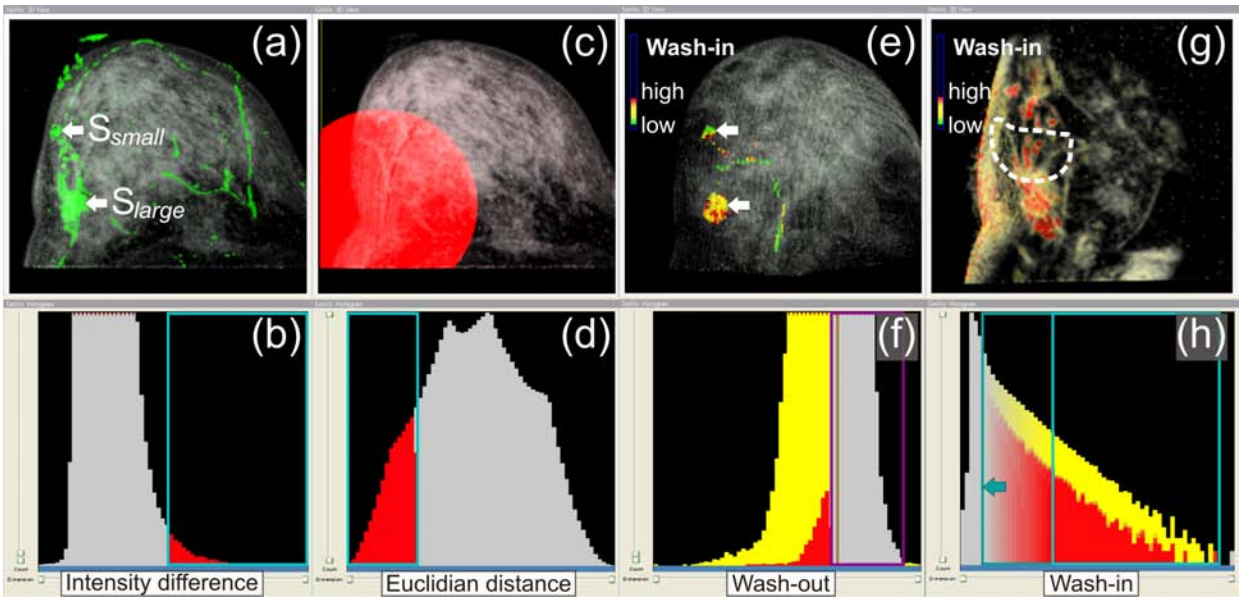

Figure 4.10: Visual analysis for the detection and characterization of suspicious breast lesions. The selection of high intensity differences between time steps t_2 and t_0 *(b)* emphasizes areas were the CA is absorbed (green regions in *(a)*). Two suspicious regions are detected (arrows). The outer breast skin is integrated as spatial reference information. The analysis is focused on a local region LR around S_{large} *(c)* by means of brushing Euclidean distances *(d)*. Areas exhibiting a rapid washout are then selected in a histogram of *Wash-out (f)*. A negative brush (purple box) is used to exclude positive and small negative values. The brown line marks the vertical zero axis. The remaining areas are visualized in *(e)* and color-coded according to *Wash-in*. Yellow to red areas indicate a rapid CA accumulation and washout. A smooth brushing of *Wash-in* within LR (h) reveals subtle spikes along the border of S_{large} (g) which are characteristic for malignant tumors. (Data is courtesy of Andreas Fessel, University Hospital Magdeburg.)

The result is color-coded by means of *Wash-in* in Figure 4.10 (e). S_{large} and S_{small} both exhibit regions with a rapid accumulation and washout and are thus likely to be malignant. S_{small} partially shows small *Slope* values which should be further investigated. Another indication confirming the suspicion of malignancy is illustrated by Figure 4.10 (g-h). A smooth brushing of high and medium *Wash-in* values within LR unveils subtle spikes (*spikulae*) along the border of S_{large}. All observations could be validated by means of a diagnostic report which stated that S_{small} presumably forms a satellite lesion connected to S_{large}.

Expert feedback. The visual analysis approach has been presented to two radiologists with a profound experience in analyzing DSC-MRI cerebral perfusion data and DCE-MRI mammographies, respectively. The discussion has been restricted to the feature specification component. Above all, both assessed the 3D visualization of the specified features embedded in spatial reference information as particularly valuable. It provides the radiologist with a more specific picture of the overall infarction or lesion extent and the location. Furthermore, an inspection of the tumor boundary in 3D may unveil features which are hard to reconstruct mentally by browsing 2D slices. The shape of the tumor boundary is crucial in assessing the dignity of the tumor. However, the 3D view should be coupled with a 2D slice view in order to access the inner parts of a feature specification result. One radiologist assessed brushing as useful for exploring the non-standardized parameter domain.

4.2.5 Function-based Feature Specification

Muigg et al. [2008] added a special attribute view (*curve view*) to the `SimVis` framework which facilitates a dense visualization of time-series data, e.g., TICs or CTCs for all voxels of a perfusion dataset. Special techniques are used to cope with overdrawing and to reduce clutter in the visualization of a multitude of curves ($>$ 10 million curves in case of a DCE-MRI mammography dataset). Dedicated *similarity brushes* are employed to define curve target shapes. Such target shapes allow for an exploitation of expert knowledge since, e.g., clinicians are trained to infer tissue characteristics from curve shape. Besides the target shape, a similarity measure is applied to match the original curves with this shape. As part of the thesis at hand, two case studies have been contributed to [Muigg et al., 2008] which will be briefly reviewed in the following. An approach similar to [Muigg et al., 2008] has been presented by Subramanian et al. [2004] for investigating DCE-MRI mammographies (Subsec. 4.1.2).

Two variants of similarity brushes have been implemented in `SimVis`. *Average Distance Brushes* employ the average distance between the target shape and the original curves as a similarity measure. *Gradient Sum Brushes* are based on the first derivatives of the target shape and the original curves. They employ the curve slope as a similarity measure and are hence, invariant to vertical translations. This property is especially attractive for the analysis of MR perfusion data since no standardized CA concentration values exist. The vertical extension of both kinds of brushes defines the range of accepted values for the respective similarity measure.

Smooth brushing has also been implemented for the similarity brushes (Subsec. 4.2.1.3). A focus range (light turquoise inner polygon) as well as a near-focus range (dark turquoise outer polygon) may be specified by the user to account for the non-standardized CA concentration values (Fig. 4.11 (a-b)). The following case studies have been accomplished by exploiting smooth gradient sum brushes for feature specification.

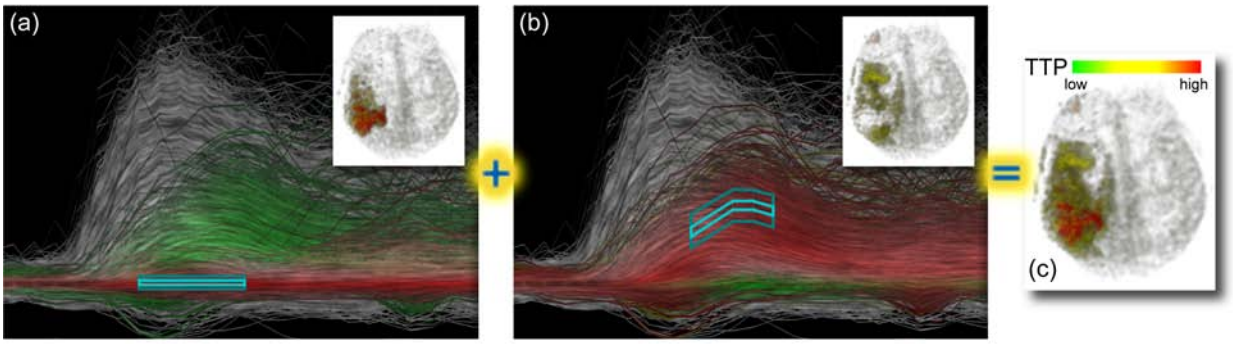

Figure 4.11: A feature set containing two different features has been defined in two curve views *(a-b)*. *(a)*: A smooth gradient sum brush (turquoise polygon) has been defined such that tissue with no significant signal enhancement is selected as the first feature (shown in its 3D context in the inset). *(b)*: A smooth gradient sum brush (turquoise polygon) has been used to specify a second feature representing tissue exhibiting reduced and delayed perfusion which is likely to correspond to the penumbra. Candidate areas are unveiled around the core (inset). *(c)*: Visualization of the overall feature set. (Image is courtesy of Philipp Muigg, SimVis GmbH, Vienna. Data is courtesy of Jonathan Wiener, Boca Raton Community Hospital.)

Ischemic stroke diagnosis. The applied dataset has been described and analyzed in Subsection 4.2.2. There, perfusion parameters and statistical analysis results constituted the basis for the feature specification. In the following however, the original 4D data converted to tracer concentration will be applied for detecting infarction core and penumbra. The analysis is illustrated by Figure 4.11. A feature set has been specified containing two features, the core and the penumbra, by using two different curve views (a-b) and similarity brushes (turquoise polygons). Each curve view shows locally selected data (red) in combination with curves selected in the overall feature set (green). This allows for an easy distinction and comparison of both features. Shading as well as an extended Line Integral Convolution (LIC) based on [Cabral and Leedom, 1993] help to convey general temporal trends in the context (gray) as well as in the selected regions (colored). The insets of Figure 4.11 (a-b) each show the respective feature in its spatial context. The color is modified according to *TTP*. Candidate areas for the penumbra appear yellowish (medium *TTP* values) whereas the infarction core is colored red (compare to Fig. 4.6). In order to visualize the extent of the infarction, the overall feature set is shown in Figure 4.11 (c-d).

Breast tumor diagnosis. The applied dataset has been described and analyzed in Subsection 4.2.4 ($Mamma_2$). There, the analysis has been based on intensity differences as well as on the descriptive perfusion parameters *Wash-in* and *Wash-out*. In the following, the original 4D data will be applied for detecting tissue exhibiting suspicious characteristics. The analysis is illustrated by Figure 4.12. In the curve view (a), a smooth gradient sum brush has been defined such that curves with a steep increasing part during the first points in time and with a steep declining part or a plateau during later points in time are selected. The corresponding feature specification result is visualized in the context of the right mamma and colored according to *Wash-in* in Figure 4.12 (b). Both structures S_{large} and S_{small} are identified as exhibiting suspicious characteristics which could be validated by means of the diagnostic report.

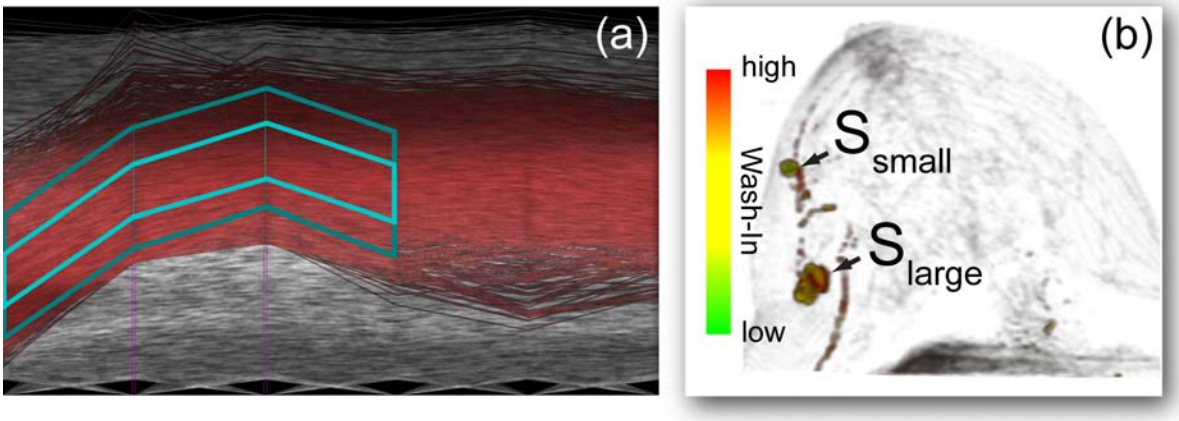

Figure 4.12: Detection of suspicious structures in breast tumor diagnosis. *(a)*: A smooth gradient sum brush (turquoise polygon) has been defined such that it resembles a curve pattern which is typical for suspicious tissue. *(b)*: The resulting selection is visualized in the context of the entire right mamma. Two suspicious structures S_{large} and S_{small} are revealed. The color indicates the accumulation speed of the contrast agent (*Wash-in*). (Image is courtesy of Philipp Muigg, SimVis GmbH, Vienna. Data is courtesy of Andreas Fessel, University Hospital Magdeburg.)

Parameter vs. function-based feature specification. The visual analysis of perfusion data by means of a function-based feature specification poses a lower demand on the preprocessing since no perfusion parameters have to be computed. Furthermore, the temporal aspect of the data is preserved and exploited. The specification of features by means of gradient sum brushes is intuitive since a priori knowledge about characteristic curve shapes may be integrated. However, selecting appropriate points in time for brush placement as well as specifying a suitable vertical brush extension such that all desired curve shapes are included requires some practice. The kinds of brushes associated with a parameter-based feature specification, e.g., rectangular brushes in a scatterplot, are instantly manageable by the user. The feature specification results of both approaches, e.g, based on the above mentioned dataset from ischemic stroke diagnosis, will be compared quantitatively in Section 4.3. This section is dedicated to a thorough comparison of four interactive feature specification approaches in the context of cerebral perfusion including the parameter and the function-based approach.

4.3 Visual Analysis of Cerebral Perfusion Data: Four Interactive Approaches and a Comparison

No absolute thresholds can yet be reliably computed for identifying salvageable tissue in DSC-MRI cerebral perfusion datasets. Instead, new approaches classify tissue by identifying common properties of signal dynamics (Subsec. 4.1.1). They generate static tissue classifications which may only be modified by fine-tuning parameters of the classification algorithm. In this section, an interactive alternative to these approaches will be presented. It is spearheaded by the feature specification component present in Subsection 4.2.1.3. The interactivity accounts for the uncertainty involved in the classification process. The user also gains a better insight into the data by interactively changing the feature specification and observing the instantly updated classification result. For feature specification, four different kinds of data are employed: (1) CTCs, (2) descriptive perfusion parameters (Subsec. 2.1.3.4), (3) enhancement trends computed in a statistical analysis (Subsec. 4.2.1.2), and (4) quantitative perfusion parameters derived via parametric modelling and deconvolution (Subsec. 2.1.3.5). The four different approaches are compared regarding the complexity of the interactive visual analysis with a focus on the involved data preprocessing as well as the feature specification. Furthermore, the respective tissue selections are compared quantitatively. The overall comparison contributes to the discussion between *data-near* and *model-near* assessment strategies and their respective opportunities.

4.3.1 Image Data and Data Preprocessing

The four analysis approaches were applied to two DSC-MRI cerebral perfusion studies from two patients who both suffered from an acute ischemic stroke. In both cases, the parietal lobe in either of the two hemispheres was affected by a thrombosis of the middle cerebral artery. The imaging details of the first study ($Brain_1$) and the related preprocessing steps have been described in detail in Subsection 4.2.2. The second study ($Brain_2$) consists of three scans acquired $\approx$ 2 hours after symptom onset, $\approx$ 4 hours later, and the next day. Thrombolytical treatment was performed following the first scan at $\approx$ 3 hours after symptom onset. Characteristic imaging parameters of the scans of the follow-up study are: gradient echo planar imaging with TR = 2000ms, TE = 60.7ms, and flip angle = 90°, matrix =128×128, slice

thickness = 5mm, slice gap = 1.5mm, in-plane resolution = 1.9×1.9mm^2, number of slices = 15, number of acquisitions = 48, and total acquisition time = 94s.

A careful visual inspection of $Brain_2$ showed that the second scan $Brain_{2\_2}$ suffered from a severe motion artifact during the first pass of CA. For a motion correction and for a registration of all scans of $Brain_2$ to the first scan $Brain_{2\_1}$, the software `RView`, [4] which employs a rigid registration algorithm [Studholme et al., 1999], was utilized. The registration supports a concurrent analysis of all three scans. Next, a Gaussian with kernel size 3×3 has been applied to reduce spatial noise, and temporal denoising has been carried out in one iteration by means of a binomial filter of size 1×3. Then, the brain tissue has been separated from the background by means of simple thresholding. A unique value has been assigned to the background voxels such that they may be easily identified in the feature specification component and in a statistical analysis. Finally, the signal intensities have been converted to CA concentration according to Equation 2.1.

For a concurrent analysis of the separate scans of $Brain_2$, the corresponding datasets have been concatenated forming one large single dataset. However, for the comparison of the visual analysis approaches in Sec. 4.3.3, each scan will be treated separately.

4.3.2 Four Interactive Approaches

Compared to an automatic classification of perfusion data, the interactive analysis approaches require the user to eventually decide which part of the tissue is ranked among ischemic and healthy tissue, respectively. Hence, a ranking strategy needs to be defined. To distinguish ischemic tissue in the feature specification component, a conservative guess (brush) is initialized and then, extended as long as the newly incorporated voxels are located only in the hemisphere affected by the stroke. This simple strategy is valid for investigating unilateral infarctions such as in $Brain_1$ and $Brain_2$. During the feature specification, infarction core and surrounding penumbral tissue are treated as a single entity. For the sake of simplicity, no smooth brushing is considered.

4.3.2.1 Analysis based on Concentration-Time Curves

The first approach is the only one that is based on time-dependent information. It directly employs the data preprocessing output, i.e., the CTCs. Muigg et al. [2008] added a curve view to the feature specification component which facilitates a dense visualization of CTCs for all voxels of a perfusion dataset (Subsec. 4.2.5). Dedicated brushes were integrated to define a curve target shape and a similarity measure is applied to match the CTCs with this shape.

The infarction core and the penumbra require the definition of two different target shapes, one describing (almost) no enhancement and one describing a delayed and diminished enhancement during the CA's first pass. In Figure 4.13 (a), gradient sum brushes are defined to detect the ischemic tissue in $Brain_1$. The horizontal and the slanted brush characterize the enhancement in the core and the penumbra, respectively. Their position and horizontal extent have been set up with respect to the location of the first pass. Together with the vertical extension and the slope, they have been adjusted according to the ranking strategy described in Subsection 4.3.2. The selection result is visualized in Fig. 4.13 (b) and colored according to TTP. The infarction core appears reddish surrounded by the yellowish penumbra. The ventricles are also included in the selection since, similar to the core, no CA is

[4] Developed by Colin Studholme; www.colin-studholme.net/software/software.html (01/16/2010)

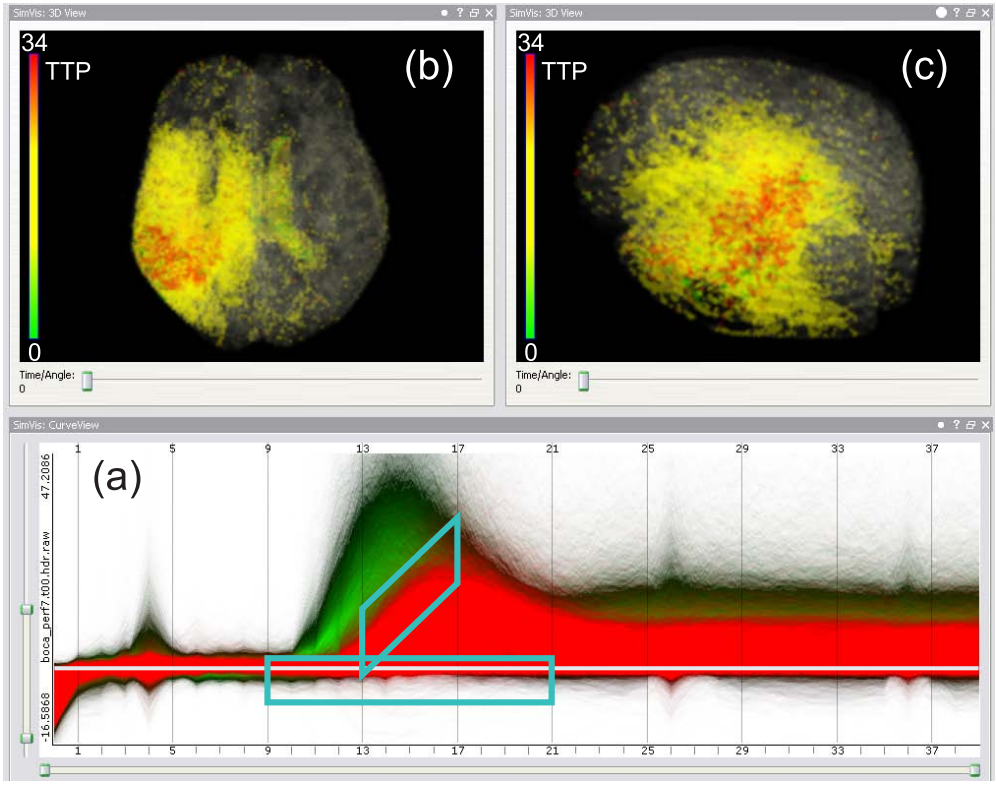

Figure 4.13: The CTCs of all voxels in $Brain_1$ are visualized in *(a)*. Two gradient sum brushes (turquoise polygons) have been defined. The selected curves are emphasized in red. The brushing reveals ischemic tissue in one hemisphere *(b)*. Its overall extension is illustrated by means of a lateral view in *(c)*. The grayish regions in *(b-c)* represent spatial reference information. (Data is courtesy of Jonathan Wiener, Boca Raton Community Hospital.)

accumulated here. A lateral view of the brain in Figure 4.13 (c) shows the extension of the infarction zone across all slices. Throughout this section, the shape of the brain is indicated as spatial reference information in all 3D views. This is achieved by brushing the gradient magnitude computed from the CA concentration at the first time step (Subsec. 4.2.2). This brushing has no impact on the infarction zone selection but also effects the coloring (slight green) of the attribute views.

Since the ventricles are not part of the ischemic tissue, they should be excluded from the selection. A subtracting *timestep brush* is employed for this purpose. Time step brushes represent simple 1D data interval brushes which may be specified per time step. To exclude the ventricles, a negative timestep brush is defined on the first time step such that large negative CA concentrations are excluded (Fig. 4.14). These values roughly represent the ventricles and major arteries after conversion from signal intensity to CA concentration (Fig. 4.21(ts1)). This is founded by the conversion equation 2.1 and the slightly higher signal intensities of the first time step as compared to the rest. The latter originate from a pending steady-state condition for the MR signal.

4.3.2.2 Analysis based on Descriptive Perfusion Parameters

The perfusion analysis based on descriptive perfusion parameters is prevailing in assessing unilateral infarctions where one hemisphere is compared to the contralateral one. It requires the derivation of the parameters in a curve shape analysis (Subsec. 2.1.3.4). Four to seven

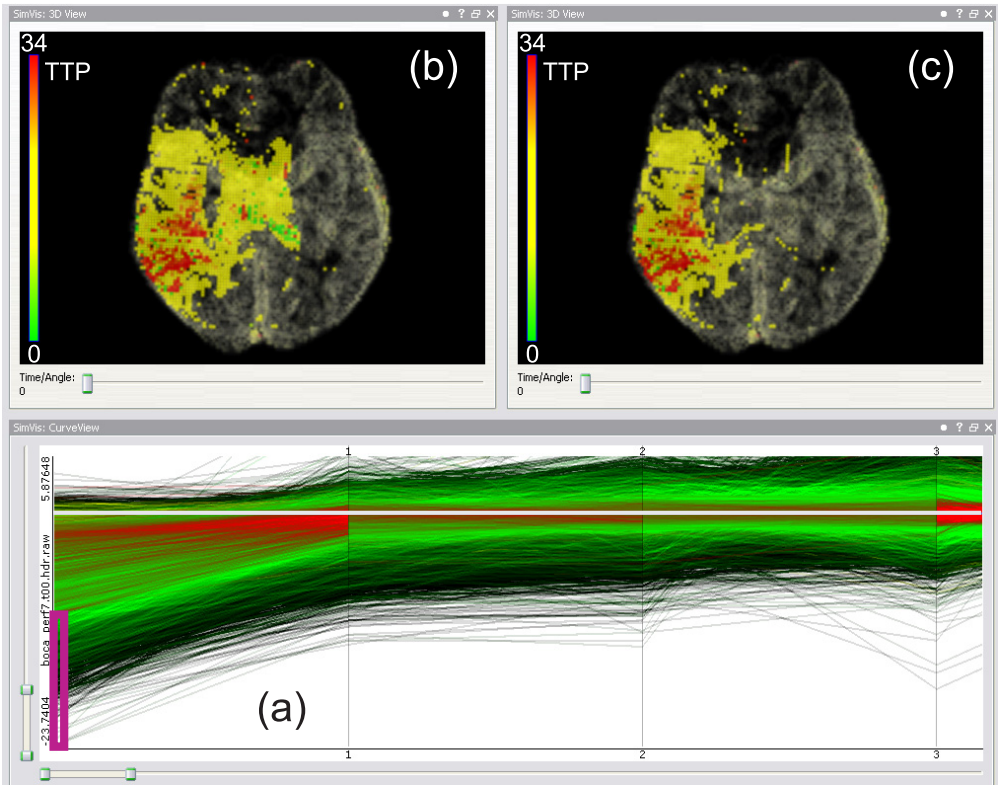

Figure 4.14: The selection from Figure 4.13 is refined in *(a)* such that the ventricles are excluded. This is illustrated in *(b)* and *(c)* only for a single slice to improve readability. In *(a)*, the CTC visualization is zoomed in on the first four time steps. The bright horizontal line represents the zero axis. A negative timestep brush (purple box) is defined such that large negative values are excluded. (Data is courtesy of Jonathan Wiener, Boca Raton Community Hospital.)

parameters are derived per voxel and constitute a special instance of multiparameter data. The feature specification component incorporates a parallel coordinates view which is perfectly suitable for assessing such data (Fig. 4.15). Each vertical line in such a view represents an axis of the n-dimensional parameter space. Each voxel containing brain tissue is represented by a polyline whose vertices are constructed on these axes based on the respective parameter value.

In Figure 4.15, a parallel coordinates view is employed to oppose all descriptive perfusion parameters derived from $Brain_2$. Each of the vertical lines represents an axis of the 7-dimensional parameter space. To generate a selection, vertical data interval brushes can be defined on each axis. At first, a brush has been defined on TTP such that high values were selected. An inspection of the corresponding polylines (emphasized in red) showed that voxels with a high TTP but a small MTT were included. This inversely proportional relationship indicates the existence of tissue with no CA accumulation (Subsec. 4.2.2). Tentatively excluding small MTT values with a negative brush (purple box) defined on MTT showed that such tissue exists in the core region but is also spread over the entire brain. Since the infarction core should remain in the selection, a trade-off has been finally achieved by restricting the negative brush to slices which do not contain ischemic tissue. The final selection result is visualized in the 3D view and colored according to TTP. The view shows the three scans of $Brain_2$ sorted by scanning order. The infarction core appears reddish in (1) and (2) and yellowish in (3). Large tissue parts of (1) and (2) are not contained in (3) anymore which indicates the existence of penumbral tissue which has benefited from the

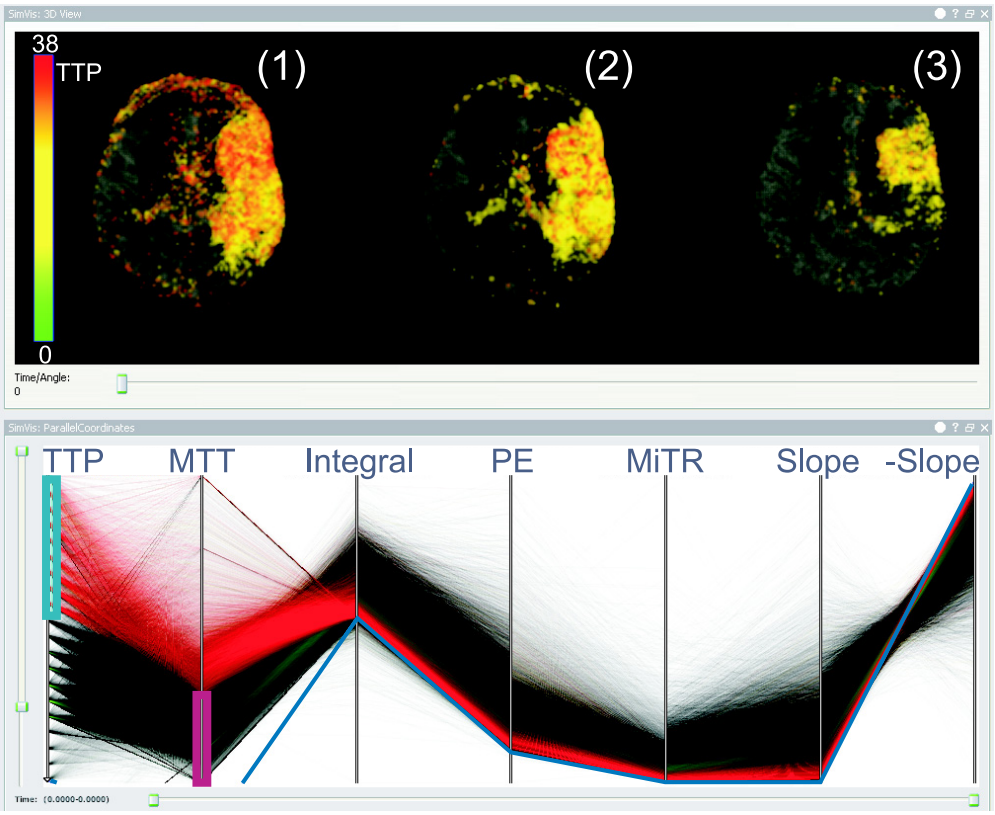

Figure 4.15: The parallel coordinates view is composed of an axis for each descriptive perfusion parameter. A brush is defined on TTP such that high values are selected. A negative brush is then defined on MTT to exclude voxels with a small MTT. The 3D view shows the follow-up study $Brain_2$ sorted by scanning order. (Data is courtesy of Arvid Lundervold, University of Bergen.)

thrombolytic therapy. Several other parameter combinations have been tested for feature specification. However, the best results could be achieved by employing TTP and MTT. Best here means that the largest compact tissue clot could be specified in the affected hemisphere accompanied by the lowest number of small disconnected structures spread over the entire brain.

4.3.2.3 Analysis based on Enhancement Trends

The work described in Subsection 4.2.2 indicated a strong information redundancy in the higher dimensional space of descriptive perfusion parameters derived from cerebral perfusion data. This redundancy could be resolved by a combination of correlation analysis and PCA. The latter revealed strong enhancement trends described by the first (pc_1) and second principal component (pc_2). These two trends could be successfully applied for the detection of ischemic tissue in $Brain_1$. Hence, it is worth investigating whether these trends may also be observed in the scans of $Brain_2$.

Before correlation analysis and PCA were carried out, the visual analysis approach introduced in Subsection 4.2.1 has been refined. Since the statistical analysis results are prone to outliers, an outlier removal technique has been introduced between background removal and auto-scaling of parameters (Fig. 4.3). It is based on the boxplot definition by Tukey [1977]. Data values are considered as outliers if they are outside the interval $[r_1 - w(r_3 - r_1), r_3 + w(r_3 - r_1)]$ with r_1 and r_3 representing the 25th and 75th percentile,

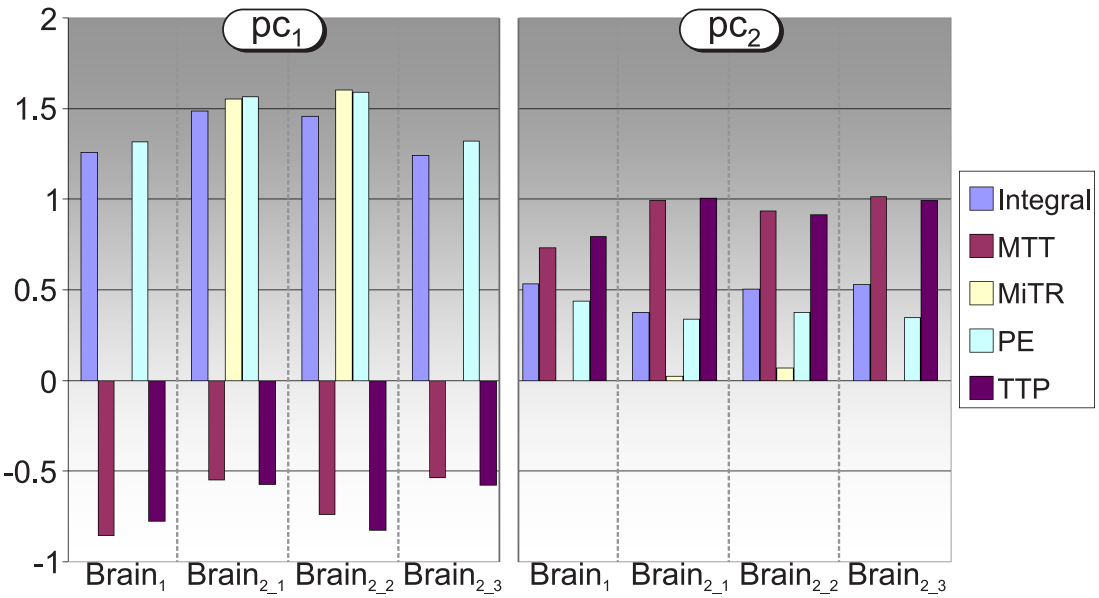

Figure 4.16: Bar chart for inspecting PCA results which have been computed based on $Brain_1$ and $Brain_2$ (three scans). The first two principal components and their loadings for the perfusion parameters are displayed. To incorporate the significance of each trend, the loadings are weighted, i.e. the bar height is scaled, with the variance explained by the corresponding pc.

respectively and a *whisker length* $w = 1.5$. However, in order to avoid the removal of pathologic features which may not be differentiable from outlier values, only one of the interval boundaries is applied per parameter. For example, small PE and high MTT values are of special interest in cerebral perfusion. Hence, only the upper and the lower bound are considered, respectively.

After the outlier removal, the correlation analysis based on all descriptive perfusion parameters has been carried out followed by an exclusion of highly correlated parameters. Then, the PCA was computed based on the reduced parameter set. The PCA results based on $Brain_2$ and $Brain_1$ are illustrated by Figure 4.16. The results achieved here for $Brain_1$ slightly differ from the ones in Subsection 4.2.1.2 (Fig. 4.5). Due to the outlier removal one strong correlation was slightly weakened (< 0.9) while a previously weaker correlation has been amplified (> 0.9). As a consequence, *Slope* and *DownSlope* instead of *Slope* and *PE* have been excluded from the parameter set before PCA.

As can be inferred from Figure 4.16, the first two pcs, i.e., the two strongest enhancement trends, are quite consistent across all datasets. Each bar of the plot represents a parameter *loading*, i.e., a weight for the linear combination of the n original variables. The prominent loadings are $Integral$ and PE for pc_1 and MTT and TTP for pc_2. $MiTR$ is only included for $Brain_{2\_1\text{-}2}$. For the remaining datasets, it was excluded before PCA due to its high correlations with other parameters. On average, both pcs together account for $\approx$ 87% of the variance in the data.

In order to employ the enhancement trends for feature specification, their respective *scores* are opposed in a scatterplot (Fig. 4.17). Since only the first two trends are considered, the scatterplot is the most appropriate attribute view. The density of data values in the plot is opacity-coded. A meaningful label for the x-axis could be "Magnitude of Enhancement" or "Magnitude and Velocity of Enhancement" ($MiTR$ included) with regard to pc_1's prominent loadings. Accordingly, the y-axis could be labeled "Time to Enhancement".

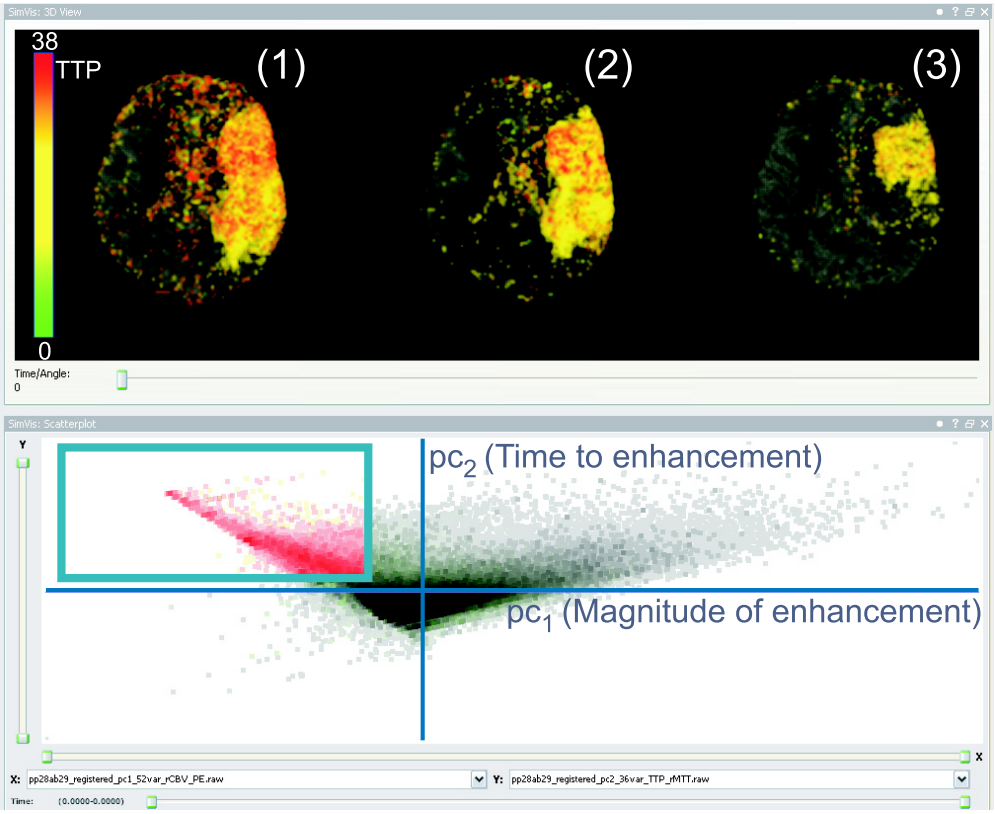

Figure 4.17: The scatterplot opposes the scores of the first (x-axis) and the second (y-axis) principal component. A brush encloses an area of low magnitude and long time to enhancement. The 3D view shows the scans of $Brain_2$ sorted by scanning order. It well resembles the one obtained in Figure 4.15. (Data is courtesy of Arvid Lundervold, University of Bergen.)

A simple rectangular brush is defined enclosing an area with a low magnitude and a long time. The 3D view shows the three scans of $Brain_2$ sorted by scanning order. The selection is colored according to TTP. It well resembles the selection based on descriptive perfusion parameters illustrated by Figure 4.15. Such a good correspondence could also be observed for $Brain_1$ here as well as in Subsection 4.2.2.

4.3.2.4 Analysis based on Quantitative Parameters

In order to obtain the quantitative perfusion parameters $rCBV$, $rCBF$, $rMTT$, and T_{max}, the arterial input function (AIF) must be determined (Subsec. 2.1.3.5). Then, the descriptive perfusion parameter *Integral* derived from the CTCs must be normalized with the corresponding parameter of the AIF in order to obtain the $rCBV$. Furthermore, the CTCs must be deconvolved with the AIF to obtain the residue function and hence, $rMTT$, $rCBF$, and T_{max}. The *Perfusion/DCE* module of the software `nordicICE` [5] has been employed for computing the quantitative parameters. It implements several deconvolution strategies. Here, the widespread standard regularized Singular Value Decomposition [Ostergaard et al., 1996] was chosen for deconvolution. The AIF was computed automatically for a user-defined subregion which was chosen such that severely diseased vessels were not included. The manual of `nordicICE` refers to the computed parameters as *semi-quantitative* since even after normalization and deconvolution, parameter values are not yet in absolute physical units and

[5] Product of NordicNeuroLab; www.nordicneurolab.com (01/16/2010)

only relative to their quantitative counterpart. A scaling is still necessary by a factor that depends on CA relaxivity, vascular structure, tissue density and hematocrit. This scaling is omitted here since it is not crucial for the comparison of the visual analysis approaches.

In `nordicICE` optionally, a gamma variate function can be fitted to each CTC and the AIF before parameter computation (Subsec. 2.1.3.3). The fitting compensates for noisy data and reduces the effect of recirculation which is essential for quantification. However, it may fail in areas with no distinctive CTC shape, i.e. abnormal hemodynamical conditions. In the following, the focus will be on investigating the impact of the fitting on the feature specification results. The selection of ischemic tissue in the four-dimensional space of quantitative perfusion parameters is carried out as described in Subsection 4.3.2.2.

In Figure 4.18 (a), a selection based on quantitative parameters whose computation involved both, fitting and deconvolution is presented. Compared to the CTC-based selection in Figure 4.13 (b), a considerable amount of small disconnected regions is included besides the large connected region representing ischemic tissue. In Figure 4.18 (b), the selection was reduced to voxels where the gamma variate fitting had failed. *NordicICE* assigns a unique value to all parameters for these voxels. The largest connected component represents the infarction core and parts of the ventricles. However, small disconnected regions which are spread over the entire brain indicate the existence of more tissue with no distinctive CTC shape. A comparison with the selection based on quantitative parameters whose computation involved no fitting supports this assumption (Fig. 4.18 (c)).

A lesson learned from investigating the fitting effects is that a straightforward estimation of the overall ischemic tissue volume is prone to overestimation if fitting is performed. Within the feature specification component, the small disconnected regions could not be separated from the infarction core by any of their attributes. Already an initial conservative brush including only the highest T_{max} values lead to a selection containing many small disconnected regions spread across the entire brain. Strictly following the initially defined tissue ranking strategy (Subsec. 4.3.2) would have meant to skip the infarction core from the selection.

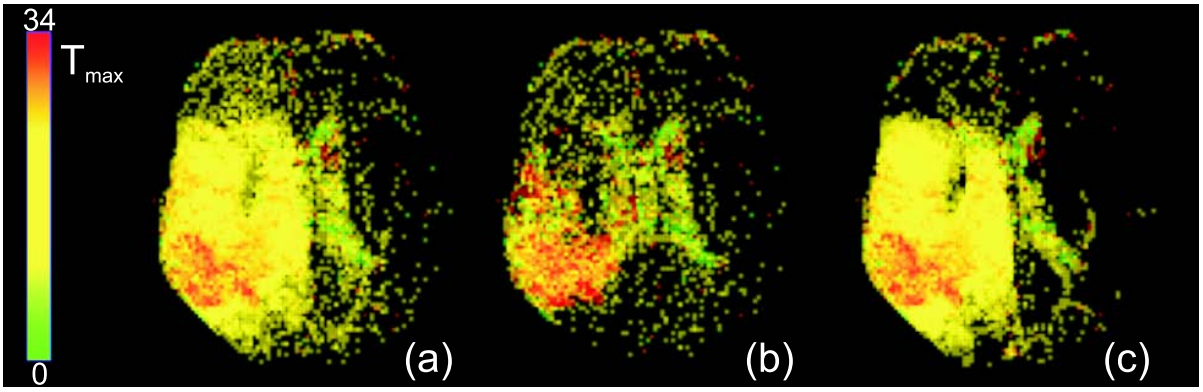

Figure 4.18: Impact of gamma variate fitting on feature specification in cerebral perfusion data. The selection in *(a)* is based on quantitative parameters whose computation involved fitting and deconvolution. In *(b)*, the selection has been reduced to voxels where the fitting had failed. In *(c)*, the selection based on the same parameters as in *(a)*, whose computation however, involved no fitting, is presented. (Data is courtesy of Jonathan Wiener, Boca Raton Community Hospital.)

4.3.3 Comparison

This section compares the four interactive approaches for feature specification and their variants. To improve readability, the following abbreviations are introduced for the Approaches based on: CTCs, with (ACTC$_{VR}$) and without (ACTC) a removal of the ventricles, descriptive perfusion parameters (ADP), enhancement trends (AET), and quantitative parameters, computed with (AQP) and without (AQP$_{NoG}$) a preceding gamma variate fitting. The approaches differ concerning the data on which the feature specification is based, the kind of attribute view used for feature specification, and the kind of applied brush (Fig. 4.19). Each approach was assessed with regard to the complexity of preprocessing necessary to generate the data on which the feature specification is based, and the complexity of the specification process itself.

The conversion of signal intensities to CA concentration is demanded by all approaches. The applied Equation 2.1 requires the determination of the Baseline phase which can easily be accomplished by a visual inspection of the averaged TIC of the entire brain tissue. No additional preprocessing is then required for ACTC and ACTC$_{VR}$. ADP further demands a delineation of the CA's first pass which may also be accomplished by visual inspection as described before. In addition, a computation of the descriptive perfusion parameters is necessary which however, can be accomplished by simple mathematics. AET does also require the computation of the descriptive perfusion parameters. Moreover, a statistical analysis of the parameters must be carried out, involving outlier removal, a correlation analysis, an exclusion of highly correlated parameters and a PCA. However, each step can be realized as a fully automatic process. AQP and AQP$_{NoG}$ both demand an AIF determination, a parameter computation and normalization, a deconvolution step and optionally, a fitting with a gamma-variate function (AQP). While most steps can be automatized, special care should be taken in AIF determination, i.e selecting a candidate region which does not include severely damaged vessels. Overall, ACTC and ACTC$_{VR}$ pose the least demands on preprocessing

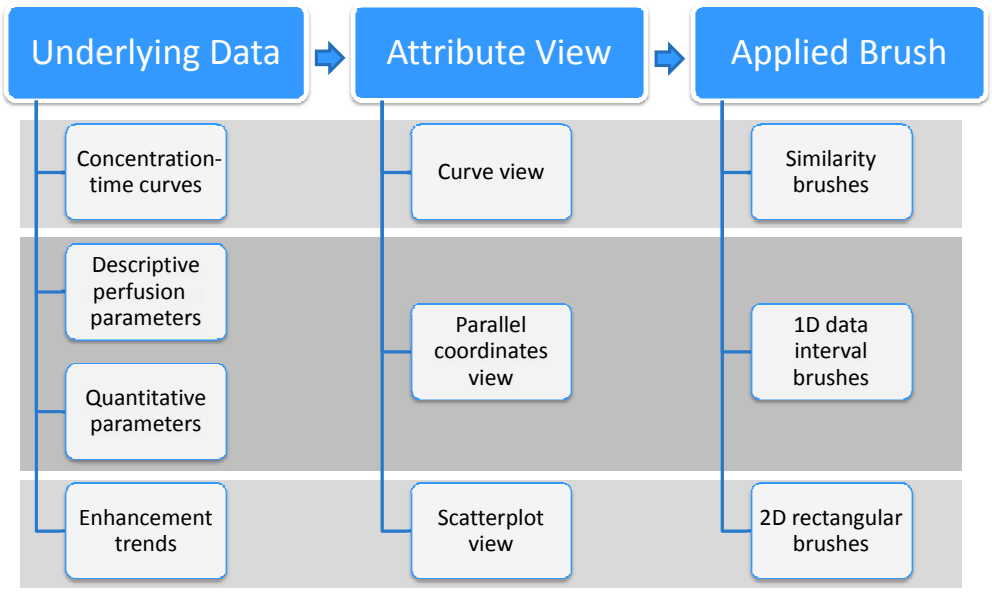

Figure 4.19: Differences between four interactive approaches to analyzing cerebral perfusion. The approaches differ with regard to the underlying data. The dimensionality of the data again guides the choice of the attribute view. Associated with each view is a dedicated kind of brush.

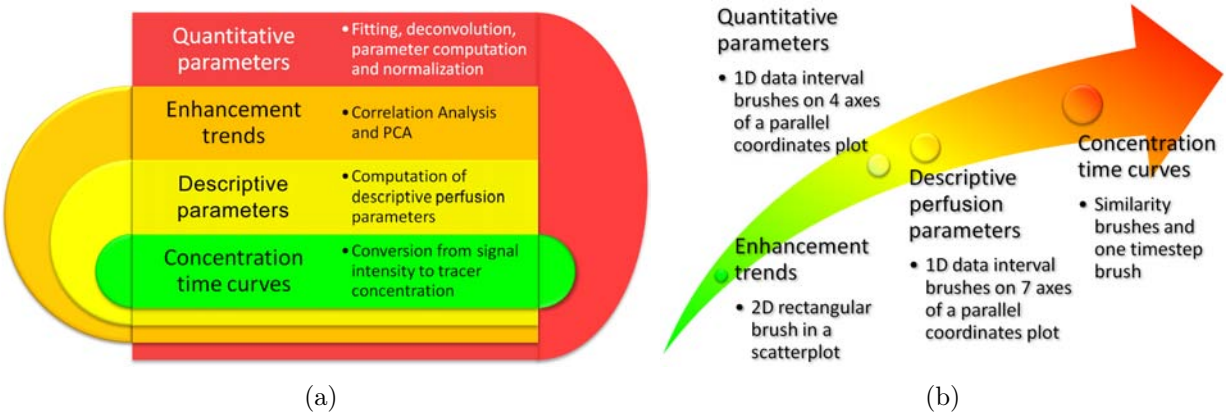

(a) (b)

Figure 4.20: Comparison of the four interactive analysis approaches regarding preprocessing efforts and complexity of the feature specification process. *(a)*: The feature specification based on CTCs requires the lowest preprocessing effort while the specification based on quantitative parameters is preceded by a complex preprocessing chain. *(b)*: Enhancement trends facilitate the quickest and easiest selection of suspicious tissue by a simple 2D rectangular brush. The specification based on CTCs is the most complex one. Handling the associated similarity brushes requires some practice.

while AET, AQP_{NoG} and AQP pose the highest demands (Fig. 4.20(a)). However, most of the necessary preprocessing can be carried out automatically in all approaches.

The complexity of the feature specification process depends on the applied attribute view and the associated brush. The gradient sum brushes used for ACTC and ACTC_{VR} are easy to set up. However, their fine-tuning requires some experience since not only CTCs having a gradient equal to the one of the brush are selected but a range of gradients as defined by the vertical extension of the brush. Furthermore, not only CTCs which pass through the brush but also vertically shifted CTCs with the desired gradient properties are selected. Although, this is a desired behavior, it still poses a discrepancy between the user expectations raised by the brush location and the selection result. Still, the gradient sum brushes provide the most intuitive way of integrating knowledge about curve shape into the feature specification. The parallel coordinates view used for ADP, AQP_{NoG} and AQP provides very simple 1D data interval brushes for each coordinate axis. However, the brushing may theoretically be carried out on seven or four axes. The practical experiences described here indicated yet, that one brush defined on the TTP/T_{max} axis delivers a good initial guess which may be refined by one or two additional (negative) brushes on other axes. The scatterplot view used for AET facilitates the definition of a 2D rectangular brush. For all datasets, this feature specification process proved to be the quickest one in yielding satisfactory selections (Fig. 4.20(b)).

The evaluation of the analysis approaches also included an investigation of their individual selection results. These were examined with respect to:

- accuracy (overlap with the "real" infarction zone),
- compactness (existence of small, disconnected regions besides the infarction zone), and
- spurious inclusion of the ventricles.

Furthermore, all selections based on the same dataset were compared regarding their pair-wise and overall overlap and the averaged CTCs of their corresponding tissue.

To assess the accuracy of a selection, it was overlaid on the original 4D perfusion scan or the converted CA concentration data and inspected visually slice by slice in cine-mode

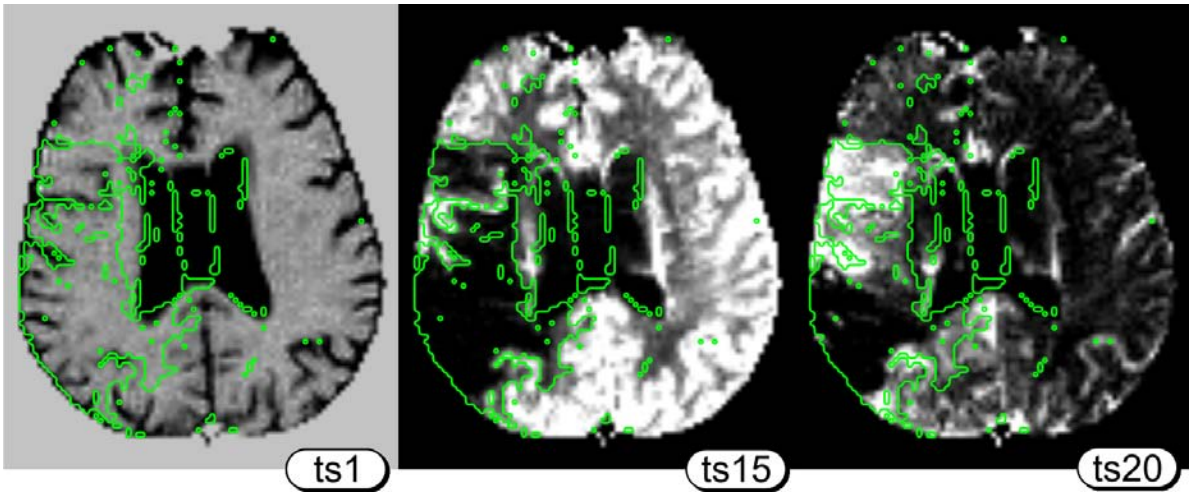

Figure 4.21: Validation of feature specification results. A slice of *Brain1* is overlaid with a feature specification result (green encircled regions) at three different time steps. The CA accumulation (bright regions) in healthy tissue is visible at an earlier time step (ts15) as compared to the penumbral tissue (ts20). (Data is courtesy of Jonathan Wiener, Boca Raton Community Hospital.)

(Fig. 4.21). In order to generate the overlay, isocontours were computed based on a binary mask image exported from the feature specification component. The visual inspection of all selections indicated no obvious under-segmentation with neither of the approaches. Over-segmentation with respect to the ventricles could be observed in all selections except for the ones based on ACTC_{VR}. A high number of small disconnected regions in the contralateral hemisphere of the infarction was observed in selections based on AQP (Fig. 4.18).

For further investigation, the compactness of each selection was determined. First, its largest connected component (LCC) was computed considering a 3D 6-connected neighborhood. For all selections, this resulted in a separation of the ischemic tissue. Next, the percentage of voxels which are part of the entire selection (ES) but not part of LCC was computed. The higher the percentage, the smaller the compactness. A peak percentage (26.8%, averaged over all datasets) could be observed for the selections based on AQP. The range of percentages for the remaining approaches was 12.2%-14.7%. The considerable deviation of the peak percentage confirms the observation of AQP being the approach resulting in the highest number of small disconnected regions.

As described in Subsection 4.3.2.1, the ventricles may be spuriously included in the selection. With non of the parameter-based approaches, it was possible to exclude the ventricles. Only the CTC-based analysis offered an opportunity by means of an additional negative timestep brush (Fig. 4.14). This suggests that a parameter-based analysis may benefit from the integration of the original time-dependent information.

An interesting question is to what extent the different selections based on the same dataset overlap. A simple measure for this is the *Dice Coefficient (DC)* [v. Rijsbergen, 1979]. The values of DC are in the range from 0 (no overlap) to 1 (identical selections). The pair-wise overlap has been computed for all selections as well as their overall overlap (Fig. 4.22). The analysis shows the smallest pair-wise overlap (ø=0.69) for all pairs including AQP. The highest values (ø=0.93) occur for the pair ACTC and ACTC_{VR} which can be expected since ACTC_{VR} is fully contained in ACTC. The remaining pair-wise overlaps are 0.79 on average.

The overall overlap is 0.53 on average (ø=0.55 when discarding ACTC_{VR}). Only discarding AQP from the computation leads to a considerable increase of the overall overlap

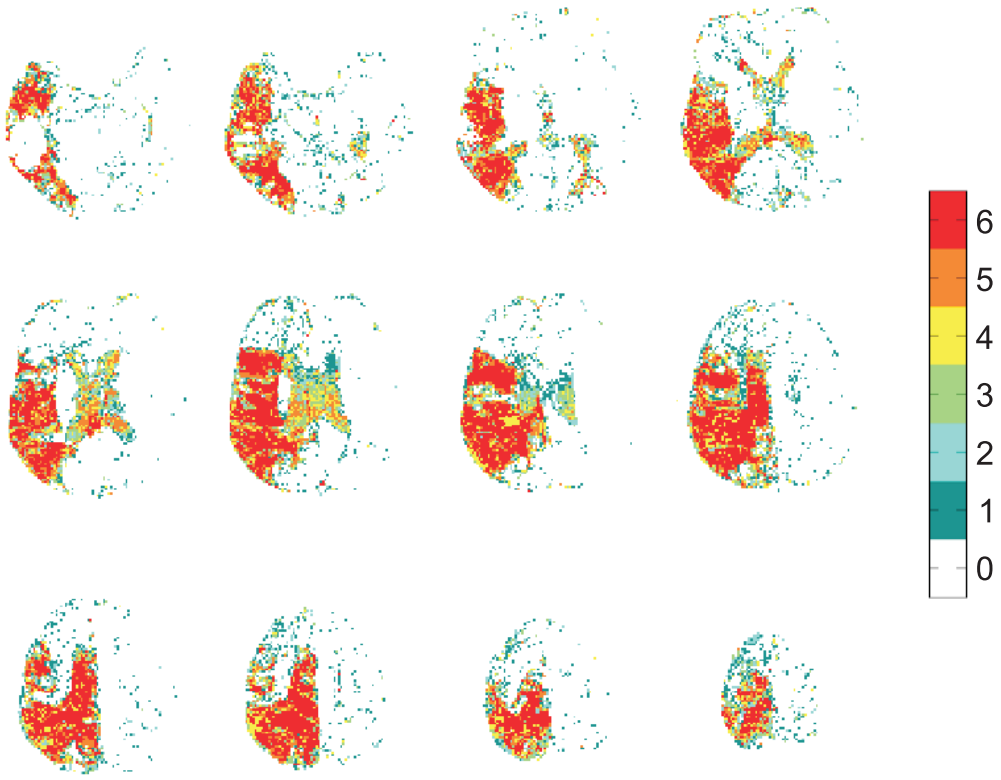

Figure 4.22: Visualization of the overall overlap of six feature specification results based on $Brain_1$. The color in each slice encodes the number of overlapping selections. (Data is courtesy of Jonathan Wiener, Boca Raton Community Hospital.)

(ø=0.16 compared to ø=0.06 for discarding the remaining approaches). This is due to the high number of small disconnected regions generated by AQP. Evaluating the overall overlap showed that despite a good-pair wise match, there still seem to be deviations across the selections. A visual inspection based on images such as Figure 4.22 indicates that many of these deviations occur aside the ischemic tissue. The respective voxels each seem to be contained only in a small subset (< 3) of selections. By contrast, the majority of tissue that is part of all selections belongs to the ischemic tissue. However, these aspects should be confirmed by a more quantitative analysis. It should also be investigated to what extent the deviations are related to the fact that the feature specification is interactive and hence user-dependent.

Another interesting aspect in examining the selections is the investigation of their counterpart in the original time-dependent perfusion data space. For that purpose, the averaged CTC has been computed for each selection together with its standard deviation at each time step. In Figure 4.23, an error bar plot computed for dataset $Brain_1$ shows the averaged CTCs of all selections together with their standard deviations. The plot is superimposed on a filled reference curve computed from the healthy brain hemisphere. A high consistency of all selections can be inferred from the averaged CTCs. While their corresponding *Integral* slightly varies, their PE is always located at timestep 18 which results in a consistent TTP. The delay with regard to the TTP of the reference curve (time step 15) is 6 seconds ((18-15)×2000ms (time between two acquisitions)) which is in the range of typical values for penumbral tissue [Olivot et al., 2009]. Further evidence provide the smaller *Integral* and PE values which indicate a diminished perfusion.

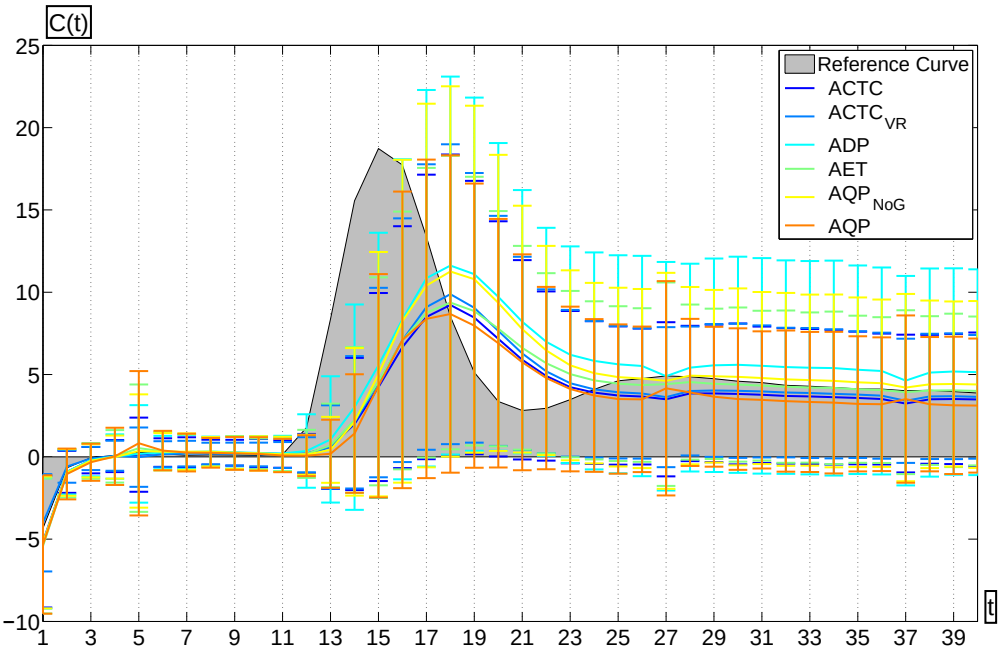

Figure 4.23: Error bar plot of the averaged CTCs corresponding to six selections based on the dataset *Brain*$_1$. The error bars represent the standard deviation of CA concentration per time step. The gray reference curve has been derived from the healthy hemisphere.

4.4 Conclusion

An interactive visual analysis approach for the streamlined evaluation of perfusion data has been presented and successfully applied to five different datasets from ischemic stroke, CHD, and breast tumor diagnosis. It integrates preprocessing techniques, statistical methods, and a feature specification component. The presented visual analysis strategy allows to assess the reliability of specific perfusion parameters, the correlation of perfusion parameters in a particular case, and enables an efficient evaluation focused on a significant subset of perfusion parameters. The statistical analysis facilitates the detection of trends in the data. Trends, representing typical enhancement patterns, may be applied for the detection of suspicious structures while trends, representing atypical enhancement patterns, may indicate preprocessing failures. Since trends are represented by a combination of several parameters, the feature specification may be more robust based on these trends than on an individual parameter. It could be shown that the reliability of a parameter may vary from dataset to dataset.

The approach has been discussed with two experienced radiologists, both familiar with perfusion imaging in the clinical routine, though not in a research context. Both rated the 3D visualization of the feature specification results embedded in spatial reference information as particularly valuable. One radiologist assessed brushing as useful for exploring the non-standardized parameter domain. Compared to the prevailing visual and highly subjective evaluation methods, the interactive visual analysis approach enables a more reproducible evaluation supported by quantitative analysis results. Thus, it may be used to answer questions regarding the diagnostic value of certain parameter combinations and to investigate the effects of a new contrast agent or changes in other imaging parameters on this value.

Muigg et al. [2008] presented a new approach for feature specification based on the visualization of a scalar function over time for an arbitrarily high number of sample points.

Dedicated similarity brushes were developed for defining curve target shapes. Similarity measures were invented to match the original curves with the target shape. In this thesis, the application of the approach to datasets from ischemic stroke and breast tumor diagnosis has been investigated. It turns out that the concept of a curve target shape and an associated similarity measure is well suited for intuitively integrating a priori knowledge of the clinician about curve shape into the feature specification process. However, the actual transformation of the knowledge into an according target shape by means of the provided user interface requires some practice.

Four different interactive approaches to analyzing cerebral perfusion data from ischemic stroke patients have been presented and compared. The approaches differ with regard to the underlying data: (1) CTCs, (2) parameters describing the CTC shape, (3) enhancement trends computed in a statistical analysis, and (4) quantitative perfusion parameters derived via parametric modelling and deconvolution with an arterial input function. The necessary preprocessing before an analysis can be carried out varies considerably between (1) and, e.g., (3) or (4). However, most of the involved steps can be automatized. The feature specification process can be intuitively accomplished in (1) by means of CTC target shapes and a similarity measure. However, it is more complex compared to, e.g., (3) where only a rectangular brush has to be defined in 2D space. For all datasets, (3) proved to be the quickest approach in yielding satisfactory results. It needs further investigation whether this is due to the simple way of defining the brush or the easily possible differentiation of the ischemic tissue in the scatterplot or both. An advantage of (1) is the ability to remove spuriously included ventricles from the selection based on the original time-dependent information. This suggests that a parameter-based analysis may benefit from the integration of the original time-dependent information.

To assess the accuracy of all approaches in detecting ischemic tissue, the selection results were superimposed on the original data. A visual inspection indicated no obvious under-segmentation with neither of the approaches. However, selections from (4), computed with a preceding gamma variate fitting, contained a high number of small disconnected regions besides the infarction zone. This could be traced back to a failure of the fitting in these regions due to the lack of a distinctive curve shape. It should be further investigated if this lack is due to local image noise or to compromised tissue perfusion with no or very little CA enhancement. The selections based on (1)-(3) and (4, without fitting), showed a considerable pair-wise overlap for the same dataset (ø=0.79). A voxel ranking with respect to the number of containing selections showed that the majority of tissue that is part of all selections belongs to the infarction zone. Most of the small disconnected tissue regions are contained only in a small subset of selections. For the comparison of all selections based on the same dataset, the corresponding averaged CTCs were superimposed on a reference CTC derived from healthy tissue. A high consistency of all selections could be inferred from this superimposition. The described perfusion deficit and delay indicated a successful inclusion of the penumbra. Compared to an algorithmic analysis, an inherent property of the interactive approach is an inter- and intra-user variability of some degree. Their impact should be examined for a larger collection of data. In addition, the possibility of differentiating between infarction core and penumbra during feature specification, e.g., by means of smooth brushing, should be further investigated.

Chapter 5

Discussion and Outlook

Perfusion data are acquired to support essential diagnostic tasks, e.g., the differentiation of infarction core and penumbra in ischemic stroke diagnosis and the early detection and diagnosis of coronary heart disease. Perfusion parameters are derived from the original time-dependent data in order to characterize regional blood flow, regional blood volume and capillary permeability. The diagnostic evaluation of perfusion data and associated perfusion parameters is a challenging and time-consuming task. Hence, simple and more advanced visual exploration techniques have been developed over the past few years to support the evaluation (Sec. 3.1). The thesis at hand contributes advanced multiparameter maps and 2D/3D glyph-based visualizations for an integrated visualization of several perfusion parameters (Sec. 3.2-3.3). Apart from being tested in the developmental and experimental phase, there are no substantial user studies with respect to advanced visual exploration techniques. To encourage this process both on the technical and on the medical side, guidelines for a visual exploration will be suggested in Section 5.1. These guidelines are inspired by diverse cooperations with clinical partners providing practical insight on how to solve practical problems and how to treat specific challenges best.

The pure visual exploration of perfusion data and associated perfusion parameters is an observer-dependent and barely reproducible task delivering no quantitative results. While being adequate in the tight schedule of clinical routine, perfusion research demands a more sophisticated approach facilitating an in-depth analysis of, e.g., parameter value distribution and inter-parameter relations. The thesis at hand contributes an interactive visual analysis approach for the streamlined investigation of perfusion including a statistical analysis (Sec. 4.2). An implementation of the approach may be used to answer crucial investigative questions in perfusion research. This has been exemplarily demonstrated in the thesis by means of comparing *data-near* and *model-near* assessment of cerebral perfusion (Sec. 4.3). Encouraged by this demonstration, the potential of the approach in answering further questions in perfusion research will be discussed in Section 5.2.

MR perfusion imaging is a very active research area in both ischemic stroke diagnosis and diagnosis of Coronary Heart Disease. Hence, techniques for the visual exploration and analysis of perfusion data must be reviewed every now and then with respect to standardization efforts in imaging and advances in imaging technology. For example, parallel imaging may soon find its way into clinical routine leading to an improved spatial coverage of the organ of interest and a higher temporal resolution. Even now many challenges remain which could not be tackled within the limited scope of this thesis. In Section 5.3, some of these challenges are discussed and and ideas which may guide future work are rendered.

The final Section 5.4 is dedicated to the transferability of the techniques developed in this thesis. This will hopefully encourage readers who are not working with MRI in ischemic stroke or CHD diagnosis to employ the techniques and adapt them to their needs. Imaging modalities other than MRI as well as different application areas of perfusion imaging and an application of Cine imaging are briefly illuminated.

5.1 Guidelines for Visual Exploration

Over the years, feedback from clinical collaborators has been collected concerning the usefulness of several visual exploration techniques. This feedback has been merged with experiences gained by colleagues also working in the fields of visualization and perfusion. Matej Mlejnek and Sven Kohle shared their experience with clinical partners regarding profile flags and volume rendering of DCE-MRI mammography data, respectively. Based on the combined wealth of experience, guidelines for the use of these techniques have been proposed and recently published in [Preim et al., 2009]. The guidelines will be reviewed and updated in the following.

It turns out that some general guidelines are valid independent of the application area. Before the guidelines are defined, the visual exploration techniques are arranged in three different classes whose separating criterion is the type of required input data:

C1 *Input data*: the original signal intensities or converted contrast agent concentrations (4D), *Techniques*: cine-movies, subtraction images, curve displays, and profile flags

C2 *Input data*: the perfusion parameters (3D), *Techniques*: parameter maps, Bull's Eye Plot (BEP), refined BEP, colored height fields, flexible lenses, color icons, glyphs

C3 *Input data*: the original signal intensities and the perfusion parameters, *Technique*: combined Maximum Intensity Projection (MIP) and Closest Vessel Projection (CVP)

The class C2 may be further subdivided into two subclasses: C2a (single parameter techniques: parameter maps, BEP) and C2b (multiparameter techniques: refined BEP, colored height fields, flexible lenses, color icons, and glyphs).

Techniques in C1 are useful for an initial inspection of the original data. Tissue characterized by a very strong or by (almost) no enhancement can be roughly identified. Cine-movies require a mental tracking of signal intensity change over time. They are useful in assessing motion artifacts, image noise, and signal inhomogeneity. Their application in breast tumor diagnosis is limited by the low temporal resolution of the data ($3-6$ points in time). Subtraction images emphasize the highest differences in signal intensity between two points in time. They are frequently used in breast tumor diagnosis to identify regions with a strong CA accumulation. Care must be taken to choose the "right" points in time. Subtraction images are also useful in assessing motion correction results. For example in breast tumor diagnosis, high intensity differences should occur only in major blood vessels and enhancing lesions. However, they may be spread over the entire mamma due to motion artifacts. Subtraction volumes provide an extension of subtraction images in 3D. They give a quick overview of the entire dataset and may be rendered, e.g., by a MIP.

Cine-movies and subtraction images may be combined with a curve display for probing the temporal course of the CA in a specific region. Several curves corresponding to different regions may be superimposed for a comparative analysis, e.g., of probably healthy and suspicious tissue. Curve displays may also be used detect motion artifacts characterized by atypical curve patterns, i.e., atypical signal intensity development. They may also be applied for determining the *Baseline* and the CA's first pass in healthy tissue. Both are crucial for the computation of perfusion parameters. Profile flags extend the concept of curve displays. They show the signal intensity development for a restricted region plotted in a graph and embedded in a volume rendering of a specific point in time or of a subtraction volume. The application of profile flags has been successfully demonstrated based on DCE-MRI mammography data. The concept should be easily transferable to cerebral perfusion

whereas an application to myocardial perfusion is arguable. The sparse spatial coverage of the myocardium by a small number of acquired slices $(3-6)$ is not appropriate for volume rendering. All techniques in C1 do not require a time-consuming preprocessing or complex user interaction. The volume rendering which provides the basis for profile flag probing can be generated in reasonable time and explored at interactive frames rates by today's common graphics hardware.

The techniques in class C2 facilitate a more thorough, reproducible and quantitative analysis of the dynamic behavior. Amongst others, they are applied for comparing the two hemispheres in cerebral perfusion, comparing rest and stress perfusion in CHD diagnosis, evaluating the effect of certain imaging parameters or CA doses, comparing perfusion across patients and across several scans of a follow-up study of the same patient or a quantitative analysis of perfusion based on a physiological model of CA distribution.

Parameter maps and the BEP (C2a) provide a simple means for inspecting a single perfusion parameter. A color-coding of the parameter values should be chosen such that suspicious values are emphasized. The determination of a parameter or a combination of parameters which most accurately describe the perfusion status is still ongoing research. Hence, the diagnosis is often based on an inspection of several parameters which is accomplished by means of a side-by-side display of parameter maps or BEPs. Techniques in C2b reduce the cognitive effort involved in a mental integration of such displays. Furthermore, they may provide additional insight into the data by unveiling features which are determined by a combination of parameters.

Colored height fields may be employed if exactly two parameters are of interest. An easily interpretable result may be achieved if one of the parameters represents the amount of delivered CA, e.g., *Integral* and *PE*, and is mapped to height. Height fields are visually attractive and may serve for the presentation of results. However, a clinical use is hampered by occlusion problems and the associated need for user interaction in 3D. Flexible lenses provide the user with an exploration facility rather than a prefabricated visualization. In a possible application scenario, an interesting feature has been detected in the original data and shall now be further examined by blending with a perfusion parameter. Synchronized lenses have been rated as particularly useful for a comparative analysis of the two hemispheres. They simplify the visual comparison by providing a spatial reference frame in the form of the lens region. If more than two parameters shall be concurrently investigated, color icons may be employed. Tests have been carried out so far for up to four parameters. The generated textures provide a good overview of the distribution of certain parameter combinations. They may unveil new features but also suppress features visible in a single parameter map. Hence, a color icon-based visualization should be linked to the underlying single parameter maps. The user may select a region characterized by a conspicuous texture causing an emphasis of this region in all parameter maps. The refined BEP may be employed for rest/stress comparisons of the same parameter or an integrated visualization of two different parameters.

Glyphs may encode several perfusion parameters depending on the number of modifiable glyph attributes. The mapping of parameters to glyph attributes should be intuitive in order to minimize the interpretive effort by the user. TIC miniatures resembling the temporal course of the CA lead to promising results since they convey the complete parameter information at a glance. The glyph-based visualization may be coupled with a feature specification component to reduce visual clutter and to direct the user to suspicious regions. In cases of densely sampled tissue, e.g., in ischemic stroke and breast tumor diagnosis, a multi-resolution glyph display may be employed gaining space for glyph drawing at lower

resolution levels. In clinical routine, 3D visualizations often serve as an overview while linked 2D representations are exploited for a detailed analysis. For example, an overview of the topology and morphology of the entire coronary tree may be given by a 3D rendering of vasculature embedded in a volume rendering of the heart. The user may select an interesting branch in 3D and further investigate vessel course and diameter distribution based on 2D multiplanar or curved multiplanar reformations of the branch as well as in common axial slices. Accordingly, glyphs may encode perfusion parameters for the whole structure of interest in a 3D view. The 3D view may be linked to 2D slice-based visualizations embedding glyphs in a texture representation of the original data. For example, an overview on the perfusion of the entire myocardium could be given segment-wise in 3D as illustrated by Figure 3.19. The overview visualization may then be linked to a 2D glyph-based voxel-wise parameter encoding as shown in Figure 3.15(c). A straightforward transfer of this scenario to ischemic stroke and breast tumor diagnosis is hampered by the more dense spatial coverage, i.e. the higher number of acquired slices. A corresponding dense 3D glyph display would lead to serious occlusion problems and introduce visual clutter.

The class C3 contains techniques which exploit the original signal intensities as well as the perfusion parameters. Kohle et al. [2002] proposed an integration of MIP and CVP for the combined visual exploration of both. First, a subtraction volume is generated and rendered via MIP. A colored CVP leading to an improved depth perception is then superimposed for all voxels exceeding a certain intensity difference. The Hue and Value component of the color encode two perfusion parameters. The approach has been proven to be useful in analyzing DCE-MRI mammography data. A transfer to ischemic stroke diagnosis seems possible though the rendering strategy must be adapted since regions exhibiting a depleted perfusion are of interest here. The combined analysis of both signal intensities and perfusion parameters has already been proven to be useful in a clinical trial for assessing breast tumor perfusion by Wiener et al. [2005]. They could show that an analysis based on MIPs of subtraction volumes and parameter maps detected many occult cancers and thereby altered and allowed more confident treatment planning.

As a consequence, techniques in C2 should be coupled with a visual representation of the temporal course of the CA, e.g., a curve display. For example, glyphs may be picked in one view and the corresponding time-intensity or concentration-time curve may be shown in the curve display. Such a linkage provides the user with access to the unaltered original data. Since clinicians are trained to interpret this data, the linkage may increase acceptance of new visualization techniques and accelerate their acquisition. Furthermore, the curve inspection may shed light on the origination of unexpected parameter values, e.g., in regions characterized by no distinctive curve shape, motion artifacts or inaccurate segmentation results.

5.2 Potential of an Interactive Visual Analysis

A thorough investigation of clinical research literature related to MR perfusion imaging for ischemic stroke and CHD diagnosis identified the following investigative questions as crucial:

- Which perfusion parameters or which combination of parameters is crucial for a specific diagnostic task?
- How are individual perfusion parameters related?

- How do imaging parameters as well as different parameter computation methods influence the expressiveness of perfusion parameters?

- How do answers to the previous questions differ from patient to patient?

In the following, the potential of an interactive visual analysis in answering these questions will be outlined. The proposed ideas are geared to clinical studies accomplished in the respective field. Most of these studies are related to two diagnostic tasks: the separation of the penumbra in ischemic stroke diagnosis and the detection of ischemic tissue in CHD diagnosis. How successful these tasks could be accomplished is frequently evaluated by means of a reference.

In ischemic stroke diagnosis, the reference is often obtained by a follow-up study [Yamada et al., 2002; Grandin et al., 2002; Schellinger et al., 2006; Kane et al., 2007; Christensen et al., 2009]. During the acute phase of the stroke, perfusion and diffusion-weighted images are acquired. Then, several perfusion parameters are derived by means of various computational methods. There is neither a consensus on which parameter best represents the perfusion status nor on which computational method should be preferred. The ischemic tissue is then delineated in a parameter map and in the diffusion-weighted images. The mismatch between both regions is supposed to represent the penumbra which has been identified as a predictor for final infarction size. It is determined for each parameter derived with each of the computational methods resulting in several mismatch candidates. In a follow-up diffusion-weighted or T2-weighted scan after therapy, the final infarct size is observed and serves as a reference.

Another way of obtaining a reference is the concurrent application of an imaging modality delivering quantitative perfusion measurements, such as PET. Studies in ischemic stroke diagnosis [Sobesky et al., 2005; Takasawa et al., 2008] as well as in CHD diagnosis [Schwitter et al., 2001; Fritz-Hansen et al., 2008] have been accomplished accordingly. The gold standard is then generated, e.g., by a thresholding the quantitative measurements.

Which perfusion parameters or which combination of parameters is crucial for a specific diagnostic task? An interesting task in ischemic stroke diagnosis is to test the difference between final and acute infarction size of inclusion in the different mismatch candidates. To which extent the tissue represented by the difference overlaps with a mismatch gives information about the predictive value of the respective parameter. Assuming that a favorite parameter has been determined, it is still likely that not all voxels belonging to the reference are part of the corresponding mismatch. Vice versa, not all voxels belonging to the mismatch may be part of the reference. The feature specification component of the visual analysis approach may be applied for a *local investigation* of such tissue (Subsec. 4.2.1.3).

As a preprocessing step, new binary attributes may be defined which indicate the inclusion of a voxel in the reference, in the different mismatch candidates and in the ischemic tissue delineated in the parameter maps and the diffusion-weighted images. These attributes facilitate a straightforward brushing of the corresponding regions, e.g., in a histogram. For example, all voxels with a value of 1 (=included) may be brushed in a histogram of the attribute characterizing the inclusion in the reference. The selection may then be refined in a second histogram of the attribute characterizing the inclusion in a mismatch candidate. A negative brush may be employed to exclude voxels which are part of both regions thereby facilitating the subsequent inspection of, e.g., the tissue which is part of the reference (final infarct size) but not part of the mismatch (prediction of final infarct size). For the resulting

tissue selection, scatterplots or parallel coordinates views may now be generated displaying the corresponding perfusion parameter distributions. A curve view may illustrate the related temporal course of the CA distribution. Together, both may give a hint on why the region was not rated as part of the mismatch candidate. Furthermore, they may indicate which perfusion parameters would have had a higher prognostic value in this region.

How are individual perfusion parameters related? The statistical analysis component of the visual analysis approach may be applied in answering this question (Subsec. 4.2.1.2). The integrated correlation analysis reveals the sign as well as the strength of proportionality. The subsequent Principal Component Analysis then reduces the set of parameters to a relevant subset explaining most of the variation in the data. Furthermore, it helps to identify trends in the data which may be applied for the detection of features or the identification of preprocessing failures. The feature specification component may as well be used for evaluating inter-parameter relations in a *multi-variate analysis*. For example, a range of parameter values may be brushed in a histogram and then displayed in the context of another parameter in a second histogram or in the context of a parameter combination in a scatterplot. Parallel coordinate views are particularly suited for assessing multiple inter-parameter relations at a glance. A range of values may be selected on one axis causing a highlighting of the associated polylines. Tracking these polylines over the remaining axis and inspecting the local, indirectly selected parameter values gives a hint on inter-parameter relations (Fig. 4.15).

How do imaging parameters as well as different parameter computation methods influence the expressiveness of perfusion parameters? Studies, e.g., in CHD diagnosis, aiming at answering this question may be based on a reference from quantitative imaging, a scan acquired with the common MR perfusion imaging settings and a scan acquired after a modification of these settings. The feature specification component may then be exploited for an analysis of the two MR scans with respect to the reference. As a preprocessing, the three scans need to be registered first. Then, the datasets corresponding to the MR scans as well as the derived parameter volumes are merged by concatenation for a concurrent visual inspection (illustrated by Figure 4.15 for a follow-up study of cerebral perfusion). A new binary attribute is defined for MR scan 1 and 2, respectively which indicates the inclusion of their voxels in the reference. This information may be easily inferred after the above mentioned registration. Voxels of MR scan 1 should be assigned a different unique value than voxels of MR scan 2. This new attribute then facilitates a straightforward brushing of the tissue representing the reference in MR scan 1 or 2, e.g., in a histogram. Two different feature sets may be specified accordingly. The corresponding perfusion parameter distributions may be conveniently explored then in a linked parallel coordinates plot opposing all perfusion parameters or one parameter derived by different computational methods. The feature sets are represented in the plot by polyline collections whose coloring identifies the set. The user may now compare the average course of the polylines collections and compare the occupied range of values per parameter for roughly assessing the impact of modified imaging parameters or computational methods on the expressiveness of perfusion parameters. In order to assess whether a specific parameter may have been exploited for delineating tissue that equals or in large parts overlaps the reference, its values may be plotted in a global histogram. If a feature set has been previously defined, a local histogram of its corresponding parameter values is automatically superimposed on the global histogram (yellow

and red bars in Fig. 4.10 (f)). The local histogram unveils whether the tissue representing the reference could have been separated, e.g., by simple thresholding.

How do answers to the previous questions differ from patient to patient? In order to answer this question, the previously described procedures may be executed for each patient and the results may be compared. It may also be useful to concatenate datasets of different patients for a concurrent analysis by means of the feature specification component. This could shed light on the origin of individual parameter value distributions in patients scanned with identical imaging settings.

5.3 Outlook

The visual exploration and analysis of perfusion data is an interesting and challenging work field bearing a great potential for further research. Remaining challenges and ideas which may guide future work are discussed in the following.

Color-, texture- and glyph-based 2D multiparameter visualizations have been presented in Section 3.2-3.3. While the benefit of the new visualizations could be demonstrated for some exemplary datasets, a systematic evaluation is missing. Color icons and glyphs seem to be the most promising techniques since > 2 perfusion parameters may be integrated in one visualization. Hence, a study should be conducted based on a large data pool and involving several clinicians that aims at evaluating both techniques. A possible task for participants of the study could be the delineation of suspicious tissue in parameter maps and in the color icon- and glyph-based visualizations. The time for delineation should be measured. Several variants of a color icon should be tested, e.g., by modifying the number of represented parameters, the parameter layout within the icon, and the colors applied for parameter mapping. Similarly, several glyph variants should be evaluated, e.g., by modifying the glyph shape and by alternating the mapping of parameters to glyph attributes. In order to maintain a manageable number of study parameters, the glyph-based visualizations should be evaluated for now on high-resolution displays without applying the multi-resolution glyph display. Once the suspicious tissue has been delineated, the participants could be asked to decide on a treatment strategy. Finally, a reference should be defined based on either a follow-up study or on quantitative perfusion measurements acquired by an alternative imaging modality (Sec. 5.2). An analysis of the study results should try to answer the following questions:

- For which parameter map or multiparameter visualization did the participants achieve the highest overlap between manually delineated tissue and the reference?
- Which parameter map or multiparameter visualization allowed for the quickest delineation of suspicious tissue?
- Does the intuitive mapping of perfusion parameters to glyph attributes as proposed in Subsection 3.3.1 outperform alternative mappings?
- Did the participants detect features in the multiparameter visualizations that they missed in the single parameter maps and vice versa?
- How did the treatment decisions based on the parameter maps and the multiparameter visualizations differ?

The 3D glyph-based visualization of myocardial perfusion has been introduced in Subsection 3.3.2 and enhanced by adding viability and functional information in Subsection 3.4.2. While the 3D visualization could serve as an initial overview of the data, a more fine granular voxel-wise analysis could be facilitated by establishing a link between the 3D visualization and the 2D glyph-based visualizations presented in Subsection 3.3.1. Furthermore, additional information could be integrated in the visualization such as precalculated segmentations of hypoperfused areas, microvascular obstruction and the peri-infarct zone which may exist at the border of necrotic tissue. The 3D visualization would strongly benefit from integrating a visual representation of the coronary arteries thus facilitating a patient-individual assignment of myocardial regions to coronary branches. Improved MR sequences for imaging the coronary arteries may lead to an imaging protocol which by default contains an according scan. The 3D visualization should be linked with the Bull's Eye Plot being the standard communication element for findings in cardiology. Animated focusing of the corresponding coronary branch after picking a segment of the Plot should be integrated (Subsec. 3.4.1.2). The transmurality and the wall thickening have been computed based on measuring surface distances in Subsection 3.4.2. The effect of previously smoothing the surfaces should be further studied. Eventually, a thorough evaluation of the comprehensive cardiac visualization should be carried out comparing diagnostic speed an accuracy with a purely visual slice-based exploration of all related scans.

An interactive feature-based approach for the streamlined visual analysis of perfusion data has been introduced in Subsection 4.2.1. The statistical analysis component comprises a Principal Component Analysis (PCA) amongst others. Since the PCA results are prone to outlier data values, an outlier removal step has been included experimentally in Subsection 4.3.2.3. The impact of outlier removal on the final feature specification result, i.e., the tissue identified a suspicious, should be further investigated. In order to facilitate an on-the-fly inspection of correlation analysis, PCA, and outlier removal results, these parts of the statistical analysis component should be transferred to the feature specification component. The user could then modify the outlier removal strategy or variantly exclude highly correlated perfusion parameters before PCA and receive an immediate visual feedback.

A very interesting clinical study which further investigates the potential of trends for detecting ischemic tissue could be conducted in ischemic stroke diagnosis. So far, the trends computed based on 5 DSC-MRI datasets (two single scan studies and one follow-up study comprising 3 scans) could be successfully applied for detecting infarction core and penumbra. The datasets were acquired using two different scanners and a different contrast agent dose. The same pattern of parameter loadings could be observed for the first two principal components which represented 75%-82% of the variance in the data. For the scores of both principal components based on one dataset, a lower and an upper threshold were manually derived such that they encompass a range of values representing ischemic tissue. The thresholds were then applied to the other datasets leading to a very good initial estimate of ischemic tissue. This observation should be reviewed in a study based on a larger data pool. Furthermore, it should be elaborated whether a trend-based detection of ischemic tissue is more robust or even more precise than a detection based on a single parameter. Since trends represent a combination of several parameters, a weak reliability of a specific parameter may be compensated by the remaining ones.

Another interesting clinical study aiming at the differentiation of normal, hypoperfused, stunned, hibernating, and necrotic myocardial tissue could be conducted by means of the visual analysis approach. For this purpose, parameters describing the transmurality of an infarction as well as wall thickness and wall thickening of the myocardium must be computed

voxel-wise and integrated as new attributes. Further meaningful attributes could be the myocardial segment comprising the voxel and the supplying coronary branch as defined by the American Heart Association [Cerqueira et al., 2002]. The different myocardial coverage of the scans must be considered in a voxel-wise attribute assignment. For the differentiation of stunned and hibernating myocardium, the user may brush suspicious wall thickening values in one attribute view and observe the corresponding perfusion parameters and transmurality in another attribute view as well as color-coded in a 3D view of the feature specification result. Hibernating and stunned myocardial tissue both are characterized by a zero transmurality (unless being part of the peri-infarct zone). In contrast to stunned myocardium, hibernating myocardium also exhibits a perfusion deficit. For the differentiation of hypoperfused and necrotic tissue, the user may brush suspicious perfusion parameter values in an attribute view and observe the feature specification result color-coded according to transmurality in the 3D view. In order to establish an anatomic reference in the 3D view, the feature specification result could be embedded in a surface representation of the left and the right ventricle.

5.4 Transferability to Different Fields

The techniques presented in this thesis may be transferred to different application areas under certain conditions. A prerequisite for the transfer of multiparameter maps (Subsec. 3.2) and 2D glyph-based visualizations (Subsec. 3.3.1) is that the underlying data represents a time-dependent variable which has been sampled over time on a regular grid and based on which parameters have been derived describing its temporal behavior. In contrast, arbitrary grid types may be handled by the statistical component and the feature specification component of the interactive visual analysis approach introduced in Subsection 4.2.1. The 3D glyph-based visualization of myocardial perfusion (Subsec. 3.3.2) and the enhancement with viability and functional information (Subsec. 3.4.2) are rather cardiac specific. They may easily be transferred to other imaging modalities but not to other fields.

In the following, the transferability of the techniques developed in this thesis is outlined with regard to perfusion data acquired by imaging modalities other than MR as well as additional application areas of perfusion imaging and an application of Cine imaging.

5.4.1 Different Imaging Modalities

This subsection is dedicated to perfusion Computed Tomography (CT) and the nuclear imaging modalities Single-Photon Emission CT (SPECT) and Positron Emission Tomography (PET) which are widely-used in ischemic stroke and CHD diagnosis, respectively.

5.4.1.1 Perfusion Computed Tomography

In cerebral perfusion CT, the first pass of an intravenously injected iodinated contrast material is monitored by means of ionizing radiation. The perfusion CT equipment and emergency settings are widely available in hospitals. Perfusion CT offers the opportunity to obtain accurate quantitative measurements [Wintermark et al., 2005b]. A possible workflow for achieving these measurement is described in [Wintermark et al., 2005a]. The analysis of perfusion CT data begins with the removal of spatial noise followed by a motion correction. Next, a curve is fitted to the measured *time attenuation curve* of each voxel, e.g., by a least-mean-squares method. Then, the quantitative parameters *rCBF*, *rCBV*, *rMTT*, and T_{max} can be derived by means of a deconvolution approach as described in Subsection 2.1.3.5.

The parameters are ideally interpreted together. The comparison of the parameters between an abnormal region and the mirrored region in the contralateral hemisphere is effective in determining the degree of a perfusion disturbance. An important objective in perfusion CT research is the reliable definition of infarction core and penumbra [Wintermark et al., 2005b].

All techniques presented in the thesis are readily transferable to the visual exploration and analysis of cerebral perfusion CT data. However, since an accurate quantification of perfusion is feasible with PCT in clinical routine, known physiological thresholds separating hypoperfused from healthy tissue should be incorporated. Color scales and parameter mapping functions for modifying glyph attributes should be redesigned such that a significant change in color, size, etc. arises from the threshold value.

5.4.1.2 Nuclear Imaging Modalities

Static SPECT and PET are the current reference standards in cardiac perfusion imaging. In the following, the focus is on static SPECT due to its higher availability, lower cost, and lower logistical effort as compared to PET. In the end of this subsection, dynamic SPECT and dynamic PET will be briefly reviewed.

In static SPECT, a radiopharmaceutical is administered which gets trapped in the myocardium. After a certain waiting time, its tissue uptake characterizing regional distribution is measured by a scintigraphic technique (3D data). Often, rest/stress tests are carried out to independently evaluate myocardial perfusion and viability. ECG-gated SPECT facilitates the imaging of myocardial contraction. The heart is imaged at different phases during the cardiac cycle. The images acquired at the end-systolic and end-diastolic phase may be used to compute myocardial wall thickness and wall thickening. The parameters which may be obtained from a rest/stress and an ECG-gated study are: uptake at rest and stress, wall thickness at end systole and end diastole, and wall thickening. Meyer-Spradow et al. [2008] propose a glyph-based SPECT visualization that integrates theses parameters as well as two additionally derived parameters: the difference between the two uptakes and a self-defined tissue conspicuousness index. Supertorus glyphs are positioned on the left ventricular surface, which has been extracted from the SPECT data. Meyer-Spradow et al. present a perfusion and a wall motion scenario for the application for their glyph-based visualization. The requirements on the different scenarios result in different parameter encodings for the ventricular surface and the glyphs. Both scenarios may be reenacted by means of a segment-wise glyph-based visualization with 3D BEP segments. A comparison of the respective parameter encodings is shown in Table 5.1. It should be noted that in order to guarantee glyph readability, the positioning of supertorii on the ventricular surface is to be preferred to a positioning of 3D BEP segments inside the ventricle (Fig. 3.18) in case of a high ventricular coverage. For example, 32 slices were acquired in [Meyer-Spradow et al., 2008] as compared to $3-6$ slices in standard myocardial perfusion MRI.

The dynamic measurement of perfusion (4D data) may be accomplished by means of dynamic SPECT (dSPECT) [Farncombe et al., 1999] or dynamic PET (dPET) [Iida et al., 1988] imaging. While common radiopharmaceutical tracers are trapped in the myocardium, diffusible tracers such as Teboroxime for dSPECT and $H_2{}^{15}O$ for dPET as well as tracers having a short half live such as ^{82}Rb for PET rapidly washout from the myocardium. The rate of tracer infusion and washout provides additional information about the function of an organ as compared to static imaging. Infusion and washout may be characterized by *time-activation curves*. Parameters derived from these curves are mostly averaged for myocardial segments to compensate for the poor spatial resolution and the low SNR usually exhibited

Scenario	Parameter	Supertorii	3D BEP segments
Perfusion	uptake stress	Surface color	Surface color
	uptake rest	Glyph color	Glyph color
	uptake difference	Glyph size	Glyph thickness
	wall thickening	Glyph roundness	Glyph height
	conspicuousness	Glyph opacity	Glyph opacity
Wall motion	uptake rest	Surface color	Surface color
	wall thickness ED	Glyph color	Glyph color
	wall thickness ES	Glyph size	Glyph height
	wall thickening	Glyph roundness	Glyph thickness
	conspicuousness	Glyph opacity	Glyph opacity

Table 5.1: Mapping of parameters extracted from a rest/stress perfusion and a functional ECG-gated SPECT study to left ventricular surface and glyph attributes. Two application scenarios are considered. The utilization of supertorus glyphs [Meyer-Spradow et al., 2008] and 3D BEP segments is compared. ED: end diastole, ES: end systole.

by those studies. However, a pixel-wise analysis by parametric images may also be possible [Lee et al., 2005]. Often, the dynamic imaging is carried out at rest and under stress.

The application of multiparameter maps, 2D glyph-based visualizations, and voxel-wise 3D glyph-based visualizations to dynamic SPECT and PET data is straightforward if parameters have been derived voxel-wise. In case of a segment-wise computation, glyph-based visualizations with 3D BEP segments and TIC miniatures may be employed. An adaptation of the 3D visualizations is necessary if the slices have not been acquired in short-axis views but in long-axis views or along arbitrary directions. The parameters obtained from a rest and a stress scan may be integrated by each of the visual exploration techniques once a reliable registration of the scans could be established. The interactive visual analysis approach is directly applicable and may assist in detecting regions with a depleted perfusion (and metabolism).

5.4.2 Different Application Areas

This subsection addresses the application of perfusion imaging in brain tumor diagnosis and and the diagnosis of renovascular disease. In addition, the application of Cine imaging to evaluating systolic heart failure is covered.

5.4.2.1 Brain Tumor Diagnosis

MR perfusion studies are acquired in the diagnosis of brain tumors for preoperatively estimating tumor grade, guiding biopsy, accurately delineating tumor margins for radiation therapy, and in follow-up examinations for the differentiation between radiation effects and recurrent tumor [Covarrubias et al., 2004]. Both, DSC- and DCE-MRI are applied measuring different quantities. DSC-MRI delivers information about blood flow, blood volume and blood transit time which correlate to tumor grade and microvessel density. The imaging parameters of DSC-MRI are similar to those described for stroke imaging (Subsec. 2.1.2.3). The acquired data are evaluated by deriving descriptive perfusion parameters from CTC shape (Subsec. 2.1.3.4) or by obtaining quantitative parameters from deconvolution approaches

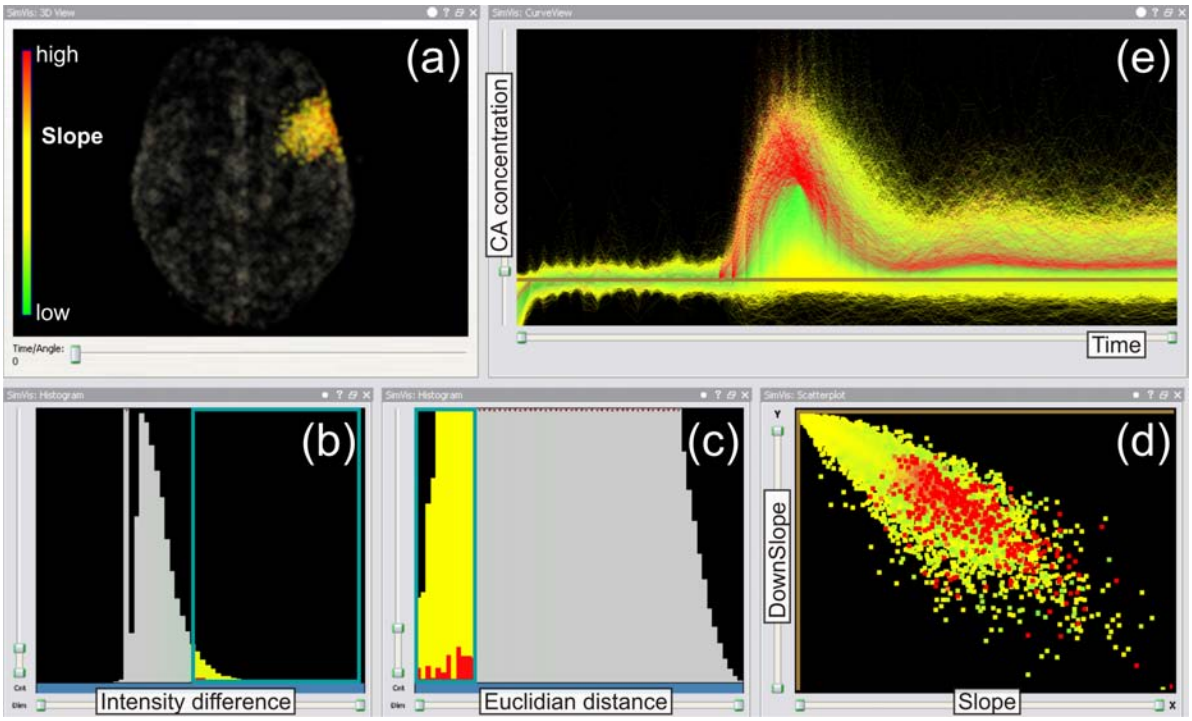

Figure 5.1: Visual analysis for the detection and characterization of brain tumors (cf. Fig. 4.10). The selection of high intensity differences between original time steps t_{21} and t_{11} *(b)* includes areas with a strong CA absorption. The analysis is focused on a suspicious region in the right anterior part of the brain by means of brushing small Euclidean distances between its center and the surrounding tissue *(c)*. The resulting region is embedded in a context rendering of the brain in *(a)* and its is colored according to *Slope*. The scatterplot in *(d)* and the curve view in *(e)* show perfusion parameter and CA concentration characteristics of the region colored in red (brown lines represent the zero axes). The observed inhomogeneous contrast enhancement and the strong rapid accumulation and washout of the CA indicate a high-grade glioma (brain tumor) which was confirmed by a neuroradiologist. (Data is courtesy of Arvid Lundervold, University of Bergen.)

(Subsec. 2.1.3.5). In contrast to stroke imaging, the quantification is often strongly hampered by CA leakage into the extravascular extracellular space due to a defect blood-brain barrier. The leakage causes T1-effects in the tissue which counteract with $T2^*$-effects thus requiring a leakage correction [Collins and Padhani, 2004]. Such a correction results in a new set of perfusion parameters which may be interesting to compare to the uncorrected counterparts [Boxerman et al., 2006].

DCE-MRI is applied for measuring transfer and rate constants related to the exchange of blood and CA between blood plasma and tumor interstitial space (permeability) as well as for determining leakage space. These quantities correlate with microvessel density and the vascular endothelial growth factor. Due to the fact that the relaxation effect lasts longer than the susceptibility effect, the temporal resolution of DCE-MRI may be decreased in oder to increase the spatial coverage. DCE-MRI data may be evaluated by means of descriptive perfusion parameters derived from TIC shape or by pharmakokinetic modeling, e.g., according to [Tofts and Kermode, 1991]. The latter includes the fitting of a model curve to the CA concentration. Transfer and rate constants as well as leakage space are then provided by the fitting equation. Both, DCE- and DSC-MRI have proven to be valuable in assessing brain tumor perfusion. A combined imaging is feasible by means of dual-echo gradient echo sequences and reduces the effect of CA leakage [Collins and Padhani, 2004].

The application of multiparameter maps and 2D glyph-based visualizations to evaluating brain tumor perfusion is straightforward. Instead of integrating different parameters, parameters corrected for CA leakage and their uncorrected counterparts may be integrated to study the effect of the correction. The visual analysis approach may support tumor grading by a local investigation of the derived perfusion parameters (Fig. 5.1). The 3D visualization of the tumor tissue may assist in inspecting its margin. Furthermore, it may be beneficial for the planning of stereotactic biopsy and radiation. The correlation analysis integrated in the statistical component of the approach may be useful in intra-parameter comparisons for assessing the impact of leakage correction. It may be enhanced by the computation of local correlations instead of a global coefficient [Sauber et al., 2006]. The follow-up analysis, e.g., after radiation therapy, is feasible and may be carried out in a similar manner as for evaluating the effect of thrombolytic therapy in stroke diagnosis (Subsec. 4.3.2.2, Fig. 4.15).

5.4.2.2 Diagnosis of Renovascular Disease

Dynamic imaging of the kidneys for evaluating the local renal perfusion is an emerging field [Prasad, 2006]. It is not yet established in clinical routine but it is gaining importance since renovascular disease is rapidly progressive. Affected patients may eventually require dialysis or a kidney transplantation. The evaluation of renal perfusion is particularly challenging and interesting since already three different CA enhancement patterns related to the three different renal compartments, renal cortex, medulla, and pelvis, may be observed in healthy subjects. MRI techniques, e.g., DCE-MRI, have been documented as highly beneficial in evaluating renal perfusion [Prasad, 2006]. Since dynamic MRI of the kidneys is yet in an experimental stage, there seems to be no consensus on applied imaging parameters. For example, Zöllner et al. [2007] investigate datasets acquired with two different magnetic field strengths, three different sequences, matrix sizes of 256×256 and 512×512, 20-44 slices, 20-118 acquisitions per slice (points in time), and regular as well as irregular temporal sampling.

Motion correction is a crucial preprocessing step in evaluating renal perfusion since the kidneys are flexible organs which are moving during acquisition due to respiration and pulsations [de Senneville et al., 2008]. Once a correct temporal inter-pixel correspondence could be established, descriptive perfusion parameters may be derived from time-intensity curves (Subsec. 2.1.3.4). These parameters are useful for comparing the two kidneys and for comparing kidneys between subjects. Quantitative parameters may as well be obtained either by employing deconvolution techniques or from using intravascular CAs [Prasad, 2006]. A crucial step in investigating renal perfusion is to separate the different compartments [Michoux et al., 2006]. Then, TICs from the individual compartments indicate tissue perfusion and glomerular filtration. The prevailing method for separating the compartments is a slice-wise manual or semi-automatic ROI definition. However, this method is time-consuming, error prone and the results are intra- and inter-observer variant. An alternative approach is the application of an Independent Component Analysis to automatically identify the compartments [Zöllner et al., 2007].

The transferability of some of the visualization techniques presented in this thesis to evaluating renal perfusion is straightforward. Multiparameter maps and 2D glyph-based visualizations may readily be applied to the derived descriptive and/or quantitative perfusion parameters. Synchronized flexible lenses (Subsec. 3.2.2) might be of particular interest for comparing regions between the two kidneys. The visual analysis approach may be employed for an interactive separation of the renal compartments (Fig. 5.2). The spatial resolution of renal perfusion data suggests the application of direct volume rendering techniques either to

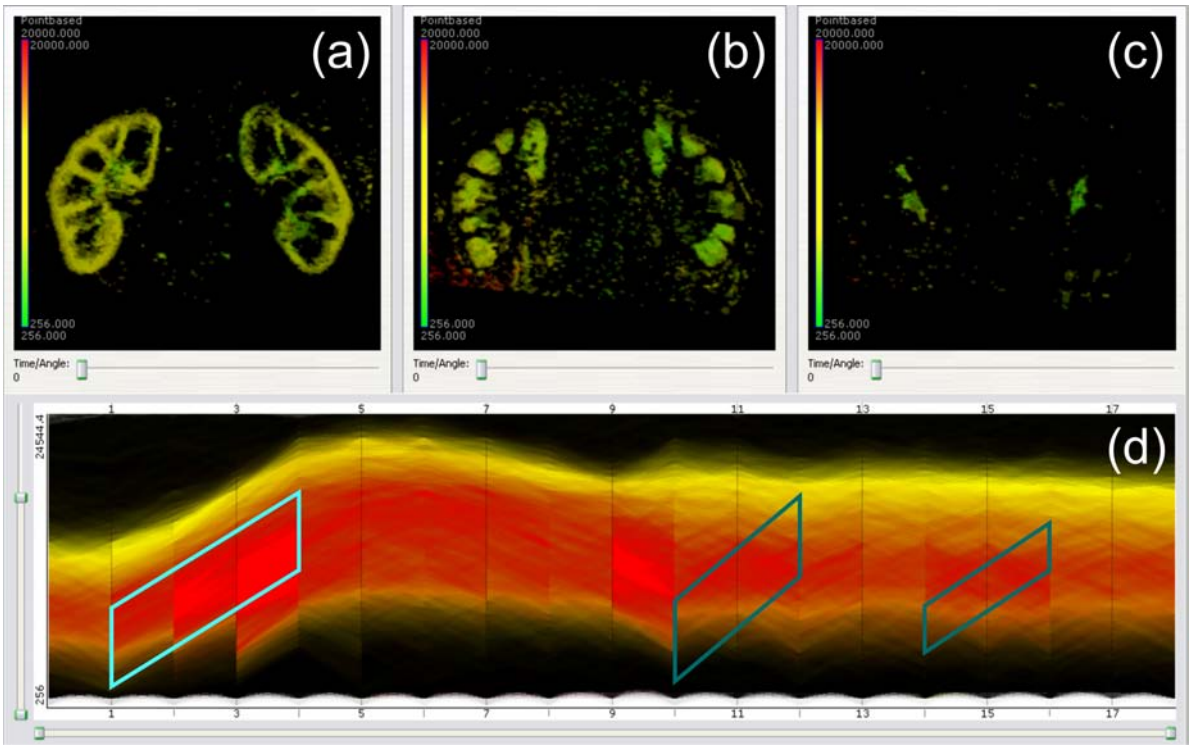

Figure 5.2: Separation of kidney compartments in evaluating renal perfusion. All TICs of a DCE-MRI renal perfusion study are visualized in *(d)*. A gradient sum brush (left bright, turquoise polygon) has been defined such that regions with a strong early CA accumulation are included. The selected curves are emphasized in red. The brushing reveals the renal cortex in *(a)*. Shifting the brush to the right (middle dark, turquoise polygon) and decreasing its horizontal extension shows the medulla in *(b)*. Note that the selected curves are only shown for the leftmost brush in *(d)*. Further shifting the brush to the right (right dark, turquoise polygon) and decreasing its vertical extension reveals the pelvis in *(c)*. (Data is courtesy of Arvid Lundervold, University of Bergen.)

individual 3D parameter volumes, to a set of parameter volumes in a multiparameter volume rendering as presented by [Kohle et al., 2002] or to the original 4D data. The latter requires a modification of the transfer function over time according to the varying CA accumulation. It may also be interesting to emphasize algorithmically or user-defined features over time in an importance-driven volume rendering [Wang et al., 2008].

5.4.2.3 Systolic Heart Failure

Heart failure is the leading cause of hospitalization in elder people. It may generally be classified as systolic or diastolic heart failure. Advanced systolic heart failure is characterized by intra- or interventricular conduction delays which disturb the synchronous beating of the ventricles thereby decreasing the heart's pumping efficiency. Systolic heart failure is seen as a widened QRS complex in the ECG. It is treated by cardiac resynchronization therapy (CRT). In CRT, a biventricular pacemaker is implanted which monitors the heartbeat and re-coordinates both ventricles if necessary. A serious issue in CRT is a proper patient selection. Parameters need to be defined that accurately predict the hemodynamic benefit of a patient. The QRS duration is currently used as such a parameter but it has been shown that it only weakly predicts CRT response. A better predictor seems to be the mechanical dyssynchrony

which may be evaluated by analyzing ventricular wall motion. Cine MRI (Subsec. 2.2.2.3) is among the techniques which have proven to be useful in this context [Lardo et al., 2005].

Chalil et al. [2007] derive parameters from *wall motion curves* to build an index that predicts CRT response. In a first step, the myocardium is delineated in all slices over all phases of a Cine MRI study, and the respective myocardial wall thickness is computed (Subsec. 2.2.3.6). Then, radial wall motion is determined as the difference in wall thickness between phase j and phase i with $j > i$. Next, the myocardium is divided into segments and the averaged wall motion is computed per segment. A wall motion curve is generated per segment by plotting the average wall motion over time (phase). Then, a variant of the sine wave function is fitted to the curve and parameters are derived from the fit: mean segmental radial wall motion, cyclic segmental radial wall motion amplitude (PE), and the segmental phase shift of the maximum radial wall motion (TTP). Finally, a tissue synchronization index is computed as the standard deviation of all segmental phase shifts. The index was proven to have a good prognostic value for CRT response.

Marsan et al. [2009] report the combined evaluation of *wall thickness curves* and MR Late Enhancement (LE) data as valuable in predicting CRT response. Wall thickness information is derived from Cine MRI data. At first, three slices representing the basal, the mid-ventricular, and the apical part, are selected from the slice stack. Then, the myocardium is delineated in all slices over all phases and divided into segments according to the 17-segment model [Cerqueira et al., 2002]. Next, the segmental average wall thickness is computed and plotted over time resulting in wall thickness curves. Finally, the time from the R-wave of the ECG to the maximum wall thickness (TTP) is computed per segment. The standard deviation of the segment times then serves as global marker for dyssynchrony. In evaluating the LE data, the myocardium is delineated in all slices, the scarred tissue is segmented, the total extent of the scar with respect to ventricular mass, and the transmurality per segment as percentage of scarred tissue are computed. The study population in [Marsan et al., 2009] received a biventricular pacemaker whose implantation was accompanied by an assessment of the location of scarred tissue in relation to the pacing lead position. About 6 months later, the CRT response was evaluated by echocardiography. The global marker for dyssynchrony derived from wall thickness curves turned out to be directly associated with response while the total extent of scarred tissue was inversely associated. Furthermore, CRT response was poor if the pacing lead position matched the location of transmural scar.

Utilizing wall motion or temporal wall thickness information in patient selection for CRT therapy is an active research field. No ultimate dyssynchrony index has been reported yet. The techniques developed in this thesis could support the research. For example, the segment-wise 3D glyph-based visualizations of myocardial perfusion could be adapted to represent parameters derived from wall motion or wall thickness curves. While the shape of 3D TIC miniatures should be adapted to the new curve shape, 3D BEP segments are immediately usable. The visualization could be enhanced by integrating viability information extracted from LE data such as scarred tissue and its transmurality (Subsec. 3.4.2). The visual analysis approach may serve a feature detection based on wall motion and wall thickness curves as well as on associated shape parameters. For that purpose, the curves and parameters need to be determined voxel-wise. This may be achieved by a segment-wise determination followed by an assignment to all voxels contained in a segment.

Bibliography

[Adams et al. 2007] Adams, Harold P.; Zoppo, Gregory del; Alberts, Mark J.; Bhatt, Deepak L.; Brass, Lawrence; Furlan, Anthony; Grubb, Robert L.; Higashida, Randall T.; Jauch, Edward C.; Kidwell, Chelsea; Lyden, Patrick D.; Morgenstern, Lewis B.; Qureshi, Adnan I.; Rosenwasser, Robert H.; Scott, Phillip A.; Wijdicks, Eelco F M.: Guidelines for the early management of adults with ischemic stroke. In: *Circulation* 115 (2007), no. 20, pp. e478–e534

[Al-Saadi et al. 2001] Al-Saadi, N.; Gross, M.; Bornstedt, A.; Schnackenburg, B.; Klein, C.; Fleck, E.; Nagel, E.: Comparison of various parameters for determining an index of myocardial perfusion reserve in detecting coronary stenosis with cardiovascular Magnetic Resonance Tomography. In: *Zeitschrift für Kardiologie* 90 (2001), no. 11, pp. 824–34

[Al-Saadi et al. 2000] Al-Saadi, N.; Nagel, E.; Gross, M.; Bornstedt, A.; Schnackenburg, B.; Klein, C.; Klimek, W.; Oswald, H.; Fleck, E.: Noninvasive detection of myocardial ischemia from perfusion reserve based on cardiovascular Magnetic Resonance. In: *Circulation* 101 (2000), no. 12, pp. 1379–83

[Astrup et al. 1981] Astrup, J.; Siesjö, B. K.; Symon, L.: Thresholds in cerebral ischemia - the ischemic penumbra. In: *Stroke* 12 (1981), no. 6, pp. 723–725

[Atkinson et al. 1990] Atkinson, D. J.; Burstein, D.; Edelman, R. R.: First-pass cardiac perfusion: Evaluation with ultrafast MR imaging. In: *Radiology* 174 (1990), no. 3 Pt 1, pp. 757–762

[Axel 1980] Axel, L.: Cerebral Blood Flow Determination by Rapid-Sequence Computed Tomography: Theoretical Analysis. In: *Radiology* 137 (1980), no. 3, pp. 679–686

[Baron 1999] Baron, J. C.: Mapping the ischaemic penumbra with PET: Implications for acute stroke treatment. In: *Cerebrovascular Diseases* 9 (1999), no. 4, pp. 193–201

[Bella and Sitek 2001] Bella, Edward V. R. D.; Sitek, Arkadiusz: Time Curve Analysis Techniques for Dynamic Contrast MRI Studies. In: *17th International Conference on Information Processing in Medical Imaging (IPMI)*, 2001, pp. 211–217

[Bendicks 2004] Bendicks, C.: *Visualisierungstechniken zur Exploration dynamischer Bilddaten*, Faculty of Computer Science, University of Magdeburg, Germany, Diplomarbeit, 2004

[Benninghoff 2004] Benninghoff, A.; Drenckhahn, D. (ed.); Zenker, W. (ed.): *Anatomie, Makroskopische Anatomie, Embryologie und Histologie des Menschen. Band 2: Herz-Kreislauf-System, lymphatisches System, endokrines System, Nervensystem, Sinnesorgane, Haut.* 16. Elsevier Urban & Fisher, 2004

[Bier et al. 1993] Bier, E.A.; Stone, M.; Pier, K.; Buxton, W.; DeRose, T.: Toolglass and Magic Lenses: The See-Through Interface. In: *ACM SIGGRAPH Computer Graphics*, 1993, pp. 73–80

[Blaas et al. 2007] BLAAS, Jorik ; BOTHA, Charl ; POST, Frits: Interactive visualization of multi-field data using dynamically linked physical and feature space views. In: *IEEE VGTC Symposium on Visualization (EuroVis)*, 2007, pp. 123–130

[Blekas et al. 2008] BLEKAS, Konstantinos ; NIKOU, Christophoros ; GALATSANOS, Nikolas P. ; TSEKOS, Nikolaos V.: A Regression Mixture Model with Spatial Constraints for Clustering Spatiotemporal Data. In: *International Journal on Artificial Intelligence Tools* 17 (2008), no. 5, pp. 1023–1041

[Bogaert et al. 2000] BOGAERT, J. ; DYMARKOWSK, S. ; BOSMANS, H.: Myocardial Perfusion. In: BOGAERT, J. (ed.) ; DUERINCKX, A.J. (ed.) ; RADEMAKERS, F.E. (ed.) ; BAERT, A.L. (ed.) ; SARTOR, K. (ed.) ; YOUKER, J.E. (ed.): *Magnetic Resonance of the Heart and the Great Vessels. Clinical Applications.* Springer, 2000, pp. 133–152

[Boxerman et al. 2006] BOXERMAN, J. L. ; SCHMAINDA, K. M. ; WEISSKOFF, R. M.: Relative cerebral blood volume maps corrected for contrast agent extravasation significantly correlate with glioma tumor grade, whereas uncorrected maps do not. In: *American Journal of Neuroradiology* 27 (2006), no. 4, pp. 859–867

[Breeuwer 2005] BREEUWER, M.: Quantification of artherosclerotic heart disease with cardiac MRI. In: *MEDICA MUNDI* 49 (2005), pp. 30–38

[Breeuwer et al. 2003] BREEUWER, M. ; PAETSCH, I. ; NAGEL, E. ; MUTHUPILLAI, R. ; FLAMM, S. ; PLEIN, S. ; RIDGWAY, J.: The detection of normal, ischemic and infarcted myocardial tissue using MRI. In: *International Congress on Computer Assisted Radiology and Surgery (CARS)* Bd. 1256, 2003, pp. 1153–1158

[Breeuwer 2002] BREEUWER, Marcel: Comprehensive visualization of first-pass myocardial perfusion: The uptake movie and the perfusogram. In: *International Society for Magnetic Resonance in Medicine (ISMRM)*, 2002

[Brix et al. 1997] BRIX, G. ; SCHREIBER, W. ; HOFFMANN, U. ; GÜCKEL, F. ; HAWIGHORST, H. ; KNOPP, M. V.: Methodological approaches to quantitative evaluation of microcirculation in tissues with dynamic Magnetic Resonance Tomography. In: *Radiologe* 37 (1997), no. 6, pp. 470–80

[Busse 2005] BUSSE, R.: Mikrozirkulation. In: SCHMIDT, R. F. (ed.) ; LANG, F. (ed.) ; THEWS, G. (ed.): *Physiologie des Menschen: Mit Pathophysiologie.* 29. Springer, 2005, pp. 619–624

[Cabral and Leedom 1993] CABRAL, Brian ; LEEDOM, Leith C.: Imaging vector fields using line integral convolution. In: *ACM SIGGRAPH Computer Graphics*, 1993, pp. 263–270

[Calamante et al. 2004] CALAMANTE, Fernando ; MØRUP, Morten ; HANSEN, Lars K.: Defining a local arterial input function for perfusion MRI using independent component analysis. In: *Magnetic Resonance Imaging* 52 (2004), no. 4, pp. 789–97

[Cerqueira et al. 2002] CERQUEIRA, Manuel D. ; WEISSMAN, Neil J. ; DILSIZIAN, Vasken ; JACOBS, Alice K. ; KAUL, Sanjiv ; LASKEY, Warren K. ; PENNELL, Dudley J. ; RUMBERGER, John A. ; RYAN, Thomas ; VERANI, Mario S.: Standardized myocardial segmentation and nomenclature for tomographic imaging of the heart: A statement for healthcare

professionals from the C ardiac Imaging Committee of the Council on Clinical Cardiology of the American Heart Association. In: *Circulation* 105 (2002), no. 4, pp. 539–42

[Chalil et al. 2007] Chalil, Shajil ; Stegemann, Berthold ; Muhyaldeen, Sarkaw ; Khadjooi, Kayvan ; Smith, Russell E A. ; Jordan, Paul J. ; Leyva, Francisco: Intraventricular dyssynchrony predicts mortality and morbidity after cardiac resynchronization therapy: a study using cardiovascular Magnetic Resonance tissue synchronization imaging. In: *Journal of the American College of Cardiology* 50 (2007), no. 3, pp. 243–252

[Chen et al. 2008] Chen, C. ; Härdle, W. ; Unwin, A. ; Chen, C. (ed.) ; Härdle, W. (ed.) ; Unwin, A. (ed.): *Handbook of Data Visualization*. 1. Springer, 2008 (Handbooks of Computational Statistics)

[Chen et al. 2006] Chen, W. ; Giger, M. L. ; Bick, U. ; Newstead, G. M.: Automatic Identification and Classification of Characteristic Kinetic Curves of Breast Lesions on DCE-MRI. In: *Medical Physics* 33 (2006), no. 8, pp. 2878–2887

[Choi et al. 2001] Choi, K.M. ; Kim, R.J. ; Gubernikoff, G. ; Vargas, J.D. ; Parker, M. ; Judd, R.M.: Transmural extent of acute myocardial infarction predicts long-term improvement in contractile function. In: *Circulation* 104 (2001), no. 10, pp. 1101–1107

[Choi et al. 2003] Choi, S.-M. ; Lee, D.-S. ; Yoo, S.-J. ; Kim, M.-H.: Interactive visualization of diagnostic data from cardiac images using 3D glyphs. In: *International Symposium on Medical Data Analysis (ISMDA)*, 2003, pp. 83–90

[Christensen et al. 2009] Christensen, Søren ; Mouridsen, Kim ; Wu, Ona ; Hjort, Niels ; Karstoft, Henrik ; Thomalla, Götz ; Röther, Joachim ; Fiehler, Jens ; Kucinski, Thomas ; Østergaard, Leif: Comparison of 10 perfusion MRI parameters in 97 sub-6-hour stroke patients using voxel-based receiver operating characteristics analysis. In: *Stroke* 40 (2009), no. 6, pp. 2055–2061

[Chua et al. 2006] Chua, S C. ; Ganatra, R H. ; Green, D J. ; Groves, A M.: Nuclear cardiology: Myocardial perfusion imaging with SPECT and PET. In: *Imaging* 18 (2006), no. 3, pp. 166–177

[Ciofolo et al. 2008] Ciofolo, Cybèle ; Fradkin, Maxim ; Mory, Benoît ; Hautvast, Gilion ; Breeuwer, Marcel: Automatic myocardium segmentation in late-enhancement MRI. In: *5th IEEE International Symposium on Biomedical Imaging (ISBI): From Nano to Macro*, 2008, pp. 225–228

[Cleveland and McGill 1984] Cleveland, W. S. ; McGill, R.: Graphical Perception: Theory, Experimentation, and Application to the Development of Graphical Methods. In: *Journal of the American Statistical Association* 79 (1984), no. 387, pp. 531–554

[Collins and Padhani 2004] Collins, David J. ; Padhani, Anwar R.: Dynamic Magnetic Resonance Imaging of tumor perfusion. Approaches and biomedical challenges. In: *IEEE Engineering in Medicine and Biology* 23 (2004), no. 5, pp. 65–83

[Coto et al. 2005] Coto, E. ; Grimm, S. ; Bruckner, S. ; Gröller, M. E. ; Kanitsar, A. ; Rodriguez, O.: MammoExplorer: An advanced CAD application for breast DCE-MRI. In: *Vision, Modeling, and Visualization (VMV)*, 2005, pp. 91–98

[Covarrubias et al. 2004] COVARRUBIAS, Diego J. ; ROSEN, Bruce R. ; LEV, Michael H.: Dynamic Magnetic Resonance perfusion imaging of brain tumors. In: *Oncologist* 9 (2004), no. 5, pp. 528–537

[Davies and Ho 1998] DAVIES, M.J. ; HO, S.Y.: Atherosclerosis: The Process. In: WEINBERG, R.W. (ed.) ; SNYDER, A. (ed.) ; MARINO-VASQUEZ, D. (ed.): *Atlas of Coronary Artery Disease*. Lippincott Williams & Wilkins, 1998, pp. 23–61

[Degani et al. 1997] DEGANI, H. ; GUSIS, V. ; WEINSTEIN, D. ; FIELDS, S. ; STRANO, S.: Mapping Pathophysiological Features of Breast Tumors by MRI at High Spatial Resolution. In: *Nature in Medicine* 3 (1997), pp. 780–782

[van Dijkman et al. 1989] DIJKMAN, P. R. ; DOORNBOS, J. ; ROOS, A. de ; LAARSE, A. van d. ; POSTEMA, S. ; MATHEIJSSEN, N. A. ; BRUSCHKE, A. V. ; VOORTHUISEN, A. E. ; CATS, V. M. ; WALL, E. E. d.: Improved detection of acute myocardial infarction by magnetic resonance imaging using gadolinium-DTPA. In: *The International Journal of Cardiovascular Imaging* 5 (1989), no. 1, pp. 1–8

[Doleisch et al. 2003] DOLEISCH, H. ; GASSER, M. ; HAUSER, H.: Interactive feature specification for focus+context visualization of complex simulation data. In: *Joint Eurographics/IEEE TCVG Symposium on Visualization (VisSym)*, 2003, pp. 239–248

[Doleisch and Hauser 2002] DOLEISCH, H. ; HAUSER, H.: Smooth Brushing For Focus+Context Visualization of Simulation Data in 3D. In: *Journal of Winter School of Computer Graphics* 10 (2002), no. 1, pp. 147–154

[Domin et al. 2007] DOMIN, Martin ; LANGNER, Sönke ; HOSTEN, Norbert ; LINSEN, Lars: Direct Glyph-based Visualization of Diffusion MR Data Using Deformed Spheres. In: *Visualization in Medicine and Life Sciences*, 2007, pp. 185–204

[Donnan et al. 2008] DONNAN, Geoffrey A. ; FISHER, Marc ; MACLEOD, Malcolm ; DAVIS, Stephen M.: Stroke. In: *Lancet* 371 (2008), no. 9624, pp. 1612–1623

[Dornheim et al. 2008] DORNHEIM, Lars ; HAHN, Peter ; OELTZE, Steffen ; TÖNNIES, Klaus-Dietz ; PREIM, Bernhard: Kontinuierliche Wanddickenbestimmung und Visualisierung des linken Herzventrikels. In: *Bildverarbeitung für die Medizin (BVM)*, 2008, pp. 333–337

[Ennis et al. 2005] ENNIS, Daniel B. ; KINDLMAN, Gordon ; RODRIGUEZ, Ignacio ; HELM, Patrick A. ; MCVEIGH, Elliot R.: Visualization of tensor fields using superquadric glyphs. In: *Magnetic Resonance in Medicine* 53 (2005), no. 1, pp. 169–176

[Farncombe et al. 1999] FARNCOMBE, T. ; CELLER, A. ; NOLL, D. ; MAEGHT, J. ; HARROP, R.: Dynamic SPECT imaging using a single camera rotation (dSPECT). In: *IEEE Transactions on Nuclear Science* 46 (1999), no. 4, pp. 1055–1061

[Finn et al. 2006] FINN, J. P. ; NAEL, Kambiz ; DESHPANDE, Vibhas ; RATIB, Osman ; LAUB, Gerhard: Cardiac MR imaging: State of the technology. In: *Radiology* 241 (2006), no. 2, pp. 338–354

[Fritz-Hansen et al. 2008] FRITZ-HANSEN, Thomas ; HOVE, Jens D. ; KOFOED, Klaus F. ; KELBAEK, Henning ; LARSSON, Henrik B W.: Quantification of MRI measured myocardial perfusion reserve in healthy humans: A comparison with positron emission tomography. In: *Journal of Magnetic Resonance Imaging* 27 (2008), no. 4, pp. 818–824

[Furnas 1986] Furnas, G.: Generalized Fisheye Views. In: *ACM CHI '86 Conf. on Human Factors in Computing Systems*, 1986, pp. 16–23

[Fuster et al. 2004] Fuster, V.; Alexander, R.W.; O'Rourke, R.A.; Roberts, R.; King, S.B.; Nash, I.S.; Prystowsky, E.N.; Cooke, D.B. (ed.); Strauss, M. (ed.); Loeb, M. (ed.); Sheinis, L.A. (ed.): *Hurst's The Heart*. 11. McGraw-Hill Professional, 2004

[Gerber et al. 2008] Gerber, Bernhard L.; Raman, Subha V.; Nayak, Krishna; Epstein, Frederick H.; Ferreira, Pedro; Axel, Leon; Kraitchman, Dara L.: Myocardial first-pass perfusion cardiovascular Magnetic Resonance: History, theory, and current state of the art. In: *Journal of Cardiovascular Magnetic Resonance* 10 (2008), no. 1, pp. 18

[Glaßer et al. 2009] Glasser, Sylvia; Schäfer, Sebastian; Oeltze, Steffen; Preim, Uta; Tönnies, Klaus-Dietz; Preim, Bernhard: A visual analytics approach to diagnosis of breast DCE-MRI data. In: *Vision, Modeling, and Visualization (VMV)*, 2009, pp. 351–362

[Glover and Pelc 1988] Glover, G.H.; Pelc, N.J.: A rapid-gated cine MRI technique. In: Kressel, H.Y. (ed.): *Magnetic resonance annual*. Raven Press, 1988, pp. 288–333

[Go et al. 1990] Go, R. T.; Marwick, T. H.; MacIntyre, W. J.; Saha, G. B.; Neumann, D. R.; Underwood, D. A.; Simpfendorfer, C. C.: A prospective comparison of rubidium-82 PET and thallium-201 SPECT myocardial perfusion imaging utilizing a single dipyridamole stress in the diagnosis of coronary artery disease. In: *Journal of Nuclear Medicine* 31 (1990), no. 12, pp. 1899–1905

[Gomez 1993] Gomez, C.: Time is brain. In: *Journal of Stroke and Cerebrovascular Diseases* 3 (1993), pp. 1–2

[Gooch et al. 1999] Gooch, Bruce; Sloan, Peter-Pike J.; Gooch, Amy; Shirley, Peter; Riesenfeld, Richard: Interactive technical illustration. In: *Symposium on Interactive 3D graphics (I3D)*, 1999, pp. 31–38

[Grandin et al. 2002] Grandin, Cécile B.; Duprez, Thierry P.; Smith, Anne M.; Oppenheim, Catherine; Peeters, André; Robert, Annie R.; Cosnard, Guy: Which MR-derived perfusion parameters are the best predictors of infarct growth in hyperacute stroke? Comparative study between relative and quantitative measurements. In: *Radiology* 223 (2002), no. 2, pp. 361–70

[Gray 1918] Gray, H.; Lewis, W.H. (ed.): *Anatomy of the Human Body*. 20. Philadelphia: Lea & Febiger 1918, Bartleby.com: 2000, 1918

[Grebe 2005] Grebe, O.: Myokardiale Ischämiediagnostik. In: Hombach, V. (ed.); Grebe, O. (ed.); Botnar, R.M. (ed.): *Kardiovaskuläre Magnetresonanztomographie: Grundlagen-Technik-klinische Anwendung*. Schattauer, 2005, pp. 351–373

[Gresh et al. 2000] Gresh, Donna L.; Rogowitz, Bernice E.; Winslow, R. L.; Scollan, D. F.; Yung, C. K.: WEAVE: A System for Visually Linking 3-D and Statistical Visualizations, Applied to Cardiac Simulation and Measurement Data. In: *IEEE Visualization (VIS)*, 2000, pp. 489–492

[Griswold et al. 2002] GRISWOLD, Mark A.; JAKOB, Peter M.; HEIDEMANN, Robin M.; NITTKA, Mathias; JELLUS, Vladimir; WANG, Jianmin; KIEFER, Berthold ; HAASE, Axel: Generalized autocalibrating partially parallel acquisitions (GRAPPA). In: *Magnetic Resonance in Medicine* 47 (2002), no. 6, pp. 1202–1210

[Grzesik et al. 2000] GRZESIK, Alexander; BERNARDING, Johannes; BRAUN, Juergen; KOENNECKE, Hans-Christian; WOLF, Karl J. ; TOLXDORFF, Thomas: Characterization of Stroke Lesions Using a Histogram-Based Data Analysis Including Diffusion- and Perfusion-Weighted Imaging. In: *SPIE Medical Imaging: Physiology and Function from Multidimensional Images* Bd. 3978, 2000, pp. 23–31

[Hahn and Peitgen 2000] HAHN, Horst K.; PEITGEN, Heinz-Otto: The skull stripping problem in MRI solved by a single 3D watershed transform. In: *Medical Image Computing and Computer-Assisted Intervention (MICCAI)* Bd. 1935, 2000, pp. 134–143

[Hansen et al. 2007] HANSEN, M. S.; ÓLAFSDÓTTIR, H.; SJÖSTRAND, K.; LARSSON, H. B.; STEGMANN, M. B. ; LARSEN, R.: Ischemic Segment Detection using the Support Vector Domain Description. In: *International Symposium on Medical Imaging*, 2007

[Haraldsson et al. 2008] HARALDSSON, Henrik; WIGSTRÖM, Lars; LUNDBERG, Magnus; BOLGER, Ann F.; ENGVALL, Jan; EBBERS, Tino ; KVITTING, John-Peder E.: Improved estimation and visualization of two-dimensional myocardial strain rate using MR velocity mapping. In: *Journal of Magnetic Resonance Imaging* 28 (2008), no. 3, pp. 604–611

[Hauser 2005] HAUSER, H.: Generalizing Focus+Context Visualization. In: BONNEAU, G.-P. (ed.); ERTL, T. (ed.) ; NIELSON, G.M. (ed.): *Scientific Visualization: The Visual Extraction of Knowledge from Data.* Springer, 2005 (Mathematics and Visualization), pp. 305–327

[Hautvast et al. 2006] HAUTVAST, G.; LOBREGT, S.; BREEUWER, M. ; GERRITSEN, F.: Automatic contour propagation in cine cardiac Magnetic Resonance images. In: *IEEE Transactions on Medical Imaging* 25 (2006), no. 11, pp. 1472–1482

[Healey and Enns 1999] HEALEY, Christopher G.; ENNS, James T.: Large datasets at a glance: Combining textures and colors in scientific visualization. In: *IEEE Transactions on Visualization and Computer Graphics* 5 (1999), no. 2, pp. 145–167

[Heiberg et al. 2005] HEIBERG, E.; WIGSTROM, L.; CARLSSON, M.; BOLGER, A.F. ; KARLSSON, M.: Time resolved three-dimensional automated segmentation of the left ventricle. In: *Computers in Cardiology*, 2005, pp. 599–602

[Hellwig et al. 2002] HELLWIG, Gesine; BRIX, Gunnar; GRIEBEL, Juergen; LUCHT, Robert; DELORME, Stefan; SIEBERT, Markus ; ENGLMEIER, Karl-Hans: Dynamic MR mammography: Three-dimensional real-time visualization of contrast enhancement in virtual reality. In: *Academic Radiology* 9 (2002), no. 11, pp. 1255–1263

[Hennemuth et al. 2007] HENNEMUTH, A.; BEHRENS, S.; KUEHNEL, C.; OELTZE, S.; KONRAD, O. ; PEITGEN, H.-O.: Novel methods for parameter based analysis of myocardial tissue in MR-images. In: *SPIE Conference on Medical Image Computing* Bd. 6511, 2007, pp. 65111N–1–65111N–9

[Hennemuth et al. 2005] Hennemuth, A. ; Bock, S. ; Boskamp, T. ; Fritz, D. ; Kühnel, C. ; Rinck, D. ; Scheuering, M. ; Peitgen, H. O.: One-click coronary tree segmentation in CT angiographic images. In: *International Congress on Computer Assisted Radiology and Surgery (CARS)*, 2005, pp. 317–21

[Hennemuth et al. 2008a] Hennemuth, Anja ; Mahnken, Andreas ; Kühnel, Caroline ; Oeltze, Steffen ; Peitgen, Heinz-Otto: CT late enhancement segmentation for the combined analysis of coronary arteries and myocardial viability. In: *Eurographics Workshop on Visual Computing for Biology and Medicine (EG VCBM)*, 2008, pp. 1–10

[Hennemuth et al. 2008b] Hennemuth, Anja ; Seeger, Achim ; Friman, Ola ; Miller, Stefan ; Peitgen, Heinz-Otto: Automatic detection and quantification of non-viable myocardium in late enhancement images. In: *International Society for Magnetic Resonance in Medicine (ISMRM)*, 2008

[Hennemuth et al. 2008c] Hennemuth, Anja ; Seeger, Achim ; Friman, Ola ; Miller, Stephan ; Klumpp, Bernhard ; Oeltze, Steffen ; Peitgen, Heinz-Otto: A comprehensive approach to the analysis of contrast enhanced cardiac MR images. In: *IEEE Transactions on Medical Imaging* 27(11) (2008), no. 11, pp. 1592–1610

[Heywang-Köbrunner et al. 1997] Heywang-Köbrunner, S.H. ; Viehweg, P. ; Heinig, A. ; Kuchler, C.: Contrast-enhanced MRI of the breast: Accuracy, value, controversies, solutions. In: *European Journal of Radiology* 24 (1997), pp. 94–108

[Hjort et al. 2005] Hjort, N. ; Butcher, K. ; Davis, S. M. ; Kidwell, C. S. ; Koroshetz, W. J. ; Röther, J. ; Schellinger, P. D. ; Warach, S. ; Østergaard, L. ; Investigators, U. C. L. A. T.: Magnetic resonance imaging criteria for thrombolysis in acute cerebral infarct. In: *Stroke* 36 (2005), no. 2, pp. 388–397

[Hoehne et al. 1981] Hoehne, K.H. ; Obermoeller, U. ; Boehm, M.: X-ray functional imaging - evaluation of the properties of different parameters. In: *Conference on Digital Radiography*, 1981, pp. 224–228

[Hunold 2007] Hunold, P.: Late Enhancement. In: Thelen, M. (ed.) ; Erbel, R. (ed.) ; Kreitner, K.-F. (ed.) ; Barkhausen, J. (ed.): *Bildgebende Kardiodiagnostik mit MRT, CT, Echokardiographie und anderen Verfahren.* Thieme, 2007, pp. 120–125

[Hunold et al. 2006] Hunold, P. ; Schlosser, T. ; Barkhausen, J.: Magnetic Resonance cardiac perfusion imaging: A clinical perspective. In: *European Radiology* 16 (2006), no. 8, pp. 1779–1788

[Iida et al. 1988] Iida, H. ; Kanno, I. ; Takahashi, A. ; Miura, S. ; Murakami, M. ; Takahashi, K. ; Ono, Y. ; Shishido, F. ; Inugami, A. ; Tomura, N.: Measurement of absolute myocardial blood flow with H215O and dynamic positron-emission tomography: Strategy for quantification in relation to the partial-volume effect. In: *Circulation* 78 (1988), no. 1, pp. 104–115

[Janoos et al. 2009] Janoos, F. ; Nouanesengsy, B. ; Machiraju, R. ; Shen, H.W. ; Sammet, S. ; Knopp, M. ; Mórocz, I.Á.: Visual analysis of brain activity from fMRI data. In: *Computer Graphics Forum* 28 (2009), no. 3, pp. 903–910(8)

[Jianu et al. 2009] JIANU, Radu ; DEMIRALP, Cagatay ; LAIDLAW, David: Exploring 3D DTI fiber tracts with linked 2D representations. In: *IEEE Transactions on Visualization and Computer Graphics* 15 (2009), no. 6, pp. 1449–1456

[Jolliffe 2002] JOLLIFFE, I. T.: *Principal Component Analysis*. 2nd. Springer, 2002 (Series in Statistics)

[Julész and Bergen 1983] JULÉSZ, B. ; BERGEN, J. R.: Textons, the fundamental elements in preattentive vision and the perception of textures. In: *Bell System Technical Journal* 62 (1983), no. 6, pp. 1619–1645

[Kane et al. 2007] KANE, Ingrid ; CARPENTER, Trevor ; CHAPPELL, Francesca ; RIVERS, Carly ; ARMITAGE, Paul ; SANDERCOCK, Peter ; WARDLAW, Joanna: Comparison of 10 different magnetic resonance perfusion imaging processing methods in acute ischemic stroke: Effect on lesion size, proportion of patients with diffusion/perfusion mismatch, clinical scores, and radiologic outcomes. In: *Stroke* 38 (2007), no. 12, pp. 3158–64

[Kao et al. 2008] KAO, Yi-Hsuan ; TENG, Michael Mu-Huo ; LIU, Kuo-Ching ; LAM, Io-Pong ; LIN, Yu-Ching: Hemodynamic segmentation of MR perfusion images in patients with unilateral carotid stenosis using independent component analysis. In: *Journal of Magnetic Resonance Imaging* 28 (2008), no. 5, pp. 1125–32

[Keefe et al. 2009] KEEFE, Daniel ; EWERT, Marcus ; RIBARSKY, William ; CHANG, Remco: Interactive coordinated multiple-view visualization of biomechanical motion data. In: *IEEE Transactions on Visualization and Computer Graphics* 15 (2009), no. 6, pp. 1383–1390

[Kholmovski et al. 2004] KHOLMOVSKI, E.G. ; VEMURI, P. ; DI BELLA, E.V.: Image reconstruction scheme for dynamic perfusion myocardium MRI study. In: *International Society for Magnetic Resonance in Medicine (ISMRM)*, 2004

[Kim et al. 1999] KIM, R. J. ; FIENO, D. S. ; PARRISH, T. B. ; HARRIS, K. ; CHEN, E. L. ; SIMONETTI, O. ; BUNDY, J. ; FINN, J. P. ; KLOCKE, F. J. ; JUDD, R. M.: Relationship of MRI delayed contrast enhancement to irreversible injury, infarct age, and contractile function. In: *Circulation* 100 (1999), no. 19, pp. 1992–2002

[Kindlmann 2004] KINDLMANN, Gordon: Superquadric tensor glyphs. In: *Joint Eurographics/IEEE TCVG Symposium on Visualization (VisSym)*, 2004, pp. 147–154

[Kindlmann and Westin 2006] KINDLMANN, Gordon ; WESTIN, Carl-Fredrik: Diffusion tensor visualization with glyph packing. In: *IEEE Transactions on Visualization and Computer Graphics* 12 (2006), no. 5, pp. 1329–1335

[Kitsiou et al. 1999] KITSIOU, A. N. ; BACHARACH, S. L. ; BARTLETT, M. L. ; SRINIVASAN, G. ; SUMMERS, R. M. ; QUYYUMI, A. A. ; DILSIZIAN, V.: 13N-ammonia myocardial blood flow and uptake: Relation to functional outcome of asynergic regions after revascularization. In: *Journal of the American College of Cardiology* 33 (1999), no. 3, pp. 678–686

[Klabunde 2005] KLABUNDE, R.E.: *Cardiovascular Physiology Concepts*. Lippincott Williams & Wilkins, 2005

[Klocke et al. 2001] Klocke, Francis J. ; Simonetti, Orlando P. ; Judd, Robert M. ; Kim, Raymond J. ; Harris, Kathleen R. ; Hedjbeli, Sascha ; Fieno, David S. ; Miller, Stephan ; Chen, Vicky ; Parker, Michele A.: Limits of detection of regional differences in vasodilated flow in viable myocardium by first-pass Magnetic Resonance perfusion imaging. In: *Circulation* 104 (2001), no. 20, pp. 2412–2416

[Kochs et al. 2005] Kochs, M. ; Merkle, N. ; Hombach, V.: Kardiale MRT-Anatomie und -Funktion. In: Hombach, V. (ed.) ; Grebe, O. (ed.) ; Botnar, R.M. (ed.): *Kardiovaskuläre Magnetresonanztomographie: Grundlagen-Technik-klinische Anwendung*. Schattauer, 2005, pp. 131–150

[Kohle et al. 2002] Kohle, S. ; Preim, B. ; Wiener, J. ; Peitgen, H.-O.: Exploration of time-varying data for medical diagnosis. In: *Vision, Modeling, and Visualization (VMV)*, 2002, pp. 31–8

[Kolominsky-Rabas 2004] Kolominsky-Rabas, Peter: *Anhaltszahlen zum Schlaganfall aus dem bevölkerungs-basierten Erlanger Schlaganfall Register im Rahmen der Gesundheitsberichterstattung (GBE) des Bundes*. 2004

[Kosior and Frayne 2007] Kosior, Jayme C. ; Frayne, Richard: PerfTool: a software platform for investigating bolus-tracking perfusion imaging quantification strategies. In: *Journal of Magnetic Resonance Imaging* 25 (2007), no. 3, pp. 653–659

[Kosior et al. 2007] Kosior, Robert K. ; Kosior, Jayme C. ; Frayne, Richard: Improved dynamic susceptibility contrast (DSC)-MR perfusion estimates by motion correction. In: *Journal of Magnetic Resonance Imaging* 26 (2007), no. 4, pp. 1167–1172

[Kramer et al. 2008] Kramer, Christopher M. ; Barkhausen, Jorg ; Flamm, Scott D. ; Kim, Raymond J. ; Nagel, Eike ; Standardized Protocols, Society for Cardiovascular Magnetic Resonance Board of Trustees Task Force o.: Standardized cardiovascular magnetic resonance imaging (CMR) protocols, society for cardiovascular magnetic resonance: Board of trustees task force on standardized protocols. In: *Journal of Cardiovascular Magnetic Resonance* 10 (2008), no. 1, pp. 35

[Kreitner and Horstick 2007] Kreitner, K.-F. ; Horstick, G.: Postoperative und postinterventionelle Bildgebung. In: Thelen, M. (ed.) ; Erbel, R. (ed.) ; Kreitner, K.-F. (ed.) ; Barkhausen, J. (ed.): *Bildgebende Kardiodiagnostik mit MRT, CT, Echokardiographie und anderen Verfahren*. Thieme, 2007, pp. 209–219

[Kuhl et al. 1999] Kuhl, C. K. ; Mielcareck, P. ; Klaschik, S. ; Leutner, C. ; Wardelmann, E. ; Gieseke, J. ; Schild, H. H.: Dynamic breast MR imaging: Are signal intensity time course data useful for differential diagnosis of enhancing lesions? In: *Radiology* 211 (1999), no. 1, pp. 101–110

[Kühnel et al. 2008] Kühnel, C. ; Hennemuth, A. ; Oeltze, S. ; Boskamp, T. ; Peitgen, H.-O.: Enhanced cardio vascular image analysis by combined representation of results from dynamic MRI and anatomic CTA. In: *SPIE Conference on Medical Image Computing*, 2008

[Kühnel et al. 2006] Kühnel, Caroline ; Hennemuth, Anja ; Bock, Susanne ; Oeltze, Steffen ; Boskamp, Tobias ; Krass, Stefan ; Preim, Bernhard ; Peitgen, Heinz-Otto:

New software assistants for cardiovascular diagnosis. In: *GI-Workshop - Softwareassistenten - Computerunterstützung für die medizinische Diagnose und Therapieplanung* Bd. Band 1, 2006, pp. 491–498

[Kuß 2006] KUSS, Anja: *Techniken zur Exploration myokardialer Perfusionsdaten*, Faculty of Computer Science, University of Magdeburg, Germany, Diplomarbeit, 2006

[Laidlaw et al. 1998] LAIDLAW, D. H.; AHRENS, E. T.; KREMERS, D.; AVALOS, M. J.; JACOBS, R. E. ; READHEAD, C.: Visualizing diffusion tensor images of the mouse spinal cord. In: *Visualization*, 1998, pp. 127–134

[Lardo et al. 2005] LARDO, Albert C.; ABRAHAM, Theodore P. ; KASS, David A.: Magnetic Resonance imaging assessment of ventricular dyssynchrony: current and emerging concepts. In: *Journal of the American College of Cardiology* 46 (2005), no. 12, pp. 2223–2228

[Latchaw et al. 2009] LATCHAW, Richard E.; ALBERTS, Mark J.; LEV, Michael H.; CONNORS, John J.; HARBAUGH, Robert E.; HIGASHIDA, Randall T.; HOBSON, Robert; KIDWELL, Chelsea S.; KOROSHETZ, Walter J.; MATHEWS, Vincent; VILLABLANCA, Pablo; WARACH, Steven ; WALTERS, Beverly: Recommendations for imaging of acute ischemic stroke. A scientific statement from the American Heart Association. In: *Stroke* (2009)

[Lee et al. 2005] LEE, Jae S.; LEE, Dong S.; AHN, Ji Y.; YEO, Jeong S.; CHEON, Gi J.; KIM, Seok-Ki; PARK, Kwang S.; CHUNG, June-Key ; LEE, Myung C.: Generation of parametric image of regional myocardial blood flow using H(2)(15)O dynamic PET and a linear least-squares method. In: *Journal of Nuclear Medicine* 46 (2005), no. 10, pp. 1687–1695

[Leutert and Schmidt 2000] LEUTERT, G.; SCHMIDT, W.: *Systematische und funktionelle Anatomie für medizinische Assistenzberufe*. 9. Elsevier Urban & Fischer, 2000

[Levkowitz et al. 1990] LEVKOWITZ, H.; SELTZER, S.E.; PICKETT, R.M. ; D'ORSI, C.J.: Color integrated displays of multimodality tomographic images. In: *Radiology* Bd. 177, 1990, pp. 248

[Levkowitz 1991] LEVKOWITZ, Haim: Color Icons: Merging color and texture perception for integrated visualization of multiple parameters. In: *IEEE Visualization (VIS)*, 1991, pp. 164–170

[Levkowitz 1997] LEVKOWITZ, Haim: *Color theory and modeling for computer graphics, visualization, and multimedia applications*. 1. Kluwer Academic Publishers, 1997 (Engineering and Computer Science)

[Ley and Kreitner 2007] LEY, S.; KREITNER, K.-F.: Funktion. In: THELEN, M. (ed.); ERBEL, R. (ed.); KREITNER, K.-F. (ed.) ; BARKHAUSEN, J. (ed.): *Bildgebende Kardiodiagnostik mit MRT, CT, Echokardiographie und anderen Verfahren*. Thieme, 2007, pp. 105–114

[Lin et al. 2006] LIN, G. S.; HINES, Horace H.; GRANT, Genine; TAYLOR, Kimberly ; RYALS, Carl: Automated quantification of myocardial ischemia and wall motion defects by use of cardiac SPECT polar mapping and 4-dimensional surface rendering. In: *Journal of Nuclear Medicine Technology* 34 (2006), no. 1, pp. 3–17

[Lloyd-Jones et al. 2009] Lloyd-Jones, Donald ; Adams, Robert ; Carnethon, Mercedes ; De Simone, Giovanni ; Ferguson, T. B. ; Flegal, Katherine ; Ford, Earl ; Furie, Karen ; Go, Alan ; Greenlund, Kurt ; Haase, Nancy ; Hailpern, Susan ; Ho, Michael ; Howard, Virginia ; Kissela, Brett ; Kittner, Steven ; Lackland, Daniel ; Lisabeth, Lynda ; Marelli, Ariane ; McDermott, Mary ; Meigs, James ; Mozaffarian, Dariush ; Nichol, Graham ; O'Donnell, Christopher ; Roger, Veronique ; Rosamond, Wayne ; Sacco, Ralph ; Sorlie, Paul ; Stafford, Randall ; Steinberger, Julia ; Thom, Thomas ; Wasserthiel-Smoller, Sylvia ; Wong, Nathan ; Wylie-Rosett, Judith ; Hong, Yuling: Heart disease and stroke statistics–2009 update: A report from the American Heart Association statistics committee and stroke statistics subcommittee. In: *Circulation* 119 (2009), no. 3, pp. e21–181

[Lombardi et al. 1999] Lombardi, M. ; Jones, R. A. ; Westby, J. ; Torheim, G. ; Southon, T. E. ; Haraldseth, O. ; Michelassi, C. ; Kvaerness, J. ; Rinck, P. A. ; L'Abbate, A.: Use of the mean transit time of an intravascular contrast agent as an exchange-insensitive index of myocardial perfusion. In: *Journal of Magnetic Resonance Imaging* 9 (1999), no. 3, pp. 402–408

[Lorensen and Cline 1987] Lorensen, William E. ; Cline, Harvey E.: Marching cubes: A high resolution 3D surface construction algorithm. In: *ACM SIGGRAPH Computer Graphics* 21 (1987), no. 4, pp. 163–169

[Lysaker et al. 2003] Lysaker, Marius ; Lundervold, Arvid ; Tai, Xue-Cheng: Noise removal using fourth-order partial differential equation with applications to medical Magnetic Resonance images in space and time. In: *IEEE Transactions on Image Processing* 12 (2003), no. 12, pp. 1579–1590

[Malyszczyk 2007] Malyszczyk, Arvid: - *DynaDataExplorer - Ein System zur angepassten, visuellen Analyse von Perfusionsdaten*, Faculty of Computer Science, University of Magdeburg, Magdeburg, Diplomarbeit, 2007

[Marsan et al. 2009] Marsan, Nina A. ; Westenberg, Jos J M. ; Ypenburg, Claudia ; Bommel, Rutger J. ; Roes, Stijntje ; Delgado, Victoria ; Tops, Laurens F. ; Geest, Rob J. d. ; Boersma, Eric ; Roos, Albert de ; Schalij, Martin J. ; Bax, Jeroen J.: Magnetic resonance imaging and response to cardiac resynchronization therapy: relative merits of left ventricular dyssynchrony and scar tissue. In: *European Heart Journal* 30 (2009), no. 19, pp. 2360–2367

[Merhige et al. 2007] Merhige, Michael E. ; Breen, William J. ; Shelton, Victoria ; Houston, Teresa ; D'Arcy, Brian J. ; Perna, Anthony F.: Impact of myocardial perfusion imaging with PET and (82)Rb on downstream invasive procedure utilization, costs, and outcomes in coronary disease management. In: *Journal of Nuclear Medicine* 48 (2007), no. 7, pp. 1069–1076

[Meyer-Spradow et al. 2008] Meyer-Spradow, Jennis ; Stegger, Lars ; Döring, Christian ; Ropinski, Timo ; Hinrichs, Klaus: Glyph-based SPECT visualization for the diagnosis of coronary artery disease. In: *IEEE Transactions on Visualization and Computer Graphics* 14 (2008), no. 6, pp. 1499–1506

[Mühler et al. 2006] MÜHLER, K.; BADE, R.; PREIM, B.: Skriptbasierte Animationen für die Operationsplanung und Ausbildung. In: *Bildverarbeitung für die Medizin (BVM)*, 2006, pp. 296–300

[Michoux et al. 2006] MICHOUX, N.; VALLÉE, J.; PECHÈRE-BERTSCHI, A.; MONTET, X.; BUEHLER, L.; VAN BEERS, B.: Analysis of contrast-enhanced MR images to assess renal function. In: *MAGMA* 19 (2006), no. 4, pp. 167–179(13)

[Milles et al. 2008] MILLES, J.; GEEST, R.J. van d.; JEROSCH-HEROLD, M.; REIBER, J.; LELIEVELDT, B.: Fully automated motion correction in first-pass myocardial perfusion MR image sequences. In: *IEEE Transactions on Medical Imaging* 27 (2008), no. 11, pp. 1611–1621

[Mäkelä et al. 2002] MÄKELÄ, Timo; CLARYSSE, Patrick; SIPILÄ, Outi; PAUNA, Nicoleta; PHAM, Quoc C.; KATILA, Toivo; MAGNIN, Isabelle E.: A review of cardiac image registration methods. In: *IEEE Transactions on Medical Imaging* 21 (2002), no. 9, pp. 1011–1021

[Mlejnek et al. 2005] MLEJNEK, Matej; ERMES, Pierre; VILANOVA, Anna; RIJT, Rob van d.; BOSCH, Harrie van d.; GERRITSEN, Frans; GRÖLLER, Meister E.: Profile Flags: A novel metaphor for probing of T2 maps. In: *IEEE Visualization (VIS)*, 2005, pp. 599–606

[Mlejnek et al. 2006] MLEJNEK, Matej; ERMES, Pierre; VILANOVA, Anna; RIJT, Rob van d.; BOSCH, Harrie van d.; GRÖLLER, Meister E.; GERRITSEN, Frans: Application-oriented extensions of profile flags. In: *IEEE VGTC Symposium on Visualization (EuroVis)*, 2006, pp. 339–346

[Mollet et al. 2005] MOLLET, Nico R.; CADEMARTIRI, Filippo; MIEGHEM, Carlos A G.; RUNZA, Giuseppe; MCFADDEN, Eugène P.; BAKS, Timo; SERRUYS, Patrick W.; KRESTIN, Gabriel P.; FEYTER, Pim J.: High-resolution spiral computed tomography coronary angiography in patients referred for diagnostic conventional coronary angiography. In: *Circulation* 112 (2005), no. 15, pp. 2318–2323

[Mouridsen et al. 2006] MOURIDSEN, Kim; CHRISTENSEN, Søren; GYLDENSTED, Louise; OSTERGAARD, Leif: Automatic selection of arterial input function using cluster analysis. In: *Magnetic Resonance in Medicine* 55 (2006), no. 3, pp. 524–31

[Muigg et al. 2008] MUIGG, Philipp; KEHRER, Johannes; OELTZE, Steffen; PIRINGER, Harald; DOLEISCH, Helmut; PREIM, Bernhard; HAUSER, Helwig: A four-level focus+context approach to interactive visual analysis of temporal features in large scientific data. In: *Computer Graphics Forum* 27 (2008), no. 3, pp. 775–782

[Müller et al. 2006] MÜLLER, Wolfgang; NOCKE, Thomas; SCHUMANN, Heidrun: Enhancing the visualization process with principal component analysis to support the exploration of trends. In: *Asia-Pacific Symposium on Information Visualisation*, 2006, pp. 121–130

[Nagel et al. 2003] NAGEL, Eike; KLEIN, Christoph; PAETSCH, Ingo; HETTWER, Sabine; SCHNACKENBURG, Bernhard; WEGSCHEIDER, Karl; FLECK, Eckart: Magnetic resonance perfusion measurements for the noninvasive detection of coronary artery disease. In: *Circulation* 108 (2003), no. 4, pp. 432–7

[Nagy and Sanchez 1990] Nagy, A. L.; Sanchez, R. R.: Critical color differences determined with a visual search task. In: *Journal of the Optical Society of America* A7 (1990), no. 7, pp. 1209–1217

[Nakajo et al. 2005] Nakajo, Hidenobu; Kumita, Shin-Ichiro; Cho, Keiichi ; Kumazaki, Tatsuo: Three-dimensional registration of myocardial perfusion SPECT and CT coronary angiography. In: *Annals of Nuclear Medicine* 19 (2005), no. 3, pp. 207–15

[Napel et al. 1993] Napel, S.; Rubin, G.D. ; Jeffrey, R.B.: STS-MIP: A new reconstruction technique for CT of the chest. In: *Journal of Computer Assisted Tomography* 17 (1993), no. 5, pp. 832–838

[Nattkemper and Wismüller 2005] Nattkemper, Tim W.; Wismüller, Axel: Tumor feature visualization with unsupervised learning. In: *Medical Image Analysis* 9 (2005), no. 4, pp. 344–51

[Nelder and Mead 1965] Nelder, J.A.; Mead, R.: A simplex method for function minimization. In: *Computer Journal* 7 (1965), no. 4, pp. 308–313

[Nesto and Kowalchuk 1987] Nesto, R. W.; Kowalchuk, G. J.: The ischemic cascade: temporal sequence of hemodynamic, electrocardiographic and symptomatic expressions of ischemia. In: *American Journal of Cardiology* 59 (1987), no. 7, pp. 23C–30C

[Netter 1990] Netter, F.H. ; Stauch, M. (ed.): *Farbatlanten der Medizin, Band 1: Herz.* 3. Georg Thieme Verlag, 1990

[Noble et al. 2004] Noble, Nicholas M.; Hill, Derek L.; Breeuwer, Marcel ; Razavi, Reza: The automatic identification of hibernating myocardium. In: *Medical Image Computing and Computer-Assisted Intervention (MICCAI)* Bd. 3217, 2004, pp. 890–898

[Nowinski et al. 2008] Nowinski, Wieslaw L.; Qian, Guoyu; Prakash, K. N.; Volkau, Ihar; Leong, Wing K.; Huang, Su; Ananthasubramaniam, Anand; Liu, Jimin; Ng, Ting T. ; Gupta, Varsha: Stroke Suite: Cad systems for acute ischemic stroke, hemorrhagic stroke, and stroke in ER. In: *Medical Imaging and Informatics*, 2008, pp. 377–386

[Oeltze et al. 2005] Oeltze, S.; Bendicks, C.; Behrens, S. ; Preim, B.: Multiparametervisualisierung zur Exploration dynamischer Bilddaten. In: *Bildverarbeitung für die Medizin (BVM)*, 2005, pp. 317–21

[Oeltze et al. 2007] Oeltze, Steffen; Doleisch, Helmut; Hauser, Helwig; Muigg, Philipp ; Preim, Bernhard: Interactive visual analysis of perfusion data. In: *IEEE Transactions on Visualization and Computer Graphics* 13 (2007), no. 6, pp. 1392–1399

[Oeltze et al. 2006] Oeltze, Steffen; Grothues, Frank; Hennemuth, Anja; Kuss, Anja ; Preim, Bernhard: Integrated visualization of morphologic and perfusion data for the analysis of coronary artery disease. In: *IEEE VGTC Symposium on Visualization (EuroVis)*, 2006, pp. 131–138

[Oeltze et al. 2009] Oeltze, Steffen; Hauser, Helwig; Rorvik, Jarle; Lundervold, Arvid ; Preim, Bernhard: Visual analysis of cerebral perfusion data – Four interactive approaches and a comparison. In: *International Symposium on Image and Signal Processing and Analysis (ISPA)*, 2009, pp. 588–595

[Oeltze et al. 2008a] OELTZE, Steffen ; HENNEMUTH, Anja ; GLASSER, Sylvia ; KÜHNEL, Caroline ; PREIM, Bernhard: Glyph-based visualization of myocardial perfusion data and enhancement with contractility and viability information. In: *Eurographics Workshop on Visual Computing for Biology and Medicine (EG VCBM)*, 2008, pp. 11–20

[Oeltze et al. 2008b] OELTZE, Steffen ; MALYSZCZYK, Arvid ; PREIM, Bernhard: Intuitive mapping of perfusion parameters to glyph shape. In: *Bildverarbeitung für die Medizin (BVM)*, 2008, pp. 262–266

[Oeltze and Preim 2005] OELTZE, Steffen ; PREIM, Bernhard: Visualization of vasculature with convolution surfaces: Method, validation and evaluation. In: *IEEE Transactions on Medical Imaging* 24 (2005), no. 4, pp. 540–548

[Olivot et al. 2009] OLIVOT, Jean-Marc ; MLYNASH, Michael ; THIJS, Vincent N. ; KEMP, Stephanie ; LANSBERG, Maarten G. ; WECHSLER, Lawrence ; BAMMER, Roland ; MARKS, Michael P. ; ALBERS, Gregory W.: Optimal Tmax threshold for predicting penumbral tissue in acute stroke. In: *Stroke* 40 (2009), no. 2, pp. 469–475

[Ortiz-Pérez et al. 2008] ORTIZ-PÉREZ, José T. ; RODRÍGUEZ, José ; MEYERS, Sheridan N. ; LEE, Daniel C. ; DAVIDSON, Charles ; WU, Edwin: Correspondence between the 17-segment model and coronary arterial anatomy using contrast-enhanced cardiac magnetic resonance imaging. In: *Journal of the American College of Cardiology* 1 (2008), no. 3, pp. 282–293

[Ostergaard et al. 1996] OSTERGAARD, L. ; WEISSKOFF, R. M. ; CHESLER, D. A. ; GYLDENSTED, C. ; ROSEN, B. R.: High resolution measurement of cerebral blood flow using intravascular tracer bolus passages. Part I: Mathematical approach and statistical analysis. In: *Magnetic Resonance in Medicine* 36 (1996), no. 5, pp. 715–25

[Paasche 2007] PAASCHE, Lydia: *Integrierte Visualisierung kardialer MRT-Daten zur Beurteilung von Funktion, Perfusion und Viabilität des Herzmuskels*, Faculty of Computer Science, University of Magdeburg, Magdeburg, Diplomarbeit, 2007

[Paasche et al. 2007] PAASCHE, Lydia ; OELTZE, Steffen ; HENNEMUTH, Anja ; KÜHNEL, Caroline ; GROTHUES, Frank ; PREIM, Bernhard: Integrierte Visualisierung kardialer MR-Daten zur Beurteilung von Funktion, Perfusion und Vitalität des Myokards. In: *Bildverarbeitung für die Medizin (BVM)*, 2007, pp. 212–216

[Panting et al. 2001] PANTING, J. R. ; GATEHOUSE, P. D. ; YANG, G. Z. ; JEROSCH-HEROLD, M. ; WILKE, N. ; FIRMIN, D. N. ; PENNELL, D. J.: Echo-planar magnetic resonance myocardial perfusion imaging: Parametric map analysis and comparison with thallium SPECT. In: *Journal of Magnetic Resonance Imaging* 13 (2001), no. 2, pp. 192–200

[Paulin 1983] PAULIN, S.: Normal coronary anatomy. In: ABRAMS, H.L. (ed.): *Coronary arteriography*. Little, Brown and Company Boston, 1983, pp. 127–174

[Peeters et al. 2009] PEETERS, T.H.J.M. ; VILANOVA, A. ; HAAR ROMENY, B.M. ter: Interactive fiber structure visualization of the heart. In: *Computer Graphics Forum* 28 (2009), no. 8, pp. 2140–2150(11)

[Petrella and Provenzale 2000] Petrella, J. R.; Provenzale, J. M.: MR perfusion imaging of the brain: Techniques and applications. In: *American Journal of Roentgenology* 175 (2000), no. 1, pp. 207–19

[Prasad 2006] Prasad, Pottumarthi V.: Functional MRI of the kidney: Tools for translational studies of pathophysiology of renal disease. In: *American Journal of Physiology - Renal Physiology* 290 (2006), no. 5, pp. F958–F974

[Preim et al. 2003] Preim, B.; Kohle, S.; Konrad-Verse, O.; Rascher-Friesenhausen, R.; Wiener, J.; Leppek, R. ; Peitgen, H.-O.: Mehrdimensionale Visualisierung dynamischer Bilddaten am Beispiel der Durchblutungsquantifizierung. In: *Simulation und Visualisierung (SimVis)*, 2003, pp. 77–88

[Preim and Bartz 2007] Preim, Bernhard; Bartz, Dirk: *Visualization in Medicine. Theory, Algorithms, and Applications*. 1. Morgan Kaufmann, 2007 (Series in Computer Graphics)

[Preim et al. 2009] Preim, Bernhard; Oeltze, Steffen; Mlejnek, Matej; Gröeller, Eduard; Hennemuth, Anja ; Behrens, Sarah: Survey of the visual exploration and analysis of perfusion data. In: *IEEE Transactions on Visualization and Computer Graphics* 15 (2009), no. 2, pp. 205–220

[Reimer and Jennings 1979] Reimer, K. A.; Jennings, R. B.: The "wavefront phenomenon" of myocardial ischemic cell death. II. Transmural progression of necrosis within the framework of ischemic bed size (myocardium at risk) and collateral flow. In: *Laboratory Investigation* 40 (1979), no. 6, pp. 633–644

[v. Rijsbergen 1979] Rijsbergen, C.J. v.: *Information Retrieval*. Butterworth, 1979

[Ringelstein and Nabavi 2007] Ringelstein, E.B.; Nabavi, D.G. ; Brandt, Th. (ed.); Hohlfeld, R. (ed.); Noth, J. (ed.) ; Reichmann, H. (ed.): *Der Ischämische Schlaganfall - Eine praxisorientierte Darstellung von Pathophysiologie, Diagnostik und Therapie*. Kohlhammer, 2007

[Ropinski and Preim 2008] Ropinski, Timo; Preim, Bernhard: Taxonomy and usage guidelines for glyph-based medical visualization. In: *Simulation und Visualisierung (SimVis)*, 2008, pp. 121–138

[Ropinski et al. 2007] Ropinski, Timo; Specht, Michael; Meyer-Spradow, Jennis; Hinrichs, Klaus H. ; Preim, Bernhard: Surface glyphs for visualizing multimodal volume data. In: *Vision, Modeling, and Visualization (VMV)*, 2007, pp. 3–12

[Rosen et al. 1990] Rosen, B. R.; Belliveau, J. W.; Vevea, J. M. ; Brady, T. J.: Perfusion imaging with NMR contrast agents. In: *Magnetic Resonance in Medicine* 14 (1990), no. 2, pp. 249–65

[Rueckert et al. 1999] Rueckert, D.; Sonoda, L. I.; Hayes, C.; Hill, D. L.; Leach, M. O. ; Hawkes, D. J.: Nonrigid registration using free-form deformations: Application to breast MR images. In: *IEEE Transactions on Medical Imaging* 18 (1999), no. 8, pp. 712–21

[Säring et al. 2009] SÄRING, D.; EHRHARDT, J.; STORK, A.; BANSMANN, M.P.; LUND, G.K. ; HANDELS, H.: Computer-assisted analysis of 4D cardiac MR image sequences after myocardial infarction. In: *Methods of Information in Medicine* 48 (2009), no. 5, pp. 377–383

[Säring et al. 2006] SÄRING, D.; STORK, A.; JUCHHEIM, S.; LUND, G.; ADAM, G. ; HANDELS, H.: HeAT: A software assistant for the analysis of LV remodeling after myocardial infarction in 4D MR follow-up studies. In: *Jahrestagung der Gesellschaft für Informatik e.V. (GI)* Bd. 1, 2006, pp. 537–543

[Sauber et al. 2006] SAUBER, Natascha; THEISEL, Holger ; SEIDEL, Hans-Peter: Multifield-graphs: An approach to visualizing correlations in multifield scalar data. In: *IEEE Transactions on Visualization and Computer Graphics* 12 (2006), no. 5, pp. 917–924

[Saver 2006] SAVER, Jeffrey L.: Time is brain–quantified. In: *Stroke* 37 (2006), no. 1, pp. 263–266

[Schellinger et al. 2006] SCHELLINGER, Peter D.; LATOUR, Lawrence L.; WU, Chen-Sen; CHALELA, Julio A. ; WARACH, Steven: The association between neurological deficit in acute ischemic stroke and mean transit time: Comparison of four different perfusion MRI algorithms. In: *Neuroradiology* 48 (2006), no. 2, pp. 69–77

[Schenk et al. 2000] SCHENK, A.; PRAUSE, G.P.M. ; PEITGEN, H.-O.: Efficient semiautomatic segmentation of 3D objects in medical images. In: *Medical Image Computing and Computer-Assisted Intervention (MICCAI)*, 2000, pp. 186–195

[Schindler et al. 1999] SCHINDLER, T. H.; MAGOSAKI, N.; JESERICH, M.; OSER, U.; KRAUSE, T.; FISCHER, R.; MOSER, E.; NITZSCHE, E.; ZEHENDER, M.; JUST, H. ; SOLZBACH, U.: Fusion imaging: Combined visualization of 3D reconstructed coronary artery tree and 3D myocardial scintigraphic image in coronary artery disease. In: *The International Journal of Cardiovascular Imaging* 15 (1999), no. 5, pp. 357–68; discussion 369–70

[Schlossbauer et al. 2008] SCHLOSSBAUER, Thomas; LEINSINGER, Gerda; WISMULLER, Axel; LANGE, Oliver; SCHERR, Michael; MEYER-BAESE, Anke ; REISER, Maximilian: Classification of small contrast enhancing breast lesions in dynamic Magnetic Resonance imaging using a combination of morphological criteria and dynamic analysis based on unsupervised vector-quantization. In: *Investigative Radiology* 43 (2008), no. 1, pp. 56–64

[Schmitt et al. 2002] SCHMITT, M.; MOHRS, O. K.; PETERSEN, S. E.; KREITNER, K.-F.; VOIGTLÄNDER, T.; WITTLINGER, T.; HORSTICK, G.; ZIEGLER, S.; MEYER, J.; THELEN, M. ; SCHREIBER, W. G.: Bestimmung der myokardialen Perfusionsreserve bei KHK-Patienten mit der kontrastmittelverstärkten MRT: Eine Vergleich zwischen semiquantitativer und quantitativer Auswertung. In: *RöFo - Fortschritte auf dem Gebiet der Röntgenstrahlen und der bildgebenden Verfahren* 174 (2002), no. 2, pp. 187–195

[Schumann and Müller 1999] SCHUMANN, Heidrun; MÜLLER, Wolfgang: *Visualisierung: Grundlagen und allgemeine Methoden.* 1. Springer, 1999

[Schünke et al. 2006] SCHÜNKE, M.; SCHULTE, E.; SCHUMACHER, U.; VOLL, M. ; WESKER, K.: *PROMETHEUS Lernatlas der Anatomie. Kopf und Neuroanatomie.* Thieme, 2006

[Schwitter et al. 2001] Schwitter, J.; Nanz, D.; Kneifel, S.; Bertschinger, K.; Büchi, M.; Knüsel, P. R.; Marincek, B.; Lüscher, T. F.; Schulthess, G. K.: Assessment of myocardial perfusion in coronary artery disease by Magnetic Resonance: A comparison with positron emission tomography and coronary angiography. In: *Circulation* 103 (2001), no. 18, pp. 2230–5

[Selle et al. 2002] Selle, Dirk; Preim, Bernhard; Schenk, Andrea; Peitgen, Heinz-Otto: Analysis of vasculature for liver surgical planning. In: *IEEE Transactions on Medical Imaging* 21 (2002), no. 11, pp. 1344–1357

[de Senneville et al. 2008] Senneville, Baudouin D.; Mendichovszky, Iosif A.; Roujol, Sébastien; Gordon, Isky; Moonen, Chrit; Grenier, Nicolas: Improvement of MRI-functional measurement with automatic movement correction in native and transplanted kidneys. In: *Journal of Magnetic Resonance Imaging* 28 (2008), no. 4, pp. 970–978

[Sobesky et al. 2005] Sobesky, Jan; Weber, Olivier Z.; Lehnhardt, Fritz-Georg; Hesselmann, Volker; Neveling, Michael; Jacobs, Andreas; Heiss, Wolf-Dieter: Does the mismatch match the penumbra? Magnetic resonance imaging and positron emission tomography in early ischemic stroke. In: *Stroke* 36 (2005), no. 5, pp. 980–985

[Sommer et al. 2002] Sommer, T.; Hofer, U.; Hackenbroch, M.; Meyer, C.; Flacke, S.; Schmiedel, A.; Schmitz, C.; Thiemann, K.; Omran, H.; Schild, H.: Submillimeter 3D coronary MR angiography with real-time navigator correction in 107 patients with suspected coronary artery disease. In: *Röfo* 174 (2002), no. 4, pp. 459–466

[Sorensen et al. 1999] Sorensen, A. G.; Copen, W. A.; Ostergaard, L.; Buonanno, F. S.; Gonzalez, R. G.; Rordorf, G.; Rosen, B. R.; Schwamm, L. H.; Weisskoff, R. M.; Koroshetz, W. J.: Hyperacute stroke: Simultaneous measurement of relative cerebral blood volume, relative cerebral blood flow, and mean tissue transit time. In: *Radiology* 210 (1999), no. 2, pp. 519–27

[Sorensen 2008] Sorensen, A. G.: Perfusion MR imaging: Moving forward. In: *Radiology* 249 (2008), no. 2, pp. 416–417

[Sorensen and Reimer 2000] Sorensen, A.G.; Reimer, P.: *Cerebral MR Perfusion Imaging. Principles and Current Applications.* Thieme, 2000

[Statistisches Bundesamt Deutschland 2007] Statistisches Bundesamt Deutschland: Todesursachen in Deutschland. In: *Fachserie* 12 (2007), no. 4, pp. 1–49

[Strohm et al. 2006] Strohm, O.; Bernhardt, P.; Niendorf, T.: *Kardiovaskuläre MRT in der Praxis: Anleitungen und Fallbeispiele.* Elsevier Urban & Fischer, 2006

[Studholme et al. 1999] Studholme, C.; Hill, D. L. G.; Hawkes, D. J.: An overlap invariant entropy measure of 3D medical image alignment. In: *Pattern Recognition* 32 (1999), no. 1, pp. 71 – 86

[Subramanian et al. 2004] Subramanian, Kalpathi R.; Brockway, John P.; Carruthers, William B.: Interactive detection and visualization of breast lesions from dynamic contrast enhanced MRI volumes. In: *Computerized Medical Imaging and Graphics* 28 (2004), no. 8, pp. 435–444

[Takasawa et al. 2008] TAKASAWA, Masashi ; JONES, P. S. ; GUADAGNO, Joseph V. ; CHRISTENSEN, Soren ; FRYER, Tim D. ; HARDING, Sally ; GILLARD, Jonathan H. ; WILLIAMS, Guy B. ; AIGBIRHIO, Franklin I. ; WARBURTON, Elizabeth A. ; ØSTERGAARD, Leif ; BARON, Jean-Claude: How reliable is perfusion MR in acute stroke? Validation and determination of the penumbra threshold against quantitative PET. In: *Stroke* 39 (2008), no. 3, pp. 870–7

[Taubin 1995] TAUBIN, Gabriel: A signal processing approach to fair surface design. In: *ACM SIGGRAPH Computer Graphics*, 1995, pp. 351–358

[Tayler 2002] TAYLER, R.: Visualizing multiple fields on the same surface. In: *IEEE Computer Graphics and Applications* 22 (2002), no. 3, pp. 6–10

[Termeer 2009] TERMEER, Maurice: *Comprehensive visualization of cardiac MRI data.* Favoritenstrasse 9-11/186, A-1040 Vienna, Austria, Institute of Computer Graphics and Algorithms, Vienna University of Technology, Diss., 2009

[Termeer et al. 2008] TERMEER, Maurice ; BESCÓS, Javier O. ; BREEUWER, Marcel ; VILANOVA, Anna ; GERRITSEN, Frans ; GRÖLLER, Meister E. ; NAGEL, Eike: Visualization of myocardial perfusion derived from coronary anatomy. In: *IEEE Transactions on Visualization and Computer Graphics* 14 (2008), no. 6, pp. 1595–1602

[Termeer et al. 2009] TERMEER, Maurice ; BESCÓS, Javier O. ; BREEUWER, Marcel ; VILANOVA, Anna ; GERRITSEN, Frans ; GRÖLLER, Meister E. ; NAGEL, Eike: *Patient-Specific Coronary Artery Supply Territory AHA Diagrams.* Version: 2009 (1). – Poster presented at SCMR 2009 (2009-01-29–2009-02-01)

[Termeer et al. 2007] TERMEER, Maurice ; BESCÓS, Javier O. ; BREEUWER, Marcel ; VILANOVA, Anna ; GERRITSEN, Frans ; GRÖLLER, Eduard: CoViCAD: Comprehensive visualization of coronary artery disease. In: *IEEE Transactions on Visualization and Computer Graphics* 13 (2007), no. 6, pp. 1632–1639

[Texas Heart Insitute 2009] TEXAS HEART INSITUTE: *Anatomy of the heart.* Version: 2009. – http://texasheart.org/HIC/Anatomy/index.cfm. Last visited on November, 5th, 2009

[Thelen et al. 2007] THELEN, M. ; ERBEL, R. ; KREITNER, K.-F. ; BARKHAUSEN, J.: *Bildgebende Kardiodiagnostik mit MRT, CT, Echokardiographie und anderen Verfahren.* Thieme, 2007

[Tofts and Kermode 1991] TOFTS, P. S. ; KERMODE, A. G.: Measurement of the blood-brain barrier permeability and leakage space using dynamic MR imaging. 1. Fundamental concepts. In: *Magnetic Resonance in Medicine* 17 (1991), no. 2, pp. 357–367

[Tory et al. 2001] TORY, Melanie ; RÖBER, Niklas ; MÖLLER, Torsten ; CELLER, Anna ; ATKINS, M. S.: 4D space-time techniques: a medical imaging case study. In: *IEEE Visualization (VIS)*, 2001, pp. 473–476

[Treisman and Gelade 1980] TREISMAN, A. ; GELADE, G.: A feature-integration theory of attention. In: *Cognitive Psychology* 12 (1980), pp. 97–136

[Treisman and Gormican 1988] TREISMAN, A. ; GORMICAN, S.: Feature analysis in early vision: Evidence from search asymmetries. In: *Psychological Review* 95 (1988), no. 1, pp. 15–48

[Tufte 1990] Tufte, Edward R.: *Envisioning Information.* Graphics Press, 1990

[Tukey 1977] Tukey, J.W.: *Exploratory Data Analysis.* Addison Wesley, 1977

[Twellmann et al. 2005] Twellmann, T. ; Lichte, O. ; Nattkemper, T. W.: An adaptive tissue characterization network for model-free visualization of dynamic contrast-enhanced Magnetic Resonance image data. In: *IEEE Transactions on Medical Imaging* 24 (2005), no. 10, pp. 1256–1266

[Villringer et al. 1988] Villringer, A. ; Rosen, B. R. ; Belliveau, J. W. ; Ackerman, J. L. ; Lauffer, R. B. ; Buxton, R. B. ; Chao, Y. S. ; Wedeen, V. J. ; Brady, T. J.: Dynamic imaging with lanthanide chelates in normal brain: Contrast due to magnetic susceptibility effects. In: *Magnetic Resonance in Medicine* 6 (1988), no. 2, pp. 164–174

[Viola et al. 2004] Viola, Ivan ; Kanitsar, Armin ; Gröller, Meister E.: Importance-Driven Volume Rendering. In: *IEEE Visualization (VIS)*, 2004, pp. 139–145

[Wald et al. 2007] Wald, Diana ; Wesarg, Stefan ; Nowak, Stefanie: Quantifizierung und Visualisierung von Narbenbereichen des Myokards. In: *Bildverarbeitung für die Medizin (BVM)*, 2007, pp. 323–327

[Wang et al. 2008] Wang, Chaoli ; Yu, Hongfeng ; Ma, Kwan-Liu: Importance-driven time-varying data visualization. In: *IEEE Transactions on Visualization and Computer Graphics* 14 (2008), no. 6, pp. 1547–1554

[Warach et al. 1996] Warach, S. ; Dashe, J. F. ; Edelman, R. R.: Clinical outcome in ischemic stroke predicted by early diffusion-weighted and perfusion magnetic resonance imaging: a preliminary analysis. In: *Journal of Cerebral Blood Flow & Metabolism* 16 (1996), no. 1, pp. 53–59

[Ware 2000] Ware, C.: *Information Visualization.* Morgan Kaufmann, 2000

[Weigle et al. 2000] Weigle, Christopher ; Emigh, William G. ; Liu, Geniva ; Taylor, Russell M. ; Enns, James T. ; Healey, Christopher G.: Oriented sliver textures: A technique for local value estimation of multiple scalar fields. In: *Graphics Interface*, 2000, pp. 163–170

[Wesarg and Nowak 2006] Wesarg, Stefan ; Nowak, Stefanie: An automated 4D approach for left ventricular assessment in clinical cine MR images. In: *GI Jahrestagung (1)*, 2006, pp. 483–490

[Wiener et al. 2005] Wiener, Jonathan I. ; Schilling, Kathy J. ; Adami, Carol ; Obuchowski, Nancy A.: Assessment of suspected breast cancer by MRI: A prospective clinical trial using a combined kinetic and morphologic analysis. In: *American Journal of Roentgenology* 184 (2005), no. 3, pp. 878–86

[Wintermark et al. 2008] Wintermark, Max ; Albers, Gregory W. ; Alexandrov, Andrei V. ; Alger, Jeffry R. ; Bammer, Roland ; Baron, Jean-Claude ; Davis, Stephen ; Demaerschalk, Bart M. ; Derdeyn, Colin P. ; Donnan, Geoffrey A. ; Eastwood, James D. ; Fiebach, Jochen B. ; Fisher, Marc ; Furie, Karen L. ; Goldmakher, Gregory V. ; Hacke, Werner ; Kidwell, Chelsea S. ; Kloska, Stephan P. ; Köhrmann, Martin ; Koroshetz, Walter ; Lee, Ting-Yim ; Lees, Kennedy R. ; Lev, Michael H. ;

LIEBESKIND, David S.; OSTERGAARD, Leif; POWERS, William J.; PROVENZALE, James; SCHELLINGER, Peter; SILBERGLEIT, Robert; SORENSEN, Alma G.; WARDLAW, Joanna; WU, Ona ; WARACH, Steven: Acute stroke imaging research roadmap. In: *Stroke* 39 (2008), no. 5, pp. 1621–1628

[Wintermark et al. 2005a] WINTERMARK, Max; FISCHBEIN, Nancy J.; SMITH, Wade S.; KO, Nerissa U.; QUIST, Marcel ; DILLON, William P.: Accuracy of dynamic perfusion CT with deconvolution in detecting acute hemispheric stroke. In: *American Journal of Neuroradiology* 26 (2005), no. 1, pp. 104–112

[Wintermark et al. 2005b] WINTERMARK, Max; SESAY, Musa; BARBIER, Emmanuel; BORBÉLY, Katalin; DILLON, William P.; EASTWOOD, James D.; GLENN, Thomas C.; GRANDIN, Cécile B.; PEDRAZA, Salvador; SOUSTIEL, Jean-François; NARIAI, Tadashi; ZAHARCHUK, Greg; CAILLÉ, Jean-Marie; DOUSSET, Vincent ; YONAS, Howard: Comparative overview of brain perfusion imaging techniques. In: *Stroke* 36 (2005), no. 9, pp. e83–99

[Wirestam and Ståhlberg 2005] WIRESTAM, R.; STÅHLBERG, F.: Wavelet-based noise reduction for improved deconvolution of time-series data in dynamic susceptibility-contrast MRI. In: *MAGMA* 18 (2005), no. 3, pp. 113–118

[Wismüller et al. 2006] WISMÜLLER, A.; MEYER-BAESE, A.; LANGE, O.; REISER, M. F. ; LEINSINGER, G.: Cluster analysis of dynamic cerebral contrast-enhanced perfusion MRI time-series. In: *IEEE Transactions on Medical Imaging* 25 (2006), no. 1, pp. 62–73

[Wittsack et al. 2002] WITTSACK, Hans-Jörg; RITZL, Afra; FINK, Gereon R.; WENSERSKI, Frank; SIEBLER, Mario; SEITZ, Rüdiger J.; MÖDDER, Ulrich ; FREUND, Hans-Joachim: MR imaging in acute stroke: Diffusion-weighted and perfusion imaging parameters for predicting infarct size. In: *Radiology* 222 (2002), no. 2, pp. 397–403

[Wünsche et al. 2004] WÜNSCHE, Burkhard C.; LOBB, Richard ; YOUNG, Alistair A.: The visualization of myocardial strain for the improved analysis of cardiac mechanics. In: *International Conference on Computer graphics and interactive techniques in Australasia and South East Asia (GRAPHITE)*, 2004, pp. 90–99

[Wu et al. 1998] WU, K. C.; ZERHOUNI, E. A.; JUDD, R. M.; LUGO-OLIVIERI, C. H.; BAROUCH, L. A.; SCHULMAN, S. P.; BLUMENTHAL, R. S. ; LIMA, J. A.: Prognostic significance of microvascular obstruction by magnetic resonance imaging in patients with acute myocardial infarction. In: *Circulation* 97 (1998), no. 8, pp. 765–72

[Wu and Liu 2007] WU, X. Y.; LIU, G. R.: Application of independent component analysis to dynamic contrast-enhanced imaging for assessment of cerebral blood perfusion. In: *Medical Image Analysis* 11 (2007), no. 3, pp. 254–265

[Xue et al. 2008] XUE, Hui; GUEHRING, Jens; SRINIVASAN, Latha; ZUEHLSDORFF, Sven; SADDI, Kinda; CHEFDHOTEL, Christophe; HAJNAL, Joseph V. ; RUECKERT, Daniel: Evaluation of rigid and non-rigid motion compensation of cardiac perfusion MRI. In: *Medical Image Computing and Computer-Assisted Intervention (MICCAI)* 11 (2008), no. Pt 2, pp. 35–43

[Xue et al. 2009] Xue, Hui ; Zühlsdorff, Sven ; Kellman, Peter ; Arai, Andrew E. ; Nielles-Vallespin, Sonia ; Chefd'Hotel, Christophe ; Lorenz, Christine H. ; Guehring, Jens: Unsupervised inline analysis of cardiac perfusion MRI. In: *Medical Image Computing and Computer-Assisted Intervention (MICCAI)*, 2009, pp. 741–749

[Yamada et al. 2002] Yamada, Kei ; Wu, Ona ; Gonzalez, R. G. ; Bakker, Dirk ; Østergaard, Leif ; Copen, William A. ; Weisskoff, Robert M. ; Rosen, Bruce R. ; Yagi, Katsumi ; Nishimura, Tsunehiko ; Sorensen, A. G.: Magnetic resonance perfusion-weighted imaging of acute cerebral infarction: Effect of the calculation methods and underlying vasculopathy. In: *Stroke* 33 (2002), no. 1, pp. 87–94

[Zachow et al. 2009] Zachow, Stefan ; Muigg, Philipp ; Hildebrandt, Thomas ; Doleisch, Helmut ; Hege, Hans-Christian: Visual exploration of nasal airflow. In: *IEEE Transactions on Visualization and Computer Graphics* 15 (2009), no. 6, pp. 1407–1414

[Zhukov and Barr 2003] Zhukov, L. ; Barr, A.: Heart-muscle fiber reconstruction from diffusion tensor MRI. In: *IEEE Visualization*, 2003, pp. 597–602

[Zierler 1962] Zierler, Kenneth L.: Theoretical basis of indicator-dilution methods for measuring flow and volume. In: *Circulation Research* 10 (1962), no. 3, pp. 393–407

[Zöllner et al. 2007] Zöllner, Frank ; Kocinski, Marek ; Lundervold, Arvid ; Rørvik, Jarle: Assessment of renal function from 3D dynamic contrast enhanced MR images using independent component analysis. In: *Bildverarbeitung für die Medizin (BVM)*, 2007, pp. 237–241

Nomenclature

AIF	Arterial Input Function
AHA	American Heart Association
BEP	Bull's Eye Plot
CA	Contrast Agent
CHD	Coronary Heart Disease
CTC	Concentration-time curve
CTCA	Computed Tomography Coronary Angiography
CXA	Coronary X-ray Angiography
DCE-MRI	Dynamic Contrast-Enhanced Magnetic Resonance Imaging
DOI	Degree of interest
DSC-MRI	Dynamic Susceptibility Contrast Magnetic Resonance Imaging
DTI	Diffusion Tensor Imaging
DWI	Diffusion-Weighted Imaging
ECG	Electrocardiogram
ICA	Independent Component Analysis
LAD	Left Anterior Descending Coronary Artery
LCA	Left Coronary Artery
LCX	Left Circumflex Coronary Artery
LE	Late Enhancement
MITR	Maximum Intensity-Time Ratio
MPRI	Myocardial Perfusion Reserve Index
MR	Magnetic Resonance
MRCA	Magnetic Resonance Coronary Angiography
MRI	Magnetic Resonance Imaging
MTT	Mean Transit Time
PCA	Principal Component Analysis
PE	Peak Enhancement
PET	Positron Emission Tomography
RCA	Right Coronary Artery
rCBF	regional Cerebral Blood Flow
rCBV	regional Cerebral Blood Volume
rMTT	regional Mean Transit Time
SPECT	Single-Photon Emission Computed Tomography
TIC	Time-intensity Curve
$\mathbf{T_{max}}$	Time To Peak of the residue function
TTP	Time To Peak